REFERENCE ONLY

UNIVERSITY OF LONDON THESIS

Degree PhD Year 2005 Name of Author CANKESTEN, K.J.

COPYRIGHT

This is a thesis accepted for a Higher Degree of the University of London. It is an unpublished typescript and the copyright is held by the author. All persons consulting the thesis must read and abide by the Copyright Declaration below.

COPYRIGHT DECLARATION

I recognise that the copyright of the above-described thesis rests with the author and that no quotation from it or information derived from it may be published without the prior written consent of the author.

LOANS

Theses may not be lent to individuals, but the Senate House Library may lend a copy to approved libraries within the United Kingdom, for consultation solely on the premises of those libraries. Application should be made to: Inter-Library Loans, Senate House Library, Senate House, Malet Street, London WC1E 7HU.

REPRODUCTION

University of London theses may not be reproduced without explicit written permission from the Senate House Library. Enquiries should be addressed to the Theses Section of the Library. Regulations concerning reproduction vary according to the date of acceptance of the thesis and are listed below as guidelines.

A. Before 1962. Permission granted only upon the prior written consent of the author. (The Senate House Library will provide addresses where possible).

B. 1962 - 1974. In many cases the author has agreed to permit copying upon completion of a Copyright Declaration.

C. 1975 - 1988. Most theses may be copied upon completion of a Copyright Declaration.

D. 1989 onwards. Most theses may be copied.

This thesis comes within category D.

☑ This copy has been deposited in the Library of UCL

☐ This copy has been deposited in the Senate House Library, Senate House, Malet Street, London WC1E 7HU.

MAGNETIC RESONANCE IMAGING AND THE DEVELOPMENT OF VASCULAR TARGETED TREATMENTS FOR CANCER

by

Katharine Jane Lankester

A thesis submitted for the degree of

Doctor of Philosophy

University of London
Faculty of Oncology

2005

Gray Cancer Institute, Northwood, Middlesex, UK
and
Department of Medical Oncology, Mount Vernon Hospital

ProQuest LLC
789 East Eisenhower Parkway
P.O. Box 1346
Ann Arbor, MI 48106-1346

ABSTRACT

The main subject of the work presented in this thesis is the further development of magnetic resonance imaging (MRI) as a non-invasive method of investigating tumour microcirculation. Two different MR techniques were used: dynamic contrast enhanced (DCE)-MRI and Blood Oxygen Level Dependent (BOLD)-MRI. Intravital microscopy was used to help interpret BOLD-MRI results. The ultimate aims were to determine whether MRI methods could be relied upon to define a drug as having vascular disrupting activity and to develop techniques to predict the effectiveness of vascular disruptive agents (VDA).

In DCE-MRI, tissue enhancement is continuously monitored over several minutes after intravenous injection of contrast medium. Modelling of contrast agent kinetics generates quantitative parameters related to tissue blood flow rate and permeability, e.g. K^{trans} (transfer constant). In a clinical study, patients had DCE-MRI examinations before and 24 hours after cytotoxic chemotherapy to establish whether any acute anti-vascular effects could be detected. No acute reductions in K^{trans} were seen. In this project, the acute effects of the VDA, combretastatin A-4-phosphate, were investigated using DCE-MRI in SW1222 tumours in mice. Responses were seen both at a clinically relevant dose and at higher doses, and a dose-response relationship established.

BOLD-MRI can detect changes in oxygenation and blood flow within tumours using deoxygenated haemoglobin as an intrinsic contrast agent. Tumours contain a variable proportion of immature vessels, which may explain differential sensitivity to VDAs. In this project, BOLD-MRI was used to assess tumour vessel maturity using consequent vasoreactivity to angiotensin II and carbon dioxide (as air-5%CO_2 or as carbogen) in an animal model. Intravital microscopy was used to directly observe response to these agents in mouse window chambers. Results suggest that response to vasoactive agents is useful for assessing vascular maturity in tumours but that more sensitive non-invasive imaging methods than BOLD-MRI are required for clinical use.

ACKNOWLEDGMENTS

Completion of the work described in this thesis would not have been possible without the contribution of many people in the Gray Cancer Institute, Mount Vernon Hospital and the Paul Strickland Scanner Centre. I should like to thank my supervisors Dr Gillian Tozer and Professor Gordon Rustin for supporting me during this PhD and providing invaluable help and advice.

The Tumour Microcirculation group at the Gray Cancer Institute has made me very welcome. I would particularly like to thank Ross Maxwell and Sally Hill for teaching me and for all their support and encouragement. Vivien Prise, Ian Wilson and Gemma Lewis all helped considerably with the *in-vivo* work and cell culture. I would also like to thank Davina Honess who has been a good source of advice.

I would like to thank Anne Clarke and the animal house staff for looking after the mice used for the *in vivo* experiments and for all their support and help. Søren Bentzen and Francesca Buffa helped with statistical advice and Mike Stratford has been very patient about questions concerning pharmacokinetics and how to use the Origin graph program. I am also grateful to Boris Vojnovic, Paul Barber and Ros Locke of the Advanced Technology group who developed the program for the analysis of the BOLD-MRI data and the equipment used for the intravital microscopy experiments. For the intravital microscopy experiments, both Paul Barber and Ian Wilson were very helpful at trouble-shooting when the microscope, computer or video were playing up. Frances Daley was very helpful with advice about preparing tumours for histology and did all the immunohistochemical staining.

I am indebted to several people at the Paul Strickland Scanner Centre, in particular Anwar Padhani and Jane Taylor for their patience and excellent advice and for giving me their time to help analyse the data. I am also grateful to James Stirling and Linda Culver, the MRI radiographers who did the scanning. Martin Leach and James D'Arcy from the MRI unit at the Royal Marsden Sutton developed the MRIW software used for the analysis in the clinical study.

At Mount Vernon Hospital, I would like to thank Jane Boxall, the research nurse, for her help and support for the clinical study. Melanie Winterbotham from Research and Development was very helpful when I was struggling with all the forms required for ethics

approval. I am very grateful to all the patients who gave up their valuable time to take part in the clinical study.

I have been supported financially by The Marie Cancer Translational Research Trust and The Cancer Treatment and Research Trust and would like to thank the trustees for their support.

Finally, I am very grateful for the love and support of my family and friends who have helped me keep things in perspective, particularly when writing up.

TABLE OF CONTENTS

Chapter 1 Introduction 10

1.1 Tumour Microcirculation 10
1.1.1 Angiogenesis 10
1.1.2 Morphology of tumour vasculature 13
1.1.3 Consequences of the structural and functional abnormalities of tumour vasculature 14
1.1.4 Implications for anti-cancer treatment 15

1.2 Tumour microcirculation as a therapeutic target 16
1.2.1 Small molecule vascular disruptive agents 17
1.2.2 Ligand-based therapies 24
1.2.3 Other vascular disruptive strategies 26

1.3 Investigation of tumour vessel maturity 29
1.3.1 Use of BOLD-MRI response to vasoactive agents to investigate vessel maturity 32

1.4 Measurement of tumour blood flow in the laboratory and the clinic 36
1.4.1 Introduction 36
1.4.2 Tracer and contrast agent kinetic techniques 36
1.4.3 Measurement of red cell flux and velocity using intravital microscopy 46
1.4.4 Measurement of red cell flux and velocity using the Doppler technique 47

1.5 MRI methods for imaging tumour microcirculation 48
1.5.1 Overview of MRI principles 48
1.5.2 Image Contrast 52
1.5.3 Dynamic Contrast Enhanced Magnetic Resonance Imaging 55
1.5.4 BOLD-MRI 63
1.5.5 The use of MRI in the assessment of vascular disruptive agents 65
1.5.6 Further development of DCE-MRI to assess vascular disruptive response 67

1.6 Aims of thesis 68

1.7 References 69

Chapter 2 DCE-MRI measurement of acute vascular disruptive effects of cytotoxic agents 85

2.1 Introduction 85
2.1.1 Background 85
2.1.2 Study objective 86

2.2 Methods 87
2.2.1 Patient selection 87
2.2.2 MRI protocol 87
2.2.3 Image analysis 88
2.2.4 Statistical analysis 90

2.3 *Results* 92
2.3.1 Patient characteristics 92
2.3.2 Reproducibility 96
2.3.3 Correlation between different parameters 97
2.3.4 Response 98

2.4 *Discussion* 101
2.4.1 T_1-weighted DCE-MRI parameters 101
2.4.2 T_2*-weighted DCE-MRI parameters: rBV, MTT and rBF 104
2.4.3 R_2* (BOLD) 107
2.4.4 Conclusions 108

2.5 *References* 109

Chapter 3 **The acute anti-vascular effects of CA-4-P on the SW1222 tumour as measured by DCE-MRI** 112

3.1 *Introduction* 112
3.1.1 Radioimmunotherapy 112
3.1.2 Rationale for study 114
3.1.3 Study objectives 115

3.2 *Methods* 116
3.2.1 Mice and tumours 116
3.2.2 Drug treatments 116
3.2.3 MRI protocol 116
3.2.4 Histological parameters 120
3.2.5 Statistical analysis 122

3.3 *Results* 123
3.3.1 Gd-DTPA relaxivity in mouse plasma at 4.7 T 123
3.3.2 Arterial input function for Gd-DTPA in the mouse 124
3.3.3 MR parameters 124
3.3.4 Histological parameters 131

3.4 *Discussion* 134
3.4.1 MR parameters 134
3.4.2 Histological parameters 136
3.4.3 Clinical relevance of this study 137
3.4.4 Conclusions 139

3.5 *References* 140

Chapter 4 **Investigation of tumour vessel maturity using air-5% CO_2/carbogen and angiotensin II using MRI and intravital microscopy** **143**

4.1 *Introduction* **143**

4.2 *Materials and Methods* **144**
4.2.1 Tumours 144
4.2.2 Histology: vascular maturation index 145
4.2.3 Effect of ATII, air-5% CO_2/carbogen and anaesthesia on mouse blood pressure 145
4.2.4 BOLD-MRI animal studies 146
4.2.5 Intravital microscopy 151

4.3 *Results* **158**
4.3.1 Histology: vascular maturation index 158
4.3.2 The effect of treatment on mouse MABP 161
4.3.3 BOLD-MRI results 163
4.3.4 Intravital microscopy results 170

4.4 *Discussion* **179**
4.4.1 T138 tumours 179
4.4.2 Mouse MABP measurements 179
4.4.3 Tumour vessel response to angiotensin II 180
4.4.4 Tumour vessel response to air-5% CO_2 and carbogen 182

4.5 *Conclusions* **183**

4.6 *References* **184**

Chapter 5 **Concluding Discussion** **185**

5.1 *Future work* **186**
5.1.1 Clinical study 186
5.1.2 CA-4-P/SW1222 study 188
5.1.3 Investigation of tumour vessel maturity 188

5.2 *References* **190**

Appendix **191**

1.1 *Conversion of signal intensity into Gd-DTPA concentration* 191
1.2 *Calculation of $T_1(0)$* **192**

List of publications and presentations **194**

List of Figures

Chapter 1

1.1	Process of vessel maturation	12
1.2	Chemical structure of A: colchicine; B: CA-4-P; C: ZD6126; D: DMXAA	19
1.3	Summary of the proposed mechanism of action of CA-4-P	21
1.4	Vascular maturation index for different human tumour types	29
1.5	Change in MRI signal intensity	33
1.6	Arterial and tissue concentration time curves	39
1.7	A: A nuclear spin, rotating about its longitudinal axis. B: Volume of tissue containing randomly orientated spins	49
1.8	The application of an external magnetic field, $\underline{B}_0$ causes the nuclear spin to precess gyroscopically around $\underline{B}_0$ (A) and to line up with their net orientations either parallel or anti-parallel to $\underline{B}_0$ (B).	49
1.9	A. The net magnetisation, $\underline{M}_0$ at equilibrium. B. Application of a RF pulse.	51
1.10	A. T_1 relaxation time-curve. B. T_2 relaxation time-curve	51
1.11	Diagram to show relationship between RF pulse, resultant signal, TR and TE	53
1.12	Graph of signal intensity versus time showing the transient dip in signal intensity due to T_2* effects following bolus injection of Gd-DTPA	55
1.13	Diagram to show derivation of IAUGC	57
1.14	Diagram to show Toft's model for Gd-DTPA uptake kinetics	59
1.15	Diagram to show Γ-variate fit to ΔR_2* curve	61
1.16	Schematic tissue concentration-time curve showing the approximations used for mean transit time	62

Chapter 2

2.1	Representative MRI maps	95
2.2	T_1-weighted parameters	99
2.3	T_2*-weighted parameters	100
2.4	ΔR_2* curves and Γ-variate fits for (A) glioblastoma multiforme and (B) pelvic tumour	106

Chapter 3

3.1	Gd-DTPA relaxivity in mouse plasma	123
3.2	Signal intensity and IAUGC maps	125
3.3	Mean tumour and muscle IAUGC for each treatment group	126
3.4	IAUGC dose-response relationship for tumour and muscle	127
3.5	Tumour IAUGC spatial heterogeneity	128
3.6	Mean tumour K^{trans} and v_e for each treatment group	130
3.7	Percentage necrosis seen at 24 hours following CA-4-P	131
3.8	Histological sections to show necrosis, αSMA and CD31 antigen staining	132
3.9	Change in functional vascular volume (%) at 4 and 24 hours post CA-4-P	133
3.10	Comparison of mouse standard arterial input functions	135

Chapter 4

4.1	A: T_1-weighted image, B: BOLD image	149
4.2	Diagram to show BOLD-MRI protocol	149
4.3	Window chamber diagrams	152
4.4	Video intravital microscopy images	156
4.5	Vascular maturation index	158
4.6	H&E sections of HT29, CaNT and T138 tumours	159
4.7	Histological sections to show αSMA and CD31 antigen staining	160
4.8	Effect of A: ATII infusion, B: 5% CO2/carbogen and C: anaesthesia on mouse MABP	162
4.9	Mean percentage change from baseline for T_2* and A_0 for the ATII protocol	164
4.10	Mean percentage change in T_2* and A_0 for gas-breathing protocol	165
4.11	Mean percentage change in signal intensity for ATII protocol (A) and gas-breathing protocol (B)	167
4.12	BOLD images of HT29 tumour showing response to ATII	168
4.13	BOLD images of kidney showing response to ATII	169
4.14	Intravital microscopy images	172
4.15	Mean percentage change in HT29 parameters for ATII protocol	174
4.16	Mean percentage change in CaNT parameters for ATII protocol	175
4.17	Mean percentage change in HT29 parameters on gas breathing protocol	177
4.18	αSMA staining of HT29 and CaNT tumours taken from window chamber preparations	178

Appendix

1.1	Calculation of $T_1(0)$	193

List of Tables

Chapter 1

1.1	Small molecule and ligand-based vascular disruptive agents in clinical or pre-clinical development	18
1.2	Effect of carbogen on tumour blood flow	34
1.3	Summary of techniques to measure TBF	37

Chapter 2

2.1	Patient details	93
2.2	Tumour pixel numbers	94
2.3	Baseline MR parameters (day 1) for individual patients	94
2.4	Tumour reproducibility analysis for T1-weighted parameters	96
2.5	Muscle reproducibility analysis for T1-weighted parameters	97
2.6	Tumour reproducibility analysis for T2*-weighted parameters	97
2.7	Correlation between baseline (day 1) parameter values	97

Chapter 3

3.1	Clinical trial schedule	115
3.2	Mean values of relaxation parameters for each treatment group	129
3.3	Parameter values for AIF	135

Chapter 4

4.1	Comparison of baseline MABP in unanaesthetised and anaesthetised mice	161
4.2	Intravital microscopy: baseline values for ATII protocol	171
4.3	Total animal and vessel numbers for ATII protocol	171
4.4	Baseline parameters for gas breathing protocol	176
4.5	Mouse and vessel numbers used for gas breathing protocol	176

Chapter 1 Introduction

This chapter describes the development of tumour vasculature, its functional and structural abnormalities and the consequences of these abnormalities for anti-cancer therapy. The identification of tumour microcirculation as a potential therapeutic target and the subsequent development of vascular disruptive agents are discussed. Tumour vessel maturation status, its implications for vascular-targeted therapies and methods for evaluating tumour vessel maturity are introduced. Methods for measuring tumour blood flow in the laboratory and the clinic are described and compared. The basic principles of magnetic resonance imaging and the specific techniques used for the work presented in this thesis are outlined. Finally the aims of the thesis are given.

1.1 Tumour microcirculation

1.1.1 Angiogenesis

Angiogenesis, defined as the growth of new capillaries from an existing vascular bed, involves the migration, proliferation and differentiation of endothelial cells (Carmeliet, 2003). Angiogenesis is crucial for normal development and persists in the adult in physiological processes such as wound healing and the female reproductive system, and in pathological processes such as neoplasia and diabetic retinopathy. The development of a blood supply is an essential requirement for a tumour to grow larger than 1-2 mm^3 in size (Folkman, 1971) and, apart from a few exceptions (see below) this is achieved via angiogenesis.

Tumour cells promote angiogenesis by the upregulation of pro-angiogenic factors such as vascular endothelial growth factor (VEGF) and its receptors (Brown et al., 1995; Hatva et al., 1995; Plate et al., 1993; Takahashi et al., 1994; Warren et al., 1995) and the down-regulation of anti-angiogenic factors such as thrombospondin-1 (Watnick et al., 2003). In addition, the nature of the tumour microenvironment is conducive towards angiogenesis as the presence of hypoxia can upregulate many pro-angiogenic genes including VEGF (Forsythe et al., 1996; Hlatky et al., 1994; Maxwell et al., 1997; Plate et al., 1993; Shweiki et al., 1992), Angiopoietin-2 (Ang-2) (Mandriota et al., 2000), nitric oxide synthase (NOS) (Melillo et al., 1995), platelet-derived growth factor (PDGF) (Kuwabara et al., 1995) and basic and acidic fibroblastic growth factors (bFGF and aFGF) (Kuwabara et al., 1995).

VEGF increases vessel permeability (Bates & Curry, 1996; Senger et al., 1986; Yuan et al., 1996) and induces endothelial cell migration and proliferation in conjunction with Ang-2 (Maisonpierre et al., 1997). Endothelial sprouts are then formed that develop into blind-ending tubes and anastomose to form vascular loops (Jain, 2003).

In normal development, the nascent vascular network is then pruned and remodelled to match the metabolic requirements of the tissue: hyperoxia decreases VEGF levels and induces vessel regression whereas hypoxia increases VEGF levels and induces vessel growth (Alon et al., 1995; Benjamin et al., 1999; Benjamin et al., 1998). Vascular remodelling may also occur by the insertion of tissue pillars that then become septa and divide the vessel - 'intussusceptive microvascular growth' (Djonov et al., 2001; Djonov et al., 2000; Patan et al., 1996). Vessels then undergo a process of maturation and stabilisation in which they acquire mural cells (smooth muscle cells in the case of arteries and veins and pericytes in the case of capillaries), a basement membrane and extracellular matrix (Carmeliet, 2000; Jain, 2003) - see **Figure 1.1.** Studies using knockout mice have shown that Angiopoietin-1 (Ang-1), its tyrosine kinase receptor Tie-2, PDGF-B and its receptor PDGFR-β are important factors for vessel maturation (Hellstrom et al., 2001; Lindahl et al., 1997; Patan, 1998; Suri et al., 1996). (Ang-1 and Ang-2 are counteracting ligands for the Tie-2 receptor (Hawighorst et al., 2002)). Transforming growth factor-beta1 (TGF-β_1) also has a role in vessel maturation as it can promote the expression of genes associated with matrix formation and smooth muscle cell differentiation (Chambers et al., 2003).

It is this association of new vessels with mural cells that appears to mark the end of growth factor dependence (Benjamin et al., 1998) and cessation of vessel growth (Crocker et al., 1970), thus 'stabilising' the vessel. *In vitro* studies have shown that pericytes in contact with endothelial cells can inhibit their proliferation (Orlidge & D'Amore, 1987), probably by local activation of TGF-β (Wakui et al., 1997).

Apart from the examples of physiological angiogenesis discussed above, the mature adult vasculature is stable and quiescent. In contrast, the presence of high levels of pro-angiogenic factors in tumours (Grunstein et al., 1999; Hawighorst et al., 2002; Holash et al., 1999; Plate et al., 1992) results in on-going angiogenesis and the persistence of immature vessels.

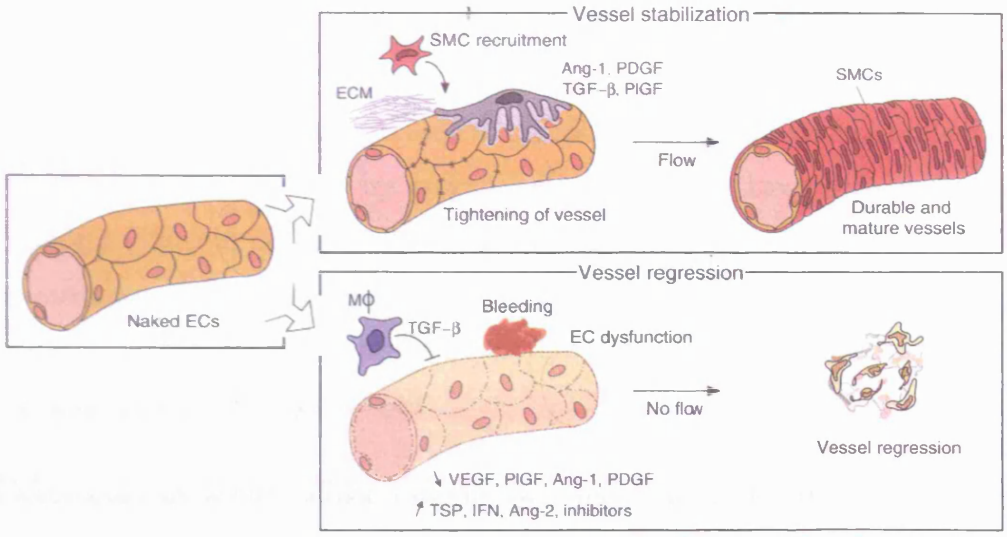

Figure 1.1: Process of vessel maturation, from (Carmeliet, 2003). EC: endothelial cell; ECM: extracellular matrix; SMC: smooth muscle cell; MΦ: macrophage; PlGF: placental growth factor (a VEGF-related protein); TSP: thrombospondin; IFN: interferon; other abbreviations as in text.

1.1.1.1 Other mechanisms involved in tumour vasculature development

There are other processes besides angiogenesis that may contribute to the development of tumour vasculature.

Circulating endothelial precursor cells may be recruited to sites of neovascularisation where they differentiate in-situ into mature endothelial cells, a process termed 'vasculogenesis' (Asahara et al., 1999).

The co-option of normal host vessels has been observed in tumours growing in lung and liver, both of which are very well-vascularised organs. In a subset of non-small cell lung carcinoma (NSCLC) specimens, an 'alveolar' pattern was observed, characterised by a lack of parenchymal destruction and the absence of both tumour-associated stroma and new vessels. Instead, neoplastic cells filled up the alveoli and the only vessels present appeared to belong to the trapped alveolar septa (Offersen et al., 2001; Passalidou et al., 2002; Pezzella et al., 1997). Similarly, a 'replacement growth' pattern has been observed in liver metastases of colorectal and breast origin in which tumour cells replaced hepatocytes and co-opted the sinusoidal blood vessels between liver plates (Stessels et al., 2004; Vermeulen et al., 2001).

Experiments in a rat glioma model suggest that even angiogenic tumours may initially co-opt normal host blood vessels (Holash et al., 1999; Yancopoulos et al., 2000). The co-opted host vessels were observed to regress, causing tumour necrosis, but successful

tumours were able to initiate angiogenesis and so survive (Holash et al., 1999; Yancopoulos et al., 2000).

'Vasculogenic mimicry' is a term used to describe the presence within tumours of vascular channels that are not lined by endothelial cells. These have been described in both melanoma (Maniotis et al., 1999) and breast carcinoma (Shirakawa et al., 2002). However, the existence of vasculogenic mimicry is controversial and McDonald et al. (McDonald et al., 2000) comment that extravasated erythrocytes in the extracellular matrix could be misinterpreted as vascular channels.

If a tumour can develop a blood supply using mechanisms that do not involve endothelial cell proliferation, then specific anti-angiogenic therapies may be ineffective. How significant a problem this may be is not known.

1.1.2 Morphology of tumour vasculature

Once established, tumour vasculature is both structurally and functionally abnormal. Common features seen in solid tumours include plexuses of wide venules and sinusoidal capillaries of varying diameter with numerous blind endings (Konerding et al., 1995). Avascular and poorly vascularised regions are prevalent throughout tumours (Konerding et al., 1999; Less et al., 1991) and up to 20-fold more tumour cells are dependent on each vessel for nutritive support than are cells in normal tissue (gut) (Konerding et al., 1999). The pattern of tumour vasculature that develops is dependent on tumour location, its biological features and the pre-existing vascular bed (Konerding et al., 1995).

Ultrastructural studies have observed the presence of wide interendothelial junctions, fenestrae, transendothelial channels formed by vesicles, and discontinuous or absent basal lamina in a significant fraction of tumour vessels (Hashizume et al., 2000; Jain, 1987a). Tumour vascular permeability is significantly higher than that of skin or muscle (Dvorak et al., 1988; Jain, 1987a; Sevick & Jain, 1991) and the degree of tumour vessel permeability is dependent on tumour type and host organ (Fukumura et al., 1997; Hobbs et al., 1998) and on VEGF (Yuan et al., 1996).

It is not clear whether tumours contain lymphatic vessels as they are difficult to identify definitively and specific markers are lacking (Jain & Fenton, 2002). However, most

evidence suggests that functional lymphatics are absent from tumours (Leu et al., 2000; Padera et al., 2002).

Tumour vessels may lack protective mechanisms such as mural cells and a basement membrane. Even if mural cells are present, they may not be functionally normal: Morikawa et al. observed abnormalities in pericyte shape and abnormal separations between αSMA[1] and CD31-positive cells on tumour vessels, indicating that pericytes were only loosely associated with endothelium (Morikawa et al., 2002).

Tumour vessels may not always have an intact endothelial cell lining. 'Mosaic' vessels have been observed that have focal regions where tumour cells appeared to be in contact with the vessel lumen (Chang et al., 2000; Hammersen et al., 1985). However, endothelial cells can be very thin, so might not be apparent in thin histological sections.

1.1.3 Consequences of the structural and functional abnormalities of tumour vasculature

As a consequence of the structural and functional abnormalities of tumour vasculature, tumour blood flow is both spatially and temporally heterogeneous (Endrich et al., 1979; Leunig et al., 1992; Tozer et al., 1990; Vaupel et al., 1989). Many solid tumours contain hypoxic regions and tumours are also more hypoxic than typical normal tissues (Adam et al., 1999; Cerniglia et al., 1997; Chaplin et al., 1998a; Martin et al., 1993; Moulder & Rockwell, 1984; Vaupel & Höckel, 1998). The degree of hypoxia depends on oxygen consumption rate as well as oxygen supply (blood flow) and will be dictated by flow through individual vessels as well as the distance between vessels. Interruption in blood supply due to transient vessel shutdown leads to 'acute' hypoxia (Brown, 1979; Chaplin et al., 1987) whereas 'chronic' hypoxia is dependent on a tumour cell's distance from the nearest blood vessel (Thomlinson & Gray, 1955).

Tumours have a lower extracellular pH than normal tissues (Wike-Hooley et al., 1984). The mechanism is thought to be increased lactic acid production due to aerobic and anaerobic glycolysis in tumour cells (Wike-Hooley et al., 1984). However, glycolysis-deficient tumours still have a low pH, so production of other acids such as carbon dioxide may also contribute to a shift to acidic pH (Newell et al., 1993).

---

[1] αSMA: alpha smooth muscle actin, used to stain smooth muscle cells and pericytes. CD31 antigen: pan-endothelial marker. **See Section 1.3.**

Tumours are characterised by an elevated interstitial fluid pressure (IFP), compared to normal tissues (Jain, 1987b; Leunig et al., 1992; Netti et al., 1996; Znati et al., 1996). IFP is higher in the centre of a tumour and approaches normal physiological pressure towards the periphery (Boucher et al., 1990; Boucher et al., 1996). Tumour interstitial hypertension is presumably due to the proliferation of tumour cells within a confined area, high vascular permeability and the possible absence of functional lymphatics (see above) (Jain, 1987a) and is a cause of reduced tumour blood flow (Milosevic et al., 1999).

1.1.4 Implications for anti-cancer treatment

Drug delivery to tumours will be compromised by an inadequate, heterogeneous blood supply. In addition, the presence of high IFP inhibits extravasation of macromolecules into the extravascular space (Jain, 1988; Jain, 1989).

Tumour response to treatment with both chemotherapy and radiotherapy will also be compromised. Hypoxic cells are more radioresistant than oxic cells (Gray et al., 1953). They are also non-proliferating and so protected against DNA-damaging treatments (Chaplin et al., 1998a). It has also been shown that hypoxia can select for a more aggressive, pro-angiogenic phenotype (Brizel et al., 1996; Hockel et al., 1999; Rofstad & Danielsen, 1999), probably by selecting for resistance to apoptosis and by inducing pro-angiogenic growth factors (Graeber et al., 1996; Zhang & Hill, 2004).

1.2 Tumour microcirculation as a therapeutic target

The dependency of solid tumours on a functional blood supply makes targeting the tumour microcirculation an attractive proposition. The theoretical advantages of this strategy are:

1. tumour vasculature is accessible to blood-borne agents;

2. treatment-resistant mutations are unlikely to emerge as tumour endothelial cells are non-transformed;

3. angiogenesis occurs in very limited circumstances in adults so targeting specific receptors on proliferating tumour endothelium is potentially safe;

4. each capillary supplies hundreds of tumour cells, potentiating the anti-tumour effect.

In reality, treatment-resistant mutations may emerge (Kerbel et al., 2001) and clinical trials have shown that vascular-targeted therapies are not without toxicity (see below).

Differences between tumour and normal vessels that could be exploited include: increased endothelial cell proliferation rate, ~20-35 times that seen in normal vessels (Denekamp, 1982; Denekamp & Hobson, 1982; Eberhard et al., 2000; Hobson & Denekamp, 1984); increased permeability (Dvorak et al., 1988); the presence of immature vessels (Eberhard et al., 2000); and abnormal vessel structure (Jain, 1988; Konerding et al., 1999). Also, gene transcripts have been identified that are expressed predominantly by tumour endothelium that could be potential targets for antibody or gene-directed therapies (St Croix et al., 2000).

Tumour microcirculation may be targeted either by inhibition of the developing neovasculature (anti-angiogenic strategies) (Folkman, 1971) or by damaging the established vasculature causing blood vessel shutdown (vascular disruptive strategies) (Denekamp, 1982). There is potential overlap between the effects of individual agents, but for the purpose of description it is easier to divide them into these two categories, depending on the aims of the treatment.

Anti-angiogenic strategies include the development of inhibitors of growth factors such as VEGF and its receptors, matrix metalloproteinase inhibitors and agents that inhibit

endothelial cells directly such as thalidomide and endostatin (Fox et al., 2001; Los & Voest, 2001).

The aim of vascular disruptive strategies is to cause a rapid and extensive shutdown of tumour blood flow in the established tumour vasculature, leading to secondary tumour cell death (Tozer et al., 2002). Denekamp et al. (Denekamp et al., 1983) found that vascular occlusion, induced by clamping the base of subcutaneous tumours for 15-24 hours, caused early and extensive tumour necrosis in an animal model. This pattern of cell death is indicative of vascular-mediated tumour cell kill (Tozer et al., 2002).

There are several different types of vascular disruptive therapies:

1. Small molecule vascular disruptive agents. These are not specifically targeted to tumour endothelium but can exploit the differences between tumour and normal tissue endothelium, producing selective vascular damage in tumour tissue.

2. Ligand-directed approaches that involve the selective targeting of tumour endothelial cells using specific antibodies or peptides.

3. Physical methods. These include hyperthermia, tumour embolisation and photodynamic therapy.

4. Gene-based approaches. In theory, gene-directed vascular-targeted therapies should be effective, but as yet there are no promising candidates.

1.2.1 Small molecule vascular disruptive agents

Low molecular weight drugs with vascular disruptive activity can be divided into two main groups: tubulin-depolymerising agents (e.g. combretastatin A4-phosphate – CA-4-P) and cytokine inducers (e.g. 3,4-dimethylxanthenone-acetic acid - DMXAA) – see **Table 1.1.** **Figure 1.2** shows the chemical structures of some of these compounds.

1.2.1.1 Tubulin-depolymerising agents: background

Tubulin is an essential component of the eukaryotic cell cytoskeleton. The cytoskeleton provides physical support for maintenance of cell shape, cell motility and also the infrastructure for the movement of organelles within the cell and for signal transduction pathways. It comprises three principal types of protein filaments: actin filaments,

microtubules made of tubulin and intermediate filaments made of vimentin and other proteins (Alberts et al., 1989).

Actin filaments form cross-linked networks and small bundles in the peripheral cytoplasm and give mechanical strength to the cell surface, allowing shape change and movement. Microtubules are formed from tubulin heterodimers consisting of α and β tubulin, which polymerise into long filaments that radiate from near the nucleus throughout the cytoplasm, forming a system of fibres along which organelles can travel (Alberts et al., 1989). Microtubules, and their associated proteins, are required for mitotic spindle formation and so are essential components of mitosis (Jordan et al., 1998).

Small molecule vascular disruptive agents
Tubulin Binding agents
CA-4-P (Oxi 2021)
CA-1-P (Oxi 4503)
ZD 6126 – phosphate prodrug of N-acetylcolchinol
AVE8062 – CA-4-P analogue, formerly AC-7700
Auristatin–PE (TZT-1027) – synthetic derivative of dolastatin 10
NPI-2358
MN-029
Cytokines or cytokine inducers
TNFα
FAA
DMXAA
Ligand-directed approaches
Agents causing direct vascular damage
Exherin
Agents inducing coagulation
Alphastatin
Tissue factor fusion proteins
Fusion proteins including toxins, anti-cytotoxics or radioisotopes
VEGF linked to diphtheria toxin
VEGF linked to gelonin
TES-23
^{111}Indium-anti-PSMA antibody
Agents directed against extracellular matrix
TNFα linked to fibronectin-isoform antibody

Table 1.1: Small molecule and ligand-based vascular disruptive agents in clinical or pre-clinical development (see text).

The vinca alkaloids are tubulin-depolymerising agents that are used clinically for cytotoxic chemotherapy (Jordan et al., 1998; Wang et al., 2000). Their cytotoxic activity is due primarily to their anti-mitotic action: they inhibit spindle formation, causing mitotic arrest

and subsequent cell death. The taxanes are another group of cytotoxic agents that inhibit spindle formation by binding to tubulin but they act by stabilising tubulin rather than by inducing depolymerisation (Jordan et al., 1998; Wang et al., 2000).

Tubulin-depolymerising agents also have vascular disruptive activity. However, the early agents studied (colchicine and the vinca alkaloids) were only found to have vascular disruptive effects at close to the maximum tolerated dose (MTD) (Baguley et al., 1991; Boyland & Boyland, 1937; Hill et al., 1993; Hill et al., 1995). Combretastatin A-4 (CA-4) was the first small molecule agent to be developed that had significant vascular disruptive effects at a tolerable dose in animal models (Dark et al., 1997).

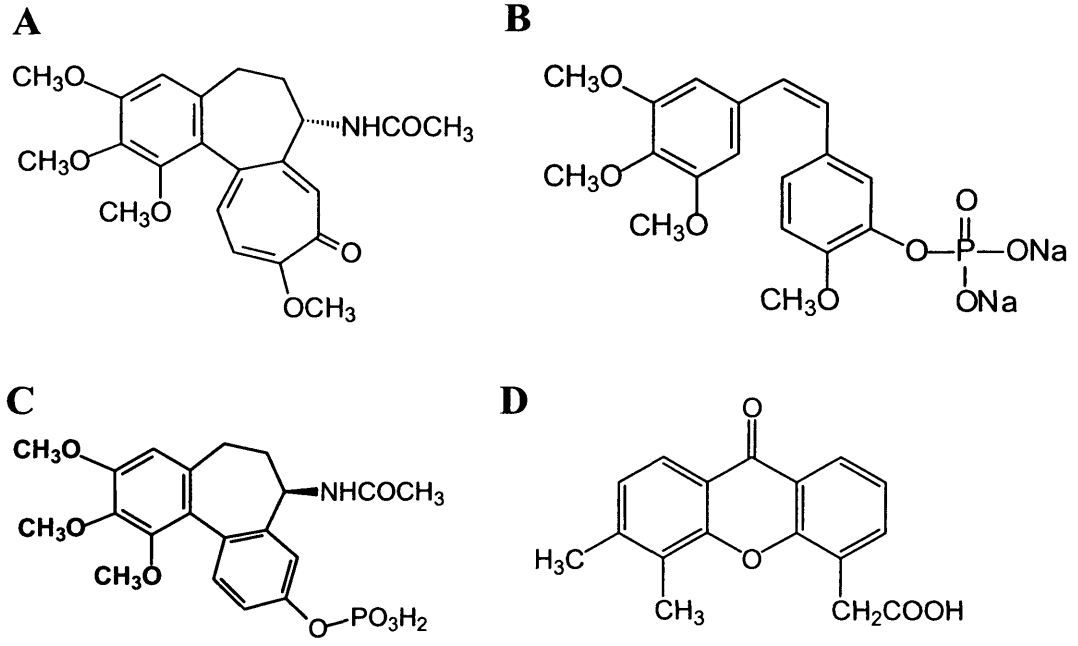

Figure 1.2: Chemical structure of **A**: colchicine; **B**: CA-4-P; **C**: ZD6126; **D**: DMXAA

1.2.1.2 Combretastatin A-4-Phosphate (CA-4-P)

The combretastatins were isolated from the African bush willow, *Combretum caffrum*, in the 1980s (Pettit et al., 1982). They are tubulin-depolymerising agents and are structurally related to colchicine, binding to the same site on tubulin (McGown & Fox, 1989). CA-4-P is the water-soluble pro-drug of CA-4 and has vascular disruptive activity at 1/10th of the MTD in mice (Dark et al., 1997). The plasma half-life of CA-4 is 0.86 hours in the rat (after 30 mg.kg^{-1} CA-4-P given intraperitoneally (Prise et al., 2002) and 1.01 hours in the mouse (after 100 mg.kg $^{-1}$ CA-4-P given intraperitoneally) (Dr M.R.L Stratford, written communication, October 1998). Plasma CA-4 half-life is longer in humans (~2-4 hours),

measured following intravenous administration of 6-90 $mg.m^{-2}$ CA-4-P (Dowlati et al., 2002; Rustin et al., 2003b; Stevenson et al., 2003).

CA-4-P (and CA-4) cause a rapid vascular shutdown in animal and human xenograft tumour models, with maximal effect at 3-6 hours - as shown by reduction in either perfused vascular volume, measured using Hoechst 33342 (Chaplin et al., 1999; Dark et al., 1997; Grosios et al., 1999), or tumour blood flow (^{125}iodoantipyrine (^{125}IAP) method) (Prise et al., 2002; Tozer et al., 1999) or fraction of cardiac output (^{86}RbCl method) (Chaplin et al., 1999; Murata et al., 2001a; Murata et al., 2001c) (see **Section 1.4**). Reduction in tumour blood flow is associated with an increase in vascular resistance (Tozer et al., 1999) and an increase in vascular permeability (Tozer et al., 2001). The consequence of blood vessel shutdown is tumour cell death, and extensive central haemorrhagic necrosis is seen at 24 hours following administration of CA-4-P at 100 $mg.kg^{-1}$ in the mouse (Bohle et al., 2000; Dark et al., 1997; Grosios et al., 1999).

In comparison, CA-4-P has little or no effect on blood flow in most normal tissues (Chaplin et al., 1999; Murata et al., 2001a; Tozer et al., 1999). For example, a ~100-fold reduction in tumour blood flow was observed at 6 hours following treatment with 100 $mg.kg^{-1}$ CA-4-P in the P22 rat carcinosarcoma, whereas there was only a 7-fold reduction in blood flow in the spleen, the most responsive normal tissue (Tozer et al., 1999). No histological changes were found in normal tissues at 24 hours following CA-4-P administration (Prise et al., 2002).

The use of MR techniques to assess the acute vascular disruptive effects of CA-4-P (and other small molecule vascular disruptive agents) is discussed in **Section 1.5.5.**

In vitro, CA-4-P leads to rapid reorganisation of the cytoskeleton of endothelial cells and changes in their morphology and function. Incubation of human umbilical endothelial cells (HUVECs) with CA-4-P results in complete depolymerisation and disruption of microtubules within 30 minutes and, in parallel, reorganisation of the actin cytoskeleton into stress fibres associated with focal adhesions (Grosios et al., 1999; Kanthou & Tozer, 2002). The cells contract and inter-cellular gaps appear if cells are grown in monolayers. In addition, a proportion of cells round up and form numerous surface blebs lined with actin (Kanthou & Tozer, 2002). CA-4-P causes the rapid phosphorylation of myosin light chains (Kanthou & Tozer, 2002), which is required for activation of actin-myosin

interactions and leads to increased contractility and stress fibre formation (van Nieuw Amerongen & van Hinsbergh, 2001). The small GTPase, Rho, and the associated Rho kinase, are responsible for actin reorganisation into stress fibres and actin-myosin mediated contraction in a variety of non-smooth muscle cell systems, including endothelial cells (van Nieuw Amerongen & van Hinsbergh, 2001). The changes in actin reorganisation in response to CA-4-P in endothelial cells were found to be mediated via the activation of this Rho pathway since they could be blocked with inhibitors of Rho and Rho kinase (Kanthou & Tozer, 2002).

These effects on the cytoskeleton and cell morphology are paralleled by changes in endothelial cell function (Galbraith et al., 2001; Kanthou & Tozer, 2002). CA-4-P increases the permeability of endothelial monolayers to macromolecules, which can also be blocked by inhibitors of Rho/Rho kinase, suggesting that morphological changes are associated with important functional changes, *in vitro* (Kanthou & Tozer, 2002). If similar changes occurred *in vivo*, then this could explain the increases seen in tumour vascular resistance (due to rounding up and blebbing of endothelial cells), vascular permeability (causing oedema and an increase in interstitial fluid pressure), coagulation and rheological changes at slightly later times and the resultant vascular collapse (Chaplin & Hill, 2002; Prise et al., 2002; Tozer et al., 2002) – see **Figure 1.3**.

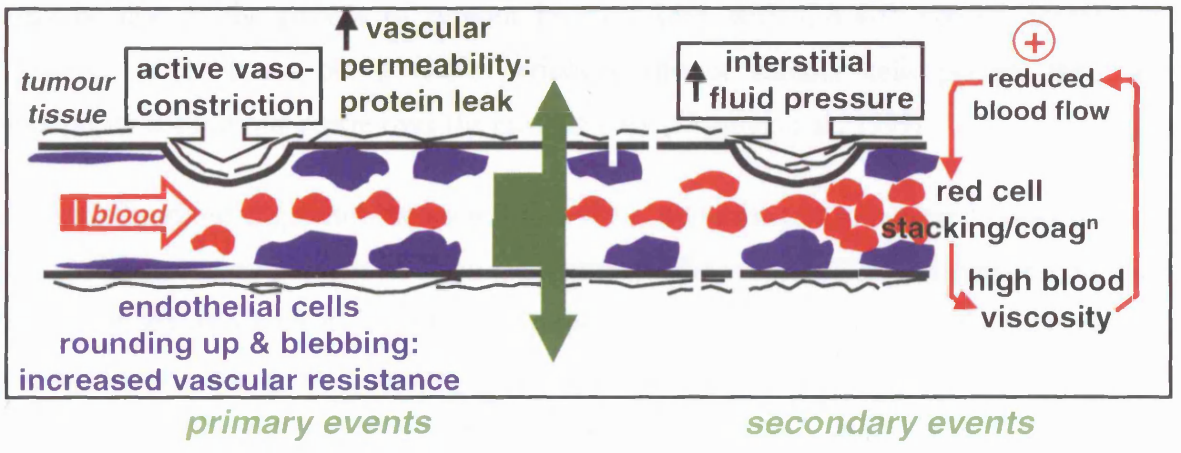

Figure 1.3: Summary of the proposed mechanism of action of CA-4-P, (Tozer et al., 2002).

CA-4-P also has direct cytotoxic effects on endothelial cells *in vitro* and is selective for proliferating cells (Dark et al., 1997). Tumour cell lines are also sensitive to CA-4-P to variable degrees (Ahmed et al., 2003) and C Kanthou, personal communication. CA-4-P is thought to primarily kill proliferating cells in mitosis – by causing spindle malformation and

nuclear DNA damage leading to cell cycle arrest in the G2/M phase of the cell cycle. It is thought that cell death then occurs via mechanisms that share characteristics with apoptosis (Kanthou et al., 2004). *In vitro* cytotoxic effects are only observed after lengthy drug exposures. For example, apoptotic changes in endothelial cells start to appear after 2-4 hours drug exposure, reaching significance at 8 hours (Kanthou et al., 2004). Therefore, considering the plasma half-life of CA-4, it is not certain how relevant these changes are *in vivo*.

However, cytotoxic effects may be relevant with administration schedules using repeated doses of CA-4-P (Tozer et al., 2002), which are much more effective (Hill et al., 2002a). CA-4-P also has anti-angiogenic effects as it can inhibit endothelial cell migration and sprout formation at non-cytotoxic doses (Ahmed et al., 2003).

Single doses of CA-4-P can kill substantial numbers of tumours cells: 100 $mg.kg^{-1}$ CA-4-P induced 1.5 log cell kill and 500 $mg.kg^{-1}$ CA-4-P induced >3 log cell kill in the CaNT tumour grown in mice (Chaplin & Hill, 2002). However, single doses of CA-4-P produce either no or only modest growth delays (Chaplin & Hill, 2002; Chaplin et al., 1999; Grosios et al., 1999; Hill et al., 2002a). In comparison, the cytotoxic agents, cisplatin and 5-fluorouracil (given at half-MTD), and also radiation produce similar or less log cell kill in the CaNT tumour but do induce growth delay (Chaplin & Hill, 2002). This discrepancy may be due to the pattern of tumour necrosis seen with CA-4-P: central necrosis is observed at 24 hours but a viable peripheral rim of tumour cells persists that can repopulate the tumour centre over the ensuing days (Chaplin et al., 1999).

Improved tumour responses are seen if CA-4-P is administered in repeated doses (Hill et al., 2002a) or as a continuous infusion (Malcontenti-Wilson et al., 2001). Improved tumour responses are also seen if CA-4-P is administered in combination with other anti-cancer therapies: cytotoxic agents (Chaplin et al., 1999; Grosios et al., 2000; Siemann et al., 2002); radiotherapy (Chaplin et al., 1999; Horsman & Murata, 2002; Li et al., 1998; Murata et al., 2001c); radioimmunotherapy (Pedley et al., 2001) and hyperthermia (Eikesdal et al., 2001; Horsman & Murata, 2002). When used in combination with radioimmunotherapy, CA-4-P has the additional benefit of increasing antibody retention in tumour (Pedley et al., 2001) (see **Chapter 3**).

Three phase I trials of CA-4-P have now been completed (Anderson et al., 2003; Dowlati et al., 2002; Galbraith et al., 2003; Rustin et al., 2003b; Stevenson et al., 2003). In the majority of patients, CA-4-P was well-tolerated with the most common side effects being cardiovascular in origin (tachycardia and hypertension – mostly grade 1[2]) and tumour pain. However, 2 patients developed cardiac ischaemia. Phase I/II trials in combination with cytotoxic agents, radiotherapy and radioimmunotherapy are now underway, with exclusion of patients at risk of ischaemic heart disease.

1.2.1.3 Other tubulin-depolymerising agents with vascular disruptive activity

ZD6126, is a water-soluble phosphate pro-drug that is converted *in vivo* into N-acetylcolchinol. N-acetylcolchinol binds reversibly to the colchicine-binding site on tubulin and has vascular disruptive activity. ZD6126 induces endothelial shape changes *in vitro* in a similar manner to CA-4-P (Davis et al., 2002; Micheletti et al., 2003). Acute blood vessel shutdown and haemorrhagic necrosis are seen *in vivo* with doses of ZD6126 up to 30-fold lower than the MTD (Davis et al., 2002). Tumour growth delay is seen with ZD6126 in combination with cytotoxic agents but not as on its own in single doses (Davis et al., 2002; Siemann & Rojiani, 2002). ZD6126 is now in early clinical trials (Evelhoch et al., 2002; Evelhoch et al., 2004; Gadgeel et al., 2002).

Other tubulin-depolymerising agents that are undergoing evaluation include: CA-1-P (Oxi 4503), a close structural analogue of CA-4-P (Hill et al., 2002b; Holwell et al., 2002); AVE8062 (formerly AC-7700), a synthetic combretastatin analogue (Nihei et al., 1999); Auristatin-PE (TZT-1027), a synthetic derivative of Dolastatin (Otani et al., 2000); NPI-2358 (Palladino et al., 2004) and MN-029 (McCreedy et al., 2004).

1.2.1.4 Small molecule cytokine inducers

DMXAA is a synthetic flavonoid with vascular disruptive activity. How it causes vascular damage is not known but is thought to involve both direct effects on tumour endothelial cells (Ching et al., 2002; Ching et al., 2004) and indirect effects via the release of cytokines, such as tumour necrosis factor-alpha (TNFα) and interferon-alpha (IFNα), and vasoactive agents such as 5HT (serotonin) and nitric oxide (Baguley, 2003; Baguley & Ching, 2002; Baguley et al., 1997; Cao et al., 2001; Thomsen et al., 1991).

[2] Radiation Therapy Oncology Group (RTOG) toxicity criteria: grade 1 is transient and asymptomatic, no treatment required.

DMXAA is a synthetic analogue of flavone acetic acid (FAA), which has vascular disruptive activity in experimental tumours (Bibby et al., 1989) but not in humans (Kaye et al., 1990; Kerr et al., 1989). The lack of clinical activity of FAA is thought to be due to species difference in response. Whereas DMXAA up-regulates TNFα mRNA in both human and murine monocyte/macrophage lineage cells, FAA had activity in murine cells only (Ching et al., 1994) and increases TNFα levels in mouse but not in human plasma (Chabot et al., 1993).

DMXAA has completed phase I trials (Galbraith et al., 2002; Jameson et al., 2003; Rustin et al., 2003a) and is now entering phase II trials, in combination with other therapies. As with CA-4-P, improved tumour responses have been seen in animal models in combination with other anti-cancer therapies (Horsman & Murata, 2002; Murata et al., 2001b; Pedley et al., 1996; Pedley et al., 1999; Siemann et al., 2002; Siim et al., 2003).

TNFα has also been investigated as an anti-cancer agent. It induces tumour regression in animal models, which is at least partially mediated by selective damage to tumour vasculature (Kallinowski et al., 1989). Systemic administration of TNFα is toxic clinically (Lejeune et al., 1998) but regional administration (via isolated limb perfusion) can be tolerated and produces tumour responses – for example, as a neoadjuvant treatment in combination with interferon-γ and melphalan for patients with extremity sarcomas (Eggermont et al., 1996).

1.2.2 Ligand-based therapies

Ligand-based therapies can be designed to expressly bind to targets on the tumour vasculature: either to cause acute vascular damage directly or to deliver cytotoxic agents, toxins or radio-isotopes to the tumour (Thorpe, 2004) (**Table 1.1**).

Novel tumour endothelium-specific targets can be identified by screening endothelial and non-endothelial cell libraries using expressed sequence tags (Huminiecki & Bicknell, 2000) or by identifying mRNA transcripts from purified endothelial cells (St Croix et al., 2000). Alternatively, specific monoclonal antibodies can be generated in mice by injecting tumour endothelial cells (Huang et al., 1997; Tsunoda et al., 1999) or *in vivo* screening of phage-display libraries can be used to identify specific markers that bind to tumour endothelium (Arap et al., 1998; Pasqualini & Ruoslahti, 1996).

Burrows & Thorpe created an animal model to test the vascular targeting approach (Burrows & Thorpe, 1993). Firstly, a major histocompatibility complex (MHC) class II antigen was induced on tumour endothelium by the transfection of neuroblastoma cells with a retrovirus containing the interferon-γ gene. Then, a fusion protein comprising the toxin, ricin, and an anti-MHC class II antigen antibody was administered. The fusion protein localised to tumour endothelial cells and induced haemorrhagic necrosis and tumour regression.

Since then, other ligand-based therapies have been developed that might potentially be translated into clinical practice. The N-cadherin antagonist, Exherin, is an example of a ligand-based approach that causes direct vascular damage (Lepekhin et al., 2003). N-cadherin is a cell adhesion molecule that holds together and stabilises endothelial cells. Exherin mimics the N-cadherin active site, preventing N-cadherin binding. Administration of Exherin caused tumour blood vessel rupture within 60 minutes of injection in a range of animal models (Lepekhin et al., 2003) It is thought to be selective for tumour vessels specifically as they lack the full support structures found in normal blood vessels.

Another approach is to selectively initiate coagulation within tumour vessels, thus inducing thrombosis and subsequent tumour necrosis. Fibrinogen E (FgnE) is a proteolytic fragment of the blood clotting protein, fibrinogen, that causes selective vascular damage in tumours (Brown et al., 2002). The peptide, alphastatin (constructed from the first 24 amino-acids of the alpha chain of human fibrinogen) produces similar results (Staton et al., 2004), although it is not clear why either FgnE or alphastatin are selective for tumour vasculature. Selective vascular damage can also be induced by the administration of fusion proteins comprising tissue factor and a tumour endothelium-specific element (Hu et al., 2003; Huang et al., 1997). Tissue factor is a cell membrane receptor protein that is the initiator of the extrinsic pathway of the coagulation cascade (Hu et al., 2003). A truncated version of tissue factor is used that is only activated when brought into contact with tumour endothelium.

Examples of fusion proteins comprising a tumour-endothelium selective agent and a toxin or cytotoxic agent include: VEGF fused to a truncated form of diphtheria toxin (Olson et al., 1997); VEGF fused to the plant toxin, gelonin (Veenendaal et al., 2002); and TES-23 (a specific anti-tumour endothelium antibody) fused to neocarzinostatin, an anti-tumour antibiotic (Tsunoda et al., 1999).

It is also possible to target radio-isotopes to tumour endothelium. Prostate specific membrane antigen (PSMA), normally expressed on prostate epithelial cells, is also expressed on the endothelium of several non-prostatic solid tumours (Chang et al., 1999a; Chang et al., 1999b). An ^{111}Indium-labelled anti-PSMA monoclonal antibody is now in a phase I trial (Nanus et al., 2003).

Tumour extracellular matrix components may be targeted instead of endothelium. Borsi et al. (Borsi et al., 2003) constructed a fusion protein composed of TNFα and an antibody to a particular fibronectin isoform (containing the extradomain B) that is a marker for angiogenesis (Tarli et al., 1999). The fusion protein accumulated in tumour neovasculature in tumour-bearing mice and induced haemorrhagic necrosis and tumour regression (Borsi et al., 2003).

1.2.3 Other vascular disruptive strategies

1.2.3.1 Physical methods

Photodynamic therapy (PDT) uses a photosensitising drug that is activated by exposure to light of a specific wavelength (Hopper, 2000). The photosensitiser is injected intravenously and the tumour site illuminated using a laser. The activated photosensitiser reacts with molecular oxygen to produce short-lived reactive oxygen species that are highly cytotoxic, causing cell kill within a narrow radius (<0.02 μm).

PDT has a vascular disruptive effect as well as causing direct tumour cell kill. It is cytotoxic for tumour endothelial and vascular smooth muscle cells, inducing apoptosis (Engbrecht et al., 1999; Wyld et al., 1997; Wyld et al., 2001) and can induce blood vessel shutdown in experimental tumours (Dolmans et al., 2002; Engbrecht et al., 1999; Gross et al., 2003; van Geel et al., 1996).

The photosensitisers, photofrin, a porphyrin derivative, and aminolaevulinic acid, which is metabolised into protoporphyrin IX, are both licensed for clinical use (Hopper, 2000). In practice, PDT is limited to superficial lesions, e.g. basal cell carcinoma (Wang et al., 2001) or local chest wall recurrences of breast carcinoma (Cuenca et al., 2004) or to endoscopically accessible tumours, e.g. Barrett's oesophagus[3] (Ackroyd et al., 2000).

[3] Barrett's oesphagus is a premalignant condition in which normal squamous mucosa is replaced by metaplastic columnar epithelium.

Hyperthermia, the heating of tumours to high temperatures (43-44 °C), can cause direct vascular damage (Song, 1998). There is selectivity for tumour vessels as normal tissues are able to dissipate heat more efficiently (by increased blood flow). Clinical trials of hyperthermia in combination with radiotherapy have shown increased response rates and even a survival benefit in some tumours (Wust et al., 2002). Tumours are typically heated to at least 43 °C for 60 minutes (Overgaard et al., 1995; Vernon et al., 1996). As with PDT, its application is limited to accessible tumours.

Liver tumours (e.g. primary hepatocellular carcinoma, neuroendocrine tumours or colorectal metastases) can be treated with tumour embolisation (Stuart, 2003). The technique involves insertion of a catheter via the femoral artery into whichever branch of the hepatic artery is supplying the liver segment containing tumour. Gelatin foam or plastic particles are then injected to embolise the tumour. Cytotoxic agents, such as doxorubicin, may be injected concomitantly. The technique can provide good palliation (Stuart, 2003) and has even improved survival in carefully selected patients with hepatocellular carcinoma (Llovet et al., 2002). However, it is an invasive technique with significant toxicity (there is a post-embolisation syndrome of pain, fever and malaise and damage to normal hepatocytes may cause liver dysfunction) that is only applicable to selected patients.

1.2.3.2 Gene therapy

In theory, tumour vasculature is an ideal target for gene therapy as it should be easier to transfect endothelial cells than tumour cells (as they are in direct contact with blood) and transfection of only a limited proportion of endothelial cells would be necessary for vessel damage (Chaplin & Dougherty, 1999).

The objective is usually to transfect target cells with a retroviral or adenoviral vector and then to administer an agent that will only have activity in the transfected cells, resulting in selective damage. Mavria and Porter have developed an experimental model system that provides proof of principle for this strategy (Mavria & Porter, 2001). Tumour vasculature was transfected with a retroviral vector containing herpes simplex virus-thymidine kinase (by co-injection of the vector with tumour cells as a subcutaneous xenograft). The pro-drug ganciclovir was then administered, resulting in its selective phosphorylation and subsequent incorporation into DNA in transfected cells, leading to extensive haemorrhagic necrosis and tumour growth delay.

Another example is the *in vitro* transduction of endothelial cells with an adenoviral vector containing a chimeric protein comprising the extra-cellular domain of the VEGF receptor, Flk-1/KDR, and the cytoplasmic domain for Fas (which is involved in the apoptotic pathway). Endothelial cell apoptosis is then triggered by administration of exogenous VEGF (Carpenito et al., 2002).

While direct injection with a viral vector might be feasible for superficial or endoscopically accessible tumours, in general safe systemic administration of gene therapy will be required for translation into clinical practice. Currently vascular disruptive gene therapy strategies are still at the pre-clinical stage.

1.3 Investigation of tumour vessel maturity

Tumours are characterised by the persistence of immature blood vessels due to on-going angiogenesis and high levels of growth factors (see **Section 1.1**).

One indication of vascular maturity is the presence of a smooth muscle cell or pericyte coating, which can be typically identified by alpha-smooth muscle actin (αSMA) or desmin immunohistochemistry (Morikawa et al., 2002). A pan-endothelial marker (e.g. von Willibrand factor (vWF) or CD31 antigen) is used to identify all vessels present in a histological section. A vascular maturation index can then be defined as the percentage of vessels staining positive for αSMA or desmin.

Vascular maturation index = (number of positive staining vessels/total vessels) x100

In one study, the vascular maturation index (using αSMA) for a panel of normal tissues (brain, gut, heart, kidney, liver, lung, skin) was 85-95% but only 60% for the corpus rubrum of the ovary (used as a model of active angiogenesis) (Goede et al., 1998). In contrast, the same index ranged from <10% to >80% in a range of different human tumours (again using αSMA) – see **Figure 1.4** (Eberhard et al., 2000).

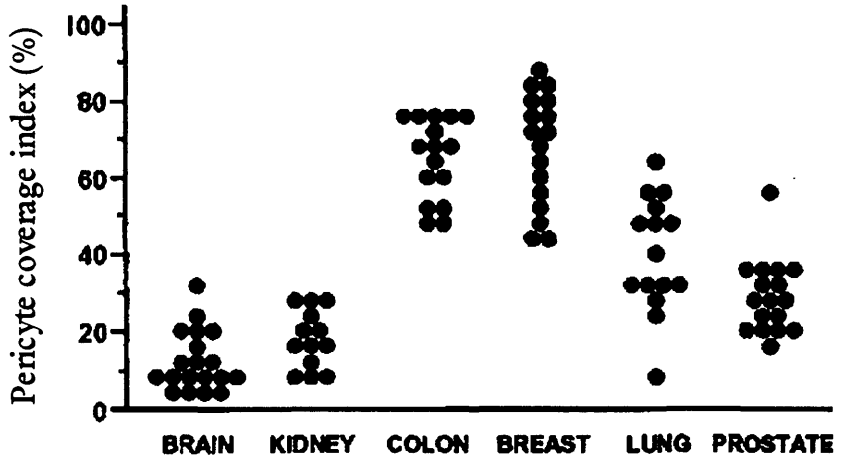

Figure 1.4: Vascular maturation index for different human tumour types from (Eberhard et al., 2000). Vascular maturation index is here termed 'pericyte coverage index'.

LH39 is another histological marker of mature vessels that has been used to obtain a vascular maturation index. It is an anti-basement membrane monoclonal antibody that

localises to mature venules and capillaries but not to newly formed vessels (Passalidou et al., 2002).

This index might be inaccurate if not all pericytes stain positively for αSMA (or desmin) or if partial pericyte coverage is missed in thin histological sections (Morikawa et al., 2002). The former point may not be a problem as Morikawa et al. found that both αSMA and desmin identified pericytes consistently in tumours. However, in normal tissues, capillaries expressed immunoreactivity to desmin but not αSMA (normal tissue arterioles and venules were identified by both markers) (Morikawa et al., 2002).

Evaluation of the proportion of immature vessels within a tumour is pertinent for several reasons. The molecular control of the maturation phase of angiogenesis is only just beginning to be understood (see **Section 1.1**) and has the potential for providing new targets for anti-angiogenesis based cancer therapy. Analysis of vessel wall maturity in tumours is a step towards identifying likely targets for disrupting angiogenesis/vascular function in tumours (Benjamin et al., 1999). Also, knowledge of the extent of tumour vessel immaturity might aid prediction of response to anti-angiogenic agents and might explain differential sensitivity to CA-4-P (and other vascular disruptive agents).

Using neonatal mouse retinal vessels as a model of angiogenesis, it can be shown that VEGF withdrawal leads to regression of capillaries that are not covered by pericytes (i.e. immature vessels) and an increase in vascular maturation index (Benjamin et al., 1998; Goede et al., 1998). An increase in vascular maturation index following VEGF withdrawal has also been demonstrated in tumours: in a mouse glioma model (with a conditional VEGF expression system) and in human prostate cancers (VEGF reduction induced by anti-androgen therapy) (Benjamin et al., 1999). These findings suggest that tumours with a high proportion of mature vessels are unlikely to have a large response to anti-VEGF inhibitors.

It is not known why CA-4-P should be selective for tumour vasculature and why some tumour types are more sensitive than others (Beauregard et al., 2001; Beauregard et al., 2002). However, the relative lack of smooth muscle cell/ pericyte investiture of the vessel walls in tumours is one potential predisposing factor influencing response. For instance, smooth muscle cell/pericyte investiture could confer structural stability to the vessels. In turn, the maturity of the vascular wall will affect its permeability to blood solutes. It has

been shown that sensitivity to CA-4-P, as measured by DCE-MRI, is proportional to the permeability of the vascular wall to macromolecules, across a range of different rodent tumour types (Beauregard et al., 2001).

Our preliminary data has shown that the human adenocarcinoma, HT29, stains well for αSMA, indicating a mature vascular wall, whereas the murine mammary carcinoma, CaNT, stains poorly. This difference may relate to the differential sensitivity to CA-4-P of the HT29 tumour versus CaNT - CaNT being more sensitive (Dr SA Hill – personal communication). The relative lack of sensitivity of the HT29 to CA-4-P has also been confirmed by other authors (Beauregard et al., 2001; Beauregard et al., 2002). Preliminary data investigating fibrosarcomas expressing different single VEGF isoforms has shown that they display a differential sensitivity to CA-4-P that corresponds to their vascular maturation index. Histological vascular maturation index was 30% and 100 % for the $VEGF_{120}$ and the $VEGF_{188}$ expressing fibrosarcomas respectively (Ireson et al., 2004). In a window chamber model, red cell velocity was reduced to ~10-20% of baseline at 3 hours, persistent at 24 hours following CA-4-P administration in the $VEGF_{120}$ fibrosarcoma, whereas red cell velocity was reduced to only 60% of baseline, with recovery by 24 hours following CA-4-P administration in the $VEGF_{188}$ fibrosarcoma (Dr SA Hill – personal communication).

If the maturity index of tumour blood vessels proves to be important for determining vascular response to CA-4-P and similar drugs, it would be useful to develop a non-invasive functional measure of tumour vessel maturation status, with the ultimate aim of translation into the clinic. Whereas a histological vascular maturation index can be obtained using human cancer specimens, it is invasive and its application is limited as an index based on a biopsy may be inaccurate due to tumour heterogeneity and it is often not practical, or indeed possible, to obtain repeat biopsies in order to assess treatment response.

Vessel response to a vasoactive agent is a functional measure that might discriminate between mature and immature tumour vessels. That is, blood vessels with a vascular smooth muscle cell/pericyte coat should be able to vasoconstrict/vasodilate effectively, whereas immature vessels should be less responsive.

Vasoactive agents act by changing blood vessel diameter, altering vascular resistance and hence tumour blood flow rate. Resistance is inversely proportional to the vessel radius raised to the fourth power - so only a small change in vessel diameter is required to have a significant effect on blood flow (Pocock & Richards, 2004).

1.3.1 Use of BOLD-MRI response to vasoactive agents to investigate vessel maturity

Blood Oxygen-Level Dependent magnetic resonance imaging (BOLD-MRI) is sensitive to changes in tumour oxygenation and blood flow and has been used as non-invasive method of monitoring tumour response to hyperoxic gases such as carbogen (95% oxygen (O_2), 5% CO_2) and to vasoactive agents (see **Section 1.5.4**).

1.3.1.1 Carbon dioxide (CO_2)

It has been proposed that BOLD-MRI can be used to non-invasively distinguish mature from immature tumour vessels by their differential response to breathing air-5% CO_2 and carbogen gas (Abramovitch et al., 1999; Neeman et al., 2001). CO_2 is a vasodilator (see below), so mature vessels should vasodilate in response to air-5% CO_2 (because of their well-developed vascular wall) resulting in an increase in tumour blood flow and a positive BOLD response, whereas immature vessels will not respond. The hypothesis is that BOLD-MRI can selectively detect mature vessels by their response to air-5% CO_2, whereas the entire functional vasculature is detected by increased signal change in response to hyperoxia (breathing carbogen) (Neeman et al., 2001).

'Vascular function' and 'vascular maturation' maps of functional and mature vessels respectively may be obtained by identifying voxels showing a significant change in signal intensity when breathing carbogen or air-5% CO_2 compared to air alone (Abramovitch et al., 1999; Neeman et al., 2001). **Figure 1.5** (from Neeman et al., 2001) shows change in signal intensity in response to air-5% CO_2 and carbogen for regions of interest containing mature and immature vessels respectively in a C6 glioma model. The difference in change in signal intensity in response to air-5% CO_2 between these two areas was significant.

Vascular maturation maps obtained by this method have been validated by spatial matching with histological staining with αSMA (Abramovitch et al., 1999; Gilead et al., 2004). (See also the discussion in **Chapter 4**).

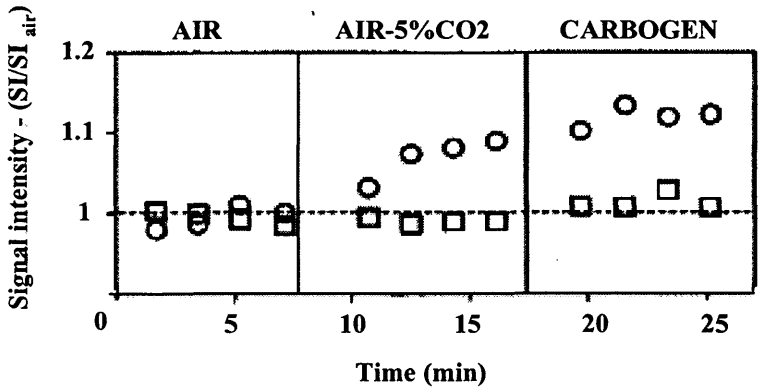

Figure 1.5: Change in MRI signal intensity over time in a region of interest with immature (squares) and mature (circles) vessels, (Neeman et al., 2001).

The rationale for the addition of 5% CO_2 to oxygen to form carbogen gas for tumour radiosensitisation is that CO_2 counteracts the vasoconstrictive influence of pure oxygen (Bird & Telfer, 1965; Du Sault, 1963; Kruuv et al., 1967). In addition, CO_2 is a respiratory stimulant and shifts the oxygen-haemoglobin curve to the right, reducing the affinity of haemoglobin for oxygen and so increasing the amount of free oxygen in the blood (Kruuv et al., 1967).

Evidence for the vasodilatory effects of CO_2 comes from studies of normal tissue vasculature. Studies using an isolated preparation of rat mesenteric small arteries to investigate the vasoactive effects of CO_2 have shown that an increase in CO_2 (from 5% at baseline to 10%) induces initial vasoconstriction then prolonged relaxation (Carr et al., 1993; Nielsen et al., 1991). Relaxation was dependent on an intact endothelium and on the presence of the vasodilator, nitric oxide (Carr et al., 1993). Further confirmation of the importance of nitric oxide comes from Iadecola (Iadecola, 1992) who found that a carbogen-induced increase in cerebral blood flow (as measured by laser Doppler flowmetry in a rat model) was virtually abolished by nitric oxide synthase inhibition.

Investigation of the effect of carbogen on tumour blood flow has produced variable results, with some authors reporting either no change or a decrease in blood flow (or surrogate marker) (**Table 1.2**). Although variation between tumour types may reflect different levels of tumour vessel maturity or a lack of sensitivity of the measurement technique, there is evidence that CO_2 can also act as a vasoconstrictor. In a window chamber model, Dewhirst et al. found that carbogen induced vasoconstriction (non-significant) in normal skin arterioles but vasodilation (again non-significant) in tumour-

feeding arterioles (Dewhirst et al., 1996). Again, using a window chamber model (without implanted tumour), Neeman et al. found that air-5% CO_2 resulted in a small but significant vasoconstriction in skin arterioles but did not affect venules or the neovasculature. This suggests that the mechanism of action of CO_2 may be organ and tumour-specific. As both O_2 and CO_2 can modulate the production of both nitric oxide and endothelin-1, local balance between these factors may be responsible for the different responses seen in tumours (Bell & Chaplin, 1998; Chaplin et al., 1998a; Chaplin et al., 1998b). A study using a P22 tumour tissue-isolated preparation found that tumour vessels failed to vasodilate in response to acetylcholine (which acts primarily via receptor stimulation of endothelial cells to release nitric oxide), suggesting that some tumours are incapable of nitric oxide production (Tozer et al., 1996).

Animal studies			
	Method	**Tumour type**	**Outcome**
(Kruuv et al., 1967).	Thermal circulation index method	C3H spontaneous tumour & S3HBA tumour in mice	Increase in TBF vs air breathing
(Grau et al., 1992)	^{86}RbCl	C3H tumour in mice	No difference in TBF vs air breathing
(Honess & Bleehen, 1995)	^{86}RbCl	RiF tumour in mice	Increase in TBF vs air breathing
(Hill et al., 1998a)	Laser Doppler flowmetry	SaF sarcoma in mice	Decrease in red cell flux
(Lanzen et al., 1998)	Laser Doppler flowmetry	R3230Ac in rat	Variable response
(Hill et al., 1998b)	Laser Doppler flowmetry	HT29 in mice	Increase in red cell flux
(Dunn et al., 1999)	Laser Doppler flowmetry	R3230Ac in rat window chamber	Decrease in red cell flux
(Thews et al., 2002)	Laser Doppler flowmetry	DS sarcoma	Increase in red cell flux
Clinical studies			
(Powell et al., 1996)	Laser Doppler flowmetry	Range of tumour types: 8 patients	No overall change
(Hulshof et al., 1998)	^{99}Tc-HMPAO SPECT (1st pass extraction)	Glioblastoma multiforme 6 patients	No change in tumour to normal brain ratio for perfusion

Table 1.2: Effect of carbogen on tumour blood flow (TBF)

1.3.1.2 Angiotensin II

It is possible that other vasoactive agents might be more appropriate for evaluation in conjunction with BOLD-MRI. It has been observed that tumour vessels are more

responsive to vasoconstrictors than vasodilators, suggesting that tumour vessels are usually in a maximally-vasodilated state (Mattsson et al., 1982), possibly as a result of tissue acidosis and hypoxia (Vaupel et al., 1989).

An ideal agent for clinical use needs to be safe, have had extensive pre-clinical experience, an established mechanism of action in the peripheral vasculature, a quick onset of action (so would have to be in an intravenous formulation or a gas) and a short half-life (of a few minutes).

The vasoconstrictor, angiotensin II (ATII), is a potential candidate for use with BOLD-MRI for the investigation of tumour vessel maturation status. It is an endogenous peripheral vasoconstrictor that is formed by the activation of the renin-angiotensin system. It increases mean arterial blood pressure (MABP) by binding to ATII receptors on vascular smooth muscle cells resulting in vasoconstriction within a few minutes of the start of an intravenous infusion. It has a short half-life, a rapid onset of action (Sato et al., 1995) and no cardiac inotropic or chronotropic effects.

ATII has been proposed as a means of increasing tumour blood flow relative to normal tissues in order to improve the delivery of cytotoxic agents. It is assumed that tumour vessels will either be incapable of response to ATII or respond to a lesser extent than normal tissues, depending on the degree of tumour vessel maturity. ATII has already been tested in clinical trials with no adverse effects (Burke et al., 2001; Goldberg et al., 1991; Hemingway et al., 1992; Noguchi et al., 1988; Sasaki et al., 1985).

The majority of studies have shown that ATII infusion increases tumour blood flow relative to normal tissues in animal models (Burton et al., 1985; Dworkin et al., 1997; Dworkin et al., 1996; Jirtle et al., 1978; Suzuki et al., 1981; Tanda et al., 1991; Tozer & Shaffi, 1993; Trotter et al., 1991) and in patients (Burke et al., 2001). Changes in absolute tumour blood flow in response to ATII will be dependent on the capacity of tumour vessels to vasoconstrict in response, which explains the variable results found. Some studies still report an increase in absolute tumour blood flow in response to ATII (Tanda et al., 1991,Sasaki, 1985 # 1316), but other studies report a decrease (Bell et al., 1996; Dworkin et al., 1997; Jirtle et al., 1978; Tozer & Shaffi, 1993).

The evaluation of BOLD-MRI response to vasoactive agents as a means of assessing tumour vessel maturity is part of the work presented in this thesis (see **Section 1.6**).

1.4 Measurement of tumour blood flow in the laboratory and the clinic

1.4.1 Introduction[4]

Tracer kinetic studies use freely diffusible or intravascular tracers to obtain tissue blood flow from the measurement of tracer concentration in the tissue of interest and in arterial blood over time. In addition, intravital microscopy and laser Doppler flowmetry can be used to obtain endpoints that are related to blood flow: red cell flux and velocity. Some techniques can only be used in animal models whereas others can be used in both animal and clinical studies. **Table 1.3** summarises the main techniques used.

1.4.2 Tracer and contrast agent kinetic techniques

In nuclear medicine studies, a trace amount of an inert radioactive substance, 'tracer', is injected into the blood and then monitored in the tissue of interest. The tracer can also be injected directly into a tissue and then its clearance measured. Tissue concentration is measured from the specific activity of the tracer. Tracer kinetic principles can be adapted for computerised tomography (CT) and magnetic resonance imaging (MRI), in which pharmacological doses of contrast agent are injected intravenously and change in contrast agent concentration measured from the change in signal intensity in image voxels.

For tracer kinetic studies, it is assumed that the physiological system is in a steady state and that blood flow in a tissue of interest is constant. There are three fundamental equations on which almost all tracer kinetic studies are based (Peters, 1998).

$$\frac{Q_t}{dt} = \frac{Q_a}{dt} - \frac{Q_v}{dt} \qquad (1)$$

where Q_t, Q_a and Q_v are the amounts of tracer in tissue, feeding arterioles and draining veins respectively (in mg or MBq for tracer, mmol for radiological contrast agents). This is Fick's principle - that the amount of tracer in an organ or tissue at a given time is equal to the difference between the amount arriving and the amount leaving (or = input rate – output rate) (Kety, 1960a; Kety, 1960b; Peters, 1998).

[4] For tracer studies, blood flow is usually expressed per unit tissue volume or mass ($ml.min^{-1}.ml^{-1}$ or $ml.min^{-1}.g^{-1}$). The term 'perfusion' can also be defined as flow per unit tissue volume or mass. However, in MRI experiments, perfusion is usually defined more generally, describing the process of delivery of arterial blood to a tissue capillary bed (Buxton, 2002) so, to avoid confusion, this latter definition of perfusion will be used.

Method	Technique	What measured?	Clinical use?	Advantages/disadvantages
First pass extraction technique	^{86}RbCl extraction	TBF as fraction of cardiac output or absolute TBF/ unit gram of tissue	No	+: relatively simple; absolute TBF if arterial sampling -: single measurements only
	Doppler Ultrasound: microbubbles	TBF as fraction of cardiac output	Yes	+: serial measurements possible -: limited to accessible tumour s
	SPECT with ^{99m}Tc-HMPAO	TBF as fraction of cardiac output or absolute TBF/ml of tissue	Yes	As for PET, but much better availability
	Dynamic CT	TBF/unit volume of tissue	Yes	+: non-invasive, CT scanners widely available -: complicated modelling/software, radiation dose to patient
Kety model for freely diffusible tracer	^{125}I or ^{14}C-labelled IAP	TBF/unit gram of tissue	No	+:Considered gold standard -: single measurements only
	^{15}O PET	TBF/unit volume of tissue	Yes	+: serial measurements possible, good time resolution -: poor spatial resolution; requires arterial cannulation; radiation dose to patient, limited availability
	DCE-MRI with Gd-DTPA	Transfer constant, K^{trans} is related to TBF and permeability-surface area product	Yes	+: widely available; non-invasive, good spatial resolution; serial measurements. -:complicated modelling, cannot easily separate TBF from permeability-surface area product
	^{133}Xenon clearance	TBF/ unit gram of tissue	Yes	+: quantitative -: superficial tumours only, radiation dose to patient
	Thermal clearance	TBF/ unit gram of tissue	Yes	-: large errors under conditions where thermal conduction is important –e.g. superficial tumours
Bolus tracking technique	DCE-MRI with Gd-DTPA	Relative TBF	Yes	+: non-invasive, serial measurements possible -: complicated modelling, ?accuracy
	Dynamic CT	TBF/unit gram of tissue		As above
Doppler effect	Laser Doppler flowmetry	Red cell flux and velocity	Yes	-: limited to accessible tumours, serial measurements not possible, invasive
	High-frequency Doppler ultrasound	Red cell flux and velocity	Yes	+: non-invasive, serial measurements possible -: superficial tumours only
Direct observation of fluorescently-labelled red cells	Intravital microscopy	Red cell flux and velocity	No	+: direct observation of tumour vessels, serial measurements -: only possible for very small tumours

Table 1.3: Summary of techniques to measure TBF

$$C = \frac{Q}{V_D} \qquad \text{(dilution equation)} \qquad (2)$$

where C is concentration ($mg.ml^{-1}$, $MBq.ml^{-1}$ or $mmol.ml^{-1}$), Q is tracer amount (mg, MBq or mmol), and V_D is the volume of distribution of the tracer (ml) - the fraction of the total tissue volume that the agent can enter.

$$\tau = \frac{V_D}{f} \qquad \text{(transit time equation)} \qquad (3)$$

were τ is time (min^{-1}) and f is blood flow ($ml.min^{-1}$). The transit time equation is based on the central volume principle (Stewart, 1894) and has been proved for tracer kinetic studies by Meier and Zierler (Meier & Zierler, 1954). It is assumed that the distribution of transit times of tracer particles does not change with time; flow of tracer particles represents blood flow; there are no stagnant pools of blood; no recirculation occurs and the tracer is injected instantaneously (Meier & Zierler, 1954).

For tracer studies, parameters are usually expressed per unit gram of tissue. However, for imaging studies they are expressed per unit volume of tissue with units: f (min^{-1}), V_D (dimensionless) and concentration, C ($mmol.ml^{-1}$).

A general expression for tissue tracer concentration can be constructed by adding up the amount of agent delivered by a certain time, weighted by the probability that the agent is still present in the tissue at that time (Buxton, 2002). If the probability that a particle of tracer that entered the tissue at time t′ is still present at time t is r(t- t′) (the 'residue function'), then the number of tracer particles entering in between t′ and t′ + dt is $fC_a(t')dt'$, where C_a is the arterial tracer concentration. Tissue concentration at time t, C_t is then:

$$C_t(t) = \int_0^t fC_a(t')r(t-t')dt' = fC_a(t) \otimes [r(t)] \qquad (4)$$

where ⊗ denotes convolution (Buxton, 2002).

Equation (4) is usually written as:

$$C_t(t) = C_a(t) \otimes [f \times r(t)] \qquad (5)$$

If the equation is thought of in terms of linear systems, then $C_a(t)$ is the input , $C_t(t)$ is the output and $fr(t)$ is the 'impulse response'.

1.4.2.1 Tumour blood flow measured by first pass extraction techniques

One method of measuring blood flow is to use radioactive or fluorescently labelled microspheres, made of glass, plastic or starch. The microspheres are injected into a large artery or the left ventricle, to make sure that they are fully mixed. They are small enough to pass through arterioles but become trapped in the capillary beds of tissues on the 'first pass' through the circulation. Therefore, they distribute to the tissues as a fraction of the cardiac output (CO) received by the tissues (see **Figure 1.6A**). The tissue concentration time curve will be sigmoidal in shape with a plateau, H such that:

$$H \propto \frac{f}{CO} \tag{6}$$

As none of the microspheres leave the tissue, r(t) = 1 for all time so equation (5) becomes (Buxton, 2002):

$$C_t(t) = fC_a(t) \tag{7}$$

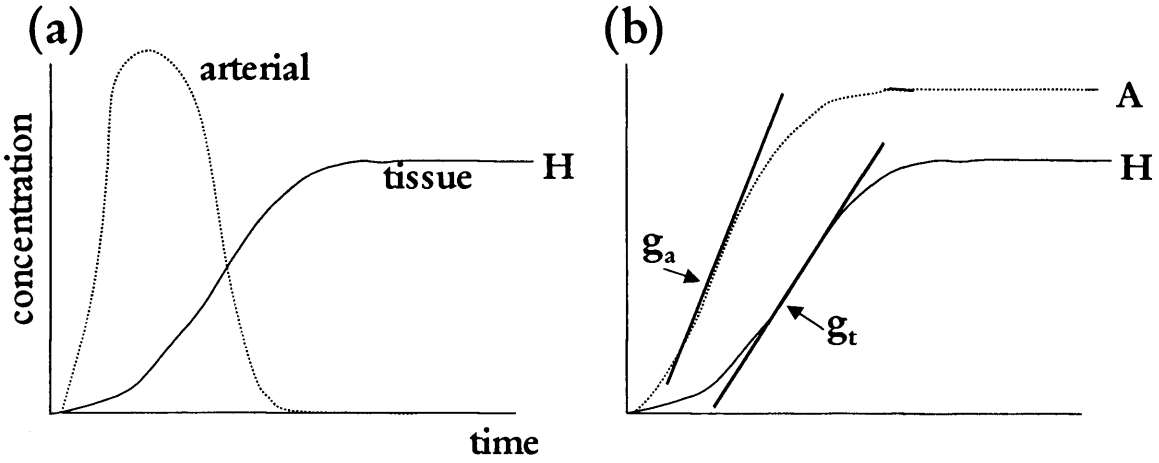

Figure 1.6: (**a**) arterial and tissue concentration time curves following injection of microspheres. (**b**) the integral of the arterial concentration curve has the same shape as the tissue concentration curve (see text).

If the arterial input function is obtained from blood sampling, then absolute measurements of blood flow can be made. A clinically applicable example of this technique is using microbubbles and intermittent Doppler ultrasound (Krix et al., 2003).

Certain chemical species, under certain circumstances, also distribute as a fraction of the cardiac output if injected intravenously (e.g. rubidium chloride) and may be used in a similar way (Sapirstein, 1958; Zanelli & Fowler, 1974). In the laboratory, ^{86}rubidium chloride (^{86}RbCl) has been used to measure the relative change in tumour blood flow rate (as change in fractional cardiac output) following CA-4-P in rodent models (Chaplin et al., 1999; Eikesdal et al., 2001; Murata et al., 2001c). Measurement of cardiac output and hence absolute tumour blood flow (per gram of tissue) is possible in rats but technically very difficult in mice. Tumour and organs are excised for measurement of radioactivity so serial measurements are not possible.

This method may be used clinically using SPECT (single photon emission computed tomography). SPECT is a nuclear medicine procedure in which a radiotracer is injected intravenously, its activity detected using a rotating gamma camera and then a cross-sectional image reconstructed. The procedure has similar advantages/disadvantages to PET (see below). Tracers such as ^{99m}Tc-HMPAO, a non-toxic lipophilic agent that is almost completely extracted during the 1st pass, are used (Hulshof et al., 1998; Langen et al., 1989; Rowell et al., 1990; Rowell et al., 1989).

Tissue blood flow can also be obtained from measurement of the maximum slope of C_t (Peters et al., 1987). Integration of the arterial concentration curve generates a curve with the same shape as the tissue concentration curve (see **Figure 1.6B**), therefore, the parameters of the two curves will be in proportion and

$$\frac{H}{A} = \frac{g_t}{g_a} \qquad (8)$$

where A is the plateau of the integrated arterial curve, g_a its maximum slope and g_t is the maximum slope of the tissue curve. A is also the area under the arterial concentration curve, before integration, and g_a the same as its peak height (Peters et al., 1987). Substituting for H:

$$\frac{f}{CO} \propto \frac{g_t}{g_a} A \qquad (9)$$

The tissue-concentration curve of a tracer that is not completely extracted on its first pass will not reach a plateau but its maximal slope will be the same as that obtained with microspheres (Miles, 1991; Peters et al., 1987). Therefore, the principles outlined above can be applied to recirculating tracers, provided that the shape of the tissue concentration time curve can be determined accurately. This is one of the methods used with dynamic CT to obtain blood flow measurements (Miles, 1991) and has been used with CT to measure tumour blood flow clinically (Hermans et al., 2003).

The advantages of dynamic CT are that it has good spatial resolution and serial measurements can be made. Also, increase in signal density is directly proportional to contrast agent concentration. However, it involves a dose of radiation for the patient and complicated software modelling is required.

1.4.2.2 Techniques based on Kety model for freely diffusible tracers

Another way of approaching blood flow measurement is to use the model originally described by Kety for tissue uptake of a freely diffusible, inert tracer (Kety, 1960a; Kety, 1960b). This model assumes that the tissue can be treated as a single, well-mixed compartment.

Equation (1) can be rewritten:

$$\frac{Q_t}{dt} = F(C_a - C_v) \qquad (10)$$

Where F is blood flow in $ml.min^{-1}$ (not at this stage, per unit volume or mass) and C_v is the tracer concentration in venous blood. C_v is difficult to measure but if the exchange of tracer between tissue and venous blood is very rapid, such that the two compartments stay in equilibrium even as the overall concentration is changing, then $C_v = C_t/\lambda$ - where λ is the partition coefficient between tissue and venous blood. For a tracer that is equally soluble in tissue and in blood, λ can be thought of as the volume of distribution. In solid tumours, however, there are non-perfused areas to which tracer cannot get access such that tracer $V_D = \alpha\lambda$, where α is the perfused fraction of tissue/tumour and so $C_v = C_t/V_D$. Substituting in equation (10):

$$\frac{Q_t}{dt} = \frac{F}{V_D}(V_D C_a - C_t) \qquad (11)$$

If the tracer used is not freely diffusible then equation (11) has to be modified to include the extraction fraction, E (the fractional loss from blood to tissue in a single passage).

If equation (11) can be expressed per unit of tissue:

$$\frac{C_t}{dt} = \frac{Ef}{V_D}(V_D C_a - C_t) \qquad (12)$$

where f is blood flow per unit volume (or mass) of tissue. If C_a is variable, but zero at time 0, then

$$C_t(t) = Ef \int_0^t C_a e^{-\frac{Ef}{V_D}t} dt \qquad (13)$$

Comparison with the general expression of tissue tracer concentration, equation (5), shows that the residue function for a freely diffusible tracer, $r(t) = e^{-ft/V_D}$.

Equation (13), known as the Kety equation, applies for injection of an intravenous bolus of tracer and is used for measurement of tumour blood flow in animals using radiolabelled iodoantipyrine (IAP) (Tozer et al., 1994). In the clinic, radiotracers suitable for positron emission tomography (PET) (Anderson & Price, 2002) are used and the method has also been adapted for DCE-MRI (see **Section 1.5**) (Tofts, 1997; Tofts & Kermode, 1991).

In the laboratory, IAP, labelled with either ^{125}iodine (^{125}I) or ^{14}carbon (^{14}C), can be used to obtain absolute measurements of blood flow (IAP is assumed to be freely diffusible so E=1) (Kety, 1960b; Tozer et al., 1994). IAP has been used to investigate the acute effects of CA-4-P (Maxwell et al., 2002; Tozer et al., 1999). Tumour levels of IAP are measured after excision by scintillation counting and serial arterial blood samples are taken for estimation of the arterial input function. It is also possible to investigate spatial distribution of blood flow (using autoradiography). The disadvantages of this method are that it is labour intensive and although routine in rats, is technically difficult in mice. Also, sequential measurements in the same animal are not possible.

PET can be used to measure blood flow both in the laboratory and clinically. A radiotracer that emits positrons (such as ^{15}O or ^{18}F) is injected as an intravenous bolus. Each positron is rapidly annihilated by collision with a nearby electron, producing 2 gamma rays. The gamma rays are at 180 degrees to each other and are detected by a band of coincident detectors. The original position of the positron can then be calculated and a 3D image formed. Blood flow can be calculated using very similar modelling to IAP with ^{15}O-labelled water as the tracer (Herscovitch et al., 1983; Raichle et al., 1983). PET has been used to measure tumour blood flow (Anderson & Price, 2002) and also to monitor response to CA-4-P in a phase I trial (Anderson et al., 2003). The advantages of using PET to measure blood flow are that it is a sensitive technique and quantitative measurements can be made relatively easily. External imaging and a very short tracer half-life means that sequential measurements can be made. The disadvantages of this method are: PET availability is currently limited; spatial resolution is poor and anatomical resolution requires co-registration with either CT or MRI; arterial cannulation is required for quantitative measurement; the patient receives a dose of radiation (Anderson & Price, 2002; Anderson et al., 2001). Also, this method is only practical with an on-site cyclotron to generate the short-lived radio-isotopes required (t½ for ^{15}O is about 2 minutes).

DCE-MRI involves the intravenous injection of contrast agent, e.g. gadopentetate dimeglumine (Gd-DTPA), while a series of images are acquired. As with dynamic CT, it is a relatively insensitive technique, requiring pharmacological doses of contrast agent (c.f. the trace amounts required for nuclear medicine studies). The advantages of using this technique are that MRI is widely available, and does not involve a dose of radiation for the patient. Images have good spatial resolution – so heterogeneity of response within a tumour can be investigated. As with PET, sequential imaging is possible. Unfortunately, there is no readily diffusible tracer available and so contrast agent uptake depends on vessel permeability as well as blood flow rate. Also, change in contrast agent concentration is not directly proportional to change in signal intensity and cannot be measured directly. The modelling is still based on that devised by Kety (Kety, 1960a; Kety, 1960b) but it incorporates a term to include vascular permeability for the contrast agent (Tofts, 1997; Tofts & Kermode, 1991) (see **Section 1.5**).

The Kety model can be adapted for interstitial injection of an inert tracer. In this case C_a will be negligible and blood flow will be related to tracer clearance from the tissue. This method has been used to calculate blood flow in tumours after local injection of ^{133}Xe or

$^{99m}TcO_4$ in animal models (Cliffe et al., 1994; Lyng et al., 1992) and clinically (with ^{133}Xe) (Mantyla et al., 1988). However, the technique is invasive, involves a dose of radiation for the patient and can only be used for superficial tumours. Similar modelling is used for thermal clearance (Samulski et al., 1987).

1.4.2.3 Bolus tracking of intravascular tracer

This technique (also known as indicator dilution analysis) was originally described for non-diffusible radioactive tracers (Meier & Zierler, 1954; Zierler, 1965) but has been adapted for imaging techniques such as DCE-MRI (Rosen et al., 1990) and dynamic CT (Axel, 1980; Cenic et al., 2000). It can be used to calculate mean transit time and blood volume and hence blood flow from the transit time equation - equation (3).

The model is based on a simple system with a single inlet and outlet with flow *f*. The system can represent an entire organ or tissue or an individual MR or CT voxel. If the tracer is injected as an instantaneous bolus then tracer concentration at the outlet will rise to a peak and then return to zero (assuming there has not been time for recirculation).

Tissue blood volume can be obtained relatively easily. All tracer that enters the system must leave so

$$\int_0^\infty fC_a(t)dt = \int_0^\infty fC_v(t)dt \qquad (14)$$

where C_a and C_v are the tracer concentrations entering and leaving the system, respectively. $C_v = C_t/V_D$ (see above). Rearranging and substituting in equation (14) gives:

$$V_D = \frac{\int_0^\infty C_t(t)dt}{\int_0^\infty C_a(t)dt} \qquad (15)$$

For an intravascular tracer, V_D=blood volume, so tissue blood volume is directly proportional to the area under the tissue concentration time curve (Axel, 1980; Buxton, 2002).

If the arterial input function, $C_a(t)$ is known, then blood flow, f may be obtained from deconvolving equation (5). Alternatively, if the mean transit time, τ, is measured, then f can be obtained by substituting in equation (3).

The fraction of tracer leaving per unit time is termed h(t). This is related to the fraction of tracer remaining, the residue function r(t) as

$$dr/dt = -h(t) \tag{16}$$

As all tracer must leave the system, $\int_0^\infty h(t)dt = 1$. The mean transit time is then given by:

$$\tau = \int_0^\infty th(t)dt \tag{17}$$

Equation (17) defines the centre of gravity or 'centroid' of h(t) and is also known its 'first moment'. τ can be expressed in terms of the tracer concentration at the outlet (the venous concentration) as

$$\tau = \frac{\int_0^\infty tC_v(t).dt}{\int_0^\infty C_v(t).dt} \tag{18}$$

- i.e. as the normalised first moment of the venous concentration-time curve (Axel, 1980; Meier & Zierler, 1954). (Also, see Peters (Peters, 1998) for a worked example of the calculation of τ).

For imaging studies, it is not possible to measure C_v and instead the first moment of the tissue concentration curve is used as an approximation for τ (Axel, 1980; Weisskoff et al., 1993). However the tissue-concentration and venous-concentration time curves are not directly comparable as $C_v(t)$ is modelled as the convolution of $C_a(t)$ with h(t), whereas $C_t(t)$ is modelled as the convolution of $C_a(t)$ with $fr(t)$, (Buxton, 2002). For the venous concentration, the impulse response is h(t) which depends primarily on the mean transit time and so the ratio of V_D/f (transit time equation), whereas for the tissue concentration,

the impulse response is $fr(t)$ which is dependent on both f and V_D, not just their ratio. Therefore, the influence of f on the tissue concentration curve cannot be cleanly separated from V_D and sensitivity to flow increases is reduced, particularly for a broad arterial input function (Buxton, 2002).

1.4.3 Measurement of red cell flux and velocity using intravital microscopy

Intravital microscopy is a powerful imaging technique that allows continuous non-invasive observation of living tissue (Jain et al., 2002). It can be used to study tumour (or normal tissue) vasculature using chronic transparent window preparations or acute (exteriorised) tissue preparations (Jain et al., 2002).

The dorsal skin flap window chamber model was developed for intravital microscopic investigation of transplanted rodent tumours (Dewhirst et al., 1987; Papenfuss et al., 1979) and has been adapted for use with human xenografts in SCID mice (Leunig et al., 1992). It involves surgical implantation of a metal or plastic frame containing a glass chamber through which the growing tumour may be observed.

The animal is placed in a jig on an adapted microscope stage so that blood vessels can be observed under magnification. A fluorescent dye (e.g. the carbocyanine dye, DiI) is used to label red-cell membranes (Unthank et al., 1993). DiI is lipophilic so dissolves in and diffuses throughout the lipids of the cell plasma membrane. Labelled red cells are then injected intravenously prior to the experiment. Video recordings are made under transmitted and fluorescent illumination for off-line-analysis at a later stage. Red cell flux (the number of red cells passing a point/min) and velocity can be measured for individual vessels within a region of interest (Tozer et al., 2001). Blood flow in a particular vessel can be calculated from vessel diameter and velocity (=diameter^2 x velocity x $\pi/4$). Intravital microscopy has been used to monitor response to CA-4-P in tumours implanted in a window chamber in rats (Tozer et al., 2001).

The effect of vascular-targeted strategies on tumour vasculature can be observed using this model e.g. vascular disruptive agents (Tozer et al., 2001) or anti-angiogenic agents (Vajkoczy et al., 2000; Yuan et al., 1996). The model can also be used to directly visualise tumour vessel response to vasoactive agents, e.g. ATII (Hori et al., 1993) and hydralazine (Dewhirst et al., 1994), and to hyperoxic gases including carbogen (Abramovitch et al., 1998; Dewhirst et al., 1996; Dunn et al., 1999).

The window chamber model has also been used to investigate related parameters such as interstitial fluid pressure (Boucher et al., 1996; Leunig et al., 1992) and tumour oxygenation (Dewhirst et al., 1999; Dewhirst et al., 1992; Kimura et al., 1996; Torres Filho et al., 1994). Tumour vessel permeability can be investigated using high molecular-weight fluorescent markers, such as FITC-dextran (Yuan et al., 1993). More recently, multi-photon fluorescent imaging has been used to facilitate accurate quantification of fluorescence in 3D images (Tozer et al., 2005).

1.4.4 Measurement of red cell flux and velocity using the Doppler technique

Laser Doppler flowmetry is a clinically applicable method where the signal recorded relates to red cell flux and velocity. The underlying principle is that light scattered from moving objects (red blood cells) within the tissue will show a change in frequency that is related to their velocity (Stern, 1975). Microprobes are inserted into the tumour and the signal recorded for up to approximately two hours (Hill et al., 1998a). The signal is then calculated relative to pre-treatment values. Laser Doppler flowmetry can be used both in animal models (Hill et al., 1998a) and clinically (Goodchild et al., 2001; Powell et al., 1996). It has been used to monitor response to CA-4-P in an animal model (Malcontenti-Wilson et al., 2001). The limitations of this technique are that only a representative sample of the tumour can be sampled and serial readings are not possible (as the microprobes cannot be positioned reproducibly). Also, there is a complicated relationship between the signal and blood flow rate, hence absolute blood flow rate cannot be calculated and it is difficult to compare measurements on different occasions and between different institutions. In humans, studies are limited to accessible tumours e.g. neck nodes or skin metastases (Powell et al., 1996).

High frequency Doppler ultrasound has also been used to monitor the effects of vascular disruptive therapy on superficial tumours (Goertz et al., 2002). It is non-invasive and can be used for serial measurements, but is limited to superficial tumours of <5-10 mm depth.

1.5 *MRI methods for imaging tumour microcirculation*[5]

1.5.1 Overview of MRI principles

Atoms with an odd number of protons or neutrons possess nuclear spin (spin angular momentum). The nucleus is positively charged, so induces a magnetic field (as it is a moving charged particle). Each of these spinning nuclei can therefore be thought of as a tiny magnet spinning on its long axis - see **Figure 1.7A.** Magnetic resonance imaging (MRI) is derived from the interactions of these nuclear 'spins' with an external applied magnetic field. Hydrogen nuclei (which possess a single proton) are usually used as they are abundant in tissue and have the strongest magnetic dipole 'moment' of any stable nucleus - so produce the strongest signal. However, other isotopes such as ^{13}carbon, ^{19}fluorine, ^{23}sodium or ^{31}phosphorus have also been used. All work presented in this thesis has been performed using ^{1}H (proton)-MRI.

The nuclear spins present in a defined volume of tissue can each be represented by a magnetic dipole moment vector with a defined magnitude and axis of rotation - **Figure 1.7.A.** These vectors are orientated randomly in all directions, so when summed, the net magnetisation vector will be zero – see **Figure 1.7.B.** If the tissue is placed in an external magnetic field, $\underline{B}_0$ (units = tesla, T), there is an interaction between the nuclear spins and $\underline{B}_0$ such that individual spins rotate, or 'precess', gyroscopically around the axis of $\underline{B}_0$ (**Figure 1.8.A**) and the magnetic dipole moment vector of each spin lines up either parallel or anti-parallel to $\underline{B}_0$ (**Figure 1.8.B**). The spins precess at a frequency proportional to the magnetic field strength of $\underline{B}_0$, known as the Larmor frequency:

$$\underline{\omega}_0 = \gamma \underline{B}_0 \qquad (19)$$

where $\underline{\omega}_0$ is the Larmor frequency (Hz), γ is the gyromagnetic ratio (Hz.T^{-1}) of the nuclear spin and $\underline{B}_0$ is the external magnetic field (T). γ is a constant which is an intrinsic property of a particular nuclear spin.

---

[5] **Bibliography for this section:**

A Training Course in Magnetic Resonance Imaging and Spectroscopy, Oct 2001. Royal Marsden NHS Trust/Institute of Cancer Research and The Institute of Physics and Engineering in Medicine.

J.P. Hornak website http://www.cis.rit.edu/htbooks/mri/inside.htm

Buxton RB. Introduction to Functional Magnetic Resonance Imaging. Cambridge University Press, Cambridge, UK

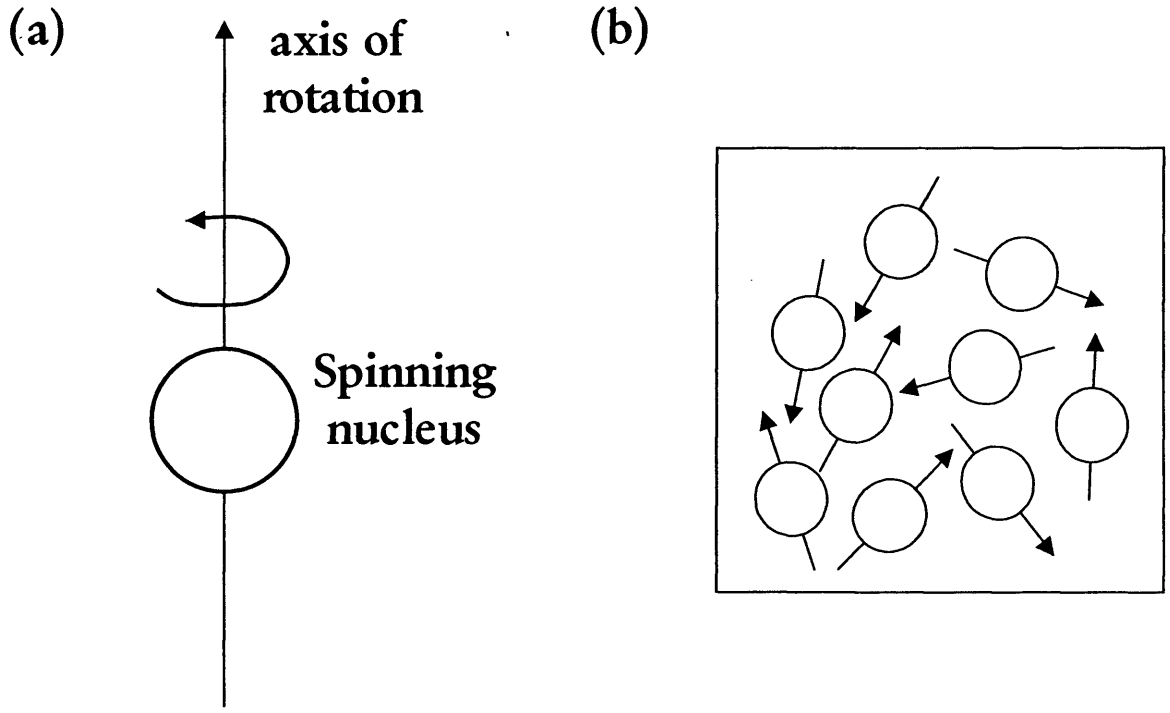

Figure 1.7 A: a nuclear spin, rotating about its longitudinal axis, B: volume of tissue containing randomly orientated spins, arrows indicate axes of rotation.

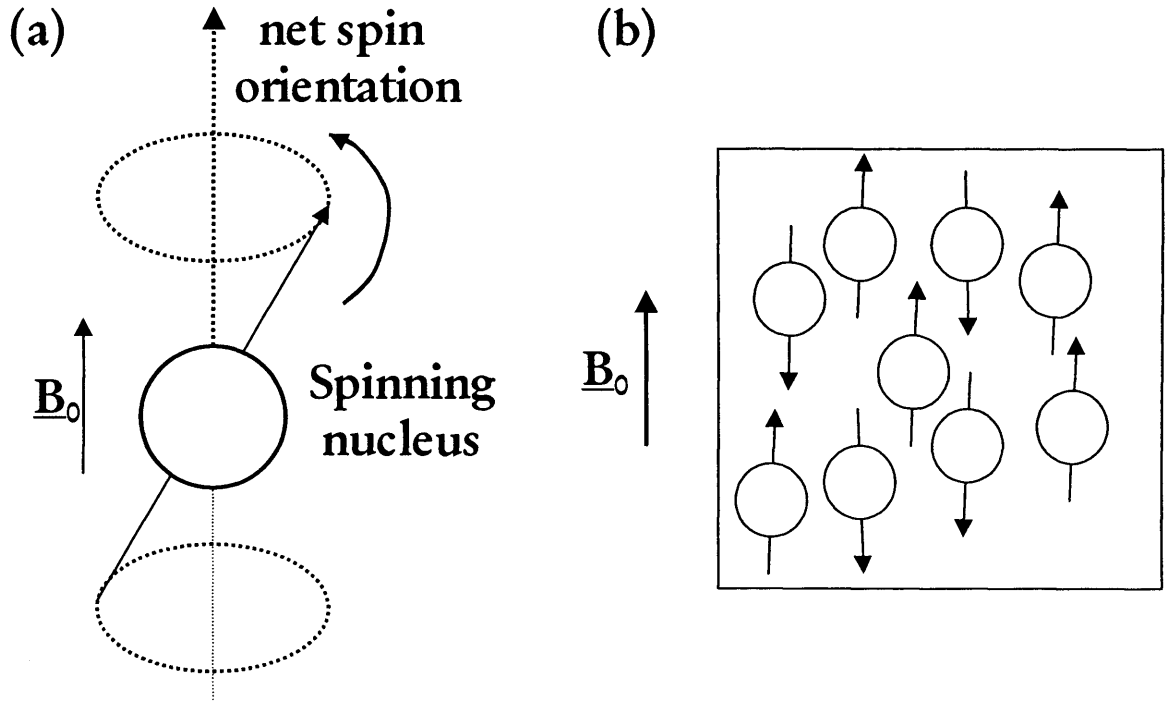

Figure 1.8 The application of an external magnetic field, $\underline{B}_0$ causes the nuclear spin to precess gyroscopically around $\underline{B}_0$ (A) and to line up with their net orientations either parallel or anti-parallel to $\underline{B}_0$ (B).

Hydrogen nuclei can exist at two energy levels. Nuclei at the lower energy level have magnetic vectors aligned parallel with $\underline{B}_0$ (spin-up) as this requires less energy than anti-parallel (spin-down) alignment. A tiny excess number of hydrogen nuclei (7 per 10 million) have magnetic vectors in parallel alignment, creating a net magnetisation vector, $\underline{M}_0$, in the same direction as $\underline{B}_0$ (**Figure 1.9.A**). These vectors can be described using Cartesian coordinates: $\underline{B}_0$ and $\underline{M}_0$ are conventionally said to be in the Z-axis and the longitudinal magnetisation vector is termed M_Z. At equilibrium, $M_Z = \underline{M}_0$ and there is no magnetisation vector in the tranverse plane (M_{XY}).

$\underline{M}_0$ is the source of the MRI signal, but cannot be detected when it is in parallel with $\underline{B}_0$. The application of a radio-frequency (RF) pulse, $\underline{B}_1$, at the Larmor (resonance) frequency, in the transverse (XY) plane (i.e. perpendicular to $\underline{B}_0$), causes the nuclear spins to precess around $\underline{B}_1$ instead so the net magnetisation vector rotates out of alignment with $\underline{B}_0$ (**Figure 1.9.B**). The flip angle, α, is the angle of rotation produced by $\underline{B}_1$. For example, a flip angle of 90^0 will rotate $\underline{M}_0$ into the transverse (XY) plane, where it is now termed $\underline{M}_1$ (**Figure 1.9.B**).

There is now a moving magnetic field in the transverse plane that can induce a voltage in a receiver coil. This electric voltage is the nuclear magnetic resonance (NMR) signal. Once the RF pulse is switched off, the net magnetisation vector will realign with $\underline{B}_0$, along the longitudinal (Z) axis (as the nuclear spins will rotate back to precess around $\underline{B}_0$). As only magnetisation in the transverse plane (XY) can induce voltage in the receiver coil, the MR signal will decay as $\underline{M}_1$ rotates back to $\underline{M}_0$ – a process known as 'free induction decay'. An MR image could then be constructed from this signal, though it is usually too fast to allow spatial encoding and so other RF pulses are generally used, in sequence with magnetic field gradients, to form encoded echoes. These can then be Fourier transformed into final images.

The RF pulse provides the energy required to excite nuclear spins from the lower energy level to the higher energy level – this is 'resonance'. The moment the RF pulse ceases, the excited spins will revert to the lower energy level in a process called 'relaxation', which is a re-establishment of thermal equilibrium. There are two relaxation processes: the recovery of longitudinal magnetisation (M_Z) and the decay of tranverse magnetisation (M_{XY}) – governed by relaxation time constants, T_1 and T_2 respectively.

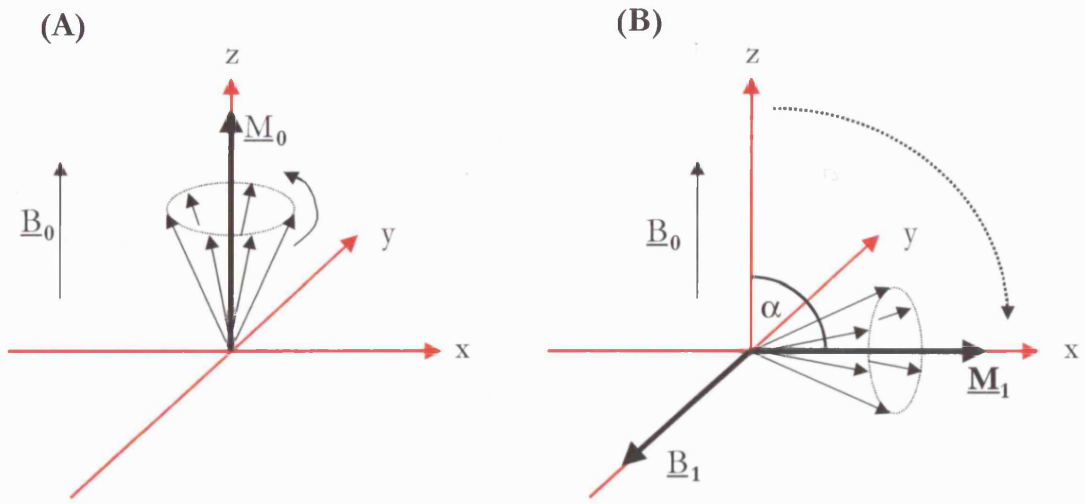

Figure 1.9: A: The net magnetisation, $\underline{M}_0$ at equilibrium, **B:** Application of a RF pulse causes $\underline{M}_0$ to rotate through a flip angle of α to give a net magnetisation of $\underline{M}_1$.

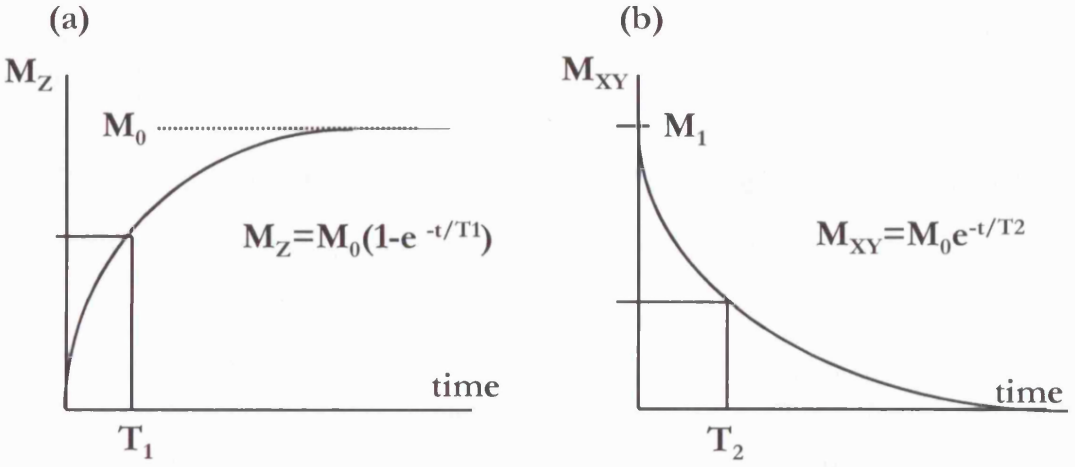

Figure 1.10 A: T_1 relaxation time-curve **B.** T_2 relaxation time-curve

T_1 ('spin-lattice' relaxation) depends on how quickly nuclear spins give up energy to the surrounding tissue or 'lattice' and is defined as the time taken for M_Z to return to 63% of its original value ($\underline{M_0}$), i.e. to increase M_Z by a factor of e (**Figure 1.10.A**).

T_2 ('spin-spin' relaxation) depends on the interaction with adjacent spins. At the end of the RF pulse, all spins are precessing in the transverse (XY) plane (assuming a 90^0 flip angle has been applied) at the same frequency and are 'in phase' with each other. Once the RF pulse is switched off, the precessional frequency of a particular spin is altered by interactions with adjacent nuclear spins, resulting in a gradual loss of phase coherence and hence transverse magnetisation. T_2 is defined as the time taken for M_{XY} to decay to 37% of its maximum value, i.e. to decrease M_{XY} by a factor of e (**Figure 1.10.B**).

B_0 is not uniform, as there are local field distortions due to magnetic susceptibility differences between different tissues. 'Magnetic susceptibility' is a measure of the degree to which a material becomes magnetised when placed in a magnetic field. Air, bone and other tissues all have different magnetic susceptibilities, resulting in distortions in $\underline{B_0}$ at interfaces between different structures. Local inhomogeneities in $\underline{B_0}$ will influence the rate of decay of transverse magnetisation. The effective transverse relaxation under these circumstances is faster than T_2 and the term T_2^* is used to describe it and:

$$\frac{1}{T_2^*} = \frac{1}{T_2} + \frac{1}{T_2'} \qquad (20)$$

where T_2' is the extra relaxation component due to $\underline{B_0}$ inhomogeneities. (Equation 20 may also be written as $R_2^* = R_2 + R_2'$, where R_2 is the relaxation rate and $= 1/T_2$).

1.5.2 Image Contrast

Tissues have characteristic T_1 and T_2 values. T_1 values in the body vary between about 0.2 and 4 seconds and are 8-10 times longer than T_2 values. To create an image, a particular sequence of RF pulses and magnetic field gradients is applied – called a MR pulse sequence. The size, direction, timing and frequency of these pulses and gradients can be manipulated such that tissues with different relaxation times will have different signal intensities and there is contrast between them in the resultant image. The repetition time, TR, is the time between one RF pulse and the next. The echo time, TE, is the time between centre of the initial pulse and the time when the MR signal is measured (see

Figure 1.11). On a 'T_1-weighted image' (short TR, short TE), tissues with a short T_1 appear bright and those with a long T_1 appear dark. The opposite occurs with a T_2 weighted image (long TR, long TE): tissues with a long T_2 appear bright whereas those with a short T_2 appear dark.

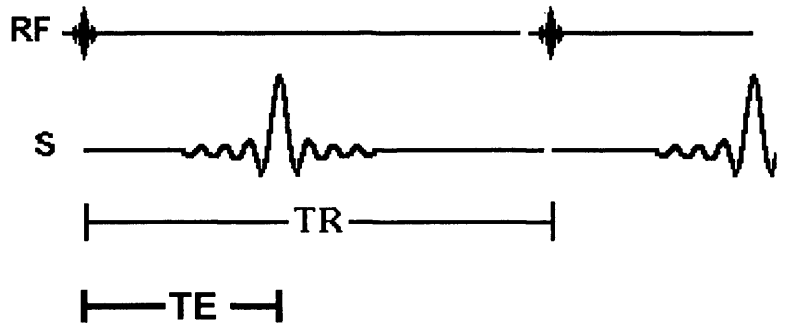

Figure 1.11: Diagram to show relationship between RF pulse, resultant signal (S), TR and TE

MRI visible protons are those within soft tissues and liquids. Solid tissues or structures such as bone have a fixed lattice and appear black on all image types. Image contrast may also be produced by using pulse sequences sensitive to the relative number of mobile protons available within a tissue. This is termed 'proton density' (PD) image contrast. For example, cerebrospinal fluid has a high proton density whereas brain tissue has a lower proton density. The proton density is responsible for the magnitude of signal generated (signal amplitude). Proton density contrast is regarded as 'basic' MR contrast as it is not dependent on tissue relaxation times. (Measured PD images do have some residual T_1 and T_2 contrast by the nature of the sequence timings used in their measurement).

Image contrast may be enhanced by the use of intravenous contrast agents such as the low molecular weight agent, gadopentetate dimeglumine (Gd-DTPA, Magnevist®). Gd-DTPA is paramagnetic[6], as the gadolinium ion contains seven unpaired electrons and so has a large magnetic dipole moment. The presence of Gd-DTPA in a tissue shortens the T_1 and T_2 relaxation times, increasing the 'relaxation rates', $1/T_1$ and $1/T_2$, such that (for T_1)

$$\frac{1}{T_{1obs}} = \frac{1}{T_1(0)} + r_1 C \qquad (21)$$

[6] A paramagnetic material will develop a weak attractive force if placed in an magnetic field.

where $1/T_{1obs}$ is the observed value in the presence of Gd-DTPA, $1/T_1(0)$ is the innate value, C is the concentration of Gd-DTPA (mM) and r_1 is the 'relaxivity' of Gd-DTPA in $mM^{-1}.s^{-1}$ (specific water relaxation rate due to Gd-DTPA, dependent on magnetic field strength). (Equation 21 may be written in a similar fashion substituting T_2 for T_1). The effect of Gd-DTPA is to **increase** signal intensity on a T_1-weighted image (as tissues with a short T_1 are bright) and to **decrease** signal intensity on a T_2 (or T_2^*) weighted image (as tissues with a short T_2 are dark). Gd-DTPA is used primarily as a T_1-agent as its effect on T_1 is greater than on T_2 for the same dose of contrast agent (as $T_1 > T_2$). The effect of Gd-DTPA is often described in terms of relaxation 'rate' constants – e.g. $R_1 = 1/T_1$ and so on.

Gd-DTPA has a low molecular weight (0.57 kD) and so diffuses out of blood vessels into the extracellular space (except in cerebral imaging when the blood-brain barrier is intact). Tumour vessels are more permeable than normal vessels (Jain, 1987a), so Gd-DTPA diffuses more rapidly into tumour extravascular extracellular space (EES) than into normal tissue EES, providing contrast by increasing tumour signal intensity on T_1-weighted images.

Gd-DTPA can also provide contrast by its effect on tissue magnetic susceptibility. The presence of Gd-DTPA within blood vessels alters the magnetic susceptibility of blood, inducing local distortions in $\underline{B}_0$. The consequence is shortening of the relaxation time, T_2^* (as nuclear spins dephase more rapidly) and a decrease in signal intensity on a T_2^*-weighted image. Protons in extravascular water adjacent to the vessel are also affected - resulting in a decrease in signal intensity over an area wider than the vessel diameter. This significantly increases contrast agent sensitivity. The effect only occurs during the brief period when Gd-DTPA is confined to the intravascular space, as T_1 effects will dominate once the contrast agent starts extravasating into the EES.

Blood Oxygen Level Dependent (BOLD)-MRI is a special technique that exploits the fact that deoxygenated haemoglobin (deoxyHb) is weakly paramagnetic and so can be used as an intrinsic contrast agent via its effects on magnetic susceptibility (Ogawa et al., 1990; Ogawa et al., 1993) - see **Section 1.5.4.**

1.5.3 Dynamic Contrast Enhanced Magnetic Resonance Imaging (DCE-MRI)

DCE-MRI involves the acquisition of a set of images as an intravenous bolus of a contrast agent, such as Gd-DTPA, is injected. The bolus of Gd-DTPA will briefly be confined within the vascular space before diffusing rapidly into tumour EES.

During the initial 'vascular' phase, a T_2*-weighted sequence can be used to detect signal change due to passage of the bolus of Gd-DTPA through the tissue capillary bed (**Figure 1.12**). Gd-DTPA can be treated as a non-diffusible, purely intravascular agent during this brief time. Modelling of this phase (using the indicator dilution theory for non-diffusible tracers (Meier & Zierler, 1954; Rosen et al., 1990; Zierler, 1965)) can produce estimates of relative tumour blood flow and volume (see **Sections 1.4.2.3** and **1.5.3.2**). Sequences with rapid image acquisition are used (e.g. images every 2 seconds for a total of 60 images).

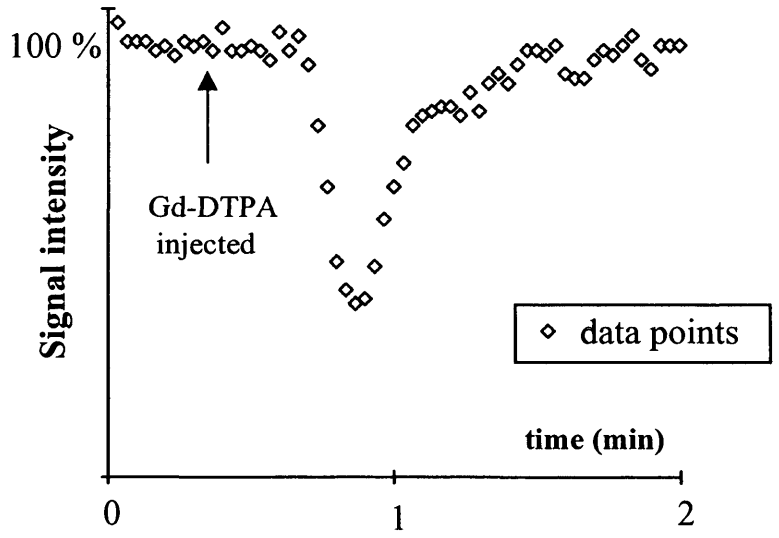

Figure 1.12: Graph of signal intensity versus time showing the transient dip in signal intensity due to T_2* effects following bolus injection of Gd-DTPA (with thanks from Dr NJ Taylor).

The contrast agent then passes rapidly into tumour EES – detected as an increase in signal intensity if a T_1-weighted sequence is used. The sequences used do not need such rapid image acquisition and typically have image time resolutions of 10-12 seconds. During this phase, Gd-DTPA can be treated as a diffusible tracer and the model developed by Kety (Kety, 1960a; Kety, 1960b) applied to produce estimates of vessel permeability, perfusion and leakage space (see **Section 1.4.2.2. and below**). There will be some T_2* effects during this phase that cannot be eliminated completely but the sequence can be optimised by appropriate choice of TR and TE values.

The change in signal intensity (ΔSI) over time following contrast agent injection can be analysed to obtain semi-quantitative parameters such as maximum gradient, maximum amplitude or area under the ΔSI-time curve (AUC). These parameters can provide information about the tumour microcirculation as they are indirectly related to tumour perfusion, vascular permeability and vessel surface area (Beauregard et al., 1998; Hawighorst et al., 1999; Mayr et al., 1996). Unlike CT imaging, the change in signal intensity on the MR image does not reflect contrast agent concentration directly but rather is a map of the effect of Gd-DTPA on the relaxation times of hydrogen nuclei present in the tissue. Therefore it is difficult to compare non-quantitative results from different institutions as different sequences, machines and injection procedures will produce different changes in signal intensity for the same change in contrast agent concentration (Parker et al., 1997). For quantitative analysis (to obtain comparable results between institutions) and tracer kinetic model application, estimation of the tissue contrast agent concentration is required.

1.5.3.1 T_1-weighted DCE-MRI kinetic parameters

The T_1-weighted quantitative parameters derived for the work presented in this thesis are IAUGC (the initial area under the Gd-DTPA concentration vs time curve) and the kinetic parameters obtained from the Tofts' model (Tofts & Kermode, 1991): the transfer constant for Gd-DTPA from plasma to tumour extracellular space, K^{trans} and the volume of the EES or leakage space, v_e. How these parameters are derived is outlined below.

1.5.3.1.1 Quantitative analysis: conversion of signal intensity to Gd-DTPA concentration

For quantitative analysis, signal intensity values have to be converted first into T_1 relaxation times and then into Gd-DTPA concentration values.

In the clinical study (see **Chapter 2**), data from a calibration experiment that involved phantoms with known T_1 relaxation time values were available. Signal intensities were converted into T_1 relaxation times using this calibration data in conjunction with proton density images (Parker et al., 1997).

The concentration of Gd-DTPA present at time t, C_t, can then be calculated from equation 22 (a rearrangement of equation 21) (Donahue et al., 1994):

$$C_t = \frac{\left(\frac{1}{T_1(t)} - \frac{1}{T_1(0)}\right)}{r_1} \qquad (22)$$

where $T_1(t)$ is the post-contrast signal intensity at time t, $T_1(0)$ is the pre-contrast relaxation time and r_1 is the longitudinal relaxivity of protons *in vivo* due to Gd-DTPA respectively. For the clinical study, r_1 was taken to be 4.5 $mM^{-1}s^{-1}$ for a 1.5 Tesla system (Donahue et al., 1994).

The method used for T_1 calculation for the CA-4-P/SW1222 study (see **Chapter 3**) is given in the **Appendix**. Relaxivity, r_1 at 4.7 Tesla was also determined for this study – the details of the method used are given in **Chapter 3**.

1.5.3.1.2 IAUGC

The IAUGC (units: mM.min or mM.s) is usually calculated for the first 60 or 90 seconds following Gd-DTPA injection (Evelhoch, 1999; Evelhoch et al., 2004). It cannot be related simply to tumour physiology, but has the advantage of being a quantitative parameter that is obtained without mathematical modelling or knowledge of the arterial input function (see below). As such, changes in voxels that are excluded from the modelling analysis are evaluated by the IAUGC parameter. It is a measure of how much contrast agent is taken up by the tumour in the first 60 or 90 seconds post-Gd-DTPA injection and is influenced by tumour blood flow rate and tumour vessel permeability. IAUGC values can be easily and robustly calculated for individual voxels in the tumour region of interest, (quantification of baseline T_1 is required). An average IAUGC value for the whole tumour can then be determined. **Figure 1.13** shows the derivation of IAUGC.

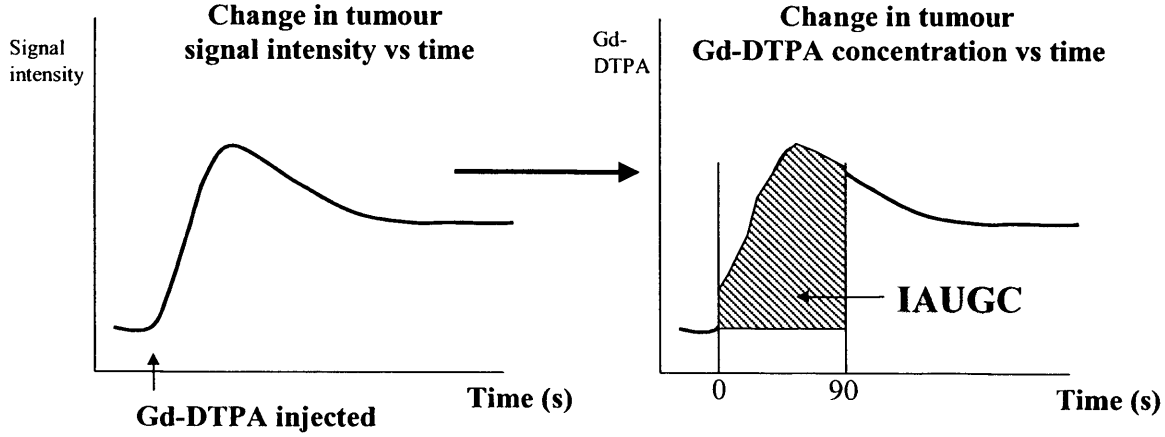

Figure 1.13: Diagram to show derivation of IAUGC

1.5.3.1.3 K^{trans} and v_e

The transfer constants for Gd-DTPA diffusion into the tumour extracellular extravascular space from blood plasma (K^{trans}) and back again (k_{ep}) can be calculated using a mathematical model (Tofts' model - see **Figure 1.14**) (Tofts et al., 1999; Tofts & Kermode, 1991).

This model is an adaptation of the Kety model, which was developed to describe the uptake of a freely diffusible inert tracer from the plasma to tissue extracellular extravascular space (Kety, 1960a; Kety, 1960b) (see **Section 1.4.2.2**). The main differences between the Tofts' and Kety models are that Gd-DTPA is not a freely diffusible tracer (which is a requirement of the Kety model) and that the transfer constants elicited are expressed per unit volume rather than per unit gram of tissue.

Using the Tofts' model, the time course of contrast agent concentration in tumour can be described by:

$$C_t(t) = K^{trans} \times C_a(t) \otimes e^{-k_{ep}t} \qquad (23)$$

where C_{at} represents the contrast agent concentration in arterial blood plasma at time t, (the 'arterial input function' or AIF), K^{trans} (min^{-1}) represents the transfer constant for transport from plasma to the tumour extravascular extracellular space (EES), k_{ep} (min^{-1}) represents the rate constant for transport from the EES to plasma and $\otimes$ denotes convolution. This equation is in the same form as equation (5) – see **Section 1.4.2**. The volume of EES per unit volume of tissue in the tumour, v_e (%), is equal to K^{trans}/k_{ep}.

K^{trans} (and k_{ep}) have both blood flow rate and permeability components as Gd-DTPA is not freely diffusible and their biological meaning is dependent on the balance between capillary permeability and blood flow in the tissue of interest (Tofts et al., 1999; Tofts, 1997). In high permeability situations, K^{trans} is equal to the blood plasma flow per unit volume of tissue. In low permeability situations, such as in the brain, it is equal to the permeability surface area product between the blood plasma and the EES (Tofts, 1997). Fit failures may occur with the derivation of K^{trans} due to the presence of either non-perfused regions, or regions of very high blood flow (see also **Section 1.5.5**).

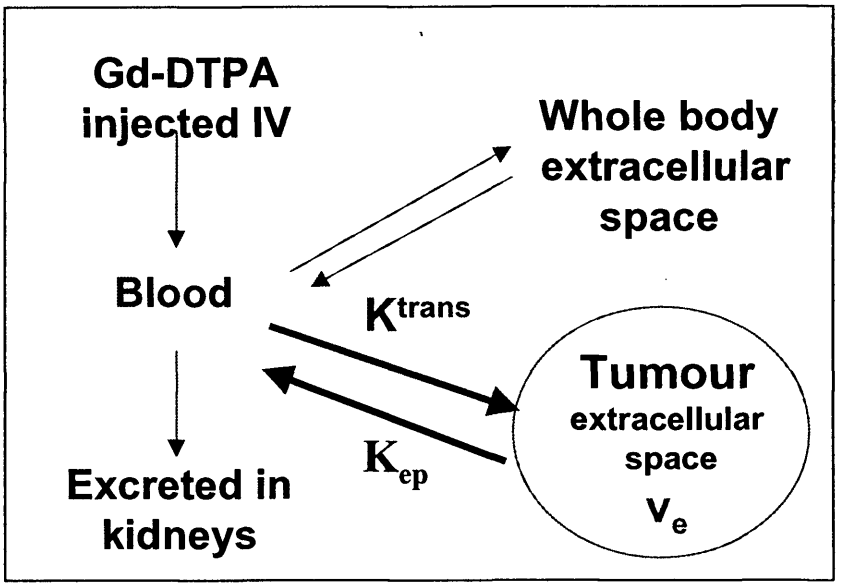

Figure 1.14: Diagram to show Toft's model for Gd-DTPA uptake kinetics.

There are a lot of assumptions when applying Tofts' model to tumours so these parameters should be regarded as the 'apparent' blood flow rate/permeability and leakage space (Parker et al., 1997). In principle, however, as the values of K^{trans} and v_e that are derived are based on Gd-DTPA concentration, comparisons between different studies and different MR centres can be made.

1.5.3.1.4 Calculation of arterial input function

The arterial input function, C_a, can be approximated to a bi-exponential function:

$$C_a = D\left[a_1 e^{-m_1 t} + a_2 e^{-m_2 t}\right] \quad (24)$$

where D is the dose of Gd-DTPA (mmol.kg^{-1}) and a_1, a_2, m_1, and m_2 are free parameters. For the clinical study (see **Chapter 2**), a standard arterial input function was used based on measurements on a group of healthy volunteers (Weinmann et al., 1984). For the SW1222/CA-4-P study, the arterial input function was derived using data from both a blood-sampling method and *in vivo* imaging (see **Chapter 3** for details). Wedeking et al. measured C_a in rats and recommended fitting to a tri-exponential function (Wedeking et al., 1990). However measurements were made out to 90 minutes post-Gd-DTPA injection. For shorter time spans, a bi-exponential function is commonly used (Checkley et al., 2003; Furman-Haran et al., 1996; Lyng et al., 1998). Although a multi-exponential decay function

better describes the total plasma concentration curve, a bi-exponential function seems sufficient to fit plasma concentration if the time range is short (Su et al., 1994).

1.5.3.2 T_2-weighted DCE-MRI (for calculation of rBV and rBF)*

The bolus-tracking technique for measurement of blood volume and flow requires an intravascular tracer (see **Section 1.4.2.3**) (Meier & Zierler, 1954; Zierler, 1965). Gd-DTPA fulfills this requirement in cerebral imaging, providing the blood brain barrier is intact. Therefore, the bolus tracking technique can be used to measure relative cerebral blood volume and flow (Rosen et al., 1990). In situations when vessels are permeable to Gd-DTPA (in visceral imaging or cerebral imaging with disruption of the blood brain barrier e.g. by tumour), the contrast agent will have a brief intravascular phase before it starts to leak out into extracellular extravascular space – so the technique can still be applied.

The intravenous bolus of contrast agent produces a transient decrease in signal intensity (and hence a transient increase in R_2*) on a T_2*-weighted image as it passes through the cerebral vascular bed. It is assumed that there is a linear relationship between contrast agent concentration and the change in transverse relaxation rate, ΔR_2* (Belliveau et al., 1990; Rosen et al., 1990; Villringer et al., 1988):

$$C(t) \propto \Delta R_2 *(t) = -\frac{1}{TE}\ln\left(\frac{S(t)}{S_0}\right) \qquad (25)$$

where S_0 and S(t) are the signal intensities at the baseline and at time t respectively and TE is the echo time of the MR sequence used (Belliveau et al., 1990; Rosen et al., 1990). It is also assumed that the amount of contrast agent that diffuses into the EES during the first pass is minimal and so does not affect the susceptibility gradient and hence ΔR_2* (Barbier et al., 1999).

The shape of the ΔR_2*-time curve will be affected by re-circulation of the Gd-DTPA bolus (see **Figure 1.15**) which can be corrected by fitting to a gamma (Γ)-variate function (Benner et al., 1997; Thompson et al., 1964). rBV is calculated from:

$$rBV = \int \Delta R_2 *(t)dt \qquad (26)$$

(see **Section 1.4.2.3.**) Blood volume measurement is relative as the constant of proportionality relating C(t) and ΔR_2^* is not known. Reproducibility is improved by normalising to the integral of the arterial-concentration time curve and then to grey or white matter in the contralateral hemisphere (in cerebral imaging). The ratio of grey to white matter cerebral blood volumes obtained using this MR technique is in good agreement with that obtained with PET (Belliveau et al., 1990; Guckel et al., 1994). Brain tumour rBV measurements have been obtained from this technique (Aronen et al., 1994; Guckel et al., 1994; Jackson et al., 2002b; Maeda et al., 1993; Rosen et al., 1991a) – and found to correlate with measurements made with PET (Rosen et al., 1991a).

If contrast is able to leak into tumour EES then T_1-shortening will occur, producing an increase in signal intensity (T_1 'shine-through') and reducing the peak of the ΔR_2^* curve (Jackson et al., 2002b). The Γ-variate function will help to correct for any T_1 effects (Boxerman et al., 1997; Rosen et al., 1991b), as will 'pre-enhancing' the tumour with a dose of contrast agent 5-10 mins prior to imaging (Jackson et al., 2002b) and choosing a small flip angle (Maeda et al., 1993). Using a double dose of contrast agent also improves sensitivity (Bruening et al., 2000).

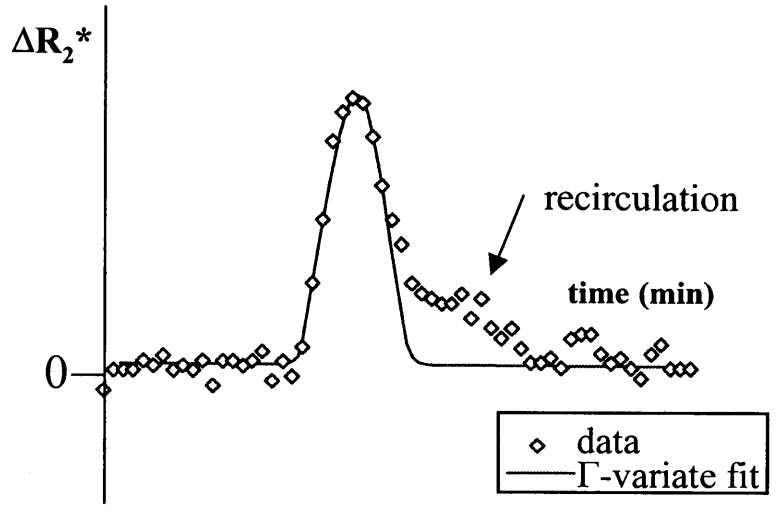

Figure 1.15: Diagram to show Γ-variate fit to ΔR_2^* curve.

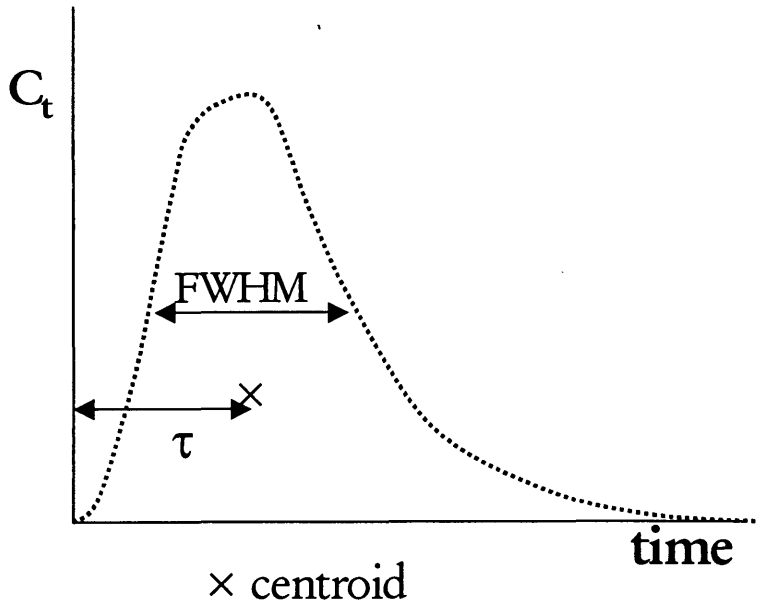

Figure 1.16: Schematic tissue concentration-time curve showing the approximations used for the mean transit time. FWHM: full-width half-maximum.

The measurement of relative blood flow (rBF) is more complex mathematically than measurement of rBV and so is more prone to error (Buxton, 2002) (see **Section 1.4.2.3**). Using the general equation for tissue tracer concentration (see the introduction to **Section 1.4.2**), rBF can be obtained by deconvolving the ΔR_2*-time curve from the arterial input function (Axel, 1983; Ostergaard et al., 1996). A more pragmatic approach, that does not require knowledge of the arterial input function, is to use either the normalised first moment, or the 'full-width half-maximum' measurement, of the ΔR_2* - time curve (**Figure 1.16**) (Perthen et al., 2002) as an approximation for the mean transit time (τ). rBF may then be obtained by substituting in the mean transit time equation.

There have been several studies comparing this MR technique with other methods of measuring cerebral blood flow in humans such as ^{133}Xe SPECT (Wirestam et al., 2000) and ^{15}O-H_2O-PET (Lin et al., 2001; Mukherjee et al., 2003; Ostergaard et al., 1998). There is positive correlation between different methods, at least for relative measurements.

This MR technique has been used to obtain estimates of rBV and rBF in visceral tumours (Ah-See et al., 2004; Jackson et al., 2002a; Taylor et al., 2004) and this particular application is discussed further in **Chapter 2**.

1.5.4 BOLD-MRI

The presence of deoxyHb in blood causes a decrease in signal intensity on a T_2*-weighted image due to its magnetic susceptibility effects (Ogawa et al., 1990; Ogawa et al., 1993). In contrast, oxyhaemoglobin does not affect magnetic susceptibility as the presence of oxygen suppresses the magnetic properties of the iron molecules, present in the heme group[7].

The BOLD-MRI signal is related to the amount of deoxyHb present and the blood volume as:

$$R_2^* \propto V[dHb]^{\beta} \qquad (27)$$

Where V is blood volume, [dHb] is deoxyHb concentration and β is ~1-1.5 depending on vessel size (Davis et al., 1998).

BOLD-MRI will be sensitive to changes in tissue oxygenation and blood flow as these factors will alter tissue deoxyHb levels. This is the basis of functional brain imaging as neuronal stimulation increases cerebral blood flow and oxygen delivery to the corresponding cortical area. The consequence is a decrease in deoxyHb levels and a transient increase in signal intensity on a BOLD image, for example, visual stimulation 'lights up' the visual cortex (Kwong et al., 1992; Ogawa et al., 1992). Tissue oxygenation and/or blood flow can also be manipulated by extrinsic factors such as breathing hyperoxic gases or administration of vasoactive agents. This has led to the development of BOLD-MRI as a non-invasive method of monitoring tumour response to hyperoxic gases such as carbogen (Abramovitch et al., 1999; Collingridge, 1997; Griffiths et al., 1997; Jordan et al., 2000; Neeman et al., 2001; Rijpkema et al., 2002; Robinson et al., 1997; Taylor et al., 2001). There have also been studies using BOLD-MRI to monitor the effects of vasoactive agents such as hydralazine (Robinson et al., 2000); calcitonin gene-related peptide (CGRP) (Howe et al., 1996) and the nitric oxide donor, isosorbide dinitrate (Jordan et al., 2000).

Analysis of the BOLD response can either be semi-quantitative, describing changes in signal intensity seen, or quantitative, in which absolute T_2* or R_2* measurements are made (a change in T_2* will be in the same direction as change in signal intensity). A multi-gradient echo sequence can be used to sample the NMR signal during transverse relaxation.

[7] DeoxyHb is paramagnetic and oxygenated haemoglobin is diamagnetic.

Assuming TR $>T_2^*$, signal intensity can be approximated by:

$$S \approx A_0 e^{-TER_2^*} \quad (28)$$

where A_0 is signal intensity extrapolated to zero echo time (the intercept on the y-axis) (Lebon et al., 1998). Sampling the transverse relaxation at several echo times allows the decay to be fitted, assuming monoexponential decay, providing R_2^* and A_0 values. A_0 is sensitive to blood flow rate whereas R_2^* is sensitive to oxygenation (Lebon et al., 1998). A_0 is dependent on the system adjusts, so rises and falls with signal intensities. ΔA_0 in a given experiment (e.g. breathing carbogen gas) will be proportional to flow.

An increase or decrease in tumour oxygenation will change deoxyHb levels and so have a direct effect on BOLD signal intensity. A change in tumour blood flow can also affect BOLD signal intensity – an increase in flow would be anticipated to decrease deoxyHb levels by flushing out deoxygenated blood with fresh, oxygenated blood. Choice of MR sequence parameters will also influence the effect of TBF on BOLD signal intensity as hydrogen spins in blood flowing into an observed slice produce a much stronger signal than stationary spins. This is termed the 'inflow effect' and occurs because spins in static tissue are already partially saturated (have a reduced signal intensity) by previous RF pulses (Howe et al., 1999). Therefore, the BOLD signal intensity change is dependent on both oxygenation and blood flow, depending on the MR sequence used (Howe et al., 1996; Howe et al., 1999).

As the BOLD signal is dependent on deoxyHb levels, an R_2^* map of a tumour ROI should be indicative of tumour hypoxia. However, the interpretation of intrinsic R_2^* maps is uncertain as the presence of oedema, haemorrhage and necrosis will all affect magnetic susceptibility and hence the BOLD signal (Robinson et al., 2003a; Robinson et al., 2003b). Regions of high signal intensity (slow R_2^*) are thought to delineate well-oxygenated/perfused areas of tumour whilst dark areas (fast R_2^*) are thought to indicate poorly perfused/necrotic regions (Robinson et al., 2000). A clinical study investigating prostate cancer hypoxia compared R_2^* maps with pimonidazole (a hypoxic marker) immuno-staining of co-registered histological sections. Preliminary results showed that regions with a fast R_2^* (defined as $\geq 28\ s^{-1}$) were positively correlated with hypoxia (with a sensitivity and specificity of 96% and 59% respectively) (Taylor et al., 2003).

1.5.5 The use of MRI in the assessment of vascular disruptive agents

T_1-weighted DCE-MRI has been used to investigate the acute effects of vascular disruptive agents in animal models: CA-4-P (Beauregard et al., 2001; Beauregard et al., 2002; Beauregard et al., 1998; Galbraith et al., 2003; Maxwell et al., 2002); DMXAA (Beauregard et al., 2002); ZD6126 (Evelhoch et al., 2004; Robinson et al., 2003a). Acute reductions in semi-quantitative and/or quantitative parameters are seen within 24 hours of treatment in a range of tumour types. Similar results were seen in phase I clinical trials of vascular disruptive agents which used change in DCE-MRI parameters as biomarkers for vascular disruptive effect: CA-4-P (Dowlati et al., 2002; Galbraith et al., 2003; Stevenson et al., 2003); DMXAA (Galbraith et al., 2002); ZD6126 (Evelhoch et al., 2004).

As K^{trans} has both blood flow and permeability components (see above), reduction in K^{trans} cannot be directly equated to the acute blood flow shutdown seen with CA-4-P using intravital microscopy. However, the use of DCE-MRI to assess response to vascular disruptive agents has been validated by Maxwell et al. (Maxwell et al., 2002). Changes in K^{trans} in response to CA-4-P in a rat carcinosarcoma model matched changes in blood flow rate measured using uptake of radiolabelled ^{125}iodoantipyrine (IAP). Reductions in absolute tumour blood flow rate at 4 and 24 hours as measured by IAP correlated with reductions in K^{trans} (and IAUGC) as measured by DCE-MRI. Although the size of the decrease seen in K^{trans} was smaller than that seen in tumour blood flow rate, the time course and dose-dependency patterns were very similar. Reductions in v_e were also seen, with no significant change in k_{ep}. Treatment with CA-4-P may alter Gd-DTPA kinetics such that, in this situation, blood flow rate is the dominant influence on K^{trans}.

The fall in v_e seen in the study by Maxwell et al. (Maxwell et al., 2002) seems counter-intuitive. CA-4-P increases vascular permeability to macromolecules (Kanthou & Tozer, 2002) which would lead to oedema and an increase in extracellular space – which is not consistent with a fall in v_e. However, as CA-4-P results in the complete shutdown of a large proportion of tumour blood vessels (Dark et al., 1997) then some tumour areas will be cut off from flowing blood – and this would explain the fall in v_e seen (Maxwell et al., 2002). Therefore, v_e represents the fraction of EES to which Gd-DTPA has access rather than the entire EES (Maxwell et al., 2002).

Lyng et al. (Lyng et al., 1998) have compared measurement of tumour blood flow rate using uptake of ^{86}rubidium chloride (^{86}RbCl) or ^{14}carbon-labelled IAP (^{14}C-IAP) with DCE-

MRI parameters in two melanoma xenograft models. They used the Kety model directly for Gd-DTPA kinetics to obtain separate values for the extraction fraction, E, and for tumour blood flow (which they designate '$PERF_{Kety}$' and which is expressed in $ml.min^{-1}$ per unit gram of tissue) (Lyng et al., 1998) – see **Section 1.4.2.2.**[8] Extraction fractions were >70% and tumour blood flow rates, as measured by $PERF_{Kety}$ (based on Gd-DTPA concentration data), were almost identical to values obtained using the $^{86}RbCl$ or ^{14}C-IAP methods for the two tumour types. In contrast, DCE-MRI parameters derived from signal-intensity or Gd-DTPA-concentration time curves (initial uptake rate, maximum uptake) did not provide reliable estimates of relative blood flow rate (Lyng et al., 1998). Although this study did not measure K^{trans} directly, it adds support to the proposition that K^{trans} is flow-dominated, at least for extra-cranial tumours. As K^{trans} incorporates E, it will under-estimate true tumour blood flow rate - by approximately 15-30% (based on Lyng et al.'s and Maxwell et al.'s data (Lyng et al., 1998; Maxwell et al., 2002).

The pattern and time course of changes in K^{trans} seen in a clinical phase I trial of CA-4-P was similar to that seen in animal models (Galbraith et al., 2003) indicating the appropriateness of using K^{trans} as a surrogate marker of vascular response to treatment. This view has been endorsed by a specialist panel meeting under the auspices of Cancer Research UK - the Pharmacodynamic/Pharmacokinetic Technologies Advisory Committee (PTAC) - who considered the measurement and analysis methodology requirements for robust application of DCE-MRI to vascular disruptive clinical trials (Leach et al., 2005).

BOLD-MRI has also been used to monitor the acute effects of vascular disruptive agents (Robinson et al., 2003a) – see the discussion sections in **Chapters 2 and 3.**

[8] In the Tofts' model, K^{trans} is expressed per unit volume of tissue. K^{trans} is related to $PERF_{kety}$ as $K^{trans} = E.PERF_{kety}.\rho(1\text{-}Hct)$, where ρ is tissue density and Hct is haematocrit (Tofts et al, 1999).

1.5.5 Further development of DCE-MRI to assess vascular disruptive response

The work presented in this thesis has attempted to explore further whether MRI methods can be relied upon to define a drug as having vascular disruptive activity. In particular, to investigate whether the acute DCE-MRI changes seen with CA-4-P do not also occur with conventional cytotoxic agents. It is assumed that the acute blood vessel shutdown seen in response to treatment with vascular disruptive agents is unique to this class of agent and so acute reductions in T_1-DCE-MRI parameters, such as K^{trans}, would not be seen in response to conventional cytotoxic agents. It is important to confirm this supposition - firstly, to aid interpretation of any DCE-MRI examinations performed to assess response to the vascular disruptive agent, and secondly, to determine any overlapping toxicities.

DCE-MRI has also been used to investigate further the acute vascular disruptive response to CA-4-P in a pre-clinical study. The combination of CA-4-P and radioimmunotherapy (using ^{131}I-A5B7, an anti-CEA antibody[9], in the SW1222 colorectal cancer xenograft) has led to tumour cures (Pedley et al., 2001) and is now being tested in a phase I clinical trial. It is presumed that the combination is effective due to additive effects and also increased antibody retention in tumour. However, the pre-clinical study used a relatively high dose of CA-4-P (200 mg.kg^{-1}) and did not investigate the effectiveness of lower doses. It would be helpful to investigate the effect of lower, more clinically relevant, doses of CA-4-P and compare the magnitude of vascular disruptive effect (using DCE-MRI) to effect on antibody retention and therapeutic efficacy.

[9] CEA: carcino-embryonic antigen

1.6 Aims of thesis

The main objective of the work presented in this thesis is the application and further development of MRI as a non-invasive method of investigating functional aspects of the tumour microcirculation. In particular, the validity and role of using DCE-MRI for assessment of acute tumour response to vascular disruptive agents and the development of BOLD-MRI as a non-invasive method of evaluating tumour vessel maturity were investigated.

The specific aims of this thesis were:

- To use T_1-weighted DCE-MRI to determine whether conventional cytotoxic agents cause any acute damage to the tumour vasculature in patients with pelvic or abdominal gynaecological tumours. In particular, to determine the reproducibility of this technique in this patient group and then to assess the acute response (<24 hours) to chemotherapy. In addition, to determine the reproducibility of BOLD-MRI (R_2*) and T_2*-weighted DCE-MRI (rBV and rBF) measurements in this patient group and to further explore the use of these parameters for the assessment of the tumour microcirculation (**Chapter 2**).

- To use T_1-weighted DCE-MRI to investigate the acute effects (at 4 and 24 hours) of 3 different dose levels of CA-4-P (30, 100 and 200 $mg.kg^{-1}$) on the SW1222 tumour in mice. (**Chapter 3**).

- To further explore BOLD-MRI as a clinically applicable technique for the assessment of tumour vascular maturity. In particular, to determine if Neeman et al's technique using BOLD-MRI response to air then air-5% CO_2/carbogen can be applied to the assessment of different tumour types with different degrees of vessel maturity (HT29, CaNT and T138). Also, to determine whether using a vasoconstrictor, Angiotensin II, with BOLD-MRI can discriminate between mature and immature vessels. In addition, to use intravital microscopy to directly observe tumour vessel response to these agents, in order to aid interpretation of BOLD-MRI results (**Chapter 4**).

1.7 References: Chapter 1

Abramovitch, R., Dafni, H., Smouha, E., Benjamin, L. & Neeman, M. (1999). In vivo prediction of vascular susceptibility to vascular susceptibility endothelial growth factor withdrawal: magnetic resonance imaging of C6 rat glioma in nude mice. *Cancer Res*, **59**, 5012-6.

Abramovitch, R., Frienkiel, D. & Neeman, M. (1998). Analysis of Subcutaneous Angiogenesis by Gradient Echo Magnetic Resonance Imaging. *Magn Reson Med*, **39**, 813-824.

Ackroyd, R., Brown, N.J., Davis, M.F., Stephenson, T.J., Marcus, S.L., Stoddard, C.J., Johnson, A.G. & Reed, M.W. (2000). Photodynamic therapy for dysplastic Barrett's oesophagus: a prospective, double blind, randomised, placebo controlled trial. *Gut*, **47**, 612-7.

Adam, M.F., Dorie, M.J. & Brown, J.M. (1999). Oxygen tension measurements of tumors growing in mice. *Int J Radiat Oncol Biol Phys*, **45**, 171-80.

Ahmed, B., Van Eijk, L.I., Bouma-Ter Steege, J.C., Van Der Schaft, D.W., Van Esch, A.M., Joosten-Achjanie, S.R., Lambin, P., Landuyt, W. & Griffioen, A.W. (2003). Vascular targeting effect of combretastatin A-4 phosphate dominates the inherent angiogenesis inhibitory activity. *Int J Cancer*, **105**, 20-5.

Ah-See, M.-L.W., Makris, A., Taylor, N.J., Harrison, M., Richman, P.I., D'Arcy, J.A., Burcombe, R.J., Pittam, M.R., Ravichandran, D., Stirling, J.J., Leach, M.O. & Padhani, A.R. (2004). T1 and T2* weighted dynamic contrast-enhanced MRI predicts for clinico-pathological response to neoadjuvant chemotherapy in primary breast cancer. In *Proc. ISMRM*, Vol. 12. pp. 1992: Kyoto, Japan.

Alberts, B., Bray, D., Lewis, J., Raff, M., Roberts, K. & Watson, J.D. (1989). *Molecular Biology of the Cell*. Garland Publishing Inc.: New York.

Alon, T., Hemo, I., Itin, A., Pe'er, J., Stone, J. & Keshet, E. (1995). Vascular endothelial growth factor acts as a survival factor for newly formed retinal vessels and has implications for retinopathy of prematurity. *Nat Med*, **1**, 1024-8.

Anderson, H. & Price, P. (2002). Clinical measurement of blood flow in tumours using positron emission tomography: a review. *Nucl Med Commun*, **23**, 131-8.

Anderson, H., Price, P., Blomley, M., Leach, M.O. & Workman, P. (2001). Measuring changes in human tumour vasculature in response to therapy using functional imaging techniques. *Br J Cancer*, **85**, 1085-93.

Anderson, H.L., Yap, J.T., Miller, M.P., Robbins, A., Jones, T. & Price, P.M. (2003). Assessment of pharmacodynamic vascular response in a phase I trial of combretastatin A4 phosphate. *J Clin Oncol*, **21**, 2823-30.

Arap, W., Pasqualini, R. & Ruoslahti, E. (1998). Cancer treatment by targeted drug delivery to tumour vasculature in a mouse model. *Science*, **279**, 377-380.

Aronen, H.J., Gazit, I.E., Louis, D.N., Buchbinder, B.R., Pardo, F.S., Weisskoff, R.M., Harsh, G.R., Cosgrove, G.R., Halpern, E.F., Hochberg, F.H. & et al. (1994). Cerebral blood volume maps of gliomas: comparison with tumor grade and histologic findings. *Radiology*, **191**, 41-51.

Asahara, T., Masuda, H., Takahashi, T., Kalka, C., Pastore, C., Silver, M., Kearne, M., Magner, M. & Isner, J.M. (1999). Bone marrow origin of endothelial progenitor cells responsible for postnatal vasculogenesis in physiological and pathological neovascularization. *Circ Res*, **85**, 221-8.

Axel, L. (1980). Cerebral blood flow determination by rapid-sequence computed tomography: theoretical analysis. *Radiology*, **137**, 679-86.

Axel, L. (1983). Tissue mean transit time from dynamic computed tomography by a simple deconvolution technique. *Invest Radiol*, **18**, 94-9.

Baguley, B.C. (2003). Antivascular therapy of cancer: DMXAA. *Lancet Oncol*, **4**, 141-8.

Baguley, B.C. & Ching, L.M. (2002). DMXAA: an antivascular agent with multiple host responses. *Int J Radiat Oncol Biol Phys*, **54**, 1503-11.

Baguley, B.C., Holdaway, K.H., Thomsen, L.L., Zhuang, L. & Zwi, L. (1991). Inhibition of growth of colon 38 adenocarcinoma by vinblastine and colchicine: evidence for a vascular mechanism. *Eur J Cancer*, **27**, 482-487.

Baguley, B.C., Zhuang, L. & Kestell, P. (1997). Increased plasma serotonin following treatment with flavone-8-acetic acid, 5,6-dimethylxanthenone-4-acetic acid, vinblastine, and colchicine: relation to vascular effects. *Oncol Res*, **9**, 55-60.

Barbier, E.L., den Boer, J.A., Peters, A.R., Rozeboom, A.R., Sau, J. & Bonmartin, A. (1999). A model of the dual effect of gadopentetate dimeglumine on dynamic brain MR images. *J Magn Reson Imaging*, **10**, 242-53.

Bates, D.O. & Curry, F.E. (1996). Vascular endothelial growth factor increases hydraulic conductivity of isolated perfused microvessels. *Am J Physiol*, **271**, H2520-8.

Beauregard, D.A., Hill, S.A., Chaplin, D.J. & Brindle, K.M. (2001). The susceptibility of tumors to the antivascular drug combretastatin A4 phosphate correlates with vascular permeability. *Cancer Res*, **61**, 6811-5.

Beauregard, D.A., Pedley, R.B., Hill, S.A. & Brindle, K.M. (2002). Differential sensitivity of two adenocarcinoma xenografts to the anti-vascular drugs combretastatin A4 phosphate and 5,6-dimethylxanthenone-4-acetic acid, assessed using MRI and MRS. *NMR Biomed*, **15**, 99-105.

Beauregard, D.A., Thelwall, P.E., Chaplin, D.J., Hill, S.A., Adams, G.E. & Brindle, K.M. (1998). Magnetic resonance imaging and spectroscopy of combretastatin A4 prodrug-induced disruption of tumour perfusion and energetic status. *Br J Cancer*, **77**, 1761-7.

Bell, K.M. & Chaplin, D.J. (1998). The effect of oxygen and carbon dioxide on tumor cell endothelin-1 production. *J Cardiovasc Pharmacol*, **31 Suppl 1**, S537-40.

Bell, K.M., Prise, V.E., Shaffi, K.M., Chaplin, D.J. & Tozer, G.M. (1996). A comparative study of tumour blood flow modification in two rat tumour systems using endothelin-1 and angiotensin II: influence of tumour size on angiotensin II response. *Int J Cancer*, **67**, 730-8.

Belliveau, J.W., Rosen, B.R., Kantor, H.L., Rzedzian, R.R., Kennedy, D.N., McKinstry, R.C., Vevea, J.M., Cohen, M.S., Pykett, I.L. & Brady, T.J. (1990). Functional cerebral imaging by susceptibility-contrast NMR. *Magn Reson Med*, **14**, 538-46.

Benjamin, L., Golijanin, D., Itin, A., Pode, D. & Keshet, E. (1999). Selective ablation of immature blood vessels in established human tumors follows vascular endothelial growth factor withdrawal [see comments]. *J Clin Invest*, **103**, 159-65.

Benjamin, L.E., Hemo, I. & Keshet, E. (1998). A plasticity window for blood vessel remodelling is defined by pericyte coverage of the preformed endothelial network and is regulated by PDGF- B and VEGF. *Development*, **125**, 1591-8.

Benner, T., Heiland, S., Erb, G., Forsting, M. & Sartor, K. (1997). Accuracy of gamma-variate fits to concentration-time curves from dynamic susceptibility-contrast enhanced MRI: influence of time resolution, maximal signal drop and signal-to-noise. *Magn Reson Imaging*, **15**, 307-17.

Bibby, M.C., Double, J.A., Loadman, P.M. & Duke, C.V. (1989). Reduction of tumor blood flow by flavone acetic acid: a possible component of therapy. *J Natl Cancer Inst*, **81**, 216-20.

Bird, A. & Telfer, A. (1965). Effect of hyperbaric oxygen on limb circulation. *The Lancet*, **1**, 355-6.

Bohle, A.S., Leuschner, I., Kalthoff, H. & Henne-Bruns, D. (2000). Combretastatin A-4 prodrug: a potent inhibitor of malignant hemangioendothelioma cell proliferation. *Int J Cancer*, **87**, 838-43.

Borsi, L., Balza, E., Carnemolla, B., Sassi, F., Castellani, P., Berndt, A., Kosmehl, H., Biro, A., Siri, A., Orecchia, P., Grassi, J., Neri, D. & Zardi, L. (2003). Selective targeted delivery of TNFalpha to tumor blood vessels. *Blood*, **102**, 4384-92.

Boucher, Y., Baxter, L.T. & Jain, R.K. (1990). Interstitial pressure gradients in tissue-isolated and subcutaneous tumors: implications for therapy. *Cancer Res*, **50**, 4478-84.

Boucher, Y., Leunig, M. & Jain, R.K. (1996). Tumor angiogenesis and interstitial hypertension. *Cancer Res*, **56**, 4264-6.

Boxerman, J.L., Rosen, B.R. & Weisskoff, R.M. (1997). Signal-to-noise analysis of cerebral blood volume maps from dynamic NMR imaging studies. *J Magn Reson Imaging*, **7**, 528-37.

Boyland, E. & Boyland, M. (1937). Studies in tissue metabolism. IX. The action of colchicine and *B.typhosus* extract. *Biochem J*, **31**, 454-460.

Brizel, D., Scully, S., Harrelson, J., Layfield, L., Bean, J., Prosnitz, L. & Dewhirst, M. (1996). Tumor oxygenation predicts for the likelihood of distant metastases in human soft tissue sarcoma. *Cancer Res*, **56**, 941-3.

Brown, J.M. (1979). Evidence for acutely hypoxic cells in mouse tumours, and a possible mechanism of reoxygenation. *Br J Radiol*, **52**, 650-6.

Brown, L.F., Berse, B., Jackman, R.W., Tognazzi, K., Guidi, A.J., Dvorak, H.F., Senger, D.R., Connolly, J.L. & Schnitt, S.J. (1995). Expression of vascular permeability factor (vascular endothelial growth factor) and its receptors in breast cancer. *Hum Pathol*, **26**, 86-91.

Brown, N.J., Staton, C.A., Rodgers, G.R., Corke, K.P., Underwood, J.C. & Lewis, C.E. (2002). Fibrinogen E fragment selectively disrupts the vasculature and inhibits the growth of tumours in a syngeneic murine model. *Br J Cancer*, **86**, 1813-6.

Bruening, R., Berchtenbreiter, C., Holzknecht, N., Essig, M., Wu, R.H., Simmons, A., Heuck, A., Maschek, A., Meusel, M., Williams, S.C., Cox, T., Knopp, M.V. & Reiser, M. (2000). Effects of three different doses of a bolus injection of gadodiamide: assessment of regional cerebral blood volume maps in a blinded reader study. *AJNR Am J Neuroradiol*, **21**, 1603-10.

Burke, D., Davies, M.M., Zweit, J., Flower, M.A., Ott, R.J., Dworkin, M.J., Glover, C., McCready, V.R., Carnochan, P. & Allen-Mersh, T.G. (2001). Continuous angiotensin II infusion increases tumour: normal blood flow ratio in colo-rectal liver metastases. *Br J Cancer*, **85**, 1640-5.

Burrows, F.J. & Thorpe, P.E. (1993). Eradication of large solid tumors in mice with an immunotoxin directed against tumor vasculature. *Proc Natl Acad Sci U S A*, **90**, 8996-9000.

Burton, M.A., Gray, B.N., Self, G.W., Heggie, J.C. & Townsend, P.S. (1985). Manipulation of experimental rat and rabbit liver tumor blood flow with angiotensin II. *Cancer Res*, **45**, 5390-3.

Buxton, R.B. (2002). *Introduction to Functional Magnetic Resonance Imaging: Principles and Techniques*. Cambridge University Press: Cambridge, UK.

Cao, Z., Baguley, B.C. & Ching, L.M. (2001). Interferon-inducible protein 10 induction and inhibition of angiogenesis in vivo by the antitumor agent 5,6-dimethylxanthenone-4-acetic acid (DMXAA). *Cancer Res*, **61**, 1517-21.

Carmeliet, P. (2000). Mechanisms of angiogenesis and arteriogenesis. *Nat Med*, **6**, 389-95.

Carmeliet, P. (2003). Angiogenesis in health and disease. *Nat Med*, **9**, 653-60.

Carpenito, C., Davis, P.D., Dougherty, S.T. & Dougherty, G.J. (2002). Exploiting the differential production of angiogenic factors within the tumor microenvironment in the design of a novel vascular-targeted gene therapy-based approach to the treatment of cancer. *Int J Radiat Oncol Biol Phys*, **54**, 1473-8.

Carr, P., Graves, J.E. & Poston, L. (1993). Carbon dioxide induced vasorelaxation in rat mesenteric small arteries precontracted with noradrenaline is endothelium dependent and mediated by nitric oxide. *Pflugers Arch*, **423**, 343-5.

Cenic, A., Nabavi, D.G., Craen, R.A., Gelb, A.W. & Lee, T.Y. (2000). A CT method to measure hemodynamics in brain tumors: validation and application of cerebral blood flow maps. *AJNR Am J Neuroradiol*, **21**, 462-70.

Cerniglia, G.J., Wilson, D.F., Pawlowski, M., Vinogradov, S. & Biaglow, J. (1997). Intravascular oxygen distribution in subcutaneous 9L tumors and radiation sensitivity. *J Appl Physiol*, **82**, 1939-45.

Chabot, G.G., Branellec, D., Sassi, A., Armand, J.P., Gouyette, A. & Chouaib, S. (1993). Tumour necrosis factor-alpha plasma levels after flavone acetic acid administration in man and mouse. *Eur J Cancer*, **29A**.

Chambers, R.C., Leoni, P., Kaminski, N., Laurent, G.J. & Heller, R.A. (2003). Global expression profiling of fibroblast responses to transforming growth factor-beta1 reveals the induction of inhibitor of differentiation-1 and provides evidence of smooth muscle cell phenotypic switching. *Am J Pathol*, **162**, 533-46.

Chang, S.S., O'Keefe, D.S., Bacich, D.J., Reuter, V.E., Heston, W.D. & Gaudin, P.B. (1999a). Prostate-specific membrane antigen is produced in tumor-associated neovasculature. *Clin Cancer Res*, **5**, 2674-81.

Chang, S.S., Reuter, V.E., Heston, W.D., Bander, N.H., Grauer, L.S. & Gaudin, P.B. (1999b). Five different anti-prostate-specific membrane antigen (PSMA) antibodies confirm PSMA expression in tumor-associated neovasculature. *Cancer Res*, **59**, 3192-8.

Chang, Y.S., di Tomaso, E., McDonald, D.M., Jones, R., Jain, R.K. & Munn, L.L. (2000). Mosaic blood vessels in tumors: frequency of cancer cells in contact with flowing blood. *Proc Natl Acad Sci U S A*, **97**, 14608-13.

Chaplin, D. & Dougherty, G. (1999). Tumour vasculature as a target for cancer therapy. *Br J Cancer*, **80 Suppl 1**, 57-64.

Chaplin, D. & Hill, S. (2002). The development of Combretastatin A4 phosphate as a vascular targeting agent. *Int J Radiat Oncol Biol Phys*, **54**, 1491-1496.

Chaplin, D., Horsman, M., Trotter, M. & Siemann, D. (1998a). Therapeutic significance of microenvironmental factors. In *Blood perfusion and microenvironment of human tumours: implications for clinical radiooncology*, Molls, M. & Vaupel, P. (eds) pp. 131-143. Springer-Verlag: Berlin.

Chaplin, D.J., Hill, S.A., Bell, K.M. & Tozer, G.M. (1998b). Modification of tumor blood flow: current status and future directions. *Semin Radiat Oncol*, **8**, 151-63.

Chaplin, D.J., Olive, P.L. & Durand, R.E. (1987). Intermittent blood flow in a murine tumor: radiobiological effects. *Cancer Res*, **47**, 597-601.

Chaplin, D.J., Pettit, G.R. & Hill, S.A. (1999). Anti-vascular approaches to solid tumour therapy: evaluation of combretastatin A4 phosphate. *Anticancer Res*, **19**, 189-95.

Checkley, D., Tessier, J.J., Kendrew, J., Waterton, J.C. & Wedge, S.R. (2003). Use of dynamic contrast-enhanced MRI to evaluate acute treatment with ZD6474, a VEGF signalling inhibitor, in PC-3 prostate tumours. *Br J Cancer*, **89**, 1889-95.

Ching, L.M., Cao, Z., Kieda, C., Zwain, S., Jameson, M.B. & Baguley, B.C. (2002). Induction of endothelial cell apoptosis by the antivascular agent 5,6-Dimethylxanthenone-4-acetic acid. *Br J Cancer*, **86**, 1937-42.

Ching, L.M., Joseph, W.R., Crosier, K.E. & Baguley, B.C. (1994). Induction of tumor necrosis factor-alpha messenger RNA in human and murine cells by the flavone acetic acid analogue 5,6-dimethylxanthenone-4-acetic acid (NSC 640488). *Cancer Res*, **54**, 870-2.

Ching, L.M., Zwain, S. & Baguley, B.C. (2004). Relationship between tumour endothelial cell apoptosis and tumour blood flow shutdown following treatment with the antivascular agent DMXAA in mice. *Br J Cancer*, **90**, 906-10.

Cliffe, S., Taylor, M.L., Rutland, M., Baguley, B.C., Hill, R.P. & Wilson, W.R. (1994). Combining bioreductive drugs (SR 4233 or SN 23862) with the vasoactive agents flavone acetic acid or 5,6-dimethylxanthenone acetic acid. *Int J Radiat Oncol Biol Phys*, **29**, 373-7.

Collingridge, D.R. (1997). Measurement and manipulation of tumour oxygen tension. In *Dept of Oncology*. University College: London.

Crocker, D.J., Murad, T.M. & Geer, J.C. (1970). Role of the pericyte in wound healing. An ultrastructural study. *Exp Mol Pathol*, **13**, 51-65.

Cuenca, R.E., Allison, R.R., Sibata, C. & Downie, G.H. (2004). Breast cancer with chest wall progression: treatment with photodynamic therapy. *Ann Surg Oncol*, **11**, 322-7.

Dark, G.G., Hill, S.A., Prise, V.E., Tozer, G.M., Pettit, G.R. & Chaplin, D.J. (1997). Combretastatin A-4, an agent that displays potent and selective toxicity toward tumour vasculature. *Cancer Res*, **57**, 1829-1834.

Davis, P.D., Dougherty, G.J., Blakey, D.C., Galbraith, S.M., Tozer, G.M., Holder, A.L., Naylor, M.A., Nolan, J., Stratford, M.R., Chaplin, D.J. & Hill, S.A. (2002). ZD6126: a novel vascular-targeting agent that causes selective destruction of tumor vasculature. *Cancer Res*, **62**, 7247-53.

Davis, T.L., Kwong, K.K., Weisskoff, R.M. & Rosen, B.R. (1998). Calibrated functional MRI: mapping the dynamics of oxidative metabolism. *Proc Natl Acad Sci U S A*, **95**, 1834-9.

Denekamp, J. (1982). Endothelial cell proliferation as a novel approach to targeting tumour therapy. *Br J Cancer*, **45**, 136-9.

Denekamp, J., Hill, S.A. & Hobson, B. (1983). Vascular occlusion and tumour cell death. *Eur J Cancer Clin Oncol*, **19**, 271-5.

Denekamp, J. & Hobson, B. (1982). Endothelial-cell proliferation in experimental tumours. *Br J Cancer*, **46**, 711-20.

Dewhirst, M., Madwed, D., Meyer, R., Ong, E., Klitzman, B., Rosner, G. & Dodge, R. (1994). Reduction in tumor blood flow in skin flap tumor after hydralazine is not due to a vascular steal phenomenon. *Radiat Oncol Invest*, **1**, 270-278.

Dewhirst, M.W., Gustafson, C., Gross, J.F. & Tso, C.Y. (1987). Temporal effects of 5.0 Gy radiation in healing subcutaneous microvasculature of a dorsal flap window chamber. *Radiat Res*, **112**, 581-91.

Dewhirst, M.W., Ong, E.T., Braun, R.D., Smith, B., Klitzman, B., Evans, S.M. & Wilson, D. (1999). Quantification of longitudinal tissue pO2 gradients in window chamber tumours: impact on tumour hypoxia. *Br J Cancer*, **79**, 1717-22.

Dewhirst, M.W., Ong, E.T., Klitzman, B., Secomb, T.W., Vinuya, R.Z., Dodge, R., Brizel, D. & Gross, J.F. (1992). Perivascular oxygen tensions in a transplantable mammary tumor growing in a dorsal flap window chamber. *Radiat Res*, **130**, 171-82.

Dewhirst, M.W., Ong, E.T., Rosner, G.L., Rehmus, S.W., Shan, S., Braun, R.D., Brizel, D.M. & Secomb, T.W. (1996). Arteriolar oxygenation in tumour and subcutaneous arterioles: effects of inspired air oxygen content. *Br J Cancer Suppl*, **27**, S241-6.

Djonov, V., Andres, A.C. & Ziemiecki, A. (2001). Vascular remodelling during the normal and malignant life cycle of the mammary gland. *Microsc Res Tech*, **52**, 182-9.

Djonov, V., Schmid, M., Tschanz, S.A. & Burri, P.H. (2000). Intussusceptive angiogenesis: its role in embryonic vascular network formation. *Circ Res*, **86**, 286-92.

Dolmans, D.E., Kadambi, A., Hill, J.S., Waters, C.A., Robinson, B.C., Walker, J.P., Fukumura, D. & Jain, R.K. (2002). Vascular accumulation of a novel photosensitizer, MV6401, causes selective thrombosis in tumor vessels after photodynamic therapy. *Cancer Res*, **62**, 2151-6.

Donahue, K., Burstein, D., Manning, W. & Gray, M. (1994). Studies of Gd-DTPA relaxivity and proton exchange rates in tissue. *Magn Reson Med*, **32**, 66-76.

Dowlati, A., Robertson, K., Cooney, M., Petros, W.P., Stratford, M., Jesberger, J., Rafie, N., Overmoyer, B., Makkar, V., Stambler, B., Taylor, A., Waas, J., Lewin, J.S., McCrae, K.R. & Remick, S.C. (2002). A phase I pharmacokinetic and translational study of the novel vascular targeting agent combretastatin a-4 phosphate on a single-dose intravenous schedule in patients with advanced cancer. *Cancer Res*, **62**, 3408-16.

Du Sault, L. (1963). The effect of oxygen on the response of spontaneous tumours in mice to radiotherapy. *Br J Radiol*, **36**, 749-54.

Dunn, T., Braun, R., Rhemus, W., Secomb, T., Tozer, G., Chaplin, D. & Dewhirst, M. (1999). The effects of hyperoxic and hypercarbic gases on tumour blood flow. *Br J Cancer*, **80**, 117-126.

Dvorak, H.F., Nagy, J.A., Dvorak, J.T. & Dvorak, A.M. (1988). Identification and characterization of the blood vessels of solid tumors that are leaky to circulating macromolecules. *Am J Pathol*, **133**, 95-109.

Dworkin, M.J., Carnochan, P. & Allen-Mersh, T.G. (1997). Effect of continuous regional vasoactive agent infusion on liver metastasis blood flow. *Br J Cancer*, **76**, 1205-10.

Dworkin, M.J., Zweit, J., Carnochan, P., Deehan, B. & Allen-Mersh, T.G. (1996). Effect of regional angiotensin II infusion on the relationship between tumour blood flow and fluorouracil uptake in a liver metastasis animal model. *Eur J Cancer*, **32A**, 1580-4.

Eberhard, A., Kahlert, S., Goede, V., Hemmerlein, B., Plate, K.H. & Augustin, H.G. (2000). Heterogeneity of angiogenesis and blood vessel maturation in human tumors: implications for antiangiogenic tumor therapies. *Cancer Res*, **60**, 1388-93.

Eggermont, A., Schraffordt Koops, H., Lienard, D., Kroon, B., van Geel, A., Hoekstra, H. & Lejeune, F. (1996). Isolated limb perfusion with high-dose tumor necrosis factor-α in combination with interferon-γ and melphalan for nonresectable extremity soft tissue sarcomas: a multicentre trial. *J Clin Oncol*, **14**, 2653-2665.

Eikesdal, H.P., Bjerkvig, R., Mella, O. & Dahl, O. (2001). Combretastatin A-4 and hyperthermia;a potent combination for the treatment of solid tumors. *Radiother Oncol*, **60**, 147-54.

Endrich, B., Reinhold, H.S., Gross, J.F. & Intaglietta, M. (1979). Tissue perfusion inhomogeneity during early tumor growth in rats. *J Natl Cancer Inst*, **62**, 387-95.

Engbrecht, B.W., Menon, C., Kachur, A.V., Hahn, S.M. & Fraker, D.L. (1999). Photofrin-mediated photodynamic therapy induces vascular occlusion and apoptosis in a human sarcoma xenograft model. *Cancer Res*, **59**, 4334-42.

Evelhoch, J., LoRusso, P., DelProposto, Z., Stark, K., Latif, Z., Morton, P., Waterton, J., Wheeler, C. & Barge, A. (2002). Dynamic contrast-enhanced MRI evaluation of the effects of ZD6126 on tumor vasculature in a phase I clinical trial. In *Proc ISMRM*, Vol. 10. pp. 2095: Honolulu, Hawaii.

Evelhoch, J.L. (1999). Key factors in the acquisition of contrast kinetic data for oncology. *J Magn Reson Imaging*, **10**, 254-9.

Evelhoch, J.L., LoRusso, P.M., He, Z., DelProposto, Z., Polin, L., Corbett, T.H., Langmuir, P., Wheeler, C., Stone, A., Leadbetter, J., Ryan, A.J., Blakey, D.C. & Waterton, J.C. (2004). Magnetic resonance imaging measurements of the response of murine and human tumors to the vascular-targeting agent ZD6126. *Clin Cancer Res*, **10**, 3650-7.

Folkman, J. (1971). Tumor angiogenesis: therapeutic implications. *New Engl J Med*, **285**, 1182-6.

Forsythe, J.A., Jiang, B.H., Iyer, N.V., Agani, F., Leung, S.W., Koos, R.D. & Semenza, G.L. (1996). Activation of vascular endothelial growth factor gene transcription by hypoxia-inducible factor 1. *Mol Cell Biol*, **16**, 4604-13.

Fox, S.B., Gasparini, G. & Harris, A.L. (2001). Angiogenesis: pathological, prognostic, and growth-factor pathways and their link to trial design and anticancer drugs. *Lancet Oncol*, **2**, 278-89.

Fukumura, D., Yuan, F., Monsky, W., Chen, Y. & Jain, R. (1997). Effect of host microenvironment on the microcirculation of human colon adenocarcinoma. *Am J Pathol*, **151**, 679-88.

Furman-Haran, E., Margalit, R., Grobgeld, D. & Degani, H. (1996). Dynamic contrast-enhanced magnetic resonance imaging reveals stress-induced angiogenesis in MCF7 human breast tumors. *Proc Natl Acad Sci U S A*, **93**, 6247-51.

Gadgeel, S.M., LoRusso, P.M., Wozniak, A.J. & Wheeler, C. (2002). A dose-escalation study of the novel vascular-targeting agent, ZD6126, in patients with solid tumors. In *Proc ASCO* pp. 438.

Galbraith, S.M., Chaplin, D.J., Lee, F., Stratford, M.R., Locke, R.J., Vojnovic, B. & Tozer, G.M. (2001). Effects of combretastatin A4 phosphate on endothelial cell morphology in vitro and relationship to tumour vascular targeting activity in vivo. *Anticancer Res*, **21**, 93-102.

Galbraith, S.M., Maxwell, R.J., Lodge, M.A., Tozer, G.M., Wilson, J., Taylor, N.J., Stirling, J.J., Sena, L., Padhani, A.R. & Rustin, G.J.S. (2003). Combretastatin A4 Phosphate has tumour anti-vascular activity in rat and man as demonstrated by dynamic magnetic resonance imaging. *J Clin Oncol*, **21**, 2831-2842.

Galbraith, S.M., Rustin, G.J.S., Lodge, M.A., Taylor, N.J., Stirling, J.J., Jameson, M., Thompson, P., Hough, D., Gumbrell, L. & Padhani, A.R. (2002). Effects of 5,6-dimethylxanthenone-4-acetic acid on human tumor microcirculation assessed by dynamic contrast-enhanced magnetic resonance imaging. *J Clin Oncol*, **20**, 3826-40.

Gilead, A., Meir, G. & Neeman, M. (2004). The role of angiogenesis, vascular maturation, regression and stroma infiltration in dormancy and growth of implanted MLS ovarian carcinoma spheroids. *Int J Cancer*, **108**, 524-31.

Goede, V., Schmidt, T., Kimmina, S., Kozian, D. & Augustin, H.G. (1998). Analysis of blood vessel maturation processes during cyclic ovarian angiogenesis. *Lab Invest*, **78**, 1385-94.

Goertz, D.E., Yu, J.L., Kerbel, R.S., Burns, P.N. & Foster, F.S. (2002). High-frequency Doppler ultrasound monitors the effects of antivascular therapy on tumor blood flow. *Cancer Res*, **62**, 6371-5.

Goldberg, J.A., Thomson, J.A., Bradnam, M.S., Fenner, J., Bessent, R.G., McKillop, J.H., Kerr, D.J. & McArdle, C.S. (1991). Angiotensin II as a potential method of targeting cytotoxic-loaded microspheres in patients with colorectal liver metastases. *Br J Cancer*, **64**, 114-9.

Goodchild, K., Hill, S., Sibtain, A., Chaplin, D. & Makris, A. (2001). Assessment of microregional blood flow in human breast carcinomas after administration of anthracycline chemotherapy. *Br J Cancer*, **85 (Suppl 1)**, 48.

Graeber, T., Osmanian, C., Jacks, T., Housman, D., Koch, C., Lowe, S. & Giaccia, A. (1996). Hypoxia-mediated selection of cells with diminished apoptotic potential in solid tumours [see comments]. *Nature*, **379**, 88-91.

Grau, C., Horsman, M.R. & Overgaard, J. (1992). Improving the radiation response in a C3H mouse mammary carcinoma by normobaric oxygen or carbogen breathing. *Int J Radiat Oncol Biol Phys*, **22**, 415-9.

Gray, L., Coger, A. & Ebert, M. (1953). The concentration of oxygen dissolved in tissues at the time of irradiation as a factor in radiotherapy. *Br J Radiol*, **26**, 638.

Griffiths, J.R., Taylor, N.J., Howe, F.A., Saunders, M., Robinson, S.P., Hoskin, P.J., Powell, M.E.B., Thoumine, M., Caine, L.A. & Baddeley, H. (1997). The response of human tumors to carbogen breathing, monitored by gradient-recalled echo magnetic resonance imaging. *Int J Radiat Oncol Biol Phys*, **39**, 697-701.

Grosios, K., Holwell, S.E., McGown, A.T., Pettit, G.R. & Bibby, M.C. (1999). In vivo and in vitro evaluation of combretastatin A-4 and its sodium phosphate prodrug. *Br J Cancer*, **81**, 1318-27.

Grosios, K., Loadman, P.M., Swaine, D.J., Pettit, G.R. & Bibby, M.C. (2000). Combination chemotherapy with combretastatin A-4 phosphate and 5-fluorouracil in an experimental murine colon adenocarcinoma. *Anticancer Res*, **20**, 229-33.

Gross, S., Gilead, A., Scherz, A., Neeman, M. & Salomon, Y. (2003). Monitoring photodynamic therapy of solid tumors online by BOLD-contrast MRI. *Nat Med*, **9**, 1327-31.

Grunstein, J., Roberts, W., Mathieu-Costello, O., Hanahan, D. & Johnson, R. (1999). Tumor-derived expression of vascular endothelial growth factor is a critical factor in tumor expansion and vascular function. *Cancer Res*, **59**, 1592-8.

Guckel, F., Brix, G., Rempp, K., Deimling, M., Rother, J. & Georgi, M. (1994). Assessment of cerebral blood volume with dynamic susceptibility contrast enhanced gradient-echo imaging. *J Comput Assist Tomogr*, **18**, 344-51.

Hammersen, F., Endrich, B. & Messmer, K. (1985). The fine structure of tumor blood vessels. I. Participation of non- endothelial cells in tumor angiogenesis. *Int J Microcirc Clin Exp*, **4**, 31-43.

Hashizume, H., Baluk, P., Morikawa, S., McLean, J.W., Thurston, G., Roberge, S., Jain, R.K. & McDonald, D.M. (2000). Openings between defective endothelial cells explain tumor vessel leakiness. *Am J Pathol*, **156**, 1363-80.

Hatva, E., Kaipainen, A., Mentula, P., Jaaskelainen, J., Paetau, A., Haltia, M. & Alitalo, K. (1995). Expression of endothelial cell-specific receptor tyrosine kinases and growth factors in human brain tumors. *Am J Pathol*, **146**, 368-78.

Hawighorst, H., Libicher, M., Knopp, M.V., Moehler, T., Kauffmann, G.W. & Gv, K. (1999). Evaluation of angiogenesis and perfusion of bone marrow lesions: role of semiquantitative and quantitative dynamic MRI. *J Magn Reson Imaging*, **10**, 286-94.

Hawighorst, T., Skobe, M., Streit, M., Hong, Y.K., Velasco, P., Brown, L.F., Riccardi, L., Lange-Asschenfeldt, B. & Detmar, M. (2002). Activation of the tie2 receptor by angiopoietin-1 enhances tumor vessel maturation and impairs squamous cell carcinoma growth. *Am J Pathol*, **160**, 1381-92.

Hellstrom, M., Gerhardt, H., Kalen, M., Li, X., Eriksson, U., Wolburg, H. & Betsholtz, C. (2001). Lack of pericytes leads to endothelial hyperplasia and abnormal vascular morphogenesis. *J Cell Biol*, **153**, 543-53.

Hemingway, D.M., Angerson, W.J., Anderson, J.H., Goldberg, J.A., McArdle, C.S. & Cooke, T.G. (1992). Monitoring blood flow to colorectal liver metastases using laser Doppler flowmetry: the effect of angiotensin II. *Br J Cancer*, **66**, 958-60.

Hermans, R., Meijerink, M., Van den Bogaert, W., Rijnders, A., Weltens, C. & Lambin, P. (2003). Tumor perfusion rate determined noninvasively by dynamic computed tomography predicts outcome in head-and-neck cancer after radiotherapy. *Int J Radiat Oncol Biol Phys*, **57**, 1351-6.

Herscovitch, P., Markham, J. & Raichle, M.E. (1983). Brain blood flow measured with intravenous H2(15)O. I. Theory and error analysis. *J Nucl Med*, **24**, 782-9.

Hill, S., Collingridge, D., Vojnovic, B. & Chaplin, D. (1998a). Tumour radiosensitization by high-oxygen-content gases: influence of the carbon dioxide content of the inspired gas on pO_2, microcirculatory function and radiosensitivity. *Int J Radiat Oncol Biol Phys*, 40, 943-951.

Hill, S., Powell, M., Goodchild, K., Griffin, T., Bell, K., Hoskin, P., Saunders, M. & Chaplin, D. (1998b). The effect of nicotinamide pretreatment on tumour perfusion during carbogen breathing: studies in mice and humans. In *10th International Conference on chemical modifiers of cancer treatment* pp. 80: Clearwater, Florida.

Hill, S.A., Chaplin, D.J., Lewis, G. & Tozer, G.M. (2002a). Schedule dependence of combretastatin A4 phosphate in transplanted and spontaneous tumour models. *Int J Cancer*, **102**, 70-4.

Hill, S.A., Lonergan, S.J., Denekamp, J. & Chaplin, D.J. (1993). Vinca alkaloids: anti-vascular effects in a murine tumour. *Eur J Cancer*, **29A**, 1320-4.

Hill, S.A., Sampson, L.E. & Chaplin, D.J. (1995). Anti-vascular approaches to solid tumour therapy: evaluation of vinblastine and flavone acetic acid. *Int J Cancer*, **63**, 119-23.

Hill, S.A., Tozer, G.M., Pettit, G.R. & Chaplin, D.J. (2002b). Preclinical evaluation of the antitumour activity of the novel vascular targeting agent Oxi 4503. *Anticancer Res*, **22**, 1453-8.

Hlatky, L., Tsionou, C., Hahnfeldt, P. & Coleman, C.N. (1994). Mammary fibroblasts may influence breast tumor angiogenesis via hypoxia-induced vascular endothelial growth factor up-regulation and protein expression. *Cancer Res*, **54**, 6083-6.

Hobbs, S.K., Monsky, W.L., Yuan, F., Roberts, W.G., Griffith, L., Torchilin, V.P. & Jain, R.K. (1998). Regulation of transport pathways in tumor vessels: role of tumor type and microenvironment. *Proc Natl Acad Sci U S A*, **95**, 4607-12.

Hobson, B. & Denekamp, J. (1984). Endothelial proliferation in tumours and normal tissues: continuous labelling studies. *Br J Cancer*, **49**, 405-13.

Hockel, M., Schlenger, K., Hockel, S. & Vaupel, P. (1999). Hypoxic cervical cancers with low apoptotic index are highly aggressive. *Cancer Res*, **59**, 4525-8.

Holash, J., Maisonpierre, P., Compton, D., Boland, P., Alexander, C., Zagzag, D., Yancopoulos, G. & Wiegand, S. (1999). Vessel cooption, regression, and growth in tumors mediated by angiopoietins and VEGF. *Science*, **284**, 1994-8.

Holwell, S.E., Cooper, P.A., Grosios, K., Lippert, J.W., 3rd, Pettit, G.R., Shnyder, S.D. & Bibby, M.C. (2002). Combretastatin A-1 phosphate a novel tubulin-binding agent with in vivo anti vascular effects in experimental tumours. *Anticancer Res*, **22**, 707-11.

Honess, D.J. & Bleehen, N.M. (1995). Perfusion changes in the RIF-1 tumour and normal tissues after carbogen and nicotinamide, individually and combined. *Br J Cancer*, **71**, 1175-80.

Hopper, C. (2000). Photodynamic therapy: a clinical reality in the treatment of cancer. *Lancet Oncol*, **1**, 212-9.

Hori, K., Zhang, Q., Saito, S., Tanda, S., Li, H. & Suzuki, M. (1993). Microvascular mechanisms of change in tumor blood flow due to angiotensin II, epinephrine, and methoxamine: a functional morphometric study. *Cancer Res*, **53**, 5528-34.

Horsman, M.R. & Murata, R. (2002). Combination of vascular targeting agents with thermal or radiation therapy. *Int J Radiat Oncol Biol Phys*, **54**, 1518-23.

Howe, F.A., Robinson, S.P. & Griffiths, J.R. (1996). Modification of tumour perfusion and oxygenation monitored by gradient recalled echo MRI and 31P MRS. *NMR Biomed*, **9**, 208-16.

Howe, F.A., Robinson, S.P., Rodrigues, L.M. & Griffiths, J.R. (1999). Flow and oxygenation dependent (FLOOD) contrast MR imaging to monitor the response of rat tumors to carbogen breathing. *Magn Reson Imaging*, **17**, 1307-18.

Hu, P., Yan, J., Sharifi, J., Bai, T., Khawli, L.A. & Epstein, A.L. (2003). Comparison of three different targeted tissue factor fusion proteins for inducing tumor vessel thrombosis. *Cancer Res*, **63**, 5046-53.

Huang, X., Molema, G., King, S., Watkins, L., Edgington, T.S. & Thorpe, P.E. (1997). Tumor infarction in mice by antibody-directed targeting of tissue factor to tumor vasculature. *Science*, **275**, 547-50.

Hulshof, M.C., Rehmann, C.J., Booij, J., van Royen, E.A., Bosch, D.A. & Gonzalez Gonzalez, D. (1998). Lack of perfusion enhancement after administration of nicotinamide and carbogen in patients with glioblastoma: a 99mTc-HMPAO SPECT study. *Radiother Oncol*, **48**, 135-42.

Huminiecki, L. & Bicknell, R. (2000). In silico cloning of novel endothelial-specific genes. *Genome Res*, **10**, 1796-806.

Iadecola, C. (1992). Does nitric oxide mediate the increases in cerebral blood flow elicited by hypercapnia? *Proc Natl Acad Sci U S A*, **89**, 3913-6.

Ireson, C.R., Hill, S.A., Lewis, G., Steele, A., Coralli, C., Dachs, G.U., Barber, P.R., Honess, D.J., Kanthou, C., Shima, D. & Tozer, G. (2004). The role of tumour vascular maturation in determining response to tubulin-binding vascular targeting agents. *Br J Cancer*, **91**, S60.

Jackson, A., Haroon, H., Zhu, X.P., Li, K.L., Thacker, N.A. & Jayson, G. (2002a). Breath-hold perfusion and permeability mapping of hepatic malignancies using magnetic resonance imaging and a first-pass leakage profile model. *NMR Biomed*, **15**, 164-73.

Jackson, A., Kassner, A., Annesley-Williams, D., Reid, H., Zhu, X.P. & Li, K.L. (2002b). Abnormalities in the recirculation phase of contrast agent bolus passage in cerebral gliomas: comparison with relative blood volume and tumor grade. *AJNR Am J Neuroradiol*, **23**, 7-14.

Jain, R. (1987a). Transport of molecules across tumor vasculature. *Cancer Metastasis Rev*, **6**, 559-93.

Jain, R.K. (1987b). Transport of molecules in the tumor interstitium: a review. *Cancer Res*, **47**, 3039-51.

Jain, R.K. (1988). Determinants of tumor blood flow: a review. *Cancer Res*, **48**, 2641-58.

Jain, R.K. (1989). Delivery of novel therapeutic agents in tumors: physiological barriers and strategies. *J Natl Cancer Inst*, **81**, 570-6.

Jain, R.K. (2003). Molecular regulation of vessel maturation. *Nat Med*, **9**, 685-93.

Jain, R.K. & Fenton, B.T. (2002). Intratumoral lymphatic vessels: a case of mistaken identity or malfunction? *J Natl Cancer Inst*, **94**, 417-21.

Jain, R.K., Munn, L.L. & Fukumura, D. (2002). Dissecting tumour pathophysiology using intravital microscopy. *Nat Rev Cancer*, **2**, 266-76.

Jameson, M.B., Thompson, P.I., Baguley, B.C., Evans, B.D., Harvey, V.J., Porter, D.J., McCrystal, M.R., Small, M., Bellenger, K., Gumbrell, L., Halbert, G.W. & Kestell, P. (2003). Clinical aspects of a phase I trial of 5,6-dimethylxanthenone-4-acetic acid (DMXAA), a novel antivascular agent. *Br J Cancer*, **88**, 1844-50.

Jirtle, R., Clifton, K.H. & Rankin, J.H. (1978). Effects of several vasoactive drugs on the vascular resistance of MT-W9B tumors in W/Fu rats. *Cancer Res*, **38**, 2385-90.

Jordan, A., Hadfield, J.A., Lawrence, N.J. & McGown, A.T. (1998). Tubulin as a target for anticancer drugs: agents which interact with the mitotic spindle. *Med Res Rev*, **18**, 259-96.

Jordan, B.F., Misson, P., Demeure, R., Baudelet, C., Beghein, N. & Gallez, B. (2000). Changes in tumor oxygenation/perfusion induced by the no donor, isosorbide dinitrate, in comparison with carbogen: monitoring by EPR and MRI. *Int J Radiat Oncol Biol Phys*, **48**, 565-70.

Kallinowski, F., Schaefer, C., Tyler, G. & Vaupel, P. (1989). In vivo targets of recombinant human tumour necrosis factor-alpha: blood flow, oxygen consumption and growth of isotransplanted rat tumours. *Br J Cancer*, **60**, 555-60.

Kanthou, C., Greco, O., Stratford, A., Cook, I., Knight, R., Benzakour, O. & Tozer, G. (2004). The tubulin-binding agent combretastatin A-4-phosphate arrests endothelial cells in mitosis and induces mitotic cell death. *Am J Pathol*, **165**, 1401-11.

Kanthou, C. & Tozer, G.M. (2002). The tumor vascular targeting agent combretastatin A-4-phosphate induces reorganization of the actin cytoskeleton and early membrane blebbing in human endothelial cells. *Blood*, **99**, 2060-9.

Kaye, S.B., Clavel, M., Dodion, P., Monfardini, S., ten Bokkel-Huinink, W., Wagener, D.T., Gundersen, S., Stoter, G., Smith, J., Renard, J. & al, e. (1990). Phase II trials with flavone acetic acid (NCS. 347512, LM975) in patients with advanced carcinoma of the breast, colon, head and neck and melanoma. *Invest New Drugs*, **8 Suppl 1**, S95-9.

Kerbel, R.S., Yu, J., Tran, J., Man, S., Viloria-Petit, A., Klement, G., Coomber, B.L. & Rak, J. (2001). Possible mechanisms of acquired resistance to anti-angiogenic drugs: implications for the use of combination therapy approaches. *Cancer Metastasis Rev*, **20**, 79-86.

Kerr, D.J., Maughan, T., Newlands, E., Rustin, G., Bleehen, N.M., Lewis, C. & Kaye, S.B. (1989). Phase II trials of flavone acetic acid in advanced malignant melanoma and colorectal carcinoma. *Br J Cancer*, **60**, 104-6.

Kety, S. (1960a). Blood-tissue exchange methods. Theory of blood-tissue exchange and its application to measurement of blood flow. *Meth Med Res*, **8**, 223-227.

Kety, S. (1960b). Measurement of local blood flow by the exchange of an inert, diffusible substance. *Meth Med Res*, **8**, 228-236.

Kimura, H., Braun, R.D., Ong, E.T., Hsu, R., Secomb, T.W., Papahadjopoulos, D., Hong, K. & Dewhirst, M.W. (1996). Fluctuations in red cell flux in tumor microvessels can lead to transient hypoxia and reoxygenation in tumor parenchyma. *Cancer Res*, **56**, 5522-8.

Konerding, M.A., Malkusch, W., Klapthor, B., van Ackern, C., Fait, E., Hill, S.A., Parkins, C., Chaplin, D.J., Presta, M. & Denekamp, J. (1999). Evidence for characteristic vascular patterns in solid tumours: quantitative studies using corrosion casts. *Br J Cancer*, **80**, 724-32.

Konerding, M.A., Miodonski, A.J. & Lametschwandtner, A. (1995). Microvascular corrosion casting in the study of tumor vascularity: a review. *Scanning Microsc*, **9**, 1233-43; discussion 1243-4.

Krix, M., Kiessling, F., Vosseler, S., Farhan, N., Mueller, M.M., Bohlen, P., Fusenig, N.E. & Delorme, S. (2003). Sensitive noninvasive monitoring of tumor perfusion during antiangiogenic therapy by intermittent bolus-contrast power Doppler sonography. *Cancer Res*, **63**, 8264-70.

Kruuv, J.A., Inch, W.R. & McCredie, J.A. (1967). Blood flow and oxygenation of tumors in mice. I. Effects of breathing gases containing carbon dioxide at atmospheric pressure. *Cancer*, **20**, 51-9.

Kuwabara, K., Ogawa, S., Matsumoto, M., Koga, S., Clauss, M., Pinsky, D.J., Lyn, P., Leavy, J., Witte, L., Joseph-Silverstein, J. & et al. (1995). Hypoxia-mediated induction of acidic/basic fibroblast growth factor and platelet-derived growth factor in mononuclear phagocytes stimulates growth of hypoxic endothelial cells. *Proc Natl Acad Sci U S A*, **92**, 4606-10.

Kwong, K.K., Belliveau, J.W., Chesler, D.A., Goldberg, I.E., Weisskoff, R.M., Poncelet, B.P., Kennedy, D.N., Hoppel, B.E., Cohen, M.S., Turner, R. & et al. (1992). Dynamic magnetic resonance imaging of human brain activity during primary sensory stimulation. *Proc Natl Acad Sci U S A*, **89**, 5675-9.

Langen, K.J., Roosen, N., Herzog, H., Kuwert, T., Kiwit, J.C., Bock, W.J. & Feinendegen, L.E. (1989). Investigations of brain tumours with 99Tcm-HMPAO SPECT. *Nucl Med Commun*, **10**, 325-34.

Lanzen, J.L., Braun, R.D., Ong, A.L. & Dewhirst, M.W. (1998). Variability in blood flow and pO2 in tumors in response to carbogen breathing. *Int J Radiat Oncol Biol Phys*, **42**, 855-9.

Leach, M.O., Brindle, K.M., Evelhoch, J.L., Griffiths, J.R., Horsman, M.R., Jackson, A., Jayson, G.C., Judson, I.R., Knopp, M.V., Maxwell, R.J., McIntyre, D., Padhani, A.R., Price, P., Rathbone, R., Rustin, G.J., Tofts, P.S., Tozer, G.M., Vennart, W., Waterton, J.C., Williams, S.R. & Workman, P. (2005). The assessment of antiangiogenic and antivascular therapies in early-stage clinical trials using magnetic resonance imaging: issues and recommendations. *Br J Cancer*, **92**, 1599-610.

Lebon, V., Carlier, P.G., Brillault-Salvat, C. & Leroy-Willig, A. (1998). Simultaneous measurement of perfusion and oxygenation changes using a multiple gradient-echo sequence: application to human muscle study. *Magn Reson Imaging*, **16**, 721-9.

Lejeune, F., Ruegg, C. & Lienard, D. (1998). Clinical applications of TNF-alpha in cancer. *Curr Opin Immunol*, **10**, 573-80.

Lepekhin, E., Jiang, X., Michaud, S., Tonary, A., Yu, W., Symonds, J.M. & Blaschuk, O.W. (2003). Early and long term effects of exherin on tumor vasculature. In *Proc ASCO*, Vol. 22. pp. 220 (abstr 883): Chicago, USA.

Less, J.R., Skalak, T.C., Sevick, E.M. & Jain, R.K. (1991). Microvascular architecture in a mammary carcinoma: branching patterns and vessel dimensions. *Cancer Res*, **51**, 265-73.

Leu, A.J., Berk, D.A., Lymboussaki, A., Alitalo, K. & Jain, R.K. (2000). Absence of functional lymphatics within a murine sarcoma: a molecular and functional evaluation. *Cancer Res*, **60**, 4324-7.

Leunig, M., Yuan, F., Menger, M.D., Boucher, Y., Goetz, A.E., Messmer, K. & Jain, R.K. (1992). Angiogenesis, microvascular architecture, microhemodynamics, and interstitial fluid pressure during early growth of human adenocarcinoma LS174T in SCID mice. *Cancer Res*, **52**, 6553-60.

Li, L., Rojiani, A. & Siemann, D. (1998). Targeting the tumor vasculature with combretastatin A-4 disodium phosphate: effects on radiation therapy. *Int J Radiat Oncol Biol Phys*, **42**, 899-903.

Lin, W., Celik, A., Derdeyn, C., An, H., Lee, Y., Videen, T., Ostergaard, L. & Powers, W.J. (2001). Quantitative measurements of cerebral blood flow in patients with unilateral carotid artery occlusion: a PET and MR study. *J Magn Reson Imaging*, **14**, 659-67.

Lindahl, P., Johansson, B.R., Leveen, P. & Betsholtz, C. (1997). Pericyte loss and microaneurysm formation in PDGF-B-deficient mice. *Science*, **277**, 242-5.

Llovet, J.M., Real, M.I., Montana, X., Planas, R., Coll, S., Aponte, J., Ayuso, C., Sala, M., Muchart, J., Sola, R., Rodes, J. & Bruix, J. (2002). Arterial embolisation or chemoembolisation versus symptomatic treatment in patients with unresectable hepatocellular carcinoma: a randomised controlled trial. *Lancet*, **359**, 1734-9.

Los, M. & Voest, E.E. (2001). The potential role of antivascular therapy in the adjuvant and neoadjuvant treatment of cancer. *Semin Oncol*, **28**, 93-105.

Lyng, H., Dahle, G.A., Kaalhus, O., Skretting, A. & Rofstad, E.K. (1998). Measurement of perfusion rate in human melanoma xenografts by contrast-enhanced magnetic resonance imaging. *Magn Reson Med*, **40**, 89-98.

Lyng, H., Skretting, A. & Rofstad, E.K. (1992). Blood flow in six human melanoma xenograft lines with different growth characteristics. *Cancer Res*, **52**, 584-92.

Maeda, M., Itoh, S., Kimura, H., Iwasaki, T., Hayashi, N., Yamamoto, K., Ishii, Y. & Kubota, T. (1993). Tumor vascularity in the brain: evaluation with dynamic susceptibility-contrast MR imaging. *Radiology*, **189**, 233-8.

Maisonpierre, P.C., Suri, C., Jones, P.F., Bartunkova, S., Wiegand, S.J., Radziejewski, C., Compton, D., McClain, J., Aldrich, T.H., Papadopoulos, N., Daly, T.J., Davis, S., Sato, T.N. & Yancopoulos, G.D. (1997). Angiopoietin-2, a natural antagonist for Tie2 that disrupts in vivo angiogenesis. *Science*, **277**, 55-60.

Malcontenti-Wilson, C., Muralidharan, V., Skinner, S., Christophi, C., Sherris, D. & O'Brien, P.E. (2001). Combretastatin A4 prodrug study of effect on the growth and the microvasculature of colorectal liver metastases in a murine model. *Clin Cancer Res*, **7**, 1052-60.

Mandriota, S.J., Pyke, C., Di Sanza, C., Quinodoz, P., Pittet, B. & Pepper, M.S. (2000). Hypoxia-inducible angiopoietin-2 expression is mimicked by iodonium compounds and occurs in the rat brain and skin in response to systemic hypoxia and tissue ischemia. *Am J Pathol*, **156**, 2077-89.

Maniotis, A.J., Folberg, R., Hess, A., Seftor, E.A., Gardner, L.M., Pe'er, J., Trent, J.M., Meltzer, P.S. & Hendrix, M.J. (1999). Vascular channel formation by human melanoma cells in vivo and in vitro: vasculogenic mimicry. *Am J Pathol*, **155**, 739-52.

Mantyla, M., Heikkonen, J. & Perkkio, J. (1988). Regional blood flow in human tumours measured with argon, krypton and xenon. *Br J Radiol*, **61**, 379-82.

Martin, L., Lartigau, E., Weeger, P., Lambin, P., Le Ridant, A.M., Lusinchi, A., Wibault, P., Eschwege, F., Luboinski, B. & Guichard, M. (1993). Changes in the oxygenation of head and neck tumors during carbogen breathing. *Radiother Oncol*, **27**, 123-30.

Mattsson, J., Lilja, J. & Peterson, H.I. (1982). Influence of vasoactive drugs on local tumor blood flow. *Eur J Cancer Clin Oncol*, **18**, 677-84.

Mavria, G. & Porter, C.D. (2001). Reduced growth in response to ganciclovir treatment of subcutaneous xenografts expressing HSV-tk in the vascular compartment. *Gene Ther*, **8**, 913-20.

Maxwell, P.H., Dachs, G.U., Gleadle, J.M., Nicholls, L.G., Harris, A.L., Stratford, I.J., Hankinson, O., Pugh, C.W. & Ratcliffe, P.J. (1997). Hypoxia-inducible factor-1 modulates gene expression in solid tumors and influences both angiogenesis and tumor growth. *Proc Natl Acad Sci U S A*, **94**, 8104-9.

Maxwell, R., Wilson, J., Prise, V., Vojnovic, B., Rustin, G., Lodge, M. & Tozer, G. (2002). Evaluation of the anti-vascular effects of combretastatin in rodent tumours by dynamic contrast enhanced MRI. *NMR Biomed*, **15**, 89-98.

Mayr, N.A., Yuh, W.T., Magnotta, V.A., Ehrhardt, J.C., Wheeler, J.A., Sorosky, J.I., Davis, C.S., Wen, B.C., Martin, D.D., Pelsang, R.E., Buller, R.E., Oberley, L.W., Mellenberg, D.E. & Hussey, D.H. (1996). Tumor perfusion studies using fast magnetic resonance imaging technique in advanced cervical cancer: a new noninvasive predictive assay. *Int J Radiat Oncol Biol Phys*, **36**, 623-33.

McCreedy, B.J., Kiyoizumi, T. & Locke, K.W. (2004). The novel vascular disrupting agent, MN-029, shows potent and selective anti-tumor activity in preclinical animal models. In *2nd International conference on vascular targeting*: Miami, Florida.

McDonald, D.M., Munn, L. & Jain, R.K. (2000). Vasculogenic mimicry: how convincing, how novel, and how significant? *Am J Pathol*, **156**, 383-8.

McGown, A.T. & Fox, B.W. (1989). Structural and biochemical comparison of the anti-mitotic agents colchicine, combretastatin A4 and amphethinile. *Anticancer Drug Des*, **3**, 249-54.

Meier, P. & Zierler, K.L. (1954). On the theory of the indicator-dilution method for measurement of blood flow and volume. *J Appl Physiol*, **6**, 731-44.

Melillo, G., Musso, T., Sica, A., Taylor, L.S., Cox, G.W. & Varesio, L. (1995). A hypoxia-responsive element mediates a novel pathway of activation of the inducible nitric oxide synthase promoter. *J Exp Med*, **182**, 1683-93.

Micheletti, G., Poli, M., Borsotti, P., Martinelli, M., Imberti, B., Taraboletti, G. & Giavazzi, R. (2003). Vascular-targeting activity of ZD6126, a novel tubulin-binding agent. *Cancer Res*, **63**, 1534-7.

Miles, K.A. (1991). Measurement of tissue perfusion by dynamic computed tomography [see comments]. *Br J Radiol*, **64**, 409-12.

Milosevic, M.F., Fyles, A.W. & Hill, R.P. (1999). The relationship between elevated interstitial fluid pressure and blood flow in tumors: a bioengineering analysis. *Int J Radiat Oncol Biol Phys*, **43**, 1111-23.

Morikawa, S., Baluk, P., Kaidoh, T., Haskell, A., Jain, R.K. & McDonald, D.M. (2002). Abnormalities in pericytes on blood vessels and endothelial sprouts in tumors. *Am J Pathol*, **160**, 985-1000.

Moulder, J.E. & Rockwell, S. (1984). Hypoxic fractions of solid tumors: experimental techniques, methods of analysis, and a survey of existing data. *Int J Radiat Oncol Biol Phys*, **10**, 695-712.

Mukherjee, P., Kang, H.C., Videen, T.O., McKinstry, R.C., Powers, W.J. & Derdeyn, C.P. (2003). Measurement of cerebral blood flow in chronic carotid occlusive disease: comparison of dynamic susceptibility contrast perfusion MR imaging with positron emission tomography. *AJNR Am J Neuroradiol*, **24**, 862-71.

Murata, R., Overgaard, J. & Horsman, M.R. (2001a). Comparative effects of combretastatin A-4 disodium phosphate and 5,6- dimethylxanthenone-4-acetic acid on blood perfusion in a murine tumour and normal tissues. *Int J Radiat Biol*, **77**, 195-204.

Murata, R., Siemann, D.W., Overgaard, J. & Horsman, M.R. (2001b). Improved tumor response by combining radiation and the vascular-damaging drug 5,6-dimethylxanthenone-4-acetic acid. *Radiat Res*, **156**, 503-9.

Murata, R., Siemann, D.W., Overgaard, J. & Horsman, M.R. (2001c). Interaction between combretastatin A-4 disodium phosphate and radiation in murine tumors. *Radiother Oncol*, **60**, 155-61.

Nanus, D.M., Milowsky, M.I., Kostakoglu, L., Smith-Jones, P.M., Vallabahajosula, S., Goldsmith, S.J. & Bander, N.H. (2003). Clinical use of monoclonal antibody HuJ591 therapy: targeting prostate specific membrane antigen. *J Urol*, **170**, S84-8; discussion S88-9.

Neeman, M., Dafni, H., Bukhari, O., Braun, R. & Dewhirst, M. (2001). In Vivo BOLD Contrast MRI Mapping of Subcutaneous Vascular Function and Maturation: Validation by Intravital Microscopy. *Magn Reson Med*, **45**, 887-898.

Netti, P., Roberge, S., Boucher, Y., Baxter, L. & Jain, R. (1996). Effect of transvascular fluid exchange on pressure-flow relationship in tumors: a proposed mechanism for tumor blood flow heterogeneity. *Microvasc Res*, **52**, 27-46.

Newell, K., Franchi, A., Pouyssegur, J. & Tannock, I. (1993). Studies with glycolysis-deficient cells suggest that production of lactic acid is not the only cause of tumor acidity. *Proc Natl Acad Sci U S A*, **90**, 1127-31.

Nielsen, H., Aalkjaer, C. & Mulvany, M.J. (1991). Differential contractile effects of changes in carbon dioxide tension on rat mesenteric resistance arteries precontracted with noradrenaline. *Pflugers Arch*, **419**, 51-6.

Nihei, Y., Suzuki, M., Okano, A., Tsuji, T., Akiyama, Y., Tsuruo, T., Saito, S., Hori, K. & Sato, Y. (1999). Evaluation of antivascular and antimitotic effects of tubulin binding agents in solid tumor therapy. *Jpn J Cancer Res*, **90**, 1387-95.

Noguchi, S., Miyauchi, K., Nishizawa, Y., Sasaki, Y., Imaoka, S., Iwanaga, T., Koyama, H. & Terasawa, T. (1988). Augmentation of anticancer effect with angiotensin II in intraarterial infusion chemotherapy for breast carcinoma. *Cancer*, **62**, 467-73.

Offersen, B.V., Pfeiffer, P., Hamilton-Dutoit, S. & Overgaard, J. (2001). Patterns of angiogenesis in nonsmall-cell lung carcinoma. *Cancer*, **91**, 1500-9.

Ogawa, S., Lee, T., Nayak, A. & Glynn, P. (1990). Oxygenation-sensitive contrast in magnetic resonance image of rodent brain at high magnetic fields. *Magn Reson Med*, **14**, 68-78.

Ogawa, S., Menon, R., Tank, D., Kim, S.-G., Merkle, H., Ellermann, J. & Ugurbil, K. (1993). Functional brain mapping by blood oxygenation level-dependent contrast magnetic resonance imaging. *Biophys J*, **64**, 803-812.

Ogawa, S., Tank, D.W., Menon, R., Ellermann, J.M., Kim, S.G., Merkle, H. & Ugurbil, K. (1992). Intrinsic signal changes accompanying sensory stimulation: functional brain mapping with magnetic resonance imaging. *Proc Natl Acad Sci U S A*, **89**, 5951-5.

Olson, T.A., Mohanraj, D., Roy, S. & Ramakrishnan, S. (1997). Targeting the tumor vasculature: inhibition of tumor growth by a vascular endothelial growth factor-toxin conjugate. *Int J Cancer*, **73**, 865-70.

Orlidge, A. & D'Amore, P. (1987). Inhibition of capillary endothelial cell growth by pericytes and smooth muscle cells. *J. Cell Biol.*, **105**, 1455-1462.

Ostergaard, L., Johannsen, P., Host-Poulsen, P., Vestergaard-Poulsen, P., Asboe, H., Gee, A.D., Hansen, S.B., Cold, G.E., Gjedde, A. & Gyldensted, C. (1998). Cerebral blood flow measurements by magnetic resonance imaging bolus tracking: comparison with [(15)O]H2O positron emission tomography in humans. *J Cereb Blood Flow Metab*, **18**, 935-40.

Ostergaard, L., Weisskoff, R.M., Chesler, D.A., Gyldensted, C. & Rosen, B.R. (1996). High resolution measurement of cerebral blood flow using intravascular tracer bolus passages. Part I: Mathematical approach and statistical analysis. *Magn Reson Med*, **36**, 715-25.

Otani, M., Natsume, T., Watanabe, J.I., Kobayashi, M., Murakoshi, M., Mikami, T. & Nakayama, T. (2000). TZT-1027, an antimicrotubule agent, attacks tumor vasculature and induces tumor cell death. *Jpn J Cancer Res*, **91**, 837-44.

Overgaard, J., Gonzalez Gonzalez, D., Hulshof, M.C., Arcangeli, G., Dahl, O., Mella, O. & Bentzen, S.M. (1995). Randomised trial of hyperthermia as adjuvant to radiotherapy for recurrent or metastatic malignant melanoma. European Society for Hyperthermic Oncology. *Lancet*, **345**, 540-3.

Padera, T.P., Kadambi, A., di Tomaso, E., Carreira, C.M., Brown, E.B., Boucher, Y., Choi, N.C., Mathisen, D., Wain, J., Mark, E.J., Munn, L.L. & Jain, R.K. (2002). Lymphatic metastasis in the absence of functional intratumor lymphatics. *Science*, **296**, 1883-6.

Palladino, M.A., Nicholson, B., Bahjat, F.R., Borgstrom, P., Neuteboom, S.T.C. & Lloyd, G.K. (2004). NPI-2358, a novel diketopiperazine that induces tumor vascular collapse. In *2nd International conference on vascular targeting*: Miami, Florida.

Papenfuss, H.D., Gross, J.F., Intaglietta, M. & Treese, F.A. (1979). A transparent access chamber for the rat dorsal skin fold. *Microvasc Res*, **18**, 311-8.

Parker, G.J., Suckling, J., Tanner, S.F., Padhani, A.R., Revell, P.B., Husband, J.E. & Leach, M.O. (1997). Probing tumor microvascularity by measurement, analysis and display of contrast agent uptake kinetics. *J Magn Reson Imaging*, **7**, 564-74.

Pasqualini, R. & Ruoslahti, E. (1996). Organ targeting in vivo using phage display peptide libraries. *Nature*, **380**, 364-366.

Passalidou, E., Trivella, M., Singh, N., Ferguson, M., Hu, J., Cesario, A., Granone, P., Nicholson, A.G., Goldstraw, P., Ratcliffe, C., Tetlow, M., Leigh, I., Harris, A.L., Gatter, K.C. & Pezzella, F. (2002). Vascular phenotype in angiogenic and non-angiogenic lung non-small cell carcinomas. *Br J Cancer*, **86**, 244-9.

Patan, S. (1998). TIE1 and TIE2 receptor tyrosine kinases inversely regulate embryonic angiogenesis by the mechanism of intussusceptive microvascular growth. *Microvasc Res*, **56**, 1-21.

Patan, S., Munn, L.L. & Jain, R.K. (1996). Intussusceptive microvascular growth in a human colon adenocarcinoma xenograft: a novel mechanism of tumor angiogenesis. *Microvasc Res*, **51**, 260-72.

Pedley, R., Hill, S., Boxer, G., Flynn, A., Boden, R., Watson, R., Dearling, J., Chaplin, D. & Begent, R. (2001). Eradication of colorectal xenografts by combined radioimmunotherapy and combretastatin A-4 3-O-phosphate. *Cancer Res*, **61**.

Pedley, R.B., Boden, J.A., Boden, R., Boxer, G.M., Flynn, A.A., Keep, P.A. & Begent, R.H. (1996). Ablation of colorectal xenografts with combined radioimmunotherapy and tumor blood flow-modifying agents. *Cancer Res*, **56**, 3293-300.

Pedley, R.B., Sharma, S.K., Boxer, G.M., Boden, R., Stribbling, S.M., Davies, L., Springer, C.J. & Begent, R.H. (1999). Enhancement of antibody-directed enzyme prodrug therapy in colorectal xenografts by an antivascular agent. *Cancer Res*, **59**, 3998-4003.

Perthen, J.E., Calamante, F., Gadian, D.G. & Connelly, A. (2002). Is quantification of bolus tracking MRI reliable without deconvolution? *Magn Reson Med*, **47**, 61-7.

Peters, A.M. (1998). Fundamentals of tracer kinetics for radiologists. *Br J Radiol*, **71**, 1116-29.

Peters, A.M., Gunasekera, R.D., Henderson, B.L., Brown, J., Lavender, J.P., De Souza, M., Ash, J.M. & Gilday, D.L. (1987). Noninvasive measurement of blood flow and extraction fraction. *Nucl Med Commun*, **8**, 823-37.

Pettit, G.R., Cragg, G.M., Herald, D.L., Schmidt, J.M. & Lohavanijaya, P. (1982). Isolation and structure of combretastatin. *Canad J Chem*, **60**, 1374-1376.

Pezzella, F., Pastorino, U., Tagliabue, E., Andreola, S., Sozzi, G., Gasparini, G., Menard, S., Gatter, K.C., Harris, A.L., Fox, S., Buyse, M., Pilotti, S., Pierotti, M. & Rilke, F. (1997). Non-small-cell lung carcinoma tumor growth without morphological evidence of neo-angiogenesis. *Am J Pathol*, **151**, 1417-23.

Plate, K.H., Breier, G., Millauer, B., Ullrich, A. & Risau, W. (1993). Up-regulation of vascular endothelial growth factor and its cognate receptors in a rat glioma model of tumor angiogenesis. *Cancer Res*, **53**, 5822-7.

Plate, K.H., Breier, G., Weich, H.A. & Risau, W. (1992). Vascular endothelial growth factor is a potential tumour angiogenesis factor in human gliomas in vivo. *Nature*, **359**, 845-8.

Pocock, G. & Richards, C. (2004). *Human Physiology - the basis of medicine*. OUP: Oxford, UK.

Powell, M.E., Hill, S.A., Saunders, M.I., Hoskin, P.J. & Chaplin, D.J. (1996). Effect of carbogen breathing on tumour microregional blood flow in humans. *Radiother Oncol*, **41**, 225-31.

Prise, V.E., Honess, D.J., Stratford, M.R., Wilson, J. & Tozer, G.M. (2002). The vascular response of tumor and normal tissues in the rat to the vascular targeting agent, combretastatin A-4-phosphate, at clinically relevant doses. *Int J Oncol*, **21**, 717-26.

Raichle, M.E., Martin, W.R., Herscovitch, P., Mintun, M.A. & Markham, J. (1983). Brain blood flow measured with intravenous H2(15)O. II. Implementation and validation. *J Nucl Med*, **24**, 790-8.

Rijpkema, M., Kaanders, J.H., Joosten, F.B., van der Kogel, A.J. & Heerschap, A. (2002). Effects of breathing a hyperoxic hypercapnic gas mixture on blood oxygenation and vascularity of head-and-neck tumors as measured by magnetic resonance imaging. *Int J Radiat Oncol Biol Phys*, **53**, 1185-91.

Robinson, S.P., Howe, F.A., Stubbs, M. & Griffiths, J.R. (2000). Effects of nicotinamide and carbogen on tumour oxygenation, blood flow, energetics and blood glucose levels. *Br J Cancer*, **82**, 2007-14.

Robinson, S.P., McIntyre, D.J., Checkley, D., Tessier, J.J., Howe, F.A., Griffiths, J.R., Ashton, S.E., Ryan, A.J., Blakey, D.C. & Waterton, J.C. (2003a). Tumour dose response to the antivascular agent ZD6126 assessed by magnetic resonance imaging. *Br J Cancer*, **88**, 1592-7.

Robinson, S.P., Rijken, P.F., Howe, F.A., McSheehy, P.M., Van Der Sanden, B.P., Heerschap, A., Stubbs, M., Van Der Kogel, A.J. & Griffiths, J.R. (2003b). Tumor vascular architecture and function evaluated by non-invasive susceptibility MRI methods and immunohistochemistry. *J Magn Reson Imaging*, **17**, 445-54.

Robinson, S.P., Rodrigues, L.M., Ojugo, A.S., McSheehy, P.M., Howe, F.A. & Griffiths, J.R. (1997). The response to carbogen breathing in experimental tumour models monitored by gradient-recalled echo magnetic resonance imaging. *Br J Cancer*, **75**, 1000-6.

Rofstad, E.K. & Danielsen, T. (1999). Hypoxia-induced metastasis of human melanoma cells: involvement of vascular endothelial growth factor-mediated angiogenesis. *Br J Cancer*, **80**, 1697-707.

Rosen, B.R., Belliveau, J.W., Aronen, H.J., Kennedy, D., Buchbinder, B.R., Fischman, A., Gruber, M., Glas, J., Weisskoff, R.M., Cohen, M.S. & et al. (1991a). Susceptibility contrast imaging of cerebral blood volume: human experience. *Magn Reson Med*, **22**, 293-9; discussion 300-3.

Rosen, B.R., Belliveau, J.W., Buchbinder, B.R., McKinstry, R.C., Porkka, L.M., Kennedy, D.N., Neuder, M.S., Fisel, C.R., Aronen, H.J., Kwong, K.K. & et al. (1991b). Contrast agents and cerebral hemodynamics. *Magn Reson Med*, **19**, 285-92.

Rosen, B.R., Belliveau, J.W., Vevea, J.M. & Brady, T.J. (1990). Perfusion imaging with NMR contrast agents. *Magn Reson Med*, **14**, 249-65.

Rowell, N.P., Flower, M.A., McCready, V.R., Cronin, B. & Horwich, A. (1990). The effects of single dose oral hydralazine on blood flow through human lung tumours. *Radiother Oncol*, **18**, 283-92.

Rowell, N.P., McCready, V.R., Tait, D., Flower, M.A., Cronin, B., Adams, G.E. & Horwich, A. (1989). Technetium-99m HMPAO and SPECT in the assessment of blood flow in human lung tumours. *Br J Cancer*, **59**, 135-41.

Rustin, G.J., Bradley, C., Galbraith, S., Stratford, M., Loadman, P., Waller, S., Bellenger, K., Gumbrell, L., Folkes, L. & Halbert, G. (2003a). 5,6-dimethylxanthenone-4-acetic acid (DMXAA), a novel antivascular agent: phase I clinical and pharmacokinetic study. *Br J Cancer*, **88**, 1160-7.

Rustin, G.J., Galbraith, S.M., Anderson, H., Stratford, M., Folkes, L.K., Sena, L., Gumbrell, L. & Price, P.M. (2003b). Phase I clinical trial of weekly combretastatin A4 phosphate: clinical and pharmacokinetic results. *J Clin Oncol*, **21**, 2815-22.

Samulski, T.V., Fessenden, P., Valdagni, R. & Kapp, D.S. (1987). Correlations of thermal washout rate, steady state temperatures, and tissue type in deep seated recurrent or metastatic tumors. *Int J Radiat Oncol Biol Phys*, **13**, 907-16.

Sapirstein, L.A. (1958). Regional blood flow by fractional distribution of indicators. *Am J Physiol*, **193**, 161-168.

Sasaki, Y., Imaoka, S., Hasegawa, Y., Nakano, S., Ishikawa, O., Ohigashi, H., Taniguchi, K., Koyama, H., Iwanaga, T. & Terasawa, T. (1985). Changes in distribution of hepatic blood flow induced by intra-arterial infusion of angiotensin II in human hepatic cancer. *Cancer*, **55**, 311-6.

Sato, H., Sugiyama, K., Hoshi, M., Urushiyama, M. & Ishizuka, K. (1995). Angiotensin II (AII) induced hypertension chemotherapy (IHC) for unresectable gastric cancer: with reference to resection after down staging. *World J Surg*, **19**, 836-42.

Senger, D.R., Perruzzi, C.A., Feder, J. & Dvorak, H.F. (1986). A highly conserved vascular permeability factor secreted by a variety of human and rodent tumor cell lines. *Cancer Res*, **46**, 5629-32.

Sevick, E.M. & Jain, R.K. (1991). Measurement of capillary filtration coefficient in a solid tumor. *Cancer Res*, **51**, 1352-5.

Shirakawa, K., Wakasugi, H., Heike, Y., Watanabe, I., Yamada, S., Saito, K. & Konishi, F. (2002). Vasculogenic mimicry and pseudo-comedo formation in breast cancer. *Int J Cancer*, **99**, 821-8.

Shweiki, D., Itin, A., Soffer, D. & Keshet, E. (1992). Vascular endothelial growth factor induced by hypoxia may mediate hypoxia-initiated angiogenesis. *Nature*, **359**, 843-5.

Siemann, D.W., Mercer, E., Lepler, S. & Rojiani, A.M. (2002). Vascular targeting agents enhance chemotherapeutic agent activities in solid tumor therapy. *Int J Cancer*, **99**, 1-6.

Siemann, D.W. & Rojiani, A.M. (2002). Antitumor efficacy of conventional anticancer drugs is enhanced by the vascular targeting agent ZD6126. *Int J Radiat Oncol Biol Phys*, **54**, 1512-7.

Siim, B.G., Lee, A.E., Shalal-Zwain, S., Pruijn, F.B., McKeage, M.J. & Wilson, W.R. (2003). Marked potentiation of the antitumour activity of chemotherapeutic drugs by the antivascular agent 5,6-dimethylxanthenone-4-acetic acid (DMXAA). *Cancer Chemother Pharmacol*, **51**, 43-52.

Song, C.W. (1998). Modification of blood flow. In *Blood perfusion and microenvironment of human tumours*, Molls, M. & Vaupel, P. (eds) pp. 193-207. Springer-Verlag, USA.

St Croix, B., Rago, C., Velculescu, V., Traverso, G., Romans, K.E., Montgomery, E., Lal, A., Riggins, G.J., Lengauer, C., Vogelstein, B. & Kinzler, K.W. (2000). Genes expressed in human tumor endothelium. *Science*, **289**, 1197-202.

Staton, C.A., Brown, N.J., Rodgers, G.R., Corke, K.P., Tazzyman, S., Underwood, J.C. & Lewis, C.E. (2004). Alphastatin, a 24-amino acid fragment of human fibrinogen, is a potent new inhibitor of activated endothelial cells in vitro and in vivo. *Blood*, **103**, 601-6.

Stern, M.D. (1975). In vivo evaluation of microcirculation by coherent light scattering. *Nature*, **254**, 56-8.

Stessels, F., Van den Eynden, G., Van der Auwera, I., Salgado, R., Van den Heuvel, E., Harris, A.L., Jackson, D.G., Colpaert, C.G., van Marck, E.A., Dirix, L.Y. & Vermeulen, P.B. (2004). Breast adenocarcinoma liver metastases, in contrast to colorectal cancer liver metastases, display a non-angiogenic growth pattern that preserves the stroma and lacks hypoxia. *Br J Cancer*, **90**, 1429-36.

Stevenson, J.P., Rosen, M., Sun, W., Gallagher, M., Haller, D.G., Vaughn, D., Giantonio, B., Zimmer, R., Petros, W.P., Stratford, M., Chaplin, D., Young, S.L., Schnall, M. & O'Dwyer, P.J. (2003). Phase I trial of the antivascular agent combretastatin A4 phosphate on a 5-day schedule to patients with cancer: magnetic resonance imaging evidence for altered tumor blood flow. *J Clin Oncol*, **21**, 4428-38.

Stewart, J. (1894). Researches on the circulation time in organs and on the influences which affect it. Parts I-III. *J Physiol*, **15**, 1.

Stuart, K. (2003). Chemoembolization in the management of liver tumors. *Oncologist*, **8**, 425-37.

Su, M.Y., Jao, J.C. & Nalcioglu, O. (1994). Measurement of vascular volume fraction and blood-tissue permeability constants with a pharmacokinetic model: studies in rat muscle tumors with dynamic Gd-DTPA enhanced MRI. *Magn Reson Med*, **32**, 714-24.

Suri, C., Jones, P.F., Patan, S., Bartunkova, S., Maisonpierre, P.C., Davis, S., Sato, T.N. & Yancopoulos, G.D. (1996). Requisite role of angiopoietin-1, a ligand for the TIE2 receptor, during embryonic angiogenesis. *Cell*, **87**, 1171-80.

Suzuki, M., Hori, K., Abe, I., Saito, S. & Sato, H. (1981). A new approach to cancer chemotherapy: selective enhancement of tumor blood flow with angiotensin II. *J Natl Cancer Inst*, **67**, 663-9.

Takahashi, A., Sasaki, H., Kim, S.J., Tobisu, K., Kakizoe, T., Tsukamoto, T., Kumamoto, Y., Sugimura, T. & Terada, M. (1994). Markedly increased amounts of messenger RNAs for vascular endothelial growth factor and placenta growth factor in renal cell carcinoma associated with angiogenesis. *Cancer Res*, **54**, 4233-7.

Tanda, S., Hori, K., Saito, S., Shinozaki, M., Zhang, Q.H. & Suzuki, M. (1991). Comparison of the effects of intravenously bolus-administered endothelin-1 and infused angiotensin II on the subcutaneous tumor blood flow in anesthetized rats. *Jpn J Cancer Res*, **82**, 958-63.

Tarli, L., Balza, E., Viti, F., Borsi, L., Castellani, P., Berndorff, D., Dinkelborg, L., Neri, D. & Zardi, L. (1999). A high-affinity human antibody that targets tumoral blood vessels. *Blood*, **94**, 192-8.

Taylor, N.J., Baddeley, H., Goodchild, K.A., Powell, M.E., Thoumine, M., Culver, L.A., Stirling, J.J., Saunders, M.I., Hoskin, P.J., Phillips, H., Padhani, A.R. & Griffiths, J.R. (2001). BOLD MRI of human tumor oxygenation during carbogen breathing. *J Magn Reson Imaging*, **14**, 156-63.

Taylor, N.J., Carnell, D.M., Smith, R.E., Hoskin, P.J., Stirling, J.J., D'Arcy, J.A., Leach, M.O. & Padhani, A.R. (2003). Evaluation of prostate gland hypoxia with quantified BOLD MRI: initial results from a correlated histological study. In *Proc ISMRM*, Vol. 11. pp. 531: Toronto, Canada.

Taylor, N.J., Lankester, K.J., Ah-See, M.-L.W., Stirling, J.J., Rustin, G.J.S., Makris, A., D'Arcy, J.A., Walker-Samuel, S., Leach, M.O. & Padhani, A.R. (2004). Reproducibility of T1 and T2* weighted dynamic contrast-enhanced MRI: a multiparametric comparison of breast and abdominal tumours. In *Proc ISMRM*, Vol. 12. pp. 1975: Kyoto, Japan.

Thews, O., Kelleher, D.K. & Vaupel, P. (2002). Dynamics of tumor oxygenation and red blood cell flux in response to inspiratory hyperoxia combined with different levels of inspiratory hypercapnia. *Radiother Oncol*, **62**, 77-85.

Thomlinson, R. & Gray, L. (1955). The histologic structure of some human lung cancers and the possible implications for radiotherapy. *Br J Cancer*, **9**, 537-549.

Thompson, H.K., Jr., Starmer, C.F., Whalen, R.E. & McIntosh, H.D. (1964). Indicator Transit Time Considered as a Gamma Variate. *Circ Res*, **14**, 502-15.

Thomsen, L.L., Ching, L.M., Zhuang, L., Gavin, J.B. & Baguley, B.C. (1991). Tumor-dependent increased plasma nitrate concentrations as an indication of the antitumor effect of flavone-8-acetic acid and analogues in mice. *Cancer Res*, **51**, 77-81.

Thorpe, P.E. (2004). Vascular targeting agents as cancer therapeutics. *Clin Cancer Res*, **10**, 415-27.

Tofts, P., Brix, G., Buckley, D., Evelhoch, J., Henderson, E., Knopp, M., Larsson, H., Lee, T., Mayr, N., Parker, G., Port, R., Taylor, J. & Weisskoff, R. (1999). Estimating kinetic parameters from dynamic contrast-enhanced T(1)-weighted MRI of a diffusable tracer: standardized quantities and symbols. *J Magn Reson Imaging*, **10**, 223-32.

Tofts, P.S. (1997). Modeling tracer kinetics in dynamic Gd-DTPA MR imaging. *J Magn Reson Imaging*, **7**, 91-101.

Tofts, P.S. & Kermode, A.G. (1991). Measurement of the blood-brain barrier permeability and leakage space using dynamic MR imaging. 1. Fundamental concepts. *Magn Reson Med*, **17**, 357-67.

Torres Filho, I.P., Leunig, M., Yuan, F., Intaglietta, M. & Jain, R.K. (1994). Noninvasive measurement of microvascular and interstitial oxygen profiles in a human tumor in SCID mice. *Proc Natl Acad Sci U S A*, **91**, 2081-5.

Tozer, G., Prise, V., Bell, K., Dennis, M., Stratford, M. & Chaplin, D. (1996). Reduced capacity of tumour blood vessels to produce endothelium-derived relaxing factor: significance for blood flow modification. *Br J Cancer*, **74**, 1955-60.

Tozer, G.M., Ameer-Beg, S.M., Baker, J., Barber, P.R., Hill, S.A., Hodgkiss, R.J., Locke, R., Prise, V.E., Wilson, I. & Vojnovic, B. (2005). Intravital imaging of tumour vascular networks using multi-photon fluorescence microscopy. *Adv Drug Deliv Rev*, **57**, 135-52.

Tozer, G.M., Kanthou, C., Parkins, C.S. & Hill, S.A. (2002). The biology of the combretastatins as tumour vascular targeting agents. *Int J Exp Pathol*, **83**, 21-38.

Tozer, G.M., Lewis, S., Michalowski, A. & Aber, V. (1990). The relationship between regional variations in blood flow and histology in a transplanted rat fibrosarcoma. *Br J Cancer*, **61**, 250-7.

Tozer, G.M., Prise, V.E., Wilson, J., Cemazar, M., Shan, S., Dewhirst, M.W., Barber, P.R., Vojnovic, B. & Chaplin, D.J. (2001). Mechanisms associated with tumor vascular shut-down induced by combretastatin A-4 phosphate: intravital microscopy and measurement of vascular permeability. *Cancer Res*, **61**, 6413-22.

Tozer, G.M., Prise, V.E., Wilson, J., Locke, R.J., Vojnovic, B., Stratford, M.R., Dennis, M.F. & Chaplin, D.J. (1999). Combretastatin A-4 phosphate as a tumor vascular-targeting agent: early effects in tumors and normal tissues. *Cancer Res*, **59**, 1626-34.

Tozer, G.M. & Shaffi, K.M. (1993). Modification of tumour blood flow using the hypertensive agent, angiotensin II. *Br J Cancer*, **67**, 981-8.

Tozer, G.M., Shaffi, K.M., Prise, V.E. & Cunningham, V.J. (1994). Characterisation of tumour blood flow using a 'tissue-isolated' preparation. *Br J Cancer*, **70**, 1040-6.

Trotter, M., Chaplin, D. & Olive, P. (1991). Effect of angiotensin II on intermittent tumour blood flow and acute hypoxia in the murine SCCVII carcinoma. *Eur J Cancer*, **27**, 887-893.

Tsunoda, S., Ohizumi, I., Matsui, J., Koizumi, K., Wakai, Y., Makimoto, H., Tsutsumi, Y., Utoguchi, N., Taniguchi, K., Saito, H., Harada, N., Ohsugi, Y. & Mayumi, T. (1999). Specific binding of TES-23 antibody to tumour vascular endothelium in mice, rats and human cancer tissue: a novel drug carrier for cancer targeting therapy. *Br J Cancer*, **81**, 1155-1161.

Unthank, J.L., Lash, J.M., Nixon, J.C., Sidner, R.A. & Bohlen, H.G. (1993). Evaluation of carbocyanine-labeled erythrocytes for microvascular measurements. *Microvasc Res*, **45**, 193-210.

Vajkoczy, P., Menger, M.D., Goldbrunner, R., Ge, S., Fong, T.A., Vollmar, B., Schilling, L., Ullrich, A., Hirth, K.P., Tonn, J.C., Schmiedek, P. & Rempel, S.A. (2000). Targeting angiogenesis inhibits tumor infiltration and expression of the pro-invasive protein SPARC. *Int J Cancer*, **87**, 261-8.

van Geel, I.P., Oppelaar, H., Rijken, P.F., Bernsen, H.J., Hagemeier, N.E., van der Kogel, A.J., Hodgkiss, R.J. & Stewart, F.A. (1996). Vascular perfusion and hypoxic areas in RIF-1 tumours after photodynamic therapy. *Br J Cancer*, **73**, 288-93.

van Nieuw Amerongen, G.P. & van Hinsbergh, V.W. (2001). Cytoskeletal effects of rho-like small guanine nucleotide-binding proteins in the vascular system. *Arterioscler Thromb Vasc Biol*, **21**, 300-11.

Vaupel, P. & Höckel, M. (1998). Oxygenation of human tumours. In *Blood perfusion and microenvironment of human tumours*, Molls, M. & Vaupel, P. (eds) pp. 63-72. Springer-Verlag: Berlin Heidelberg.

Vaupel, P., Kallinowski, F. & Okunieff, P. (1989). Blood flow, oxygen and nutrient supply, and metabolic microenvironment of human tumors: a review. *Cancer Res*, **49**, 6449-65.

Veenendaal, L.M., Jin, H., Ran, S., Cheung, L., Navone, N., Marks, J.W., Waltenberger, J., Thorpe, P. & Rosenblum, M.G. (2002). In vitro and in vivo studies of a VEGF121/rGelonin chimeric fusion toxin targeting the neovasculature of solid tumors. *Proc Natl Acad Sci U S A*, **99**, 7866-71.

Vermeulen, P.B., Colpaert, C., Salgado, R., Royers, R., Hellemans, H., Van Den Heuvel, E., Goovaerts, G., Dirix, L.Y. & Van Marck, E. (2001). Liver metastases from colorectal adenocarcinomas grow in three patterns with different angiogenesis and desmoplasia. *J Pathol*, **195**, 336-42.

Vernon, C.C., Hand, J.W., Field, S.B., Machin, D., Whaley, J.B., van der Zee, J., van Putten, W.L., van Rhoon, G.C., van Dijk, J.D., Gonzalez Gonzalez, D., Liu, F.F., Goodman, P. & Sherar, M. (1996). Radiotherapy with or without hyperthermia in the treatment of superficial localized breast cancer: results from five randomized controlled trials. International Collaborative Hyperthermia Group. *Int J Radiat Oncol Biol Phys*, **35**, 731-44.

Villringer, A., Rosen, B.R., Belliveau, J.W., Ackerman, J.L., Lauffer, R.B., Buxton, R.B., Chao, Y.S., Wedeen, V.J. & Brady, T.J. (1988). Dynamic imaging with lanthanide chelates in normal brain: contrast due to magnetic susceptibility effects. *Magn Reson Med*, **6**, 164-74.

Wakui, S., Furusato, M., Muto, T., Ohshige, H., Takahashi, H. & Ushigome, S. (1997). Transforming growth factor-beta and urokinase plasminogen activator presents at endothelial cell-pericyte interdigitation in human granulation tissue. *Microvasc Res*, **54**, 262-9.

Wang, I., Bendsoe, N., Klinteberg, C.A., Enejder, A.M., Andersson-Engels, S., Svanberg, S. & Svanberg, K. (2001). Photodynamic therapy vs. cryosurgery of basal cell carcinomas: results of a phase III clinical trial. *Br J Dermatol*, **144**, 832-40.

Wang, T.H., Wang, H.S. & Soong, Y.K. (2000). Paclitaxel-induced cell death: where the cell cycle and apoptosis come together. *Cancer*, **88**, 2619-28.

Warren, R.S., Yuan, H., Matli, M.R., Gillett, N.A. & Ferrara, N. (1995). Regulation by vascular endothelial growth factor of human colon cancer tumorigenesis in a mouse model of experimental liver metastasis. *J Clin Invest*, **95**, 1789-97.

Watnick, R.S., Cheng, Y.N., Rangarajan, A., Ince, T.A. & Weinberg, R.A. (2003). Ras modulates Myc activity to repress thrombospondin-1 expression and increase tumor angiogenesis. *Cancer Cell*, **3**, 219-31.

Wedeking, P., Eaton, S., Covell, D.G., Nair, S., Tweedle, M.F. & Eckelman, W.C. (1990). Pharmacokinetic analysis of blood distribution of intravenously administered 153Gd-labeled Gd(DTPA)2- and 99mTc(DTPA) in rats. *Magn Reson Imaging*, **8**, 567-75.

Weinmann, H.J., Laniado, M. & Mutzel, W. (1984). Pharmacokinetics of GdDTPA/dimeglumine after intravenous injection into healthy volunteers. *Physiol Chem Phys Med NMR*, **16**, 167-72.

Weisskoff, R.M., Chesler, D., Boxerman, J.L. & Rosen, B.R. (1993). Pitfalls in MR measurement of tissue blood flow with intravascular tracers: which mean transit time? *Magn Reson Med*, **29**, 553-8.

Wike-Hooley, J.L., Haveman, J. & Reinhold, H.S. (1984). The relevance of tumour pH to the treatment of malignant disease. *Radiother Oncol*, **2**, 343-66.

Wirestam, R., Ryding, E., Lindgren, A., Geijer, B., Holtas, S. & Stahlberg, F. (2000). Absolute cerebral blood flow measured by dynamic susceptibility contrast MRI: a direct comparison with Xe-133 SPECT. *Magma*, **11**, 96-103.

Wust, P., Hildebrandt, B., Sreenivasa, G., Rau, B., Gellermann, J., Riess, H., Felix, R. & Schlag, P.M. (2002). Hyperthermia in combined treatment of cancer. *Lancet Oncol*, **3**, 487-97.

Wyld, L., Burn, J.L., Reed, M.W. & Brown, N.J. (1997). Factors affecting aminolaevulinic acid-induced generation of protoporphyrin IX. *Br J Cancer*, **76**, 705-12.

Wyld, L., Reed, M.W. & Brown, N.J. (2001). Differential cell death response to photodynamic therapy is dependent on dose and cell type. *Br J Cancer*, **84**, 1384-6.

Yancopoulos, G.D., Davis, S., Gale, N.W., Rudge, J.S., Wiegand, S.J. & Holash, J. (2000). Vascular-specific growth factors and blood vessel formation. *Nature*, **407**, 242-8.

Yuan, F., Chen, Y., Dellian, M., Safabakhsh, N., Ferrara, N. & Jain, R.K. (1996). Time-dependent vascular regression and permeability changes in established human tumor xenografts induced by an anti-vascular endothelial growth factor/vascular permeability factor antibody. *Proc Natl Acad Sci U S A*, **93**, 14765-70.

Yuan, F., Leunig, M., Berk, D.A. & Jain, R.K. (1993). Microvascular permeability of albumin, vascular surface area, and vascular volume measured in human adenocarcinoma LS174T using dorsal chamber in SCID mice. *Microvasc Res*, **45**, 269-89.

Zanelli, G.D. & Fowler, J.F. (1974). The measurement of blood perfusion in experimental tumors by uptake of 86Rb. *Cancer Res*, **34**, 1451-6.

Zhang, L. & Hill, R.P. (2004). Hypoxia enhances metastatic efficiency by up-regulating Mdm2 in KHT cells and increasing resistance to apoptosis. *Cancer Res*, **64**, 4180-9.

Zierler, K.L. (1965). Equations for Measuring Blood Flow by External Monitoring of Radioisotopes. *Circ Res*, **16**, 309-21.

Znati, C.A., Rosenstein, M., Boucher, Y., Epperly, M.W., Bloomer, W.D. & Jain, R.K. (1996). Effect of radiation on interstitial fluid pressure and oxygenation in a human tumor xenograft. *Cancer Res*, **56**, 964-68.

Chapter 2 DCE-MRI measurement of acute vascular disruptive effects of cytotoxic agents

2.1 Introduction

The hypothesis of the study presented in this chapter was that taxane and platinum cytotoxic agents would not have significant acute (within 24 hours) anti-vascular effects as determined by DCE-MRI.

2.1.1 Background

DCE-MRI has been used to evaluate vascular disruptive and anti-angiogenic agents in both xenograft studies and human trials. Significant reductions in tumour DCE-MRI kinetic parameters are seen within 4-24 hours of vascular disruptive therapy (Dowlati et al., 2002; Evelhoch et al., 2002; Galbraith et al., 2003; Galbraith et al., 2002b; Maxwell et al., 2002; Stevenson et al., 2003) and by 48 hours with anti-angiogenic agents (Checkley et al., 2003a; Checkley et al., 2003b; Gossmann et al., 2002; Jayson et al., 2002; Morgan et al., 2003) (see also **Section 1.5.5**).

As DCE-MRI is used in early clinical trials to confirm that vascular disruptive and anti-angiogenic agents target vasculature, it is important to know whether cytotoxic agents also have acute effects on vasculature. As well as classifying agents according to their method of action, such information would also help in planning combination therapy and interpreting DCE-MRI results of such combination therapy.

The acute effects of cytotoxic agents on DCE-MRI kinetic parameters have not previously been reported, although measurements have been performed after 1-2 cycles of treatment (Ah-See et al., 2004; Barentsz et al., 1998; Reddick et al., 1999; Wolf et al., 2003). However, at this time-point objective tumour shrinkage and pathological response are also seen, so changes in DCE-MRI parameters may be due to a reduction in blood flow secondary to tumour cell kill rather than a direct anti-vascular effect. Animal studies suggest that apart from possibly the vinca alkaloids, significant acute vascular disruptive effects are unlikely (Chaplin & Hill, 2002) but significant anti-angiogenic effects might be more of an issue (Miller et al., 2001).

All chemotherapy regimens tested in this study included a taxane and/or platinum agent, as these are likely candidates for combination therapy in future clinical trials. The taxanes

exert their cytotoxic effects by inhibiting spindle formation but act by stabilising microtubules rather than inducing depolymerisation, so do not have vascular disruptive properties (Jordan et al., 1998; Wang et al., 2000). The platinums are alkylating agents that bind to DNA, inducing cross-link formation (Cavalli et al., 2000). Belotti et al. found that both cisplatin and paclitaxel have anti-angiogenic effects *in vitro*, but only paclitaxel had anti-angiogenic effects *in vivo* (Belotti et al., 1996).

2.1.2 Study objective

The objective was to investigate the acute DCE-MRI effects of conventional cytotoxic agents measured 24 hours after the start of the first cycle of treatment. Two pre-treatment scans were performed on consecutive days to estimate the measurement error associated with DCE-MRI. A third scan was performed 20-24 hours after treatment and the significance of any changes were determined with reference to the 'reproducibility' of the technique. Patients with gynaecological cancers (mostly ovarian) with pelvic or abdominal masses were selected, as this group reflects our practice and to avoid tumour movement with respiration during imaging.

The T_1-weighted DCE-MRI kinetic parameters, K^{trans}, v_e, k_{ep} and IAUGC, were measured. In addition, T_2*-weighted DCE-MRI imaging was used to obtain estimates of tumour relative blood volume and blood flow and BOLD-MRI was used to obtain estimates of tumour R_2*.

2.2 *Methods*

2.2.1 Patient Selection

Local ethics committee approval for the trial protocol and written informed consent from all participating patients were obtained. Eligibility criteria for the study were: histologically confirmed cancer at an anatomical site suitable for imaging with MRI; tumour mass ≥3 cm in diameter; patient due to start first cycle of taxane or platinum-based chemotherapy regimen; calculated creatinine clearance[1] >50 ml.min^{-1}; WHO performance status ≤2[2]; age ≥18 years; no history of allergic reaction to contrast agents.

2.2.2 MRI protocol

The MRI studies were performed on a 1.5 Tesla Magnetom Symphony scanner (Siemens Medical Systems, Erlangen, Germany), using a body phased array coil. In the first scanning session, initial T_1 and T_2 weighted anatomical images were obtained to select four suitable contiguous slices through the centre of a tumour mass. Care was taken to place the patient in the same position on the follow-up sessions, in order to obtain the same anatomical slice location. The following MR sequences were then acquired (slice thickness was 8 mm for all sequences, field of view (FOV) was 350 x 350 mm for sequences 1-3 and 128 x 128 mm for sequence 4):

Multiple spoiled GRE images were acquired on a single central slice with increasing TE times (5-75 ms and TR 100 ms, flip angle (α) 40°, in-plane resolution 1.37 x 2.19 mm) – for calculation of R_2* (BOLD).

A proton density (PD)-weighted spoiled gradient-recalled echo (GRE) sequence: TE 4.7 ms; TR 350 ms; α 6°; in-plane resolution 1.37 x 2.19 mm; 4 slices – for calculation of T_1 relaxation rates, see below.

A dynamic series of 40 T_1-weighted GRE images: TE 4.7 ms, TR 11 ms, α 35°, in-plane resolution 1.37 x 2.19 mm, total imaging time of 8 min 5 s – using the same slice positions

---

[1]: Calculated creatinine clearance (ml.min^{-1}) = [(140-age in years) x 1.04 x weight in kg]/plasma creatinine in μmol.l^{-1} (the Cockcroft-Gault equation).

[2] World Health Organisation performance status scale: 0=normal activities, 1=light work, 2=resting <50% of day, 3=resting >50% of day, 4=bed-bound.

as the PD sequence. Gadopentetate dimeglumine (Gd-DTPA, Magnevist(R), Schering Health Care Ltd., Burgess Hill, UK) was the contrast agent used, injected intravenously using a power injector (dose 0.1 mmol.kg^{-1} bodyweight) at 4 ml.s^{-1} during the fifth acquisition.

A dynamic series of 60 T_2*-weighted spoiled GRE images were then acquired on a single central slice (TE 20 ms, TR 30 ms, α 40^0, in-plane resolution 2.73 x 2.73 mm). A second Gd-DTPA injection (dose 0.2 mmol.kg^{-1}, at 4 ml.s^{-1}) was administered after the tenth acquisition.

System gain and scaling factors were maintained between acquisition of the proton density and T_1-weighted dynamic series of images, to enable the calculation of tissue contrast agent concentration (Parker et al., 1997). Patient blood pressure and pulse were measured on each day before imaging.

2.2.3 Image Analysis

Images were transferred to a Sun Ultra 60 workstation, (Sun Microsystems, Mountain View, CA, USA) and analysed using specialist software (Magnetic Resonance Imaging Workbench (MRIW), Institute of Cancer Research, London UK) (Parker et al., 1998). Using information from anatomical and post-contrast T_1 images, regions of interest (ROIs) were carefully drawn around the tumour edges by a trained radiologist who carefully excluded areas of artefacts and blood vessels. An elliptical ROI was also placed in an area of muscle (usually gluteus maximus as the majority of patients had pelvic tumours) on the central imaging slice. Similar ROIs were used for all three MR examinations in an individual patient.

2.2.3.1 Calculation of T_1-weighted parameters

MRIW software was used to convert MRI signal intensities into T_1 relaxation rates and then to Gd-DTPA concentrations for individual voxels, using the methods described by Parker (Parker et al., 1997). The relaxivity, r_1, was taken to be 4.5 mM^{-1}s^{-1} at 1.5 Tesla (Donahue et al., 1994) (see **Section 1.5**).

The following T_1-weighted parameters were calculated in the MRIW software: IAUGC, K^{trans}, k_{ep} and v_e. IAUGC was calculated over the first 60 seconds following injection of contrast agent, taking the onset time as the median value of the whole tumour ROI. Then,

the data were fitted to a standard compartmental model (Kety, 1960), to characterise the arterial influx of Gd-DTPA into the tumour extracellular extravascular space and its venous efflux to obtain K^{trans}, k_{ep} and v_e. An assumed arterial input function (AIF) was used for the modelling procedure (Tofts, 1997; Weinmann et al., 1984) as described previously (Galbraith et al., 2002a).

Voxels with negative or zero values of IAUGC were excluded from analysis. For the modelled data, non-enhancing voxels, voxels containing enhancing modelling failures and voxels with K^{trans} values <0.001 or >5 min^{-1} were excluded from analysis. The analysis was performed on concatenated data from all slices containing tumour, and the central slice for muscle, taking the median voxel value as representative of central tendency. Median rather than the mean voxel values were used as histogram distributions of some kinetic parameters were skewed.

2.2.3.2 *Calculation of T_2*-weighted DCE-MRI parameters: rBV and rBF*

ΔR_2* values were calculated for each time point and fitted using a Γ-variate function using MRIW software. rBV is then the integral of the ΔR_2*-time curve (using the Γ-variate fit) - see **Section 1.5.3.2.**

The relative mean transit time (MTT)[3] was approximated by measuring the width of the ΔR_2*-time curve at half its maximum value ('full-width, half-maximum') (Perthen et al., 2002). rBF was then obtained by substituting in the transit time equation (see **Section 1.4.2.3**).

A single global value for the entire ROI was obtained by taking the median of all the individual voxel values of the parameters. Parameter values >100,000 were excluded from analysis.

2.2.3.3 *Calculation of R_2* (BOLD)*

R_2* maps were calculated using IDL(R) (Research Systems, Inc, Boulder, CO, USA). A straight line was fitted to a plot of $\ln S_t$ against TE for each voxel, of which the gradient is $-R_2$* (re-arranging equation 28, **Section 1.5.4**). Voxels with either negative or zero values were excluded from analysis.

[3] For MRI, the abbreviation, MTT is usually used for mean transit time instead of τ.

2.2.4 Statistical Analysis

A reproducibility analysis was performed for each measured parameter. This has been done previously for T_1-weighted parameters (Galbraith et al., 2002a) but not for T_2*-weighted parameters.

The statistical analysis used to determine reproducibility has been described previously (Bland & Altman, 1996a; Bland & Altman, 1996b; Galbraith et al., 2002a; Padhani et al., 2002). The key statistical parameters are the 95% confidence intervals for change for a group of n patients and for an individual patient (the latter also known as the repeatability statistic). The 95% confidence intervals can then be used to determine whether a change in a kinetic parameter following an intervention is statistically significant or not (see below). The within-patient coefficient of variation was also calculated, as other MRI researchers have quoted this parameter.

In summary, for each patient, the difference d between the two pre-treatment measurements of a parameter was calculated. Data were transformed using natural logarithms if the variability of d was found to depend on its mean value (Bland & Altman, 1996b). The square root of the mean squared difference, dsd, ($=\sqrt{[(\Sigma d^2)/n]}$ where n is the number of patients) was then calculated. The 95% confidence interval for change for a group of n patients is then equal to $\pm(1.96 \times dsd/\sqrt{n})$. For an individual patient, n=1 so the 95% confidence interval for change is equal to $\pm(1.96 \times dsd)$, which is also known as the repeatability statistic, r (Bland & Altman, 1996a).

The within-patient standard deviation $wSD = dsd/\sqrt{2}$, as there are two pre-treatment measurements. This is a measure of the precision of the measurement error. The difference between a patient's parameter measurement and the true value is expected to be less than 1.96 x wSD for 95% of observations. The within-patient coefficient of variation, wCV, is then obtained by dividing wSD by the group mean pre-treatment value for each parameter. wCV quantifies measurement error relative to the size of the (positive) kinetic parameters. If data had to be transformed, then wCV was approximated by $wCV = e^{wSD}-1$ (Bland & Altman, 1996b).

The results of the reproducibility analysis were then used to assess whether there had been a statistically significant change in kinetic parameters due to chemotherapy, either for individual patients or the group. As there were two pre-treatment measurements (days 1

and 2), the mean of the two pre-treatment examinations was taken as the pre-treatment value for each parameter. The null hypothesis was that there would be no difference between this combined pre-treatment value and the post-treatment value.

For individual patients, the repeatability statistic, *r*, expressed as a percentage of the group mean pre-treatment value for each parameter, gives a range within which the difference between pre and post-treatment values would be expected to lie for 95% of observations, assuming that the null hypothesis is true. If the difference falls outside this range for a particular kinetic parameter, then a significant change was deemed to have occurred. Similarly, to assess mean response in the group, the 95% confidence interval for change, expressed as a percentage of the group mean pre-treatment value, gives the range required.

In addition, Spearman's ρ was used to determine whether there was a significant correlation between any of the baseline (day 1) parameter values (JMP Statistics (version 3.2.6, SAS Institute, Inc, Cary, North Carolina, USA).

2.3 *Results*

2.3.1 Patient characteristics

24 female patients were imaged in total. The average age was 56 years old (range 29 to 74 years). Data from four patients were excluded from analysis (3 technical failures, 1 voluntary patient motion). Data could not be obtained from all slices on day 3 for one patient (no.19 in **Table 2.1**) due to internal organ motion. One patient was unable to complete the post-treatment scan but data from the two pre-treatment scans were included in the reproducibility analysis (no.20 in **Table 2.1**). Therefore, for T_1-weighted DCE-MRI parameters, there were 20 complete data sets for the reproducibility analysis and 18 complete data sets for the response analysis. For T_2*-weighted DCE-MRI parameters (rBV, MTT, rBF) there were only 16 complete data sets for reproducibility and response analysis, as 4 patients did not complete this section on at least one of the imaging days. There were 20 complete data sets for the R_2* (BOLD) reproducibility and response analysis.

The average time from the start of chemotherapy to the third scan was 21 hours (range 17 to 23 hours).

Table 2.1 shows patient details including diagnosis, chemotherapy regimen used and response to treatment. Response was assessed after three cycles of chemotherapy either on CT or MRI imaging or by CA125 measurements[4] (based on RECIST[5] or CA125 criteria) (Rustin, 2003; Therasse et al., 2000).

Table 2.2 gives total voxel numbers and the percentage of voxels that were non-enhancing or were modelling failures. Baseline (day 1) MR parameter values for each patient are given in **Table 2.3.**

Figure 2.1 shows a baseline T_1-weighted image and also K^{trans}, rBV and R_2* MR images from days 1, 2 and 3 (data from patient 4).

[4] CA125 is a serum tumour marker that may be raised in ovarian cancer.

[5] RECIST: The 'Response Evaluation Criteria in Solid Tumours' group have issued guidelines for assessment of radiographic and clinical response based on % change in tumour size (Therasse et al., 2000).

N	Age	Tumour type	Tumour site	Chemotherapy regimen*	Previous treat-ments	Outcome‡
1	55	Adeno-carcinoma, ovary	pelvis	**C**: AUC 6†	1	Stable disease
2	70	Mixed mullerian tumour/carcinosarcoma	pelvis	**P** 60 mg.m^{-2}, **A** 60 mg.m^{-2}	0	Not evaluable#
3	59	Adeno-carcinoma, ovary	pelvis	**C**: AUC 6	0	Stable disease
4	46	Adeno-carcinoma, ovary	anterior abdominal wall	**C**: AUC 5, **T** 175 mg.m^{-2}	0	Stable disease
5	66	Adeno-carcinoma – ?ovary or colon	para-aortic lymph nodes	**C**: AUC 5	0	Progressive disease
6	73	Clear cell carcinoma, ovary	pelvis	**C**: AUC 6	2	Stable disease
7	42	Primary peritoneal carcinoma	pelvis	**P** 25 mg.m^{-2}, **D** 60 mg.m^{-2} weekly	5	Stable disease
8	65	Mixed mullerian tumour	pelvis	**P** 70 mg.m^{-2}, **E** 70 mg.m^{-2}	0	Partial response
9	62	Adeno-carcinoma, ovary	pelvis	**P** 60 mg.m^{-2}, **D** 40 mg.m^{-2} weekly	1	Partial response
10	57	Adeno-carcinoma, ovary	pelvis	**D** 80 mg.m^{-2} day 1, **G** 1250 mg.m^{-2}days 1 & 8	2	Partial response
11	49	Granulosa cell tumour, ovary	pelvis	**B** 30mg days 2,8,15, **E** 165 mg.m^{-2} days 1-3, **P** 50 mg.m^{-2} days 1 & 2.	0	Partial response
12	45	Adeno-carcinoma, ovary	pelvis	**C**: AUC 6	0	Stable disease
13	54	Adeno-carcinoma, ovary	pelvis	**C**: AUC 6	2	Partial response
14	59	Primitive neuro-ectodermal tumour	pelvis	**P** 50 mg.m^{-2} days 1&2, **E** 150 mg.m^{-2} days 1,2,3	0	Partial response
15	46	Adeno-carcinoma, ovary	pelvis	**C**: AUC 6	1	Stable disease
16	66	Adenocarcinoma ovary	pelvis	**P** 60 mg.m^{-2} weekly, **Etop** 50mg PO od	4	Not evaluable
17	67	primary peritoneal carcinoma	pelvis	**C**: AUC 6, **T** 175 mg.m^{-2}	1	Partial response
18	52	Adenocarcinoma, endometrium	pelvis	**P** 60 mg.m^{-2}, **A** 60 mg.m^{-2}	0	Partial response
19	29	Squamous cell carcinoma, cervix	cervix	**P** 60 mg.m^{-2}, **M** 300 mg.m^{-2}, **B** 30 mg.m^{-2}	0	Not evaluable
20	74	Poorly differentiated carcinoma ?ovary	anterior abdominal wall	**C**: AUC 5	0	Not evaluable

Table 2.1 Patient details: Patient order corresponds with data in **Figures 2.2 & 2.3.** N: patient number. *All chemotherapy regimens were given i.v. and repeated every three weeks unless otherwise stated. Chemotherapy drugs: **A**: adriamycin; **B**: bleomycin; **C**: carboplatin; **D**: docetaxol; **E**: epirubicin; **Etop**: etoposide; **G**: gemcitabine; **M**: methotrexate; **T**: Paclitaxel. **PO**: orally, **AUC**: area under the curve, **bd**: twice daily. †Carboplatin dose calculated according to AUC (area under the plasma-concentration time curve) based on method described by Calvert et al (Calvert et al., 1989). ‡based on RECIST or CA-125 criteria. # Not evaluable: patient only received 1 cycle of chemotherapy.

Patient number	Total voxels	non-enhancing voxels (%)	enhancing voxels with modelling failures (%)
1	849	37.3	5.5
2	5119	17.2	2.1
3	1375	4.8	5.1
4	2179	12.9	8.8
5	858	3.5	2.0
6	2317	47.8	28.1
7	1299	38.0	15.5
8	3128	12.3	5.3
9	3735	25.9	9.7
10	2207	11.1	19.7
11	1515	15.2	8.1
12	2889	2.5	15.6
13	149	0.0	7.4
14	226	10.6	36.7
15	1679	5.8	7.2
16	245	1.2	4.5
17	1149	1.5	12.9
18	4664	7.5	14.3
19	3445	3.7	39.8
20	1789	13.8	18.3

Table 2.2: Tumour voxel numbers (central tumour slice).

	T_1-parameters				T_2*-parameters			
N	K^{trans}	v_e (%)	k_{ep}	IAUGC	rBV	MTT	rBF	R_2*
1	0.152	33.84	0.449	2.19	86.4	25.1	3.41	12.14
2	0.244	46.49	0.524	4.30	317.0	28.6	10.925	16.96
3	0.233	39.21	0.594	4.24	266.7	25.8	10.12	22.62
4	0.252	40.71	0.620	5.34	241.7	26.3	9.47	20.23
5	0.270	52.22	0.517	5.65	83.2	22.5	3.58	16.21
6	0.207	27.12	0.763	2.14	59.8	27.7	1.46	12.28
7	0.349	38.32	0.911	5.30	163.4	23.1	6.50	21.04
8	0.282	38.37	0.736	5.57	308.9	23.4	12.94	16.47
9	0.284	36.83	0.772	4.23	294.4	24.3	11.89	9.08
10	0.311	34.16	0.911	4.90	311.2	26.0	11.75	20.03
11	0.243	36.85	0.660	4.90	136.2	26.8	4.9	25.46
12	0.327	27.62	1.184	4.82	217.3	22.8	9.29	26.39
13	0.405	47.71	0.849	9.50	150.5	21.2	7.10	17.13
14	0.511	45.05	1.135	8.44	280.3	23.9	11.86	36.51
15	0.433	30.48	1.419	6.82	373.8	23.7	15.62	16.6
16	0.500	48.20	1.037	8.47	308.5	24.3	12.00	31.98
17	0.550	44.20	1.244	9.44	483.0	24.9	19.15	19.12
18	0.630	43.87	1.437	10.56	366.3	22.8	15.71	28.15
19	0.589	65.21	0.903	12.08	425.7	26.2	16.32	19.51
20	1.081	40.28	2.684	9.04	400.1	25.1	16.07	28.83

Table 2.3: Baseline MR parameters (day 1) for individual patients

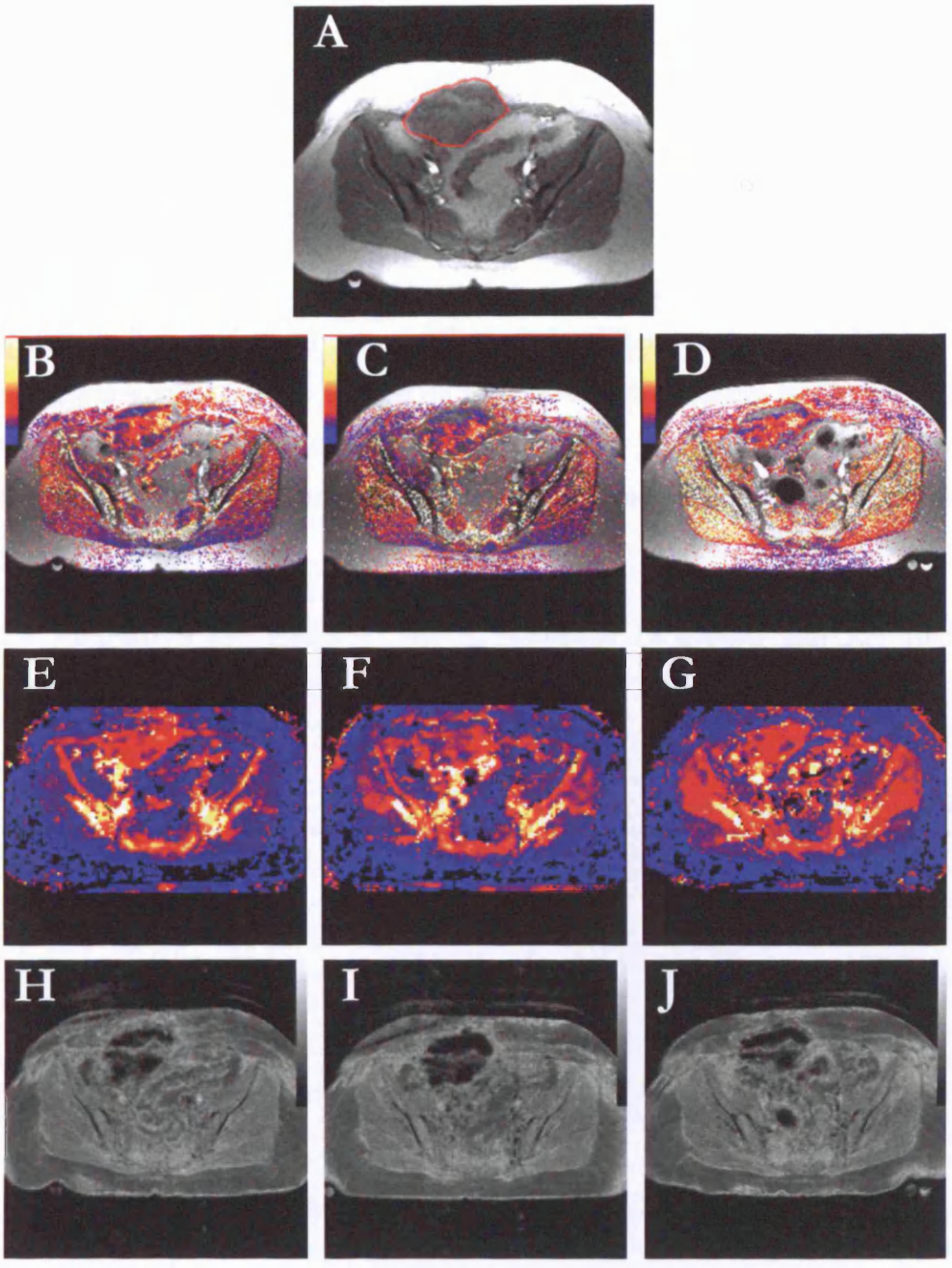

Figure 2.1 Representative MRI maps (patient 4). **A:** T_1-weighted image with tumour outlined in red; **B, C, D:** K^{trans} maps from day 1, 2 & 3 respectively. **E, F, G**: rBV maps from days 1, 2 & 3 respectively. **H, I, J**: R_2^* maps form days 1, 2 & 3 respectively.

The absolute % change in MABP and pulse between the mean pre-treatment value (day 1 and day 2) and day 3 were 7.7% (±1.4) and 8.9% (±2.8) respectively but these changes were not significant (paired t-test). 6 patients had changes in MABP >10% (range 11-21%) and 3 patients had changes in pulse greater than 10% (range 18-45%) but none of these patients had a significant parameter change apart from patient # 1 (decrease in MABP of 12%) (see below).

2.3.2 Reproducibility

Tables 2.4 and 2.5 summarise the results of the T_1-weighted DCE-MRI reproducibility analysis for tumour and muscle (as a representative normal tissue). Data for K^{trans} and k_{ep} were logarithmically transformed as variability of the difference between the two pre-treatment measures was found to depend on their mean values (Bland & Altman, 1996b). Therefore, the repeatability expressed as a % of group mean pre-treatment value is asymmetric about the mean. The repeatability for the tumour's central slice is given for comparison with the 4-slice data.

Table 2.6 summarises the results of the T_2*-weighted DCE-MRI and R_2* (BOLD) reproducibility analysis for tumour.

	TUMOUR (all 4 slices)			
	K^{trans} (min^{-1})	v_e (%)	k_{ep} (min^{-1})	IAUGC (mM.s)
mean	0.39	40.6	0.95	6.36
dsd	0.26	4.74	0.23	1.09
r	0.51	9.29	0.44	2.14
r (%)	-40.0 to +66.7%	±22.9%	-35.9 to +55.9%	±33.7%
CI (%)	-10.8 to +12.1%	±5.1%	-9.5 to +10.5%	±7.5%
wSD	0.18	3.35	0.16	0.77
wCV (%)	20.3%	8.3%	17.4%	12.1%
r (%) single slice	-39.2 to +64.4%	±26.2%	-39.8 to +65.9%	±48.9%

Table 2.4: Tumour reproducibility analysis for T_1-weighted parameters. 4-slice concatenated data. K^{trans} and k_{ep} data are logarithmically transformed. **Mean**: group mean pre-treatment value; **dsd**: square root of the mean squared difference; **r**: individual patient repeatability; **r (%)**: repeatability as a % of group mean pre-treatment value; **CI**: group 95% confidence interval for change as a % of group mean pre-treatment value; **wSD**: within-patient standard deviation; **wCV**: within-patient coefficient of variation.

	MUSCLE (central slice)			
	K^{trans} (min^{-1})	v_e (%)	k_{ep} (min^{-1})	IAUGC (mM.s)
mean	0.15	19.78	0.79	3.79
dsd	0.55	2.59	0.54	1.53
r	1.07	5.08	1.06	2.99
r (%)	-65.9 to +192.9%	±25.7%	-65.1 to +188.3	±79.0%
CI (%)	-21.9 to +28.0%	±5.9%	-21.6 to +27.5%	±18.1%
wSD	0.39	1.83	0.38	1.08
wCV (%)	47.40%	9.28%	46.55%	28.50%

Table 2.5: Muscle reproducibility analysis for T_1-weighted parameters. n=19 as one muscle ROI failed to fit on day 2.

	TUMOUR (central slice)			
	rBV	MTT (s)	rBF (s^{-1})	R_2* (s^{-1})
mean	233.4	24.9	9.53	21.6
dsd	64.98	1.19	2.26	5.44
r	127.3	2.34	4.42	10.6
r (%)	±54.5%	±9.4%	±46.4%	±48.6%
CI (%)	±13.6%	±2.4%	±11.6%	±11.0%
wSD	45.9	0.84	1.60	3.84
wCV (%)	19.7%	3.4%	16.8%	17.5%

Table 2.6: Tumour reproducibility for T_2*-weighted parameters. rBV and rBF are expressed per unit volume of tissue hence rBV has no units and rBF is in s^{-1}.

2.3.3 Correlation between different parameters

Table 2.7 shows the correlation between different parameters. Parameters showing very strong correlations (>0.8) were K^{trans} and k_{ep}, K^{trans} and IAUGC, and rBV and rBF.

K^{trans}								
v_e	0.42 NS							
k_{ep}	**0.87** p<0.0001	-0.03 NS						
IAUGC	**0.86** p<0.0001	**0.68** p=0.01	0.58 p=0.01					
rBV	**0.69** p<0.001	0.28 NS	0.59 p=0.01	0.55 p=0.01				
MTT	-0.40 NS	-0.14 NS	-0.34 NS	-0.40 NS	0.1 NS			
rBF	**0.77** p<0.0001	0.33 NS	**0.64** p<0.01	**0.65** p<0.01	**0.96** p<0.0001	-0.05 NS		
R_2*	0.51 p<0.05	0.25 NS	0.54 p=0.01	0.44 NS	0.23 NS	-0.07 NS	0.28 NS	
	K^{trans}	v_e	k_{ep}	IAUGC	rBV	MTT	rBF	R_2*

Table 2.7: Correlation between baseline (day 1) parameter values. Values showing strong (>0.6) or very strong correlation (>0.8) shown in **bold.** NS: not significant.

2.3.4 Response

2.3.4.1 *T_1-weighted DCE-MRI parameters*

Figure 2.2 shows tumour pre-treatment values (mean of the two pre-treatment examinations), the post-treatment values and repeatability ranges for K^{trans}, v_e, k_{ep} and IAUGC respectively for each patient. Patients are ordered by mean pre-treatment K^{trans} to demonstrate that the repeatability range is dependent on the mean pre-treatment value. There were no significant changes post-treatment in K^{trans} (**Figure 2.2 A**). One patient had a significant decrease in v_e (# 11) (**Figure 2.2 B**). One patient had a significant increase in k_{ep} (# 7) (**Figure 2.2 C**). Two patients had a significant increase in IAUGC (# 2 and # 10) and one patient (# 11) had a significant decrease in IAUGC (**Figure 2.2 D**).

When data were analysed for the group as a whole, there were no significant changes in K^{trans}, k_{ep} or IAUGC. However, there was a 5.5% decrease in v_e that was marginally significant, as the group 95% confidence interval for v_e was ±5.1% (see **Table 2.4**).

2.3.4.2 *T_2*-weighted DCE-MRI and R_2* (BOLD) parameters*

Figure 2.3 shows tumour pre-treatment values (mean of the two pre-treatment examinations), the post-treatment values and repeatability ranges for rBV, MTT, rBF and R_2* respectively for each patient. Patients are ordered by mean pre-treatment K^{trans} as for **Figure 2.2.**

3 patients had a significant increase in rBV (# 7, # 15, # 17) and one had a significant decrease in rBV (# 1). 1 patient had a significant increase (# 16) and 1 patient a significant decrease (# 1) in MTT. The same three patients had an increase in rBF (# 7, # 15, # 17) and two had a significant decrease (# 1 and # 16).

When patients were analysed as a group, there were no significant changes in rBV, MTT or rBF.

One patient had a significant increase in R_2* (# 1). There was no significant change in group R_2*.

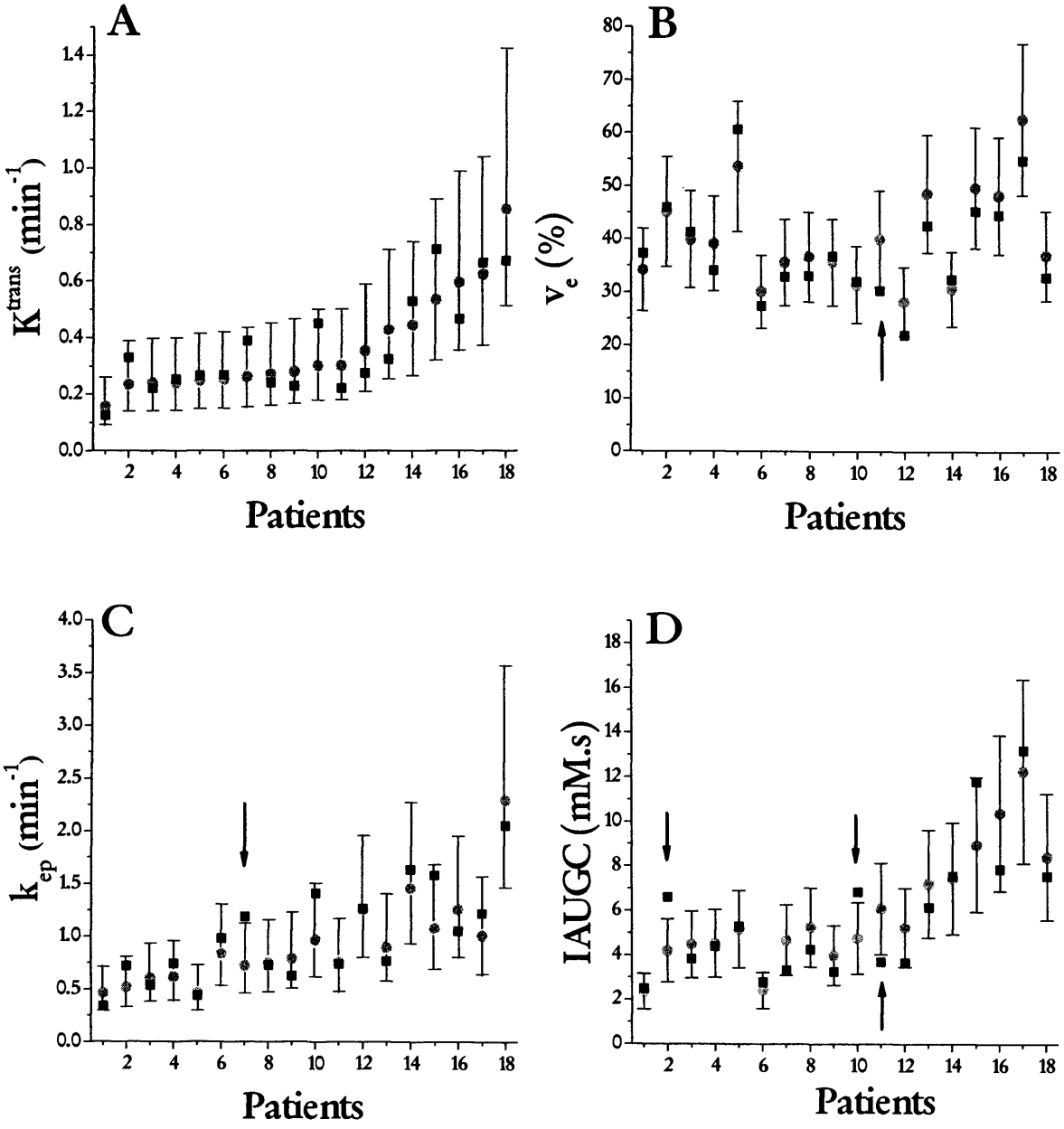

Figure 2.2: T_1-weighted parameters: A: K^{trans}, B: v_e, C: k_{ep}, D: IAUGC. The mean pre-treatment values (grey circle), post-treatment value (black square) and the repeatability range for each parameter. Significant day 3 values are marked with an arrow. Patients are ordered by mean pre-treatment K^{trans}.

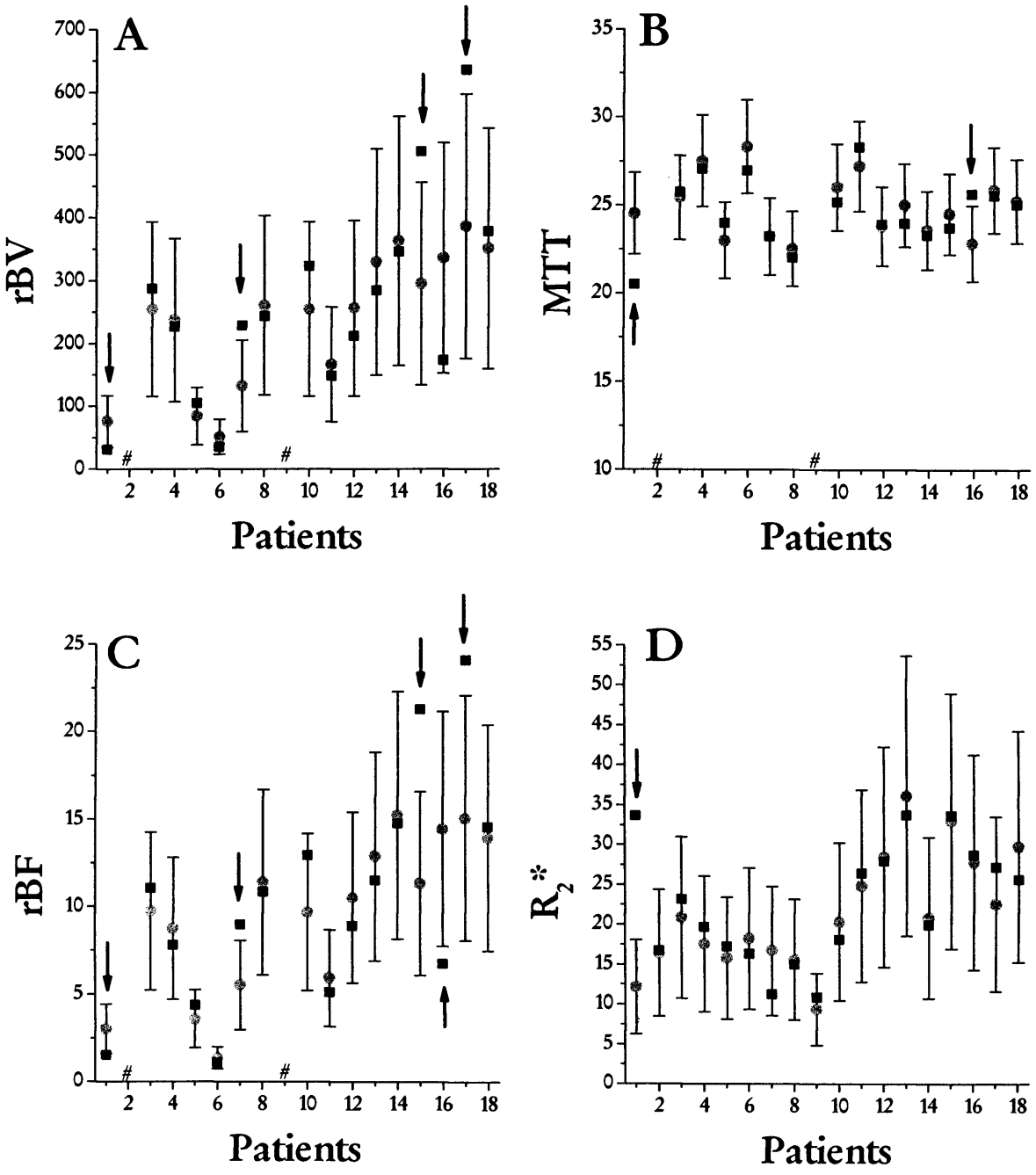

Figure 2.3: T_2*-weighted parameters. A: rBV, B: MTT C: rBF, D: R_2*. The mean pre-treatment values (grey circle), post-treatment value (black square) and the repeatability range for each parameter are shown. Significant day 3 values are marked with an arrow. Patients are ordered by mean pre-treatment K^{trans}. # missing data

2.4 Discussion

2.4.1 T_1-weighted DCE-MRI parameters

2.4.1.1 Reproducibility

The reproducibility analysis was very similar for the concatenated 4-slice and the single slice data (see **Table 2.4**) – therefore, it would be reasonable to use a single central tumour slice for subsequent studies.

The reproducibility analysis can be compared with other studies. For the phase I trial of CA-4-P performed at Mount Vernon hospital, Galbraith et al. reported an individual patient repeatability (as % of mean pre-treatment value) for tumour K^{trans} for a group of 16 patients of –45 to +83% (Galbraith et al., 2002a). The improvement between Galbraith et al.'s study and the current study is probably due to the use of a power injector and scanning on consecutive days – whereas Galbraith et al.'s study used manual injections and patients had repeat scans up to a week apart. A reproducibility analysis was also performed for the phase I trial of ZD6126 (Evelhoch et al., 2004). For 19 patients that were scanned 2-6 days apart, *wCV* was 18% for tumour IAUGC. From the data given in the paper, the individual patient repeatability (as % of mean pre-treatment value) can be calculated as ±48.9% (Evelhoch et al., 2004). In comparison, IAUGC reproducibility in the current study was ±33.7% (4-slice) and ±48.9% (central slice).

Reproducibility is not likely to improve significantly unless an individualised AIF is used. The change in contrast agent concentration in tumour-feeding arterioles is approximated by imaging an artery within the same image slice. It is technically difficult to obtain an individual AIF due to flow and pulsation artefacts within the chosen artery and, also, T_2^* effects can reduce signal intensity in regions of high contrast agent concentration, particularly at the top of the bolus passage (Rijpkema et al., 2001; van Laarhoven et al., 2003). However, techniques for measuring individual AIF have been published that improve reproducibility - e.g. the repeatability was ±20% for k_{ep} for a set of 11 patients with solid tumours, using an AIF obtained from the carotid or internal iliac artery (Rijpkema et al., 2001; van Laarhoven et al., 2003). An alternative strategy is to normalise to another tissue to correct for any change in cardiac output using a 'vascular normalisation function'. For example, repeatability for 11 patients with liver metastases, was ±27% for

k_{ep} using spleen to obtain a vascular normalisation function (van Laarhoven et al., 2003). This approach may not improve reproducibility, however, if a particular treatment also has an effect on the selected normal tissue. For, example CA-4-P produces ~7-fold reduction in blood flow in the spleen at 6 hours (measured using the IAP method in rat) (Tozer et al., 1999), so spleen may be an inappropriate comparator for vascular disruptive agents.

Mean pre-treatment parameter values were significantly lower for muscle than for tumour (unpaired t-test). Consequently, due to an increase in noise and variability, the reproducibility analysis for muscle was much worse than for tumour (see **Tables 2.4** and **2.5**). This has been noted by other authors using MRI (Evelhoch et al., 2004; Padhani et al., 2002) and the inherent variability of muscle blood flow measurements has also been observed using the IAP method (Tozer et al., 1999). It had been proposed that normalisation of tumour parameter values to muscle might improve reproducibility (Evelhoch et al., 2001). However, this was based on murine data and does not appear to be translated into human studies (Evelhoch et al., 2004). That reproducibility is worse when normalised to muscle has been confirmed using our data (for example, the individual repeatability for K^{trans} becomes –71.9% to +255.8% when the concatenated data is normalised to the muscle ROI).

It is not clear whether the poor muscle reproducibility is due to inherent variability or is a reflection of changes in cardiac output. Each patient's blood pressure and pulse were recorded before imaging – as an indication of cardiovascular status - but changes in these parameters did not correspond to MR parameter change. Measurement of cardiac output prior to imaging would help settle this issue.

2.4.1.2 Response

Our data show no significant change in group or individual K^{trans} at 24 hours following treatment with cisplatin or taxane based chemotherapy. In comparison, at 24 hours following treatment with ≥52 $mg.m^{-2}$ CA-4-P, a significant mean reduction in group K^{trans} of 29% was observed in a phase I trial for a group of 16 patients (Galbraith et al., 2003). Significant reductions in group v_e and IAUGC (of 11% and 18% respectively) were also observed in the CA-4-P phase I trial.

Given the wide within-patient variation in K^{trans} and IAUGC, it is not possible to confirm that the cytotoxic agents tested have no effect on tumour vascularity. However, based on

the results from this study, one is unlikely to expect large anti-vascular effects (and hence significant reductions in DCE-MRI kinetic parameters) in the acute setting due to cytotoxic agents alone. Therefore, if reductions in DCE-MRI kinetic parameters are seen in phase I trials of combination cytotoxic and vascular disruptive agents, one may presume they are due to the vascular disruptive agent.

These conclusions are supported by animal data. Chaplin and Hill (Chaplin & Hill, 2002) compared the effects of CA-4-P with a number of cytotoxic agents, including cisplatin and paclitaxel, in the murine CaNT tumour, using functional vascular volume (measured using Hoechst 33342) to assess vascular disruptive activity. No reduction was seen with any of the cytotoxic agents whereas a >80% reduction was seen following treatment with CA-4-P at 24 hours following drug administration (Chaplin & Hill, 2002). The only group of cytotoxic agents that has been found to have vascular disruptive activity in animal models is the vinca alkaloids. However, sustained effects are only seen at close to the maximum tolerated dose (MTD) (Baguley et al., 1991; Chaplin et al., 1996; Hill et al., 1993; Hill et al., 1995; Sersa et al., 2001).

The reason for the small reduction in group v_e is uncertain. For the one patient who had significant reduction in individual v_e, the magnitude of reduction was only just outside the repeatability range (see **Figure 2.2**). An acute reduction in v_e may occur if the ability of Gd-DTPA to access the extracellular extravascular space is reduced (Maxwell et al., 2002). Otherwise, it is plausible that early loss of cytokine production (e.g. VEGF) by tumour cells in response to chemotherapy results in a reduction of vascular permeability and interstitial fluid pressure that could reduce v_e. Such a change in permeability might not be detected by changes in K^{trans}, as K^{trans} is flow-dominated in tumours (Maxwell et al., 2002; Tofts, 1997).

Two patients had small but significant increases in IAUGC (see **Figure 2.2**). One patient (# 10) went on to have a partial response to chemotherapy whereas the other (# 2) was not evaluable for response (see **Table 2.1**). These increases do not fit into a pattern consistent with an anti-vascular effect (see above) and the cause for this effect is also uncertain but could be related to increased blood flow resulting from reductions in interstitial fluid pressure. Griffon-Etienne et al. reported on the use of intravital microscopy to measure red cell flux and found an increase in the first few days following administration of paclitaxel or docetaxel (Griffon-Etienne et al., 1999). An increase in relative tumour blood flow rate has also been seen following cyclophosphamide and 5-fluorouracil (measured

using the ^{86}RbCl method) (Braunschweiger, 1988; Li et al., 1991). These changes may be due to reduced blood vessel compression secondary to tumour cell kill rather than a direct anti-vascular effect (Griffon-Etienne et al., 1999).

The day 1 and 2 values were checked for the patients with significant parameter changes and no anomalies found. Significant changes were only just outside the repeatability range (see **Figure 2.2**) and it is possible that the small changes seen in v_e and IAUGC are due to chance rather than real events. A statistical correction factor can be applied for multiple-parameter comparisons – the Bonferroni correction (Bland & Altman, 1995). However, application of the Bonferroni correction would be too conservative in this instance, as the measured parameters are not independent of each other.

2.4.1.3 Correlation between T_1-weighted parameters

K^{trans} was significantly correlated with k_{ep} but not with v_e, as would be expected. IAUGC was found to correlate very strongly with K^{trans} and strongly with v_e (see **Table 2.7**), - reflecting its value as a 'summary' T_1-parameter.

2.4.2 T_2*-weighted DCE-MRI parameters: rBV, MTT and rBF

2.4.2.1 Reproducibility and response

Jackson et al. have performed a reproducibility analysis for rBV for 11 patients with glioma (scanned 36-56 hours apart) and for 5 patients with hepatic neoplasms (scanned 48-56 hours apart) (Jackson et al., 2002; Jackson et al., 2001). Unfortunately, the analysis is not directly comparable with our data as different reproducibility statistics are quoted.

A reproducibility analysis was not performed for muscle T_2*-weighted DCE-MRI parameters as the reduced field of view meant that imaging wrapping obscured the muscle ROI for the majority of patients.

As for the T_1-weighted DCE-MRI parameters (except v_e), there were no significant changes for the group for these parameters but a few individuals had either significant increases or decreases in certain parameters (see **Figure 2.3**). It is difficult to comment about these results, as the validity of the application of this technique to visceral tumours is not known (see below).

rBV and rBF correlated strongly with each other (as would be expected) and also correlated strongly with K^{trans}, k_{ep} and IAUGC (especially rBF). The fact that significant individual changes were not consistent across different parameters, suggests that they might be artefactual.

2.4.2.2 *Potential problems with this technique*

The potential problems of applying the T_2* DCE-MRI technique for measurement of rBV and rBF to visceral tumours include:

1. T_1 effects will be worse than in the brain due to tumour vessel permeability (see **Section 1.5.3.2**);

2. in the brain, it is possible to normalise to the contralateral hemisphere, there is no suitable equivalent for visceral tumours;

3. there are no validation studies comparing this technique with other methods of measuring tumour blood flow in visceral tumours.

We attempted to optimise the technique by using a double dose of contrast agent, pre-enhancement (from the immediately preceding T_1-dynamic sequence) and a Γ-variate fit rather than the raw ΔR_2*-data (see **Section 1.5.3.2**). However, the approximation of MTT by the full-width half-maximum of the ΔR_2*-curve is likely to have led to an overestimation of the true MTT and an underestimation of rBF (Perthen et al., 2002).

In practise, a Γ-variate function may be fitted to the ΔR_2*-curve as long as the initial rise and the peak of the curve are clearly delineated. **Figure 2.4** shows a ΔR_2*-curve and Γ-variate fit for a glioblastoma multiforme (brain tumour) and a pelvic carcinoma for comparison. However, if T_1 effects occur during the first half of the curve, then its maximum height will be reduced and rBV underestimated.

It is not known whether normalising to an area of muscle in the same imaging slice would improve measurement accuracy, as a muscle reproducibility analysis was not performed. However, if liver tumours are imaged, then normalising to spleen might be appropriate (although as for T_1-parameters, this will be a problem if a treatment intervention also affects splenic blood flow).

Given all these problems, the values obtained for rBV and rBF in visceral tumours using T_2*-weighted DCE-MRI are not likely to be accurate. However, as with T_1-weighted parameters, they may still be useful for assessment of response to treatment. If **change** in rBF (measured using MRI) in response to an agent or intervention was found to be positively correlated with change in tumour blood flow measured using a 'gold standard' technique (such as the ^{125}IAP or ^{86}RbCl methods), then this MR technique would be a useful addition to existing methods of investigating tumour microcirculation.

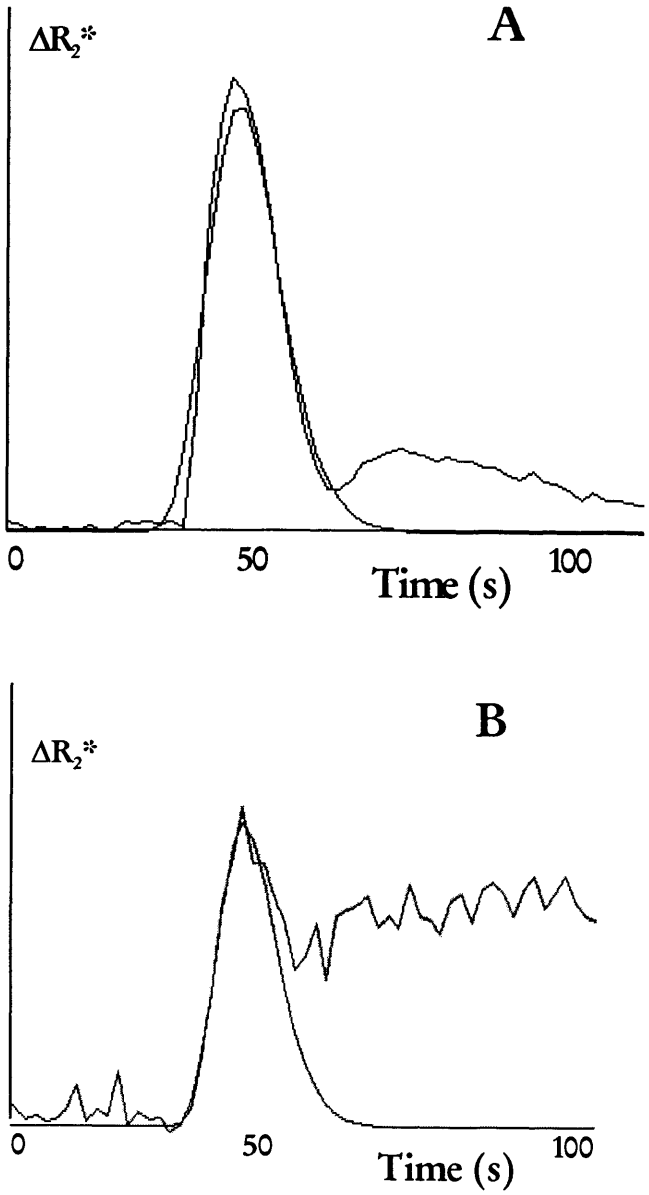

Figure 2.4: ΔR_2* curves and Γ-variate fits for (A) glioblastoma multiforme and (B) pelvic tumour (with thanks to Dr NJ Taylor).

Despite the caveats, we have obtained a reproducibility analysis for these parameters and have found that there are no significant changes in rBV, MTT or rBF for the group of patients following chemotherapy. rBV and rBF also correlated strongly with K^{trans}. In ongoing studies at Mount Vernon investigating the acute effects of vascular disruptive and anti-angiogenic agents, T_2*-weighted parameters are being measured in addition to the usual T_1-weighted parameters. Hopefully, this will provide further information regarding the usefulness or otherwise of including rBV and rBF measurements in the assessment of these agents.

2.4.3 R_2* (BOLD)

The mean baseline (day 1) R_2* value was 20.8 (±1.6) s^{-1}. Rijpkema et al. (Rijpkema et al., 2002) reported a mean baseline R_2* of 29.56 (±1.29) s^{-1} for 11 patients with head and neck squamous cell carcinomas (also measured using a 1.5 T system). The difference may be due to the higher levels of hypoxia seen in head and neck squamous cell carcinomas.

We have performed a reproducibility analysis for R_2*, which will be helpful for comparison with future studies. There were no changes for the group in R_2* post-treatment with chemotherapy but one patient had a significant decrease. R_2* did not correlate strongly with any of the other parameters. The individual patient repeatability for R_2* was ±7.7% for 13 patients with prostate carcinoma (Taylor et al., 2002). However, for this study, the two scans were performed on the same day, 30-40 minutes apart and the patient remained still in the scanner throughout. In comparison, the individual patient repeatability for R_2* for the current study was ±48.6%; showing that the necessity of repositioning the patient in the scanner and a 24-hour interval between scans worsens reproducibility. A reproducibility analysis of kidney R_2* measurements performed in 8 normal volunteers reported a wCV of 12% for both kidney cortex and medulla for four separate measurements spread over 3-10 months (Li et al., 2004). The improved reproducibility compared to our data is likely to be due to the fact that kidney tissue is more homogeneous than tumour.

R_2* measurements made at 24 hours following an anti-vascular intervention are probably not likely to be very helpful, as the presence of necrosis, haemorrhage and/or oedema will influence R_2* measurement (Robinson et al., 2003a; Robinson et al., 2003b). However, R_2* measurements made very early following administration of a vascular disruptive agent may

be indicative of acute blood vessel shutdown as R_2* is sensitive to hypoxia. Robinson et al. detected an increase in R_2* (consistent with an increase in hypoxia) at 35 minutes after administration of the vascular disruptive agent, ZD6126, in an animal model (Robinson et al., 2005). The increase in R_2* at this time-point was associated with blood flow shutdown as indicated by reduced tumour uptake of Hoechst 33342. Gross et al. investigated the effects of a novel photodynamic therapy drug (that acts as a vascular disruptive agent) in melanoma xenografts using BOLD-MRI (Gross et al., 2003). An increase in R_2* was seen within a few minutes of illumination (to activate the drug) – consistent with oxygen consumption by the photochemical reaction and acute blood vessel shutdown (Gross et al., 2003). For future studies, R_2* could be used to determine optimal timings for DCE-MRI studies of vascular disruptive agents. The advantages of using R_2* for such a purpose are that it is completely non-invasive, is relatively straightforward and can be repeated without delay.

2.4.4 Conclusions

The hypothesis that taxane/platinum-based chemotherapy regimens do not cause significant anti-vascular disruptive effects within 24 hours of treatment, as measured by DCE-MRI, has been proved – at least for the parameter K^{trans}.

This is the first demonstration that cytotoxic agents differ from vascular disruptive agents in their effect on DCE-MRI parameter, thus validating the use of DCE-MRI a biomarker of targeting activity.

In addition, a reproducibility analysis was performed for T_2*-weighted parameters: rBV, rBF, MTT and for R_2*. The usefulness of these parameters for the assessment of vascular disruptive agents remains to be determined.

2.5 References – Chapter 2

Ah-See, M.-L.W., Makris, A., Taylor, N.J., Harrison, M., Richman, P.I., D'Arcy, J.A., Burcombe, R.J., Pittam, M.R., Ravichandran, D., Stirling, J.J., Leach, M.O. & Padhani, A.R. (2004). T1 and T2* weighted dynamic contrast-enhanced MRI predicts for clinico-pathological response to neoadjuvant chemotherapy in primary breast cancer. In Proc. ISMRM, Vol. 12. pp. 1992: Kyoto, Japan.

Baguley, B.C., Holdaway, K.H., Thomsen, L.L., Zhuang, L. & Zwi, L. (1991). Inhibition of growth of colon 38 adenocarcinoma by vinblastine and colchicine: evidence for a vascular mechanism. Eur J Cancer, 27, 482-487.

Barentsz, J.O., Berger-Hartog, O., Witjes, J.A., Hulsbergen-van der Kaa, C., Oosterhof, G.O., VanderLaak, J.A., Kondacki, H. & Ruijs, S.H. (1998). Evaluation of chemotherapy in advanced urinary bladder cancer with fast dynamic contrast-enhanced MR imaging. Radiology, 207, 791-7.

Belotti, D., Vergani, V., Drudis, T., Borsotti, P., Pitelli, M., Viale, G., Giavazzi, R. & Taraboletti, G. (1996). The microtubule-affecting drug paclitaxel has antiangiogenic activity. Clin Cancer Res, 2, 1843-9.

Bland, J. & Altman, D. (1996a). Measurement error [corrected and republished article originally printed in BMJ 1996 Jun 29; 312(7047):1654] [see comments]. BMJ, 313, 744.

Bland, J. & Altman, D. (1996b). Measurement error proportional to the mean [published erratum appears in BMJ 1996 Sep 21; 313(7059):744]. BMJ, 313, 106.

Bland, J.M. & Altman, D.G. (1995). Multiple significance tests: the Bonferroni method [see comments]. BMJ, 310, 170.

Braunschweiger, P. (1988). Effect of cyclophosphamide on the pathophysiology of RIF-1 solid tumors. Cancer Res, 48, 4206-10.

Calvert, A.H., Newell, D.R., Gumbrell, L.A., O'Reilly, S., Burnell, M., Boxall, F.E., Siddik, Z.H., Judson, I.R., Gore, M.E. & Wiltshaw, E. (1989). Carboplatin dosage: prospective evaluation of a simple formula based on renal function. J Clin Oncol, 7, 1748-56.

Cavalli, F., Hansen, H.H. & Kaye, S.B. (2000). Textbook of Medical Oncology. Martin Dunitz ltd: London.

Chaplin, D. & Hill, S. (2002). The development of Combretastatin A4 phosphate as a vascular targeting agent. Int J Radiat Oncol Biol Phys, 54, 1491-1496.

Chaplin, D.J., Pettit, G.R., Parkins, C.S. & Hill, S.A. (1996). Antivascular approaches to solid tumour therapy: evaluation of tubulin binding agents. Br J Cancer Suppl, 27, S86-8.

Checkley, D., Tessier, J.J., Kendrew, J., Waterton, J.C. & Wedge, S.R. (2003a). Use of dynamic contrast-enhanced MRI to evaluate acute treatment with ZD6474, a VEGF signalling inhibitor, in PC-3 prostate tumours. Br J Cancer, 89, 1889-95.

Checkley, D., Tessier, J.J., Wedge, S.R., Dukes, M., Kendrew, J., Curry, B., Middleton, B. & Waterton, J.C. (2003b). Dynamic contrast-enhanced MRI of vascular changes induced by the VEGF-signalling inhibitor ZD4190 in human tumour xenografts. Magn Reson Imaging, 21, 475-82.

Donahue, K., Burstein, D., Manning, W. & Gray, M. (1994). Studies of Gd-DTPA relaxivity and proton exchange rates in tissue. Magn Reson Med, 32, 66-76.

Dowlati, A., Robertson, K., Cooney, M., Petros, W.P., Stratford, M., Jesberger, J., Rafie, N., Overmoyer, B., Makkar, V., Stambler, B., Taylor, A., Waas, J., Lewin, J.S., McCrae, K.R. & Remick, S.C. (2002). A phase I pharmacokinetic and translational study of the novel vascular targeting agent combretastatin a-4 phosphate on a single-dose intravenous schedule in patients with advanced cancer. Cancer Res, 62, 3408-16.

Evelhoch, J., He, Z., Polin, L., Corbett, T., Blakey, D. & Waterton, J. (2001). Dynamic Contrast-Enhanced MRI Evaluation of the Effects of ZD6126 on Tumor Vasculature. In Proc. ISMRM, Vol. 9. pp. 481: Glasgow, UK.

Evelhoch, J., LoRusso, P., DelProposto, Z., Stark, K., Latif, Z., Morton, P., Waterton, J., Wheeler, C. & Barge, A. (2002). Dynamic contrast-enhanced MRI evaluation of the effects of ZD6126 on tumor vasculature in a phase I clinical trial. In Proc. ISMRM, Vol. 10. pp. 2095: Honolulu, Hawaii.

Evelhoch, J.L., LoRusso, P.M., He, Z., DelProposto, Z., Polin, L., Corbett, T.H., Langmuir, P., Wheeler, C., Stone, A., Leadbetter, J., Ryan, A.J., Blakey, D.C. & Waterton, J.C. (2004). Magnetic resonance imaging measurements of the response of murine and human tumors to the vascular-targeting agent ZD6126. Clin Cancer Res, 10, 3650-7.

Galbraith, S., Lodge, M., Taylor, N., Rustin, G., Bentzen, S., Stirling, J. & Padhani, A. (2002a). Reproducibility of dynamic contrast enhanced MRI in human muscle and tumours - comparison of quantitative and semi-quantitative analysis. NMR Biomed, 15, 132-142.

Galbraith, S.M., Maxwell, R.J., Lodge, M.A., Tozer, G.M., Wilson, J., Taylor, N.J., Stirling, J.J., Sena, L., Padhani, A.R. & Rustin, G.J.S. (2003). Combretastatin A4 Phosphate has tumour anti-vascular activity in rat and man as demonstrated by dynamic magnetic resonance imaging. J Clin Oncol, 21, 2831-2842.

Galbraith, S.M., Rustin, G.J.S., Lodge, M.A., Taylor, N.J., Stirling, J.J., Jameson, M., Thompson, P., Hough, D., Gumbrell, L. & Padhani, A.R. (2002b). Effects of 5,6-dimethylxanthenone-4-acetic acid on human tumor microcirculation assessed by dynamic contrast-enhanced magnetic resonance imaging. J Clin Oncol, 20, 3826-40.

Gossmann, A., Helbich, T.H., Kuriyama, N., Ostrowitzki, S., Roberts, T.P., Shames, D.M., van Bruggen, N., Wendland, M.F., Israel, M.A. & Brasch, R.C. (2002). Dynamic contrast-enhanced magnetic resonance imaging as a surrogate marker of tumor response to anti-angiogenic therapy in a xenograft model of glioblastoma multiforme. J Magn Reson Imaging, 15, 233-40.

Griffon-Etienne, G., Boucher, Y., Brekken, C., Suit, H.D. & Jain, R.K. (1999). Taxane-induced apoptosis decompresses blood vessels and lowers interstitial fluid pressure in solid tumors: clinical implications. Cancer Res, 59, 3776-82.

Gross, S., Gilead, A., Scherz, A., Neeman, M. & Salomon, Y. (2003). Monitoring photodynamic therapy of solid tumors online by BOLD-contrast MRI. Nat Med, 9, 1327-31.

Hill, S.A., Lonergan, S.J., Denekamp, J. & Chaplin, D.J. (1993). Vinca alkaloids: anti-vascular effects in a murine tumour. Eur J Cancer, 29A, 1320-4.

Hill, S.A., Sampson, L.E. & Chaplin, D.J. (1995). Anti-vascular approaches to solid tumour therapy: evaluation of vinblastine and flavone acetic acid. Int J Cancer, 63, 119-23.

Jackson, A., Haroon, H., Zhu, X.P., Li, K.L., Thacker, N.A. & Jayson, G. (2002). Breath-hold perfusion and permeability mapping of hepatic malignancies using magnetic resonance imaging and a first-pass leakage profile model. NMR Biomed, 15, 164-73.

Jackson, A., Kassner, A., Zhu, X.P. & Li, K.L. (2001). Reproducibility of T2* blood volume and vascular tortuosity maps in cerebral gliomas. J Magn Reson Imaging, 14, 510-6.

Jayson, G.C., Zweit, J., Jackson, A., Mulatero, C., Julyan, P., Ranson, M., Broughton, L., Wagstaff, J., Hakannson, L., Groenewegen, G., Bailey, J., Smith, N., Hastings, D., Lawrance, J., Haroon, H., Ward, T., McGown, A.T., Tang, M., Levitt, D., Marreaud, S., Lehmann, F.F., Herold, M. & Zwierzina, H. (2002). Molecular imaging and biological evaluation of HuMV833 anti-VEGF antibody: implications for trial design of antiangiogenic antibodies. J Natl Cancer Inst, 94, 1484-93.

Jordan, A., Hadfield, J.A., Lawrence, N.J. & McGown, A.T. (1998). Tubulin as a target for anticancer drugs: agents which interact with the mitotic spindle. Med Res Rev, 18, 259-96.

Kety, S. (1960). Blood-tissue exchange methods. Theory of blood-tissue exchange and its application to measurement of blood flow. Meth Med Res, 8, 223-227.

Li, L.P., Storey, P., Pierchala, L., Li, W., Polzin, J. & Prasad, P. (2004). Evaluation of the reproducibility of intrarenal R2* and DeltaR2* measurements following administration of furosemide and during waterload. J Magn Reson Imaging, 19, 610-6.

Li, S., Wehrle, J., Glickson, J., Kumar, N. & Braunschweiger, P. (1991). Tumor bioenergetics and blood flow in RIF-1 murine tumors treated with 5-fluorouracil. Magn Reson Med, 22, 47-56.

Maxwell, R., Wilson, J., Prise, V., Vojnovic, B., Rustin, G., Lodge, M. & Tozer, G. (2002). Evaluation of the anti-vascular effects of combretastatin in rodent tumours by dynamic contrast enhanced MRI. NMR Biomed, 15, 89-98.

Miller, K.D., Sweeney, C.J. & Sledge, G.W., Jr. (2001). Redefining the target: chemotherapeutics as antiangiogenics. J Clin Oncol, 19, 1195-206.

Morgan, B., Thomas, A.L., Drevs, J., Hennig, J., Buchert, M., Jivan, A., Horsfield, M.A., Mross, K., Ball, H.A., Lee, L., Mietlowski, W., Fuxuis, S., Unger, C., O'Byrne, K., Henry, A., Cherryman, G.R., Laurent, D., Dugan, M., Marme, D. & Steward, W.P. (2003). Dynamic contrast-enhanced magnetic resonance imaging as a biomarker for the pharmacological response of PTK787/ZK 222584, an inhibitor of the vascular endothelial growth factor receptor tyrosine kinases, in patients with advanced colorectal cancer and liver metastases: results from two phase I studies. J Clin Oncol, 21, 3955-64.

Padhani, A.R., Hayes, C., Landau, S. & Leach, M.O. (2002). Reproducibility of quantitative dynamic MRI of normal human tissues. NMR Biomed, 15, 143-53.

Parker, G., Suckling, J., Tanner, S., Padhani, A., Husband, J. & Leach, M. (1998). MRIW: parametric analysis software for contrast-enhanced dynamic MR imaging in cancer. Radiographics, 18, 497-506.

Parker, G.J., Suckling, J., Tanner, S.F., Padhani, A.R., Revell, P.B., Husband, J.E. & Leach, M.O. (1997). Probing tumor microvascularity by measurement, analysis and display of contrast agent uptake kinetics. J Magn Reson Imaging, 7, 564-74.

Perthen, J.E., Calamante, F., Gadian, D.G. & Connelly, A. (2002). Is quantification of bolus tracking MRI reliable without deconvolution? Magn Reson Med, 47, 61-7.

Reddick, W., Taylor, J. & Fletcher, B. (1999). Dynamic MR imaging (DEMRI) of microcirculation in bone sarcoma. J Magn Reson Imaging, 10, 277-85.

Rijpkema, M., Kaanders, J.H., Joosten, F.B., van der Kogel, A.J. & Heerschap, A. (2001). Method for quantitative mapping of dynamic MRI contrast agent uptake in human tumors. J Magn Reson Imaging, 14, 457-63.

Rijpkema, M., Kaanders, J.H., Joosten, F.B., van der Kogel, A.J. & Heerschap, A. (2002). Effects of breathing a hyperoxic hypercapnic gas mixture on blood oxygenation and vascularity of head-and-neck tumors as measured by magnetic resonance imaging. Int J Radiat Oncol Biol Phys, 53, 1185-91.

Robinson, S.P., Kalber, T.L., Howe, F.A., McIntyre, D.J., Griffiths, J.R., Blakey, D.C., Whittaker, L., Ryan, A.J. & Waterton, J.C. (2005). Acute tumor response to ZD6126 assessed by intrinsic susceptibility magnetic resonance imaging. Neoplasia, 7, 466-74.

Robinson, S.P., McIntyre, D.J., Checkley, D., Tessier, J.J., Howe, F.A., Griffiths, J.R., Ashton, S.E., Ryan, A.J., Blakey, D.C. & Waterton, J.C. (2003a). Tumour dose response to the antivascular agent ZD6126 assessed by magnetic resonance imaging. Br J Cancer, 88, 1592-7.

Robinson, S.P., Rijken, P.F., Howe, F.A., McSheehy, P.M., Van Der Sanden, B.P., Heerschap, A., Stubbs, M., Van Der Kogel, A.J. & Griffiths, J.R. (2003b). Tumor vascular architecture and function evaluated by non-invasive susceptibility MRI methods and immunohistochemistry. J Magn Reson Imaging, 17, 445-54.

Rustin, G.J. (2003). Use of CA-125 to Assess Response to New Agents in Ovarian Cancer Trials. J Clin Oncol, 21, 187-93.

Sersa, G., Krzic, M., Sentjurc, M., Ivanusa, T., Beravs, K., Cemazar, M., Auersperg, M. & Swartz, H.M. (2001). Reduced tumor oxygenation by treatment with vinblastine. Cancer Res, 61, 4266-71.

Stevenson, J.P., Rosen, M., Sun, W., Gallagher, M., Haller, D.G., Vaughn, D., Giantonio, B., Zimmer, R., Petros, W.P., Stratford, M., Chaplin, D., Young, S.L., Schnall, M. & O'Dwyer, P.J. (2003). Phase I trial of the antivascular agent combretastatin A4 phosphate on a 5-day schedule to patients with cancer: magnetic resonance imaging evidence for altered tumor blood flow. J Clin Oncol, 21, 4428-38.

Taylor, N.J., Lankester, K.J., Stirling, J.J., Rustin, G.J.S., Hoskin, P.J. & Padhani, A.R. (2002). Reproducibility of human tumour R2* maps obtained from BOLD images. In Proc. ISMRM, Vol. 10. pp. 2065: Honolulu, Hawaii.

Therasse, P., Arbuck, S.G., Eisenhauer, E.A., Wanders, J., Kaplan, R.S., Rubinstein, L., Verweij, J., Van Glabbeke, M., van Oosterom, A.T., Christian, M.C. & Gwyther, S.G. (2000). New guidelines to evaluate the response to treatment in solid tumors. European Organization for Research and Treatment of Cancer, National Cancer Institute of the United States, National Cancer Institute of Canada. J Natl Cancer Inst, 92, 205-16.

Tofts, P.S. (1997). Modeling tracer kinetics in dynamic Gd-DTPA MR imaging. J Magn Reson Imaging, 7, 91-101.

Tozer, G.M., Prise, V.E., Wilson, J., Locke, R.J., Vojnovic, B., Stratford, M.R., Dennis, M.F. & Chaplin, D.J. (1999). Combretastatin A-4 phosphate as a tumor vascular-targeting agent: early effects in tumors and normal tissues. Cancer Res, 59, 1626-34.

van Laarhoven, H.W., Rijpkema, M., Punt, C.J., Ruers, T.J., Hendriks, J.C., Barentsz, J.O. & Heerschap, A. (2003). Method for quantitation of dynamic MRI contrast agent uptake in colorectal liver metastases. J Magn Reson Imaging, 18, 315-20.

Wang, T.H., Wang, H.S. & Soong, Y.K. (2000). Paclitaxel-induced cell death: where the cell cycle and apoptosis come together. Cancer, 88, 2619-28.

Weinmann, H.J., Laniado, M. & Mutzel, W. (1984). Pharmacokinetics of GdDTPA/dimeglumine after intravenous injection into healthy volunteers. Physiol Chem Phys Med NMR, 16, 167-72.

Wolf, W., Presant, C., Waluch, V. & Leberthon, B. (2003). A unique methodology using dynamic contrast enhanced MRI (DEMRI) for quantifying anti-angiogenic effects (AAE) of chemotherapy: AAE of docetaxel (DOC) correlate with tumor response (TR). In Proc. ASCO pp. 824: Chicago.

Chapter 3 The acute anti-vascular effects of CA-4-P on the SW1222 tumour as measured by DCE-MRI

3.1 Introduction

These experiments detailed in this chapter were part of the pre-clinical work required for the Cancer Research UK (CR-UK) phase I/II trial of CA-4-P in combination with radioimmunotherapy (RIT), using ^{131}Iodine (^{131}I)-labelled A5B7 a murine anti-carcinoembryonic antigen (CEA) monoclonal antibody, in advanced gastrointestinal carcinoma.

The purpose was to use DCE-MRI to investigate the acute effects of CA-4-P on the human colon carcinoma xenograft, SW1222 in order to establish whether a dose-response relationship could be determined and also the magnitude and duration of anti-vascular effect at a 'clinically relevant' dose (see below).

3.1.1 Radioimmunotherapy

In RIT, a radiolabelled antibody localises to a tumour-associated antigen, thus targeting radiation directly to a tumour. ^{131}I is the most commonly used radio-isotope (Napier & Begent, 1998). It has a beta (β) emission of moderate energy (0.61 MeV) which has a maximum particle range of 2 mm (equivalent to ~40 cell diameters) and also a gamma (γ)-emission that enables imaging with a γ-camera to quantify normal tissue and tumour bio-distribution (Goldenberg, 2002). In both clinical and animal studies, the dose-limiting toxicity for RIT is myelosuppression as the bone marrow is perfused by blood containing radioactivity and also is irradiated by γ-rays from radio-isotope in neighbouring organs (Ledermann et al., 1991; Napier & Begent, 1998).

The majority of studies investigating RIT in colorectal carcinoma have used antibodies raised against CEA (Napier & Begent, 1998). CEA is expressed by a wide range of common epithelial malignancies; but the highest concentrations are seen in colorectal adenocarcinomas (Chung et al., 1994; Goldenberg et al., 1976). Normal tissues, especially colonic mucosa, may show very weak positive staining for CEA (Chung et al., 1994; Goldenberg et al., 1976).

RIT has produced high response rates and has led to long term remissions in radiosensitive tumours, such as non-Hodgkin's lymphoma, (Kaminski et al., 2000; Press et al., 1993) but has had only limited success in solid tumours (Goldenberg, 2002; Napier & Begent, 1998). In the case of colorectal carcinoma, only a few responses have been seen in phase I/II trials - particularly with bulky tumours (Lane et al., 1994; Ledermann et al., 1991; Napier & Begent, 1998). The reasons for the poor responses seen in solid tumours are that they are more radioresistant than lymphomas and there is non-uniform antibody distribution. Antibody delivery is compromised in poorly-vascularised tumour regions and, even in well-vascularised regions, antibodies may not be extravasated efficiently (Jain, 1989; Jain & Baxter, 1988). A comparison of stained histological sections with radioluminography, showed that most anti-CEA antibody was retained in the outer, well-perfused areas with little antibody retention in poorly-vascularised tumour regions (Flynn et al., 1999; Pedley et al., 2002).

Tumour size is another important factor: an inverse logarithmic relationship between tumour size and ^{131}I-labelled anti-CEA antibody uptake into tumour was found in patients, with absolute antibody uptake being the most important factor determining radiation dose to the tumour (Behr et al., 1997). Patients with small volume disease have improved response rates: if tumour masses are $\leq$3 cm then objective response rates of up to 26% are seen (Behr et al., 1999; Behr et al., 2002).

The limited effectiveness of RIT as a single agent in colorectal cancer has led to its investigation in combination with other anti-cancer therapies. The combination of ^{131}I-A5B7 and a vascular disruptive agent, such as CA-4-P, is an obvious choice, due to their complementary actions (as CA-4-P is most effective in the tumour centre, with sparing of the tumour rim (Dark et al., 1997). ^{131}I-A5B7 (at 7.4 MBq intravenously) together with CA-4-P (at 200 mg.kg^{-1} intraperitoneally, given 48 hours after the antibody) has been tested using SW1222 colorectal xenografts grown in nude mice (Pedley et al., 2001). The combination eradicated tumours in 5/6 mice (85%) with no evidence of tumour re-growth when the experiment was terminated >9 months later. As single agents, CA-4-P had no effect on tumour growth whereas ^{131}I-A5B7 produced significant growth inhibition of about 35 days but no cures. The addition of CA-4-P increased trapping of ^{131}I-A5B7 in tumours with an average of 90% more radio-antibody retained at 96 hours following ^{131}I-A5B7 administration compared to controls treated with antibody alone (Pedley et al., 2001).

The combination of ^{131}I-A5B7 (18.5 MBq i.v.) and the vascular disruptive agent, DMXAA (27.5 mg.kg^{-1} intraperitoneally, given 48 hours after the antibody), produced similar results in another colorectal xenograft, LS174T (Pedley et al., 1996).

The combination of ^{131}I-A5B7 and CA-4-P may be effective for two reasons. Either the mechanism is simple additive killing of the tumour centre by CA-4-P and the rim by ^{131}I-A5B7, or, CA-4-P may enhance the effect of ^{131}I-A5B7 by increased antibody retention following CA-4-P-induced vessel collapse (Pedley et al., 2001).

The timing of vascular disruptive agent administration is important as it affects the level of antibody retention in tumour. Maximum tumour levels of ^{131}I-A5B7 are reached 24-48 hours after administration (Pedley et al., 1994). The administration of DMXAA at this time (48 hours after ^{131}I-A5B7) resulted in significantly higher antibody retention compared to controls treated with antibody alone at assessment a further 48 hours later (96 hours after ^{131}I-A5B7). However, if DMXAA was given either 3 hours before or concomitantly with ^{131}I-A5B7, antibody retention was significantly reduced (Pedley et al., 1996).

3.1.2 Rationale for study

Following on from the successful preclinical studies using the SW1222 (and other) colorectal xenografts, a phase I clinical trial of the combination of ^{131}I-A5B7 and CA-4-P was proposed in patients with advanced gastrointestinal carcinoma (the trial started in January 2004). The schedule for the clinical study is given in **Table 3.1**. The timing of the combination treatment in Week 2 (CA-4-P given 48 and 72 hours after ^{131}I-A5B7) is designed to ensure maximum antibody retention. The starting dose for CA-4-P was 33 mg.kg^{-1}, increasing to 50 mg.kg^{-1}, if tolerated. A single dose of CA-4-P is given alone in Week 1 so that DCE-MRI examinations may be performed to measure CA-4-P's acute anti-vascular effect. (DCE-MRI examinations cannot be performed in Week 2 as the patient has to be isolated for up to 5 days following ^{131}I-A5B7). The DCE-MRI data will be related retrospectively to patient outcome to see if the magnitude of reduction in DCE-MRI kinetic parameters due to CA-4-P can predict response to the combination treatment.

Week 1	Monday	DCE-MRI examination
	Tuesday	DCE-MRI examination
	Wednesday	**CA-4-P** DCE-MRI examination 4-6 hours later
Week 2	Monday	**^{131}I-A5B7**
	Wednesday	**CA-4-P**
	Thursday	**CA-4-P**
Weeks 3-8	Wednesday	**CA-4-P**

Table 3.1: Clinical Trial Schedule

Despite the good effect of the combination in animal studies (Pedley et al., 2001), the dose of CA-4-P was very high and there is no information on whether lower doses (which may be more clinically relevant) are effective. Also, there is no information on how DCE-MRI effects relate to antibody retention and therapeutic efficacy.

The aim of this pre-clinical study was therefore to determine a dose response and time-course for CA-4-P using DCE-MRI in the SW1222 tumour. The results will provide information regarding the magnitude of change in vascular parameters that might be anticipated in the clinical trial and help relate the change in vascular parameters to the therapeutic effects of the CA-4-P/^{131}I-A5B7 approach in the same animal model (Pedley et al., 2001).

3.1.3 Study objectives

The objectives were to determine if there were any changes in the quantitative MR parameters (IAUGC, K^{trans} and v_e) using the same tumour and strain of mice (MF1 nude females) as used in the therapeutic study (Pedley et al., 2001). The arterial input function was determined, as this is required for calculation of the parameters K^{trans} and v_e. Relaxation parameters (T_1, T_2 and T_2^*) were calculated. Histological measures of CA-4-P effect were also determined in terms of the functional vascular volume (using Hoechst 33342) and percentage tumour necrosis.

3.2 Methods

3.2.1 Mice and tumours

SW1222 cells (provided by Dr RB Pedley, Royal Free Hospital) were maintained in L-15 (Leibovitz) medium (Life Technologies, UK) supplemented with 10% foetal calf serum (Sigma, UK) plus 2 mM glutamine (Life Technologies) and incubated in a humidified incubator at 37° C in air-5%CO_2. $5x10^6$ cells were implanted subcutaneously onto the rear dorsum of 4-8 week old female MF1 nude mice (Harlan UK ltd, Bicester) anaesthetised with Metofane (methoxyflurane, Janssen Pharmaceuticals, Ontario, Canada). Animals were selected for treatment after approximately 2-4 weeks when their tumours reached a geometric mean diameter (GMD) of 6-9 mm. All animal experiments were performed in full compliance with government regulations and UKCCCR guidelines on animal welfare and were approved by the local Ethical Review Committee (Home office licence number: PPL 70/4552).

3.2.2 Drug treatments

Animals either received intraperitoneal (i.p.) injections of CA-4-P (Oxigene Inc. Watertown, MA, USA) or 0.9% saline. CA-4-P was dissolved in 0.9% saline at a concentration of 10 $mg.ml^{-1}$.

Mice were treated with either CA-4-P (at 30, 100 or 200 $mg.kg^{-1}$) or 0.9% saline at either 4 or 24 hours prior to DCE-MRI - making 8 treatment groups in total. The time recorded was the time from drug treatment to injection of contrast agent (Gd-DTPA) during MR imaging. A window of ± 15 minutes for the 4-hour time point and ± 60 minutes for the 24-hour time point was allowed.

3.2.3 MRI protocol

Each mouse was sedated with an i.p. injection of 0.3 $ml.kg^{-1}$ Hypnorm (fentanyl citrate 0.315 $mg.ml^{-1}$ & fluanisone 10 $mg.ml^{-1}$ – Janssen-Cilag, UK) that had been diluted 1:10 with water. The mouse was then anaesthetised temporarily with Halothane (Merial Animal Health ltd, Harlow, UK) vaporised using a 50:50 mixture of oxygen and nitrous oxide (both BOC, UK) so that an intravenous (i.v.) line could be placed in a tail vein and the mouse restrained in a Perspex jig. The mouse was then placed in a 6 cm quadrature birdcage coil in a 4.7 T Varian MR system for scanning. The temperature inside the

magnet was maintained to 35-37 ° C using a hot air blower and mouse temperature was monitored continuously via a fine copper rectal thermocouple. The rectal thermocouple did produce local field inhomogeneities but these did not impact on the tumour ROI.

The following MRI sequences were performed:

1. Initial T_1 and T_2 weighted images to select a suitable plane through the tumour centre

2. Spin echo sequence with two echo times to estimate baseline T_2: TE 11 & 60 ms, TR 1000 ms, FOV 40 x 45 mm, slice thickness 2 mm.

3. Multi-gradient echo sequence to calculate baseline T_2*: TE 4-32 ms, TR 234 ms, FOV 40 x 45 mm, slice thickness 2 mm, flip angle 45°, 8 echo times.

4. Inversion recovery (IR) sequence to calculate pre-contrast tumour T_1 values: TE 10 ms, TR 2420 ms, inversion times (IR) 100, 400, 800, 1600 & 2400 ms.

5. A 100-image dynamic gradient echo sequence: TE 2.5 ms, TR 60 ms, flip angle 70°, FOV 40x45 mm, in-plane resolution 0.16 mm x 0.45 mm, slice thickness 2 mm, time resolution 6 s, 100 images in total. Gd-DTPA was injected as an i.v. bolus at 0.1 $mmol.kg^{-1}$ (0.1 $mmol.ml^{-1}$ concentration) during the sixth acquisition over 5 seconds via an infusion pump. Contrast was injected for a total of 6 seconds to allow for the dead space in the i.v. line, estimated to be 5 µl. A 25 g mouse would therefore receive 25 µl of contrast agent solution.

After scanning, mice were killed by cervical dislocation.

3.2.3.1 Determination of relaxivity

The relaxivity, r_1, (in $mM^{-1}.s^{-1}$) of a given contrast agent is defined as the change in relaxation rate per unit of contrast agent concentration (Donahue et al., 1994). r_1 is required for calculation of the concentration of Gd-DTPA in plasma or tissue (see **Section 1.5**). A set of Gd-DTPA plasma reference tubes was made using blood obtained from non-tumour bearing mice. Blood samples (~0.5 ml per mouse) were centrifuged at 10,000 rpm for 2 minutes to obtain plasma. 10 reference tubes (ranging from 0 to 1 mM concentration) were made by adding 20 µl of Gd-DTPA (at varying concentrations) or saline to 200 µl of plasma. The reference tubes were placed in the magnet (at 35 °C) and

their T_1 values calculated using an inversion recovery MRI sequence: TE 10 ms, TR 6005 ms, inversion times (IR) 100, 250, 500, 1000, 2000, 4000 & 6000 ms. A graph of $1/T_1$ versus Gd-DTPA concentration was then plotted and r_1 calculated as described in **Section 1.5.**

3.2.3.2 Arterial input function

The arterial input function (AIF) is required for derivation of quantitative kinetic parameters such as K^{trans}. It is technically very difficult to obtain an AIF for individual mice so a cohort mouse AIF was determined instead. AIF was estimated using two different methods: *in vivo* imaging of blood vessels and by estimating the Gd-DTPA concentration in blood samples from individual mice.

3.2.3.2.1 *In vivo* method

Non-tumour bearing MF1 nude mice (n=5) were anaesthetised for i.v. cannulation then sedated and placed in a jig in the scanner as above. A suitable transverse slice in which large vessels could be seen clearly (just superior to the kidneys) was chosen. A 100-image dynamic gradient echo sequence was acquired: TE 1.5 ms TR 30 ms, flip angle 30°, slice thickness 2 mm, FOV 40 x 45 mm, in-plane resolution 0.31 x 0.45 mm, time resolution 3 s. Gd-DTPA was injected after 30 seconds (0.01 $mmol.kg^{-1}$, $1/10^{th}$ of the dose used above, but in the same volume) as an i.v. bolus over 5 seconds, as before. Contributions from in-flow effects were minimised by pre-saturation of signals outside of the slice selected for imaging. Voxels from major blood vessels (inferior vena cava and aorta) were identified from a T_1-weighted gradient-echo image obtained without pre-saturation, since the vessels showed up as high signal intensity due to flow into the slice. The mean signal intensity of these 'vessel' voxels (a combination of the inferior vena cava and the aorta) was calculated for the dynamic MRI sequence.

3.2.3.2.2 Blood sampling method

Animals used for the *in vivo* method above were killed at ~4-5 min after injection of Gd-DTPA and plasma samples obtained. Additional animals were treated similarly (but not placed in the MRI magnet) and were killed at 1-2 min or 10-12 min to provide additional time points (14 animals used in total). The T_1 values of the plasma samples were measured using an inversion recovery sequence as described above and the Gd-DTPA concentration estimated.

Data obtained from both blood sampling and *in vivo* methods were simultaneously fitted to a bi-exponential model (see **Section 1.5**). The values obtained were compared with standard mouse AIFs from the literature (Checkley et al., 2003a; Furman-Haran et al., 1996; Lyng et al., 1998).

3.2.3.3 Data processing

Images were processed using Matlab version 5 (The Mathworks, Nantick, MA USA). A region of interest (ROI) was drawn around the tumour using the initial T_1-weighted image. Data were analysed on an individual pixel by pixel basis. Individual images were reviewed and the ROI adjusted if there had been movement. Individual images that were blurred due to excessive movement were removed. One mouse had abnormally high baseline signal intensity values (thought to be due to movement in and out of the imaging plane), so was rejected.

The change in signal intensity due to contrast medium accumulation in each pixel was calculated over the imaging period. This was then converted into T_1 relaxation time changes using the method described by Hittmair et al (Hittmair et al., 1994). $T_1(0)$ was determined using the inversion recovery sequence. The concentration of Gd-DTPA in each ROI pixel present at time t, can then be calculated (see **Section 1.5** and the **Appendix**).

3.2.3.4 Calculation of MRI parameters

Representative parameter values were calculated for tumour and muscle ROIs using the median of all pixels in each ROI. Mean parameter values for each treatment group were then calculated from this data.

IAUGC (mM.s) was calculated for the first 90 seconds post-contrast (Evelhoch, 1999). K^{trans} (min^{-1}) and v_e (%) were obtained by fitting the Tofts' model (Tofts et al., 1999; Tofts & Kermode, 1991) to the Gd-DTPA concentration-time data using the standard AIF obtained for the MF1 mice (see above).

For the relaxation parameters, T_1 was calculated from the inversion recovery sequence, T_2 was estimated from the signal intensities at the two echo times measured and T_2^* was calculated using the method described in **Chapter 4**.

3.2.3.5 *IAUGC spatial heterogeneity*

The spatial heterogeneity of IAUGC values was evaluated using Matlab version 5. Mean IAUGC values were calculated for three regions determined by their distance from the edge of the tumour: rim (within 4 layers of pixels from the edge, corresponding to a distance of < 1 mm); intermediate (5-10 layers from the edge, or 1-3 mm); centre (>10 layers from the edge, or >3 mm).

3.2.4 Histological parameters

Tumours were excised from mice after imaging for histological analysis. Mice were killed by cervical dislocation and tumours excised and cut in half in the same plane as the MRI slice used for scanning. One half was fixed in formalin (Sigma-Aldrich, UK) for subsequent staining of a central tumour section with hematoxylin and eosin (H&E - Sigma-Aldrich, UK) and for alpha-smooth muscle actin αSMA (Sigma-Aldrich, UK). The other tumour half was placed in zinc fixative for subsequent staining of a central tumour section for CD31 antigen[1] (Pharmagen, UK). 1 litre zinc fixative consists of 0.5 g calcium acetate, 5.0 g zinc acetate and 5.0 g zinc chloride (all Sigma-Aldrich, UK) plus 0.5 M Tris buffer at pH 7.4 [12.1 g Tris base (FSA laboratory supplies, UK), 900 ml deionised water and 81.5 ml 1.0 N hydrochloric acid (VWR, UK)]. The method used for immunohistochemical staining involved sequential incubation of unconjugated primary antibody specific to the target antigen, a biotinylated secondary antibody which reacts with the primary antibody, enzyme-labelled streptavidin or avidin (which reacts with biotin) and a substrate chromogen. The enzyme and substrate used were horse radish peroxidase (HRP) and diaminobenzidine (DAB). Immunohistochemical staining was performed by Mrs Frances Daley, Gray Cancer Institute and the details given below.

Tumours were embedded in paraffin then 4 μm sections cut from the tumour centre. Sections were then dewaxed in xylene and rehydrated through grade alcohol (100, 90 and 70%) to water. Sections were washed in Tris-buffered saline (TBS) in between each application of reagent.

CD31 antigen. Peroxidase blocking reagent (S2001 - DakoCytomation, Ely UK) and then serum free protein block (X0909 - DakoCytomation, Ely UK) were each applied for 5 minutes (to block endogenous peroxidases and non-specific background staining

[1] CD31 antigen, also known as PECAM-1 (platelet endothelial cell adhesion molecule), is highly expressed on endothelial cells, concentrated on the junctions between them. It is used as a pan-endothelial marker.

respectively). Rat anti-mouse CD31 antibody (550274 - Pharmigen BD Bioscience, San Diego CA) was then applied, diluted 1/500 in TBS for 1 hour at room temperature. Biotinylated rabbit anti-rat antibody (EO468 - DakoCytomation, Ely UK) was then applied as the secondary antibody, diluted 1/400 in TBS for one hour at room temperature. Avidin complexed with HRP (Dako ABComplex/HRP, DakoCytomation, Ely UK) was applied for one hour at room temperature then DAB solution was applied for five minutes. Sections were rinsed in distilled water and counterstained in Gill's haematoxylin (Surgipath Europe Ltd, Peterborough UK) for 5-60 seconds, as a nuclear counter-stain. Sections were washed and dehydrated through graded alcohols, cleared in xylene and mounted in DPX (360294H Merck, UK) mounting media.

αSMA. (All reagents for this method (except primary antibody) were supplied in the Ultravision Mouse Detection kit (TQ-015-HD), Stratech Scientific Ltd, Cambridge UK). Sections were blocked with endogenous peroxidase for 15 minutes at room temperature then Ultra V block was applied to block reactive immunoglobulins and sections incubated for 60-70 minutes at room temperature. αSMA antibody (Sigma-Aldrich, UK) was then applied, diluted 1/20,000. Biotinylated goat anti-mouse antibody and then streptavidin peroxidase were applied, each for 10-15 minutes at room temperature. DAB was then applied for five minutes with hydrogen peroxide. Sections then placed in Gill's haematoxylin (Surgipath Europe Ltd, Peterborough UK) for 5-60 seconds. Sections then washed again and dehydrated through graded alcohol's, cleared in xylene and mounted in DPX (360294H Merck, UK) mounting media.

3.2.4.1 Necrosis

The percentage necrosis in H&E-stained histological sections was scored for tumours imaged at 24 hours. Using a grid eyepiece graticule marked in 100 squares, each tumour section was assessed at x10 magnification, by scoring each square as undamaged tumour or necrosis. The percentage necrosis was then calculated for each tumour. In addition, the rim of viable tissue remaining was measured for tumours imaged at 24 hours for the 100 $mg.kg^{-1}$ and 200 $mg.kg^{-1}$ dose levels.

3.2.4.2 Vascular maturation index

Tumour vascular maturation index was calculated for the control group (animals treated with saline at both time-points) and for the group treated with 30 $mg.kg^{-1}$ CA-4-P, 24 hours

prior to imaging. The vascular maturation index was defined as the percentage αSMA staining divided by the percentage of CD31 antigen staining. The amount of staining was determined using a random point scoring system based on that described by Chalkley (Chalkley, 1943; Smith et al., 1988). An eyepiece graticule with a random array of 25 points was used and the tumour assessed at x40 magnification. Points falling on areas of staining were recorded as positive. This procedure was repeated over different areas of tissue until a total of 120 fields had been scored. The total score was then divided by 30 to give the percentage staining for that tumour. Vascular maturation index was expressed as the mean value for each tumour type (± 1 standard error of the mean). Separate sections taken from the tumour centre had to be used for αSMA and CD31 antigen staining as they have different fixing methods.

3.2.4.3 Functional vascular volume

The measurement of functional vascular volume was performed by Dr SA Hill and Ms GA Lewis, in a separate experiment. Functional vascular volume was assessed in control tumours and at 4 or 24 hours following treatment with 30, 100 or 200 $mg.kg^{-1}$ of CA-4-P using Hoechst 33342 (Sigma-Aldrich, Dorset, UK) as reported previously (Smith et al., 1988). The fluorescent DNA-binding dye was dissolved in 0.9% saline at a concentration of 6.25 $mg.ml^{-1}$ and injected i.v. at a dose of 10 $mg.kg^{-1}$. Tumours were excised and frozen 1 minute later. Sections were cut at three levels through the tumour and observed under UV light illumination. Perfused vessels were identified by their fluorescent outlines. Vascular volumes were determined using a random point scoring system (based on that described by Chalkley (Chalkley, 1943; Smith et al., 1988). At least 100 fields were scored at each of the tumour levels.

3.2.5 Statistical analysis

Kinetic parameters were analysed using a statistical software package (JMP Statistics, version 3.2.6. SAS Institute Inc., Cary, North Carolina, USA). A one way analysis of variance (ANOVA) was used to look for a significant difference between treatment groups. If the ANOVA was significant ($p<0.05$) then an appropriate post-test comparison of individual means was performed to look for significant differences between dose levels. Linear regression analysis was used to test for a dose-response relationship.

3.3 Results

There were six animals for analysis per treatment group. The mean time from implantation to treatment with CA-4-P was 21.4 (±0.9) days. Mean mouse weight was 26.8 (±0.3) g and mean tumour GMD was 7.4 (±0.1) mm^3. There were no significant differences between the 8 treatment groups for time from implantation, mouse weight, tumour GMD or in the time from treatment with CA-4-P to injection of Gd-DTPA (on ANOVA).

3.3.1 Gd-DTPA relaxivity in mouse plasma at 4.7 T

Relaxivity, r_1 was calculated as 4.195 $mM^{-1}.s^{-1}$ at 35°C (see **Figure 3.1**). This is similar to other values quoted at 4.7 T: 4.02±0.14 $mM^{-1}.s^{-1}$ (Donahue et al., 1994), 4.3 $mM^{-1}.s^{-1}$ (Furman-Haran et al., 1996) and 3.8 $mM^{-1}.s^{-1}$ (Checkley et al., 2003b).

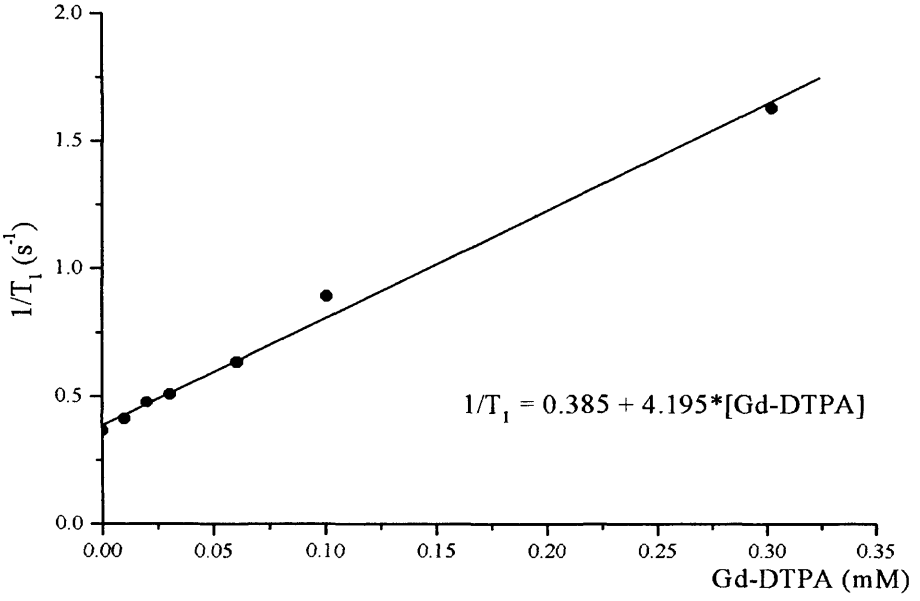

Figure 3.1: Gd-DTPA relaxivity in mouse plasma

3.3.2 Arterial input function for Gd-DTPA in the mouse

The blood-sampling and *in-vivo* imaging data were simultaneously fitted to a model arterial input function (see **Section 1.5**).

$$C_a(t) = D\left[a_1 e^{(-m_1 t)} + a_2 e^{(-m_2 t)}\right]$$

where D=0.1 mmol.kg^{-1}, the bolus dose of Gd-DTPA, a_1= 10.19 kg.l^{-1}, m_1= 4.65 s^{-1}, a_2=3.81 kg.l^{-1} and m_2 =0.09 s^{-1}.

3.3.3 MRI parameters

Figure 3.2 shows the change in signal intensity following contrast agent injection for an untreated tumour and a tumour treated 4 hours previously with 200 mg.kg^{-1} of CA-4-P. IAUGC maps of the same tumours are also shown. The acute blood vessel shutdown caused by CA-4-P is clearly demonstrated.

3.3.3.1 IAUGC

Figure 3.3 shows the mean IAUGC (mM.s) values for tumour and muscle at 4 and 24 hours following treatment with CA-4-P. IAUGC was found to be highly discriminatory between dose groups at 4 hours following treatment with CA-4-P (ANOVA, $p<0.00001$). A significant reduction in tumour IAUGC was seen at all dose levels at 4 hours following treatment with CA-4-P in comparison with the control group (relative reduction: 38.1%, 71.6% and 85.9% for 30, 100 and 200 mg.kg^{-1} respectively). There was a significant difference between treatment groups (ANOVA, p=0.005) at 24 hours with a significant reduction at the 100 and 200 mg.kg^{-1} dose levels (relative reduction 53.8% and 57.7% respectively) but not at 30 mg.kg^{-1}. Recovery was greater at the 30 mg.kg dose level than at 100 mg.kg^{-1}. There was no significant difference between any of the treatment groups and the control groups for muscle IAUGC.

The dose-response relationship for the IAUGC is shown in **Figure 3.4.** Linear regression analysis was highly significant for a dose-response relationship at 4 hours (r =-0.80, $p<0.0001$) and significant at 24 hours (r=-0.58, $p<0.01$) for tumour but not for muscle (r=-0.02 and –0.17 for 4 and 24 hours respectively).

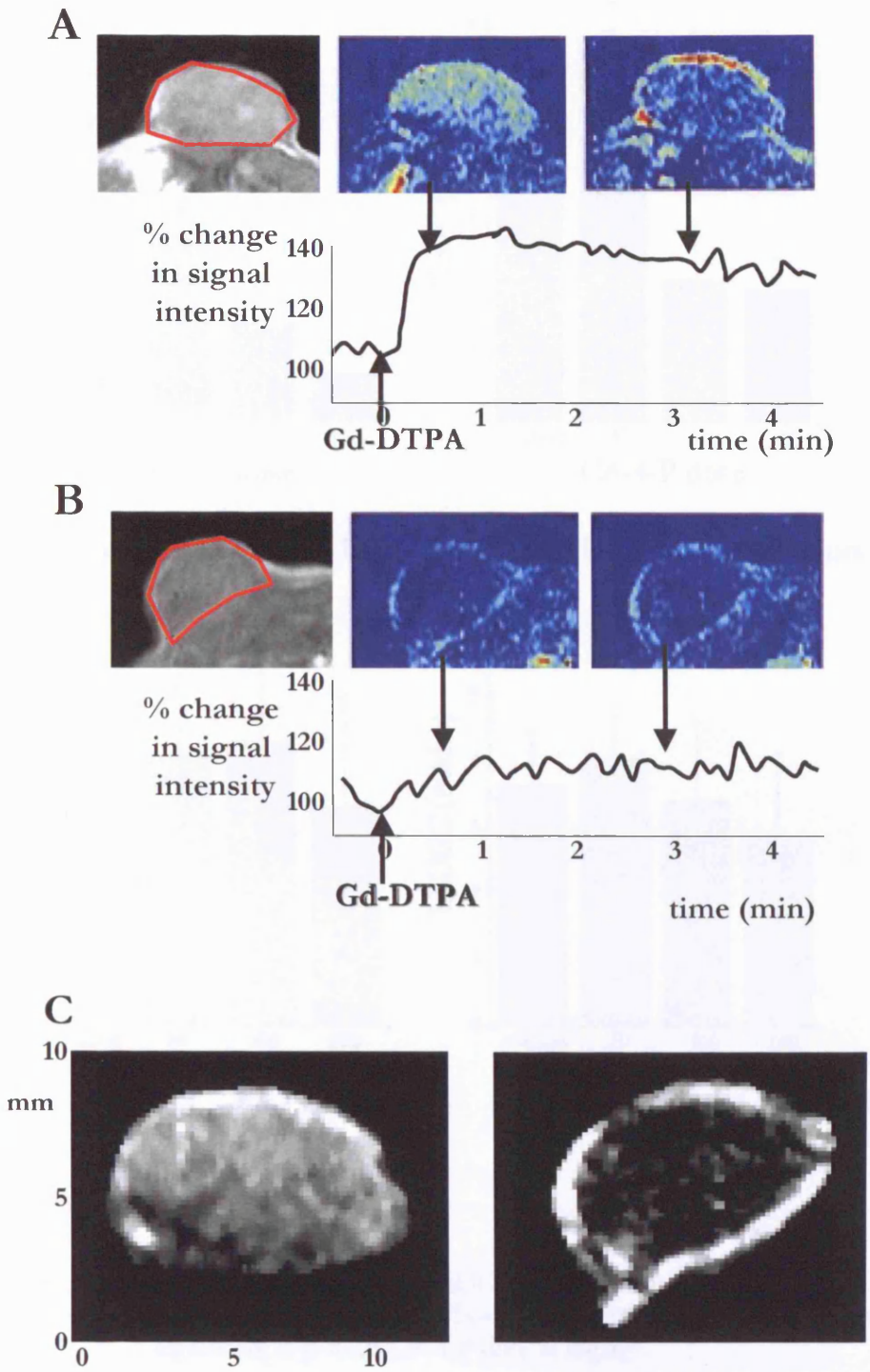

Figure 3.2: Change in signal intensity over time due to Gd-DTPA injection in (**A**): an untreated SW122 tumour and (**B**) in a SW122 tumour treated 4 hours previously with 200 mg.kg^{-1} CA-4-P **C:** IAUGC maps of the same tumours as in **A** & **B**.

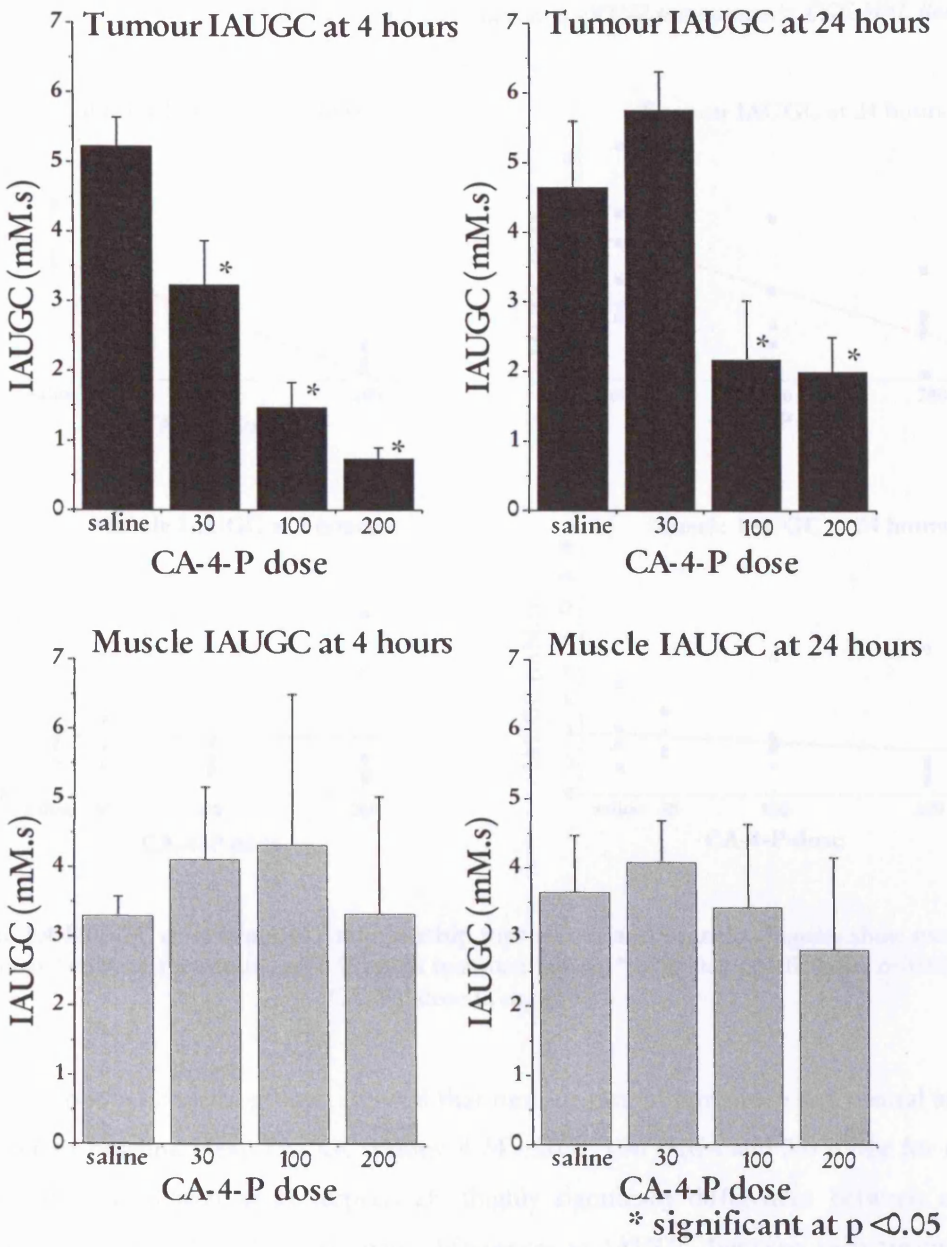

Figure 3.3 Mean tumour and muscle IAUGC for each treatment group.
Figures show mean ±standard error of the mean. N=6 for each treatment group. * indicates significant at $p < 0.05$ CA-4-P dose in $mg.kg^{-1}$.

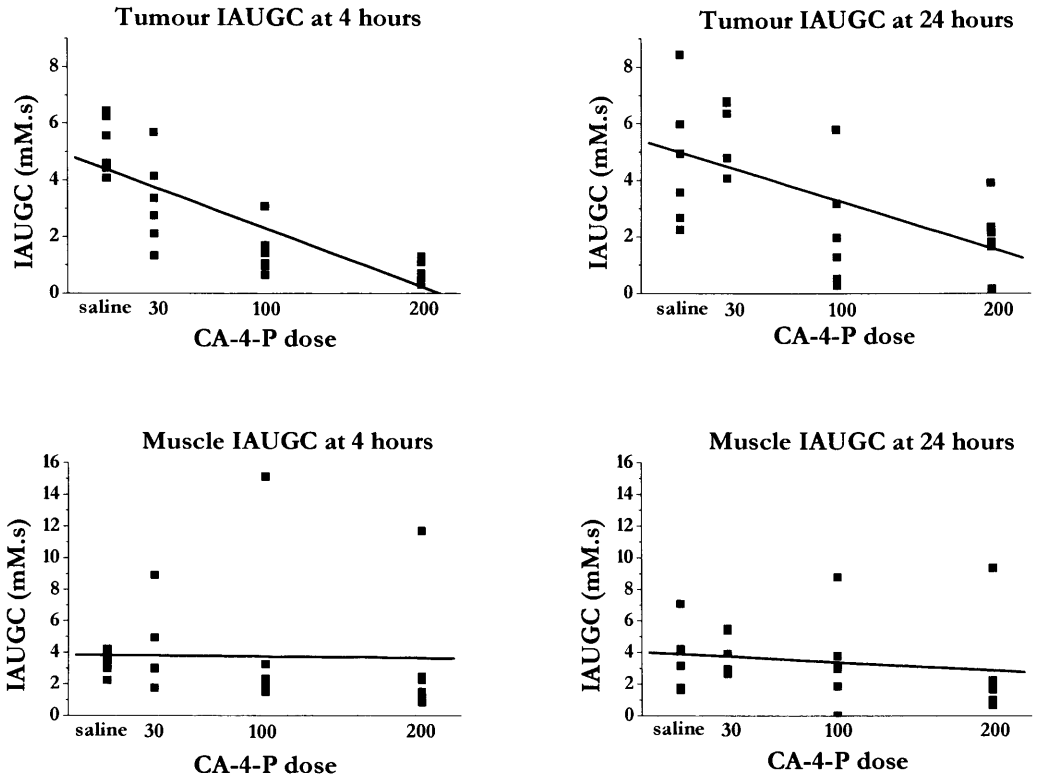

Figure 3.4 IAUGC dose-response relationship for tumour and muscle. Figures show mean ±standard error of the mean. n=6 for each treatment group. * indicates significant at $p<0.05$. CA-4-P dose in $mg.kg^{-1}$.

Analysis of pooled control groups showed that tumour rim, intermediate and central areas had different baseline mean IAUGC values: 4.74 mM.s, 3.36 mM.s and 3.0 mM.s for rim, intermediate and central areas respectively (highly significant differences between each group by paired t-test). The percentage differences in IAUGC between each treatment group and the controls for each region are summarised in **Figure 3.5**. For every dose and time, the order of change (reduction) in the group mean IAUGC was the same: centre > intermediate > rim. The ratio of centre:rim IAUGC was found to be significantly lower at 4 hours after 100 and 200 $mg.kg^{-1}$ CA-4-P and at 24 hours after 100 $mg.kg^{-1}$ CA-4-P than in the corresponding control groups.

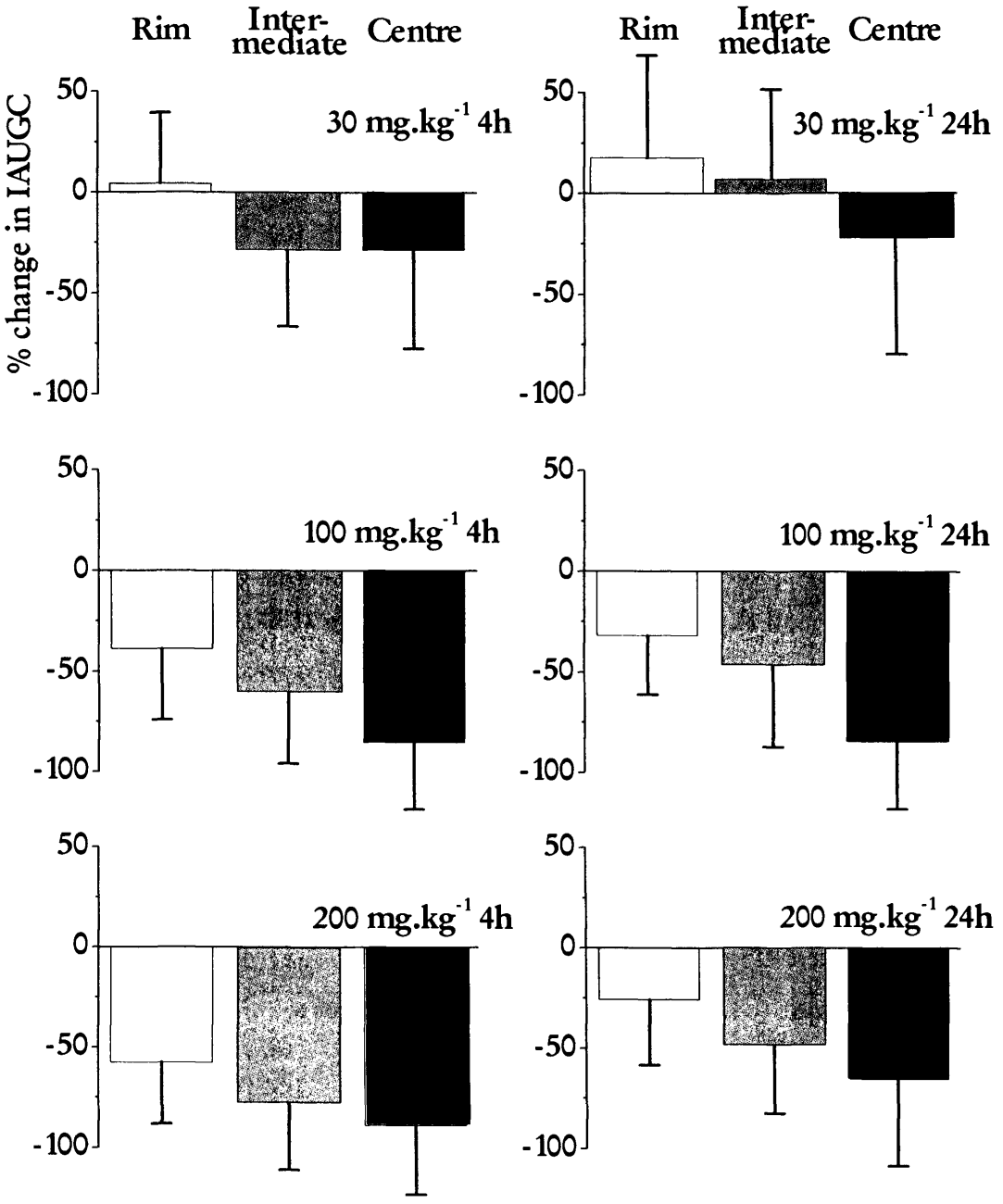

Figure 3.5 Tumour IAUGC spatial heterogeneity, showing difference in change in IAUGC for tumour rim (white), intermediate zone (grey) and centre (black) for different doses of CA-4-P. Figures show mean ±standard error of the mean. n=6 for each treatment group.

3.3.3.2 K^{trans} and v_e

The results for tumour K^{trans} and v_e are shown in **Figure 3.6.** On ANOVA, there was a significant difference between treatment groups at 4 hours following treatment with CA-4-P for both K^{trans} ($p<0.00001$) and v_e ($p<0.001$). A significant reduction in K^{trans} at all three dose levels and at 100 and 200 $mg.kg^{-1}$ in v_e was seen at 4 hours versus control (relative reduction: 57.8%, 76.4% and 86.0% for K^{trans}, and 44.3% and 69.8% for v_e, respectively). At 24 hours, there was a significant reduction in K^{trans} at 200 $mg.kg^{-1}$ (relative reduction: 60.6%) but no significant change in v_e at any dose level. K^{trans} and v_e did not discriminate between groups at 24 hours (ANOVA, not significant). As with IAUGC, there were no significant changes in muscle K^{trans} or v_e at any time point or dose level (data not shown).

There was also a significant dose response relationship for K^{trans} on linear regression analysis: $r=-0.72$ ($p<0.0001$) at 4 hours and $r=-0.48$ ($p<0.05$) at 24 hours.

3.3.3.3 Relaxation parameters (T_1, T_2, T_2*)

The results are shown in **Table 3.2.** There was a significant increase in baseline T_1 at 4 hours for 100 and 200$mg.kg^{-1}$ but no significant change at 24 hours. There was a significant increase in T_2 at 24 hours for 100 and 200$mg.kg^{-1}$ but no significant changes at 4 hours. There was no significant changes in T_2* at either time.

	4 hours				24 hours			
	saline	30 $mg.kg^{-1}$	100 $mg.kg^{-1}$	200 $mg.kg^{-1}$	saline	30 $mg.kg^{-1}$	100 $mg.kg^{-1}$	200 $mg.kg^{-1}$
T_1 (s)	1.84 (±0.06)	1.99 (±0.06)	**2.05 (±0.06)**	**2.40 (±0.26)**	2.02 (±0.19)	1.96 (±0.15)	2.45 (±0.31)	2.07 (±0.09)
T_2 (ms)	37.5 (±0.8)	39.8 (±4.0)	37.0 (±2.3)	40.1 (±2.1)	40.1 (±1.7)	40.5 (±2.4)	**52.3 (±2.7)**	**50.0 (±1.3)**
T_2* (ms)	6.4 (±0.3)	7.5 (±0.6)	7.7 (±0.6)	6.7 (±0.3)	6.4 (±0.4)	7.5 (±0.5)	8.1 (±1.5)	8.2 (±0.6)

Table 3.2: Mean values of relaxation parameters for each treatment group at 4 and 24 hours following treatment (± standard error of the mean), values significantly different ($p<0.05$) to control are shown in **bold.**

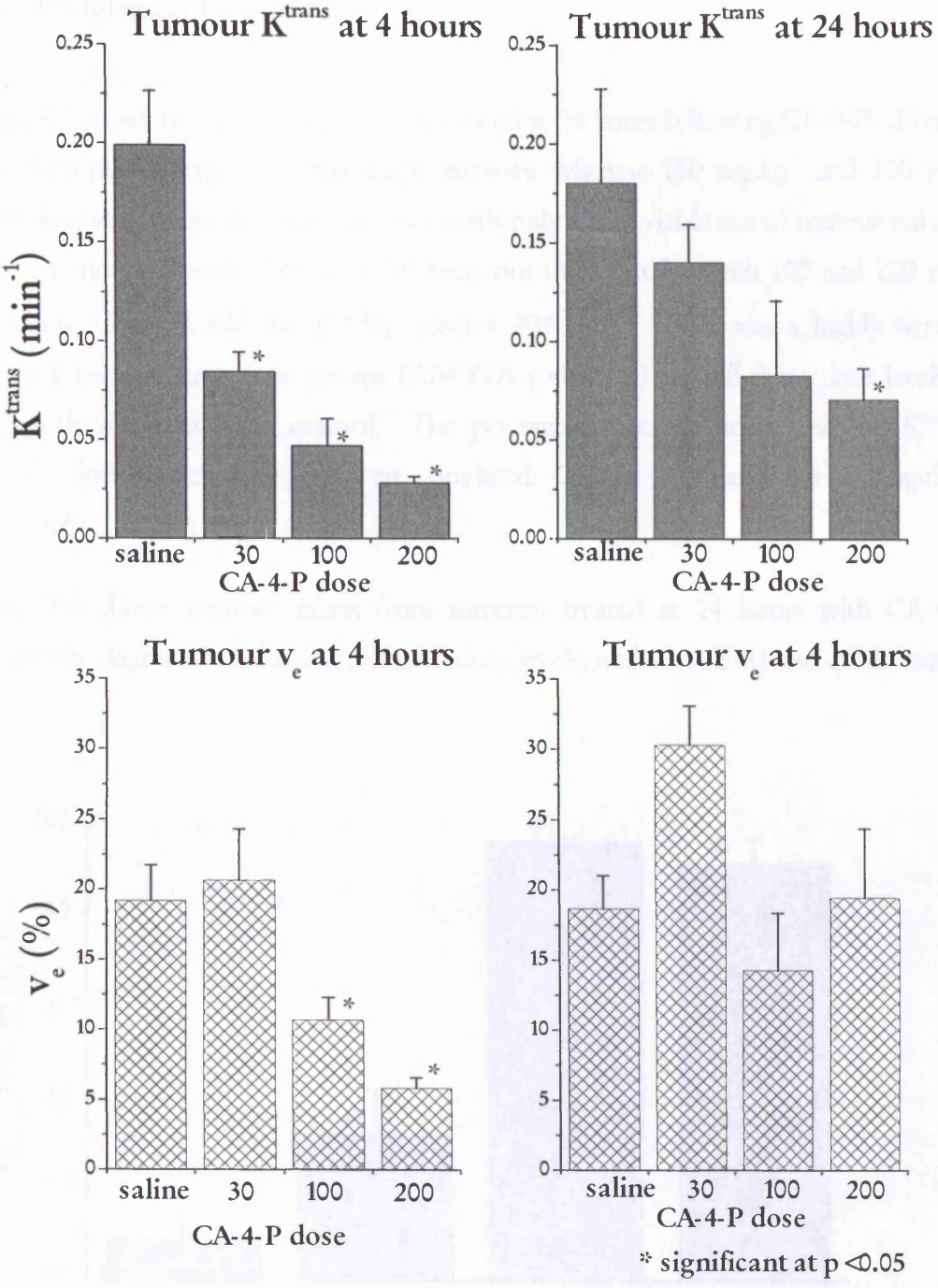

Figure 3.6: Mean tumour K^{trans} and v_e for each treatment group. Figures show mean ±standard error of the mean. n=6 for each treatment group. * indicates significant at $p < 0.05$ CA-4-P dose in $mg.kg^{-1}$.

3.3.4 Histological Parameters

3.3.4.1 Necrosis

Figure 3.7 shows the percentage necrosis scored at 24 hours following CA-4-P. 30 $mg.kg^{-1}$ CA-4-P produced patchy haemorrhagic necrosis whereas 100 $mg.kg^{-1}$ and 200 $mg.kg^{-1}$ produced extensive haemorrhagic necrosis with only a thin viable rim of tumour remaining. There was no significant difference between rim thickness between 100 and 200 $mg.kg^{-1}$ (mean rim thickness 407 μm (±120), median 204 μm). There was a highly significant difference between treatment groups (ANOVA $p<0.0001$) and all three dose levels were significantly different from control. The percentage necrosis score and the K^{trans} and IAUGC values at each dose level were correlated: -0.80 ($p<0.05$) and -0.6 (not significant) respectively.

Figure 3.8 shows sections taken from tumours treated at 24 hours with CA-4-P to demonstrate degree of necrosis at different dose levels, and also CD31 and αSMA staining.

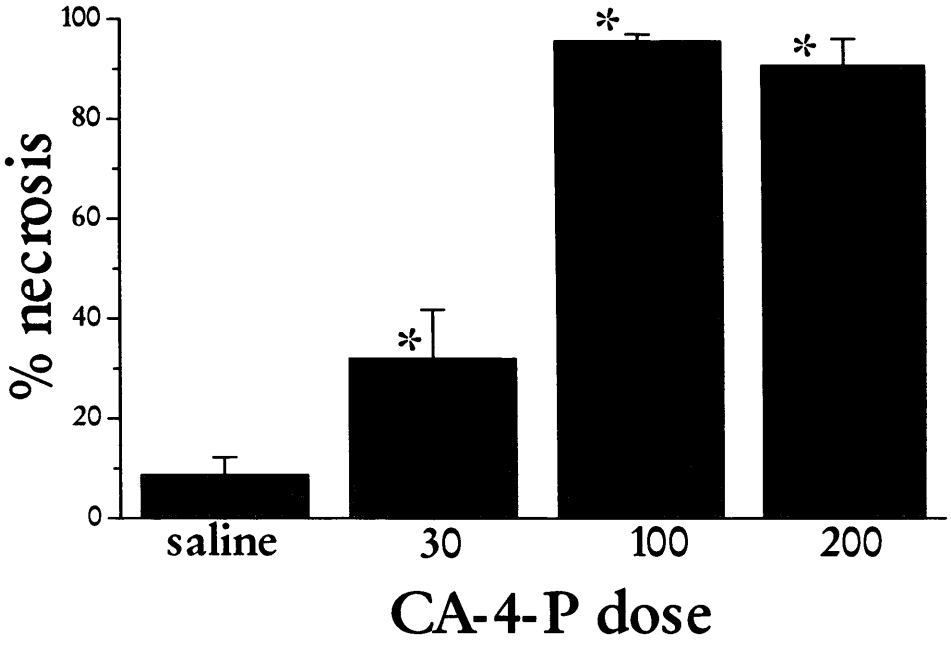

Figure 3.7: Percentage necrosis seen at 24 hours following CA-4-P ($mg.kg^{-1}$). Figures show mean ±standard error of the mean. N=6 for each treatment group. * indicates significant at $p<0.05$. CA-4-P dose in $mg.kg^{-1}$.

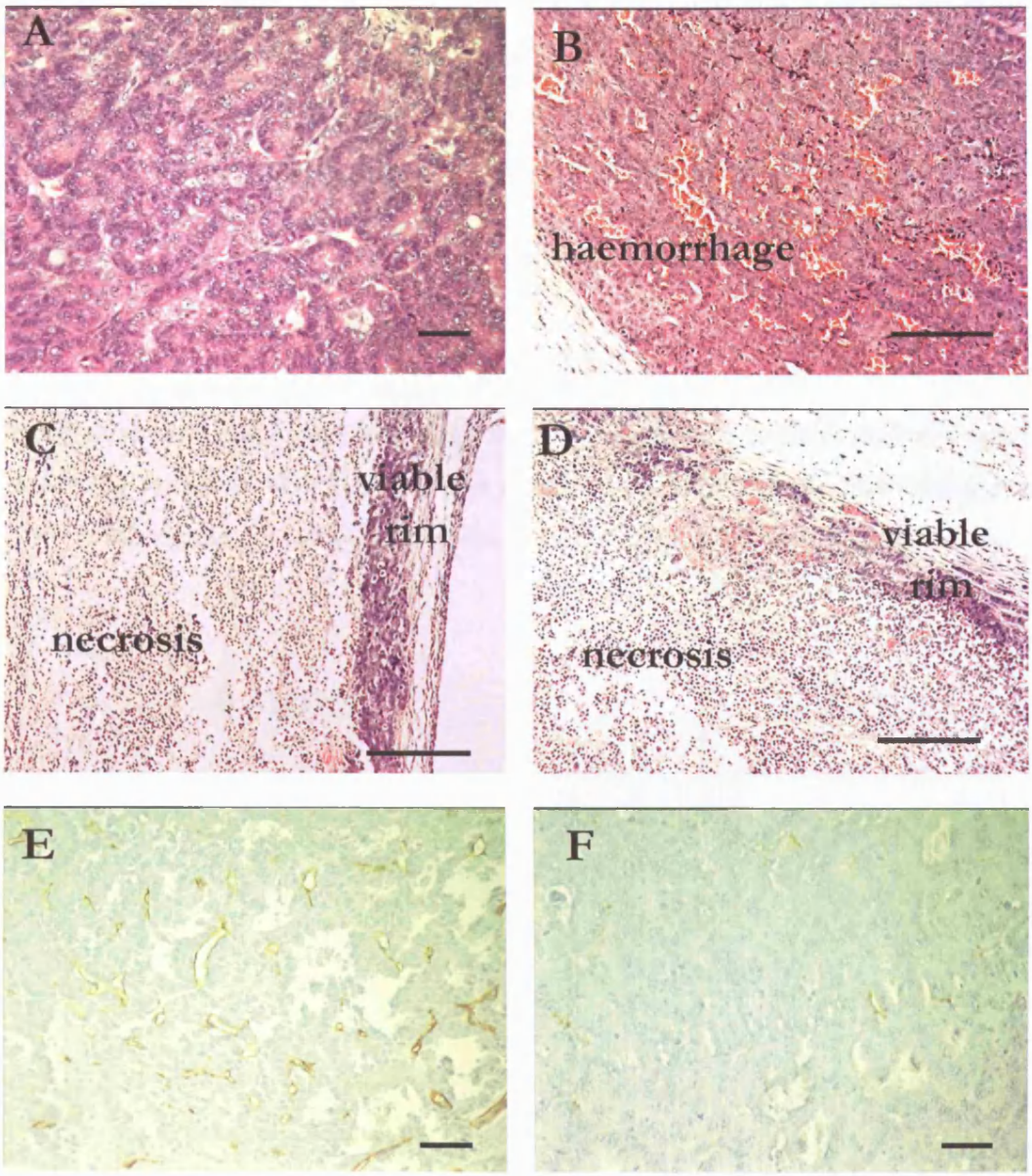

Figure 3.8: H&E sections showing extent of necrosis at 24 hours following treatment with CA-4-P. **A:** Saline; **B:** 30 mg.kg^{-1}; **C:** 100 mg.kg^{-1}; **D:** 200 mg.kg^{-1}. **E** & **F**: sections stained for CD31 antigen and αSMA staining respectively. A, E & F at x 20 magnification, rest taken with x10 magnification objective, bar represents 200 μm.

3.3.4.2 Vascular Maturation Index

Some tumour sections showed very faint or no staining for CD31 antigen and had to be discarded, leaving 8 tumours from the group treated with saline and 5 tumours from the group treated with 30 $mg.kg^{-1}$ CA-4-P at 24 hours prior to imaging for determination of vascular maturation index. The mean vascular maturation index (VMI) was 11.1% (±2.2) and 17.9% (±3.4) for the control group and the group treated with 30 $mg.kg^{-1}$ at 24 hours respectively. However, there was no significant difference between the two groups (unpaired t-test).

3.3.4.3 Functional vascular volume

Figure 3.9 shows the percentage functional vascular volume for controls and at 4 and 24 hours following treatment with CA-4-P. The reduction in functional vascular volume seen with CA-4-P was significant for all dose levels, apart from 30 $mg.kg^{-1}$ at 24 hours.

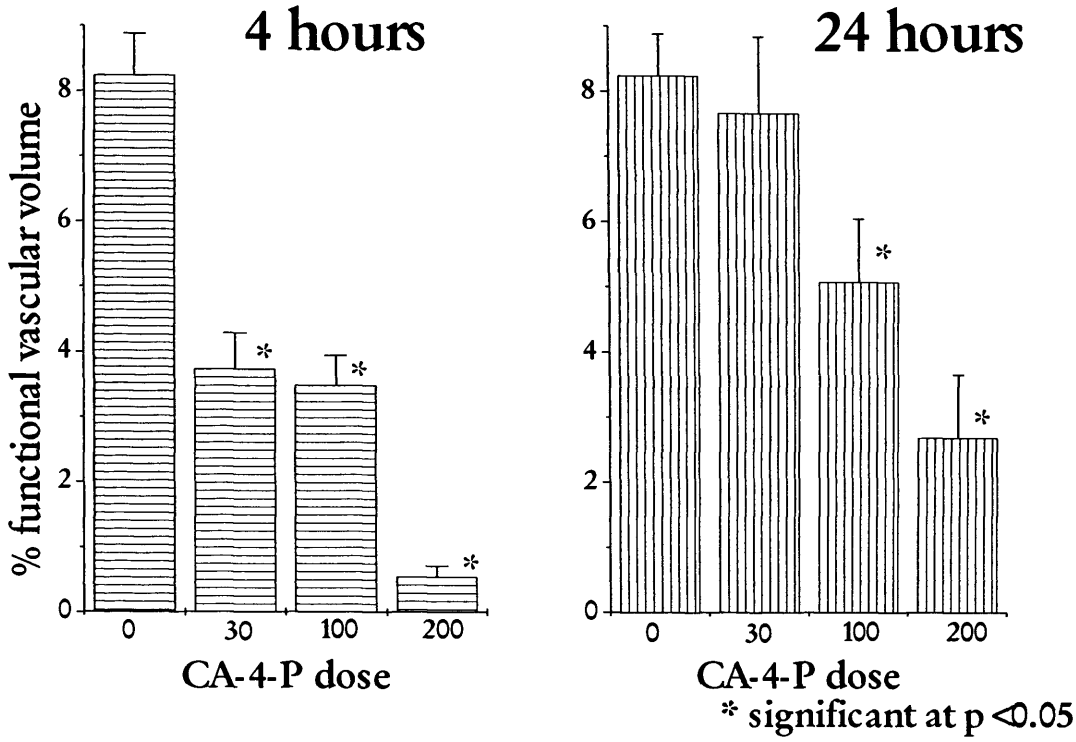

Figure 3.9 Change in functional vascular volume (%) at 4 and 24 hours post CA-4-P. Figures show mean ±standard error of the mean. n=15 for control. n=11, 8 & 7 for 30, 100 and 200 $mg.kg^{-1}$ CA-4-P at 4 hours respectively and n=10, 11 and 12 for 30, 100 and 200 $mg.kg^{-1}$ CA-4-P at 24 hours respectively. * indicates significant at $p<0.05$ CA-4-P dose in $mg.kg^{-1}$.

3.4 Discussion

3.4.1 MRI parameters

There was a significant decrease in the IAUGC in tumour (but not in muscle) for all three dose levels at 4 hours which persisted at the highest dose (200 $mg.kg^{-1}$) at 24 hours. There was a clear dose response relationship both at 4 and 24 hours, highly significant at 4 hours (using linear regression analysis of IAUGC).

The parameters K^{trans} and v_e were less sensitive indicators of CA-4-P effects. However, their calculation requires more mathematical modelling than for IAUGC - so more variability would be expected. In particular, the modelling procedure involves use of a Gd-DTPA arterial input function (AIF). The AIF used in the present study was obtained using a 'vessel' ROI (a combination of the IVC and aorta as it was not possible to distinguish clearly the two on MR images) and a simultaneous fit of data from *in-vivo* imaging and blood sampling. However, the resultant AIF appears to be a good approximation based on:

1. compatibility with previously published mouse AIF model parameters (Checkley et al., 2003a; Furman-Haran et al., 1996; Lyng et al., 1998) see **Figure 3.10** and **Table 3.3**.

2. generally good fitting of tumour and muscle data.

3. plausible values of K^{trans} and v_e were obtained.

However, the AIF used for modelling was obtained from a group of mice and no corrections could be made for individual variability or due to any systemic CA-4-P effects. It is possible, though difficult, to obtain an individual mouse AIF: Zhou et al. extracted AIF from signal intensity changes in left ventricular blood, with tumours implanted subcutaneously on the shoulder to be in the same imaging plane (Zhou et al., 2004). Pathak et al. used a tail RF coil to extract an AIF from mouse tail vein, with a second coil used to obtain images from a tumour region of interest (Pathak et al., 2004). However, the latter technique has a temporal resolution of 75 seconds so is only suitable for macromolecular contrast agents.

Reference	a_1	m_1	a_2	m_2	comments
Current study (GCI)	10.19	4.65	3.81	0.09	Simultaneous fit
(Furman-Haran et al., 1996)	4.3	0.43	3.2	0.057	Obtained from blood samples
(Lyng et al., 1998)	19.33	4.4	2.33	0.05	*In vivo* imaging (left ventricle)
(Checkley et al., 2003b)	11.95	1.17	4.67	0.054	*In vivo* imaging aorta and IVC

Table 3.3 Parameter values for AIF

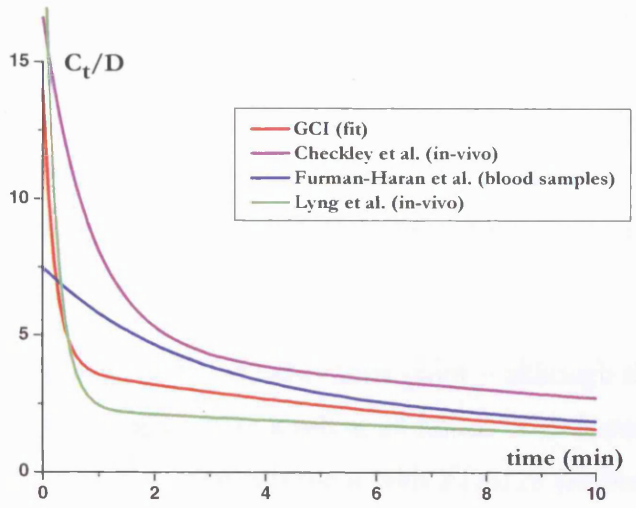

Figure 3.10: Comparison of mouse standard arterial input functions. GCI: Gray Cancer Institute (current study).

3.4.1.1 IAUGC spatial heterogeneity

The analysis of spatial heterogeneity of IAUGC values compared to distance from the edge of the tumour provides evidence that in this tumour model:

1. blood flow is higher towards the tumour rim than in the centre of untreated tumours;

2. the magnitude of CA-4-P anti-vascular effects is higher in the tumour centre than in the rim.

Previous quantitative approaches to evaluating the spatial selectivity of CA-4-P (i.e. whether the effects are greater in the tumour centre than in the rim) have been inconsistent (Maxwell et al., 2002; Maxwell et al., 2000; Tozer et al., 1999). The sensitivity differences

between rim and centre in this tumour model are consistent with the hypothesis that CA-4-P and RIT may have complementary actions, in a spatial sense (Pedley et al., 2001).

3.4.1.2 MR relaxation parameters

Interpretation of the changes in MR relaxation times (T_1, T_2 and T_2*) is uncertain, since there are several factors (e.g. blood oxygenation, blood volume, haemorrhage, necrosis, oedema) which can affect each parameter. Long relaxation times are associated with high fractional tumour water contents, probably due to free interstitial water (Belfi et al., 1991; Lyng et al., 1997; Rofstad et al., 1994). The presence of necrosis and haemorrhage can shorten relaxation times, due to the presence of paramagnetic ions (Jakobsen et al., 1995; Rofstad et al., 1994; Van Bruggen et al., 1990). Jakobsen et al. (Jakobsen et al., 1995) made the distinction between newly formed massive necrosis (e.g. due to vascular damage) and necrosis which had developed gradually during tumour growth. In the case of the former, the effect of increased oedema might overshadow the effect of increased concentrations of paramagnetic ions – resulting in longer relaxation times. This is consistent with our results: an increase in T_1 identified 4 hours after CA-4-P (100, 200 $mg.kg^{-1}$) and an increase in T_2 at 24 hours.

There were no significant changes in T_2* at either time point – although there was a trend towards an increase in T_2* at the higher dose levels at 24 hours. This is consistent with the decrease in R_2* seen at 24 hours following treatment with ZD6126 (Robinson et al., 2005) (see the discussion in **Chapter 2**).

3.4.2 Histological parameters

Changes in functional vascular volume and percentage necrosis seen in the SW1222 tumour following CA-4-P administration are similar to that seen in other tumours (Chaplin et al., 1999; Dark et al., 1997; Grosios et al., 1999). Hill et al. reported that 25 $mg.kg^{-1}$ of CA-4-P reduced functional vascular volume to ~65% of control values at 6 hours, with almost complete recovery (to 80-90%) by 24 hours in the CaNT (Hill et al., 2002). This finding is similar to the effect of 30 $mg.kg^{-1}$ CA-4-P on the SW1222 tumour: reduction to ~55% of control at 4 hours, recovering to >90% of control at 24 hours. The size and pattern of change in the MR parameters are similar to the changes seen in functional vascular volume at the corresponding time points.

It has been proposed that vascular maturation index may predict response to anti-angiogenic agents and VEGF withdrawal can lead to an increase in vascular maturation index, due to regression of immature vessels (see **Section 1.3**) (Benjamin et al., 1998). Vessel maturity may also be important in determining response to vascular disruptive agents. If immature vessels are more sensitive to CA-4-P, then an increase in vascular maturation index might be anticipated. This hypothesis was investigated by comparing vascular maturation indices calculated for control tumour and tumours that had been treated with 30 $mg.kg^{-1}$ CA-4-P 24 hours previously. This dose and time-point was used as necrosis was too extensive at the higher dose levels for αSMA and CD31 antigen scoring and the 4-hour time-point was judged to be too early for any tumour vessel regression to have occurred. There was a trend towards an increase in vascular maturation index following treatment with CA-4-P but this was not significant. However, results may have been confounded by small numbers and the presence of necrosis in the tumour sections from treated animals.

3.4.3 Clinical relevance of this study

DCE-MRI will be used in the clinical study so that early anti-vascular changes may be related to eventual response to the combination treatment. There are certain differences between the DCE-MRI protocol used here and the protocol that will be used in the clinical study. In the clinical study, patients will have three MRI scans – two before CA-4-P and one 4-6 hours afterwards. The advantage of this strategy is that patients act as their own control and also a reproducibility study can be performed. Serial MRI measurements are technically difficult using mice (requiring repeated venous cannulation) so separate control groups were used.

It is assumed that a certain level of anti-vascular response to CA-4-P will be required for enhancement of RIT. The dose of CA-4-P used in the preclinical study of ^{131}I-A5B7 and CA-4-P was 200 $mg.kg^{-1}$ (Pedley et al., 2001). The dose with equivalent effectiveness in a human (expressed in $mg.m^{-2}$) can be estimated either using a conversion factor[2] (Chodera & Feller, 1978) or by comparison of pharmacokinetic data (e.g. AUC for the active metabolite CA4 (Rustin et al., 2003)) Whichever method is used, the equivalent human

[2] The equivalent dose in humans (in $mg.m^{-2}$) for a particular dose in mouse (in $mg.kg^{-1}$) can be calculated by multiplying the mouse dose by 3.083 Chodera, A. & Feller, K. (1978). Some aspects of pharmacokinetic and biotransformation differences in humans and mammal animals. *Int J Clin Pharmacol Biopharm*, **16**, 357-60..

dose for 200 $mg.kg^{-1}$ in the mouse is approximately 10 times higher than the maximum tolerated dose in the phase I clinical trial of CA-4-P as a single agent (Rustin et al., 2003).

The effect of the combination of ^{131}I-A5B7 and more clinically relevant doses of CA-4-P on tumour growth has not been established. However, indirect evidence for the supposition that a clinically relevant dose of CA-4-P may still be effective in combination with ^{131}I-A5B7 comes from a comparison of the effect of these three dose levels on tumour antibody retention (Lankester et al., 2004). SW1222 tumour-bearing mice received a small dose of ^{131}I-A5B7 and then either 30, 100 or 200 $mg.kg^{-1}$ CA-4-P i.p. 48 hours later or no further treatment (control). The mice were bled and tissues excised 96 hours after ^{131}I-A5B7 administration and comparative activity assessed using a γ-counter. All three doses significantly increased antibody retention in tumour (increases of 71%, 78% and 90% vs control for 30, 100 and 200 $mg.kg^{-1}$ CA-4-P respectively) but not in normal tissues (Dr RB Pedley, personal communication). The percentage increases were not significantly different between the three treatment groups. The timing of CA-4-P in relation to ^{131}I-A5B7 was based on previous data showing that maximum efficacy is achieved if the vascular disruptive agent is given 24-48 hours after the radio-antibody (Pedley et al., 1996) (see the introduction to this chapter).

So, while 30 $mg.kg^{-1}$ of CA-4-P produced only a transient decrease in tumour vascular function (and limited necrosis), it still increased antibody retention in tumour significantly. It is not clear why this is the case, but it is possible that a significant number of tumour vessels are permanently lost following treatment and so antibody is less likely to escape from the tumour. If antibody clearance from tumour at this time (48 hours) is high, then a decrease in tumour blood flow reduction at this time may be particularly beneficial.

The mean reduction in IAUGC seen at 4 hours at the 30 $mg.kg^{-1}$ dose level (38%) is similar to that seen in the phase I clinical study (33% for patients treated at >52 $mg.m^{-2}$ (Galbraith et al., 2003). This suggests that the 30 $mg.kg^{-1}$ dose level is equivalent to a clinically relevant human dose. The dose levels of CA-4-P for the ^{131}I-A5B7/CA-4-P clinical trial will be 45 $mg.m^{-2}$ and 55 $mg.m^{-2}$. So, reductions of this magnitude might be anticipated to occur in the clinical trial.

3.4.4 Conclusions

There is a clear dose-response relationship for treatment with CA-4-P, in the SW1222 tumour. Significant reductions in kinetic parameters are seen at clinically relevant drug doses (30 $mg.kg^{-1}$) and are of a similar magnitude to those seen in the previous clinical study (Galbraith et al., 2003). The data presented here indicate that although a lower dose of CA-4-P (30 $mg.kg^{-1}$ in this case) results in a substantially lower and shorter duration anti-vascular effect, there is relatively little difference in radio-antibody retention between the 3 doses used. The likelihood of this dose of CA-4-P enhancing RIT therefore probably depends on the importance of radio-antibody trapping as opposed to sustained anti-vascular damage as the main mechanism of the interaction.

3.5 References –Chapter 3

Behr, T.M., Liersch, T., Canelo, R., Wörmann, B., Hiddemann, W., Ringe, B., Becker, H. & Becker, W. (1999). Radioimmunotherapy of small volume disease of colorectal cancer: results of a clinical phase I/II trial. *European Journal of Cancer*, **35 (suppl 5)**, S51.

Behr, T.M., Liersch, T., Greiner-Bechert, L., Griesinger, F., Behe, M., Markus, P.M., Gratz, S., Angerstein, C., Brittinger, G., Becker, H., Goldenberg, D.M. & Becker, W. (2002). Radioimmunotherapy of small-volume disease of metastatic colorectal cancer. *Cancer*, **94**, 1373-81.

Behr, T.M., Sharkey, R.M., Juweid, M.E., Dunn, R.M., Ying, Z., Zhang, C.H., Siegel, J.A. & Goldenberg, D.M. (1997). Variables influencing tumor dosimetry in radioimmunotherapy of CEA-expressing cancers with anti-CEA and antimucin monoclonal antibodies. *J Nucl Med*, **38**, 409-18.

Belfi, C.A., Medendorp, S.V. & Ngo, F.Q. (1991). The response of the KHT sarcoma to radiotherapy as measured by water proton NMR relaxation times: relationships with tumor volume and water content. *Int J Radiat Oncol Biol Phys*, **20**, 497-507.

Benjamin, L.E., Hemo, I. & Keshet, E. (1998). A plasticity window for blood vessel remodelling is defined by pericyte coverage of the preformed endothelial network and is regulated by PDGF- B and VEGF. *Development*, **125**, 1591-8.

Chalkley, H. (1943). Method for the quantitative morphologic analysis of tissues. *J Natl Cancer Inst*, **4**, 47-53.

Chaplin, D.J., Pettit, G.R. & Hill, S.A. (1999). Anti-vascular approaches to solid tumour therapy: evaluation of combretastatin A4 phosphate. *Anticancer Res*, **19**, 189-95.

Checkley, D., Tessier, J.J., Kendrew, J., Waterton, J.C. & Wedge, S.R. (2003a). Use of dynamic contrast-enhanced MRI to evaluate acute treatment with ZD6474, a VEGF signalling inhibitor, in PC-3 prostate tumours. *Br J Cancer*, **89**, 1889-95.

Checkley, D., Tessier, J.J., Wedge, S.R., Dukes, M., Kendrew, J., Curry, B., Middleton, B. & Waterton, J.C. (2003b). Dynamic contrast-enhanced MRI of vascular changes induced by the VEGF-signalling inhibitor ZD4190 in human tumour xenografts. *Magn Reson Imaging*, **21**, 475-82.

Chodera, A. & Feller, K. (1978). Some aspects of pharmacokinetic and biotransformation differences in humans and mammal animals. *Int J Clin Pharmacol Biopharm*, **16**, 357-60.

Chung, J.K., Jang, J.J., Lee, D.S., Lee, M.C. & Koh, C.S. (1994). Tumor concentration and distribution of carcinoembryonic antigen measured by in vitro quantitative autoradiography. *J Nucl Med*, **35**, 1499-505.

Dark, G.G., Hill, S.A., Prise, V.E., Tozer, G.M., Pettit, G.R. & Chaplin, D.J. (1997). Combretastatin A-4, an agent that displays potent and selective toxicity toward tumour vasculature. *Cancer Res*, **57**, 1829-1834.

Donahue, K., Burstein, D., Manning, W. & Gray, M. (1994). Studies of Gd-DTPA relaxivity and proton exchange rates in tissue. *Magn Reson Med*, **32**, 66-76.

Evelhoch, J.L. (1999). Key factors in the acquisition of contrast kinetic data for oncology. *J Magn Reson Imaging*, **10**, 254-9.

Flynn, A.A., Green, A.J., Boxer, G.M., Casey, J.L., Pedley, R.B. & Begent, R.H. (1999). A novel technique, using radioluminography, for the measurement of uniformity of radiolabelled antibody distribution in a colorectal cancer xenograft model. *Int J Radiat Oncol Biol Phys*, **43**, 183-9.

Furman-Haran, E., Margalit, R., Grobgeld, D. & Degani, H. (1996). Dynamic contrast-enhanced magnetic resonance imaging reveals stress-induced angiogenesis in MCF7 human breast tumors. *Proc Natl Acad Sci U S A*, **93**, 6247-51.

Galbraith, S.M., Maxwell, R.J., Lodge, M.A., Tozer, G.M., Wilson, J., Taylor, N.J., Stirling, J.J., Sena, L., Padhani, A.R. & Rustin, G.J.S. (2003). Combretastatin A4 Phosphate has tumour anti-vascular activity in rat and man as demonstrated by dynamic magnetic resonance imaging. *J Clin Oncol*, **21**, 2831-2842.

Goldenberg, D.M. (2002). Targeted therapy of cancer with radiolabeled antibodies. *J Nucl Med*, **43**, 693-713.

Goldenberg, D.M., Sharkey, R.M. & Primus, F.J. (1976). Carcinoembryonic antigen in histopathology: immunoperoxidase staining of conventional tissue sections. *J Natl Cancer Inst*, **57**, 11-22.

Grosios, K., Holwell, S.E., McGown, A.T., Pettit, G.R. & Bibby, M.C. (1999). In vivo and in vitro evaluation of combretastatin A-4 and its sodium phosphate prodrug. *Br J Cancer*, **81**, 1318-27.

Hill, S.A., Chaplin, D.J., Lewis, G. & Tozer, G.M. (2002). Schedule dependence of combretastatin A4 phosphate in transplanted and spontaneous tumour models. *Int J Cancer*, **102**, 70-4.

Hittmair, K., Gomiscek, G., Langenberger, K., Recht, M., Imhof, H. & Kramer, J. (1994). Method for the quantitative assessment of contrast agent uptake in dynamic contrast-enhanced MRI. *Magnetic resonance in medicine*, **31**, 567-571.

Jain, R.K. (1989). Delivery of novel therapeutic agents in tumors: physiological barriers and strategies. *J Natl Cancer Inst*, **81**, 570-6.

Jain, R.K. & Baxter, L.T. (1988). Mechanisms of heterogeneous distribution of monoclonal antibodies and other macromolecules in tumors: significance of elevated interstitial pressure. *Cancer Research*, **48**, 7022-32.

Jakobsen, I., Kaalhus, O., Lyng, H. & Rofstad, E.K. (1995). Detection of necrosis in human tumour xenografts by proton magnetic resonance imaging. *British Journal of Cancer*, **71**, 456-61.

Kaminski, M.S., Estes, J., Zasadny, K.R., Francis, I.R., Ross, C.W., Tuck, M., Regan, D., Fisher, S., Gutierrez, J., Kroll, S., Stagg, R., Tidmarsh, G. & Wahl, R.L. (2000). Radioimmunotherapy with iodine (131)I tositumomab for relapsed or refractory B-cell non-Hodgkin lymphoma: updated results and long-term follow-up of the University of Michigan experience. *Blood*, **96**, 1259-66.

Lane, D.M., Eagle, K.F., Begent, R.H., Hope-Stone, L.D., Green, A.J., Casey, J.L., Keep, P.A., Kelly, A.M., Ledermann, J.A., Glaser, M.G. & et al. (1994). Radioimmunotherapy of metastatic colorectal tumours with iodine-131- labelled antibody to carcinoembryonic antigen: phase I/II study with comparative biodistribution of intact and F(ab')2 antibodies. *Br J Cancer*, **70**, 521-5.

Lankester, K.J., Maxwell, R.J., Pedley, R.B., Hill, S.A., Rustin, G.J.S. & Tozer, G.M. (2004). Acute anti-vascular effects of combretastatin A4 phosphate (CA-4-P) on the SW1222 tumour as measured by dynamic contrast enhanced (DCE)-MRI. *British Journal of Cancer*, **91**, S16.

Ledermann, J.A., Begent, R.H., Massof, C., Kelly, A.M., Adam, T. & Bagshawe, K.D. (1991). A phase-I study of repeated therapy with radiolabelled antibody to carcinoembryonic antigen using intermittent or continuous administration of cyclosporin A to suppress the immune response. *Int J Cancer*, **47**, 659-64.

Lyng, H., Dahle, G.A., Kaalhus, O., Skretting, A. & Rofstad, E.K. (1998). Measurement of perfusion rate in human melanoma xenografts by contrast-enhanced magnetic resonance imaging. *Magn Reson Med*, **40**, 89-98.

Lyng, H., Tufto, I., Skretting, A. & Rofstad, E.K. (1997). Proton relaxation times and interstitial fluid pressure in human melanoma xenografts. *Br J Cancer*, **75**, 180-3.

Maxwell, R., Wilson, J., Prise, V., Vojnovic, B., Rustin, G., Lodge, M. & Tozer, G. (2002). Evaluation of the anti-vascular effects of combretastatin in rodent tumours by dynamic contrast enhanced MRI. *NMR Biomed*, **15**, 89-98.

Maxwell, R., Wilson, J., Tozer, G., Barber, P. & Vojnovic, B. (2000). Segmentation of magnetic resonance images according to contrast agent uptake kinetics using a competitive neural network. In *Artificial neural networks in medicine and biology*, Malmgren, H., Borga, M. & Niklasson, L. (eds) pp. 93-98. Springer-Verlag: London.

Napier, M. & Begent, R. (1998). Radioimmunotherapy of Gastrointestinal Cancer. In *Cancer Radioimmunotherapy*, Riva, P. (ed) pp. 333-388. Harwood Academia: Boston.

Pathak, A.P., Artemov, D. & Bhujwalla, Z.M. (2004). Novel system for determining contrast agent concentration in mouse blood in vivo. *Magn Reson Med*, **51**, 612-5.

Pedley, R., Hill, S., Boxer, G., Flynn, A., Boden, R., Watson, R., Dearling, J., Chaplin, D. & Begent, R. (2001). Eradication of colorectal xenografts by combined radioimmunotherapy and combretastatin A-4 3-O-phosphate. *Cancer Res*, **61**.

Pedley, R.B., Begent, R.H., Boden, J.A., Boxer, G.M., Boden, R. & Keep, P.A. (1994). Enhancement of radioimmunotherapy by drugs modifying tumour blood flow in a colonic xenograft model. *Int J Cancer*, **57**, 830-5.

Pedley, R.B., Boden, J.A., Boden, R., Boxer, G.M., Flynn, A.A., Keep, P.A. & Begent, R.H. (1996). Ablation of colorectal xenografts with combined radioimmunotherapy and tumor blood flow-modifying agents. *Cancer Res*, **56**, 3293-300.

Pedley, R.B., El-Emir, E., Flynn, A.A., Boxer, G.M., Dearling, J., Raleigh, J.A., Hill, S.A., Stuart, S., Motha, R. & Begent, R.H. (2002). Synergy between vascular targeting agents and antibody-directed therapy. *Int J Radiat Oncol Biol Phys*, **54**, 1524-31.

Press, O.W., Eary, J.F., Appelbaum, F.R., Martin, P.J., Badger, C.C., Nelp, W.B., Glenn, S., Butchko, G., Fisher, D., Porter, B. & et al. (1993). Radiolabeled-antibody therapy of B-cell lymphoma with autologous bone marrow support. *N Engl J Med*, **329**, 1219-24.

Robinson, S.P., Kalber, T.L., Howe, F.A., McIntyre, D.J., Griffiths, J.R., Blakey, D.C., Whittaker, L., Ryan, A.J. & Waterton, J.C. (2005). Acute tumor response to ZD6126 assessed by intrinsic susceptibility magnetic resonance imaging. *Neoplasia*, **7**, 466-74.

Rofstad, E.K., Steinsland, E., Kaalhus, O., Chang, Y.B., B, H.v. & Lyng, H. (1994). Magnetic resonance imaging of human melanoma xenografts in vivo: proton spin-lattice and spin-spin relaxation times versus fractional tumour water content and fraction of necrotic tumour tissue. *International Journal of Radiation Biology*, **65**, 387-401.

Rustin, G.J., Galbraith, S.M., Anderson, H., Stratford, M., Folkes, L.K., Sena, L., Gumbrell, L. & Price, P.M. (2003). Phase I clinical trial of weekly combretastatin A4 phosphate: clinical and pharmacokinetic results. *J Clin Oncol*, **21**, 2815-22.

Smith, K.A., Hill, S.A., Begg, A.C. & Denekamp, J. (1988). Validation of the fluorescent dye Hoechst 33342 as a vascular space marker in tumours. *Br J Cancer*, **57**, 247-53.

Tofts, P., Brix, G., Buckley, D., Evelhoch, J., Henderson, E., Knopp, M., Larsson, H., Lee, T., Mayr, N., Parker, G., Port, R., Taylor, J. & Weisskoff, R. (1999). Estimating kinetic parameters from dynamic contrast-enhanced T(1)-weighted MRI of a diffusable tracer: standardized quantities and symbols. *J Magn Reson Imaging*, **10**, 223-32.

Tofts, P.S. & Kermode, A.G. (1991). Measurement of the blood-brain barrier permeability and leakage space using dynamic MR imaging. 1. Fundamental concepts. *Magn Reson Med*, **17**, 357-67.

Tozer, G.M., Prise, V.E., Wilson, J., Locke, R.J., Vojnovic, B., Stratford, M.R., Dennis, M.F. & Chaplin, D.J. (1999). Combretastatin A-4 phosphate as a tumor vascular-targeting agent: early effects in tumors and normal tissues. *Cancer Res*, **59**, 1626-34.

Van Bruggen, N., Syha, J., Busza, A.L., King, M.D., Stamp, G.W., Williams, S.R. & Gadian, D.G. (1990). Identification of tumor hemorrhage in an animal model using spin echoes and gradient echoes. *Magn Reson Med*, **15**, 121-7.

Zhou, R., Pickup, S., Yankeelov, T.E., Springer, C.S., Jr. & Glickson, J.D. (2004). Simultaneous measurement of arterial input function and tumor pharmacokinetics in mice by dynamic contrast enhanced imaging: effects of transcytolemmal water exchange. *Magn Reson Med*, **52**, 248-57.

Chapter 4 Investigation of tumour vessel maturity using air-5% CO_2/ carbogen and angiotensin II using MRI and intravital microscopy

4.1 Introduction

This chapter contains details of the experiments performed to determine whether BOLD-MRI response to a vasoactive agent could provide a functional measure of tumour vascular maturation status.

The aim was to determine the utility of air-5% CO_2/carbogen breathing and angiotensin II (ATII) administration to discriminate between different tumour types on the basis of vessel maturity.

Histological vascular maturation index was determined for three different tumour types: the human colon carcinoma xenograft, HT29 (high numbers of mature vessels), the murine mammary tumour, CaNT (very few mature vessels), and the spontaneous mammary tumour, T138 (variable numbers of mature vessels) in mice.

Tumour BOLD-MRI response to air-5% CO_2/carbogen or ATII was used as a functional measure of vessel maturity and compared to the histological measurements for all three tumour types. The hypothesis was that breathing 5% CO_2 (in the form of air-5% CO_2 or carbogen) should cause mature vessels to vasodilate, resulting in an increase in T_2*, A_0 and BOLD signal intensity in the HT29, a fall in signal intensity or maybe no change in the CaNT (depending on change in perfusion pressure) and a variable response in T138. Conversely, an intravenous infusion of ATII should cause mature vessels to vasoconstrict, resulting in a decrease in T_2*, A_0 and BOLD signal intensity in the HT29, no change or an increase in these parameters (due to increased perfusion pressure) in the CaNT and, again, a variable response in the T138.

In order to determine whether the vasoactive agents tested were having the hypothesised effect, intravital microscopy was used to directly observe HT29 and CaNT tumour vessels and to determine the capacity of tumour blood vessels to vasodilate or constrict in response to air-5% CO_2/carbogen and to ATII respectively, and the consequence of vasoactivity on tumour blood flow rate.

The effects of the vasoactive agents and anaesthesia on mouse blood pressure were also determined in order to aid interpretation of results.

4.2 *Materials and Methods*

All animal experiments were performed in full compliance with government regulations and UKCCCR guidelines on animal welfare and were approved by the local Ethical Review Committee (Home office license number PPL 70/4552).

4.2.1 Tumours

HT29 human colorectal adenocarcinoma tumour cells were maintained in Dulbecco's modified Eagle's Medium (DMEM, Life Technologies, UK) supplemented with 10% foetal calf serum (Sigma, UK), 100 $U.ml^{-1}$ penicillin (Sigma, UK), 100 $\mu g.ml^{-1}$ streptomycin (Sigma) and 2 mM glutamine (Life Technologies) and incubated in a humidified incubator at 37^0 C in 5% CO_2/air.

$2x10^6$ cells were implanted subcutaneously on the rear dorsum of female CB17 SCID mice aged 10-16 weeks, briefly anaesthetised with metofane (methoxyflurane, Janssen Pharmaceutica, Ontario, Canada). Tumours were selected for scanning approximately 21 days later at 8-10 mm diameter.

The murine adenocarcinoma NT (CaNT) was maintained by passage between donor animals (tumour pieces were stored in liquid nitrogen, up to 10 passages from animal to animal permitted). The tumour was implanted subcutaneously on to the rear dorsum of 10-16 week old female CBA/Gy f TO mice (CBA), by injecting 0.05 ml of a crude cell suspension prepared by mechanical dissociation of an excised tumour from a donor animal. Tumours were selected for scanning approximately 21 days later at 8-10 mm diameter.

The T138 mouse strain has an inherited predisposition to develop mammary tumours and, between 5 and 18 months of age, ≥90% of females develop tumours. The tumours are predominantly well-differentiated glandular or acinar adenocarcinomas, although occasionally adenosquamous carcinomas and undifferentiated tumours develop. Female mice were checked for tumours weekly. Suitable tumours growing in the flank or groin were selected for scanning when approximately 8-10 mm in diameter. (These tumour sites were chosen so that the tumour would not move with respiration).

4.2.2 Histology: Vascular Maturation Index

Tumours were excised from mice after BOLD-MRI imaging (see below) for histological analysis. Mice were killed by cervical dislocation and tumours excised and cut in half in the same plane as the MRI slice used for scanning. One half was fixed in formalin (Sigma-Aldrich, UK) and then a central tumour section stained with hematoxylin and eosin (H&E - Sigma-Aldrich, UK) and for αSMA (Sigma-Aldrich, UK). The other tumour half was placed in zinc fixative for subsequent staining of a central tumour section for CD31 antigen (Pharmagen, UK) (see **Chapter 3** for method). Immunohistochemistry was performed by Mrs Frances Daley, Gray Cancer Institute. The vascular maturation index was then calculated for each tumour type (see **Chapter 3** for method).

4.2.3 Effect of ATII, air-5% CO_2 and carbogen, and anaesthesia on mouse blood pressure

SCID, CBA and T138 mice were anaesthetised with 10 $ml.kg^{-1}$ of a mixture of Hypnorm (fentanyl citrate 0.315 $mg.ml^{-1}$ & fluanisone 10 $mg.ml^{-1}$ - Janssen-Cilag, UK) and Hypnovel (midazolam 5 $mg.ml^{-1}$ – Phoenix Pharma, UK) diluted 1:1:2 with water. Top-up anaesthetic was given as an i.p. infusion as required.

The left femoral artery was cannulated and connected to a physiological pressure transducer (Spectramed, model no. P23XL, Gould Electronics, UK) connected to a chart recorder or computer, in order to measure mean arterial blood pressure (MABP). The effect of ATII infusion or breathing air-5% CO_2 or carbogen was then observed. Mice were killed by cervical dislocation at the end of the experiment.

4.2.3.1 Effect of ATII on mouse blood pressure

After an initial baseline recording, ATII was infused i.v. via a tail vein at 2 $\mu g.kg^{-1}.min^{-1}$ at a concentration of 10 $\mu g.ml^{-1}$ for approximately 15 minutes. Blood pressure was then recorded for a further 5-10 minutes. The first two minutes of data following the start of the ATII infusion was omitted from analysis to allow blood pressure to stabilise. The average MABP before and during ATII infusion was determined for each mouse and results compared using a paired Student's t-test.

4.2.3.2 *Effect of breathing air-5% CO_2 or carbogen on mouse blood pressure*

After an initial baseline recording during which mice breathed air via a mask, air-5% CO_2 and then carbogen were administered for approximately 8 minutes each at 1 $l.min^{-1}$. Blood pressure was then recorded for a further ~8 minutes with the mouse breathing air. The first two minutes after the switch from breathing one gas to the next was omitted from analysis. The average MABP was calculated for each treatment block. Data was then normalised to the mean pre-treatment value and a one-way analysis of variance (ANOVA) used to determine if there was a significant difference in mouse MABP when breathing the different gas mixtures.

4.2.3.3 *Effect of anaesthesia on mouse blood pressure*

In addition, the effect of anaesthesia on mouse blood pressure was determined, using the same anaesthetic protocol as above. This work was performed by Mrs V Prise (Gray Cancer Institute), using a non-invasive tail cuff blood pressure analysis system (Kent Scientific Corporation, Connecticut, USA). MABP was recorded in unanaesthetised animals during anaesthesia. A paired Student's t-test was used to determine whether there was a significant change in MABP due to anaesthesia.

4.2.4 BOLD-MRI animal studies

Mice were anaesthetised as for the blood pressure experiments. For the ATII protocol, an i.v. catheter was placed in a tail vein for ATII infusion. Mice were then placed in a 6 cm diameter quadrature birdcage coil (Varian, Palo Alto, CA, USA) in a 4.7 Tesla Varian MR system. An i.p. infusion of Hypnorm, diluted 1:10 with water, was started after approximately 30 minutes at 3 $\mu l.min^{-1}$ to maintain a constant level of anaesthesia. For the initial experiments, temperature was maintained using tubing containing circulating warm water. The mouse's rectal temperature was checked after scanning and any with a temperature less than 35^0 C were rejected. For later experiments, a hot air blower and continuous temperature monitoring with a rectal thermocouple was utilised.

4.2.4.1 BOLD-MRI protocols

Initial T_1-weighted sagital and transverse scans were obtained for localisation. Two different BOLD-MRI sequences were used for separate experiments.

A. A **multi-echo, single-slice sequence** comprising 8 images acquired every minute for 32 minutes: TE 5-40 ms in 5 ms steps, TR 117 ms, flip angle 45^0, slice thickness 1 mm, spatial resolution 0.16 x 0.31 mm, FOV 35 x 40 mm.

B. A **single-echo, multi-slice sequence** comprising 1 image acquired per minute for 32 minutes with 9 transverse slices (7 through tumour and 2 through kidney): TE 20 ms, TR 600 ms, flip angle 20^0, slice thickness 1 mm, spatial resolution 0.1 x 0.4 mm, FOV 35 x 40 mm, total imaging time 32 min).

Initial experiments were done with the multi-echo, single-slice sequence (**A**) from which quantitative images (T_2* and A_0) as well as signal intensity can be generated (see below). The intention was to obtain values for T_2* and A_0 in order to discriminate between any change in oxygenation from change in blood flow (see **Section 1.5.4**). However, on initial analysis, there was a problem with data fitting such that there was correlation between T_2* and A_0, whereas they should be independent variables. Therefore, it was decided to continue with the single-echo, multi-slice sequence (**B**). Only signal intensity data could be obtained from this sequence (so change in oxygenation and flow could not be separated) but it had the advantage of being a multi-slice sequence, so normal tissue (kidney) data could also be acquired. Subsequently, improved analysis software became available and the data from the multi-echo, single-slice sequence (**A**) was re-analysed.

ATII protocol: after an initial 8 background images had been acquired, ATII (Sigma, UK) was infused at 2 $\mu g.kg^{-1}.min^{-1}$ i.v. (at 10 $\mu g.ml^{-1}$ concentration) for 16 images, then a further 8 images were acquired after stopping the ATII infusion. This dose-rate and concentration of ATII has been used previously in mice (Hirst et al., 1991; Trotter et al., 1991).

Gas breathing protocol: scanning time was divided into 8 minute treatment periods with the mouse breathing air, air-5% CO_2, carbogen, then air again for the 1st, 2nd, 3rd and 4th treatment periods respectively - all at 1 $l.min^{-1}$ (all gases obtained from BOC, UK). A vacuum-based gas scavenger was used to minimise changes in oxygen content within the magnet bore.

Experiments using the gas breathing protocol were delayed until the gas-scavenger could be acquired. As preliminary results with the single-echo multi-slice sequence were negative for CaNT, the experiment was not repeated using the multi-echo single-slice protocol for this tumour.

4.2.4.2 Image Analysis

Multi-echo single-slice sequence

Images were processed using Matlab version 5 (The Mathworks, Nantick, MA USA). A region of interest (ROI) was drawn around the tumour using the initial T_1-weighted image (**Figure 4.1**). T_2* (ms) and A_0 (arbitrary units) pixel-maps were then calculated for each time-point using in-house computer software (Time Resolved Image Analysis, version 2) from the equation below - see **Section 1.5.4.**

$$S = A_0 e^{-\frac{TE}{T_2^*}}$$

The images produced at odd and even echo times were symmetrical. Alternate images were then reversed so that the whole series of images could be used for T_2* calculation. However, when this was done, it was observed that those images produced at odd echo times had different signal intensity to those produced at even echo times (i.e. they were predicting different A_0 values) and also had a slightly different position. Therefore, only one set of echo times could be used for T_2* calculation (the odd echo times: TE 5, 15, 25, and 35 ms).

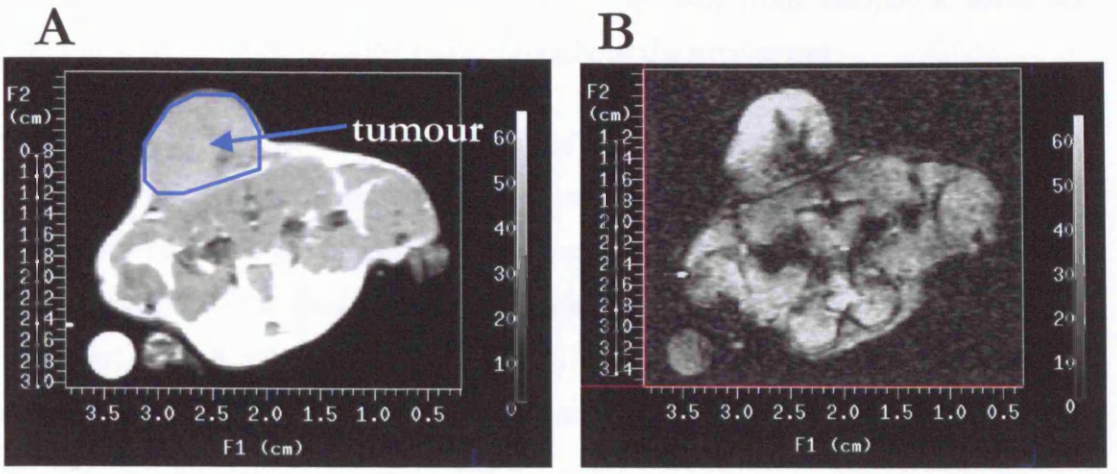

Figure 4.1: **A:** Anatomical T_1-weighted image (baseline, pre-contrast) showing transverse section through SCID mouse with dorsal subcutaneous tumour (HT29). **B**: corresponding BOLD image (animal breathing air).

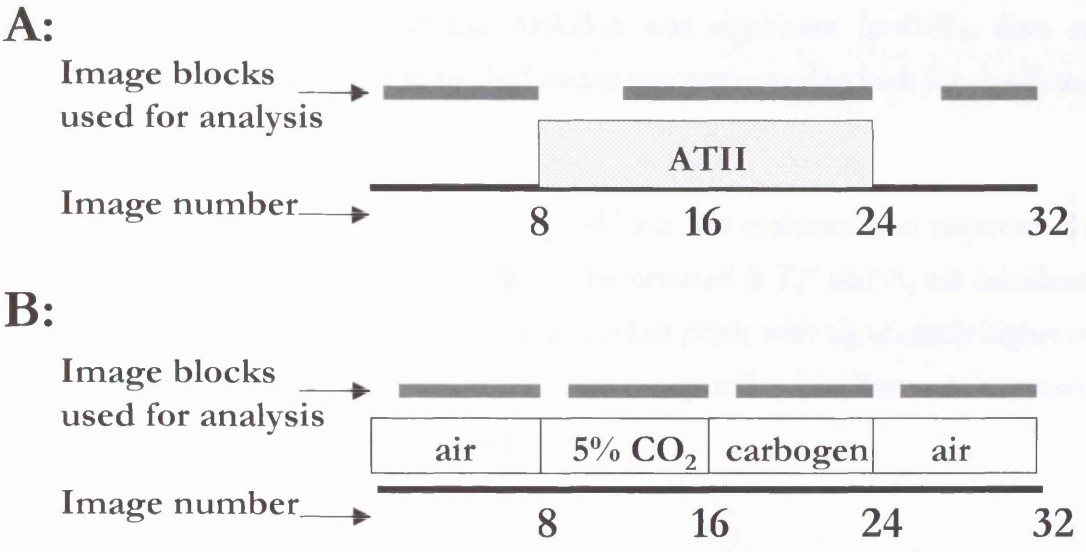

Figure 4.2 Diagram to show BOLD-MRI protocol for the ATII **(A)** and gas breathing experiments **(B)**.

Animated GIF images were generated using ImageMagick (ImageMagick™ 6.0.4 www.imagemagick.org) and used to check for movement with the GIMP animation playback feature (GNU Image Manipulation Program, www.gimp.org). Individual images, during which movement was occurring, were excluded and the ROI re-positioned for subsequent images, if necessary. Animals were excluded from analysis if there was movement in and out of the imaging plane throughout the experiment.

For both protocols the first image was not used (as it was not fully saturated). For the ATII protocol, the 1st four images following onset of ATII infusion and the 2 images immediately after the end of the infusion were excluded (to allow for the ATII infusion to take effect/wear off). The remaining images during the ATII infusion were divided into 3 treatment blocks of 4 images each for analysis. For the gas-breathing protocol, the 1st image of each of the 4 treatment blocks (air, air-5% CO_2, carbogen, air) was excluded (**Figure 4.2**).

The median values of tumour T_2* and A_0 were determined for each image and then the mean of these median values obtained for each treatment block. The mean values for each treatment block were then averaged to obtain mean values for each tumour group and then normalised to the mean baseline value. T_2* and A_0 values for each treatment block were then compared using ANOVA. If the ANOVA was significant ($p<0.05$), then an appropriate post-test comparison of individual means was performed to look for significant differences between treatment blocks.

In addition, tumour response on an individual pixel basis was evaluated – as response in a proportion of vessels within a tumour might not be detected if T_2* and A_0 are calculated for the whole tumour ROI. The percentage of individual pixels with significantly higher or lower values of T_2* and A_0 for each treatment block compared to baseline were measured (using a t-test for unknown and unequal variances).

Single-echo, multi-slice sequence

Images were processed as above using Matlab version 5 (The Mathworks, Nantick, MA USA). ROIs were drawn around the tumour and kidney using the initial T_1-weighted image. Animated GIF images were used to check for movement as before. The mean signal intensity at each time-point was calculated for the central tumour slice (slice 6), for 5 central tumour slices concatenated together (slices 4-8) and for a single kidney slice (slice

2). Images at the start of treatment blocks were excluded as for the multi-echo, single-slice protocols (see above). Mean signal intensity was then determined for each treatment block and analysed as above.

4.2.5 Intravital Microscopy

Mice were anaesthetised and ATII and air-5% CO_2/carbogen administered as per the BOLD-MRI protocol. In addition, a control group was used for each protocol (saline infusion for ATII protocol and air for gas breathing protocol) so that the effect of time and repeated observations on parameter stability could be assessed.

Window chambers were surgically implanted into the dorsal skin of male SCID and CBA mice weighing ~30-35 g, for HT29 and CaNT tumours respectively. The window chambers consisted of a double-sided aluminium frame containing parallel glass windows 5 mm in diameter and held ~0.35 - 0.4 mm apart, producing a cylindrical chamber (see **Figure 4.3**). Surgery was carried out under general anaesthesia using i.p. injection of 0.2 ml of a Hypnorm and Hypnovel mixture, diluted 1:1:2 with water. Animals were kept warm using heated pads throughout the surgical procedure and aseptic technique was used throughout. The dorsal skin was shaved and remaining stubble removed with a depilatory cream (Nair®, Carter-Wallis ltd, Folkestone, UK). The window chamber frame, with one glass window already in place, was secured to the dorsal skin flap using stainless steel screws and sutures, sandwiching a double layer of skin. A circular full skin section approximately 15 mm in diameter was surgically removed, exposing the fascia of the opposing skin layer. This fascia was removed and tumour fragments of ~1 mm in size were placed onto the exposed subcutaneous skeletal muscle. Subcutaneous transplants of HT29 and CaNT tumours were used as donors. The window chamber was then filled with sterile saline and the second glass window secured in place with a brass clip. Animals were given an i.p. injection of 0.5 ml dextrose-saline and a s.c. injection of 0.1 ml (0.3 $mg.ml^{-1}$ concentration) of buprenorphine (® Vetergesic, Reckitt & Coleman Products ltd, Hull, UK) immediately after surgery, to provide post-op hydration and analgesia respectively. 1% chloramphenicol ointment (Martindale Pharmaceuticals ltd, Romford, UK) was applied to the sutures and screws to prevent infection. Animals were kept on a warmed pad until recovery from anaesthesia.

Subsequently, animals were kept in a warm room at ~30° C (humidity 55 ±10%). They were fed a soft diet and weighed and checked daily until the day of the experiment.

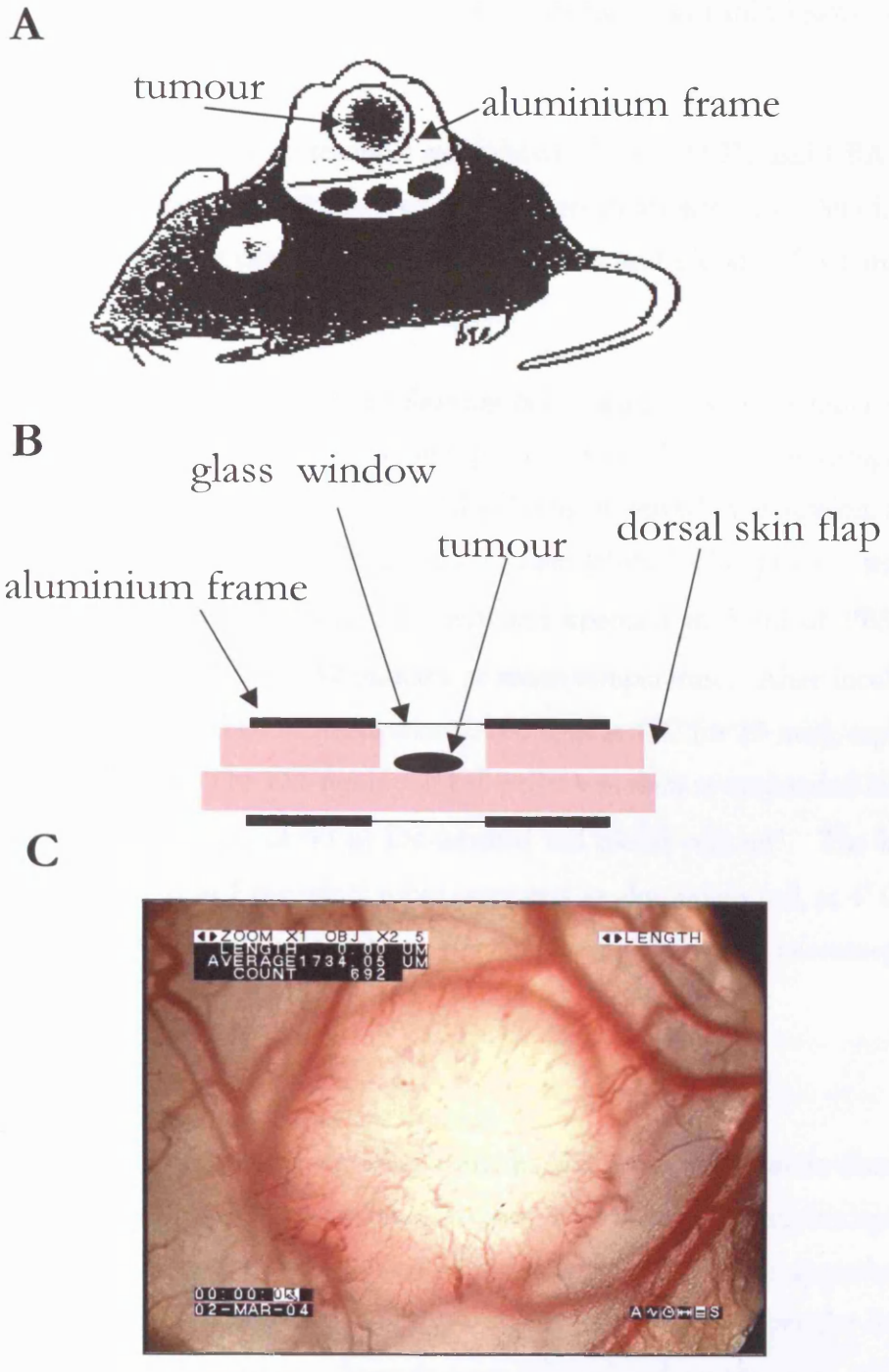

Figure 4.3: A: window chamber secured in mouse dorsal skin flap (from (Jain et al., 2002); **B**: diagram to show window chamber in cross-section. **C**: HT29 tumour growing in chamber, viewed with x2.5 objective.

4.2.5.1 *Method for labelling of red blood cells with DiI*

The fluorescent marker, DiI (1,1'-dioctadecyl-3,3,3',3'-tetramethylindocarbocyanine perchlorate, D-282, Molecular Probes Europe BV, Leiden, The Netherlands), which effectively binds to cell membranes (Unthank et al., 1993) was dissolved in ethanol (5 mg DiI in 10 ml in ethanol) and then stored in Eppendorf tubes (in 1 ml aliquots), wrapped in aluminium foil, at -20° C.

Blood was obtained under deep terminal anaesthesia. Donor SCID and CBA mice were anaesthetised with Metofane (methoxyflurane, Janssen Pharmaceutica, Ontario, Canada). The chest cavity was then opened, the great vessels cut and blood (~0.5-1 ml) collected from the chest cavity using a heparinised syringe.

Red blood cells were labelled with DiI following published protocols (Kimura et al., 1996; Unthank et al., 1993). Red blood cells were separated from plasma by centrifugation (3000 rpm at 4°C for 5 min), the buffy coat (white blood cells) removed by aspiration, and the red blood cells washed in sterile phosphate-buffed saline (PBS). This process was repeated twice. 50 µl of packed red blood cells were re-suspended in 5 ml of PBS and then incubated with 50 µl of DiI for 30 minutes at room temperature. After incubation, any unbound dye was removed by centrifugation (3000 rpm at 4° C for 10 min), aspiration and two washings with PBS. The DiI-red blood cell pellet was then re-suspended in 0.95 ml of PBS to give a concentration of 50 µl DiI-labelled red blood cells.ml^{-1}. The labelled red blood cells were stored in Eppendorf tubes, wrapped in aluminium foil, at 4° C and used within 4 days. Viability and uniformity of labelling were checked by microscopy prior to use.

4.2.5.2 *Intravital microscopy experiments*

Intravital microscopy was carried out when tumours had reached >2 mm in diameter (~10-15 days after surgery). An inverted Nikon Diaphot 200 fluorescence microscope was used that had a stage modified in-house for taking mice. Animals were anaesthetised with Hypnorm and midazolam as above, and top-up anaesthesia given as per the BOLD-MRI experiments via an i.p. infusion. Animals were then placed on the stage such that the window chamber was located centrally above the objectives using locating screws. Rectal temperature was maintained between 35 and 37 °C throughout the experiment using a thermostatically controlled heating pad beneath the animal, an infrared overhead lamp and gauze padding.

Before the start of each experiment, an aliquot of DiI (~0.05 ml) was injected i.v. Tumour preparations were alternately viewed under transmitted visible light (for the subsequent measurement of vessel diameter) and under fluorescence ε-illumination using a 100-W mercury arc lamp (for the subsequent measurement of red blood cell flux and velocity under fluorescence conditions). Fluorescence was set up to excite and detect the emissions from red blood cells labelled with DiI (550 and 565 nm wavelengths respectively). Window chamber preparations were viewed under transmitted light using x2.5, x10 and x20 magnification objectives. A tumour region of interest (ROI) was then selected using the x20 magnification objective that included a range of differently sized vessels in which red blood cells could be viewed clearly under visible and fluorescence illumination. At each time point, this ROI was monitored for 30 s using transmitted light and then for 60 s using ε-illumination using the x20 magnification objective. Observations were recorded in a digital format, using a Sony DSR-30P digital videocassette recorder, for subsequent off-line analysis (25 frames per second). If possible, a skin arteriole within the window chamber was also viewed under transmitted light at each time point (for ~5 s) so that diameter measurements could be made. Skin arterioles were identified by their shape, direction of blood flow and close association with veins. XY stage micrometers could be used to return to a specific ROI (to within <10 μm) when required. Return to a specific focal plane within the ROI (Z direction) could be ensured by reference to specific vascular features within the field of view.

For the ATII protocol, experiments were performed using both the HT29 and CaNT tumours. After baseline observations had been made, either ATII (2 $\mu g.kg^{-1}.min^{-1}$, 10 $\mu g.ml^{-1}$ concentration, the same dose as used for the BOLD-MRI experiments) or saline (at same infusion rate as for ATII) was infused for 15 minutes. Observations were then made at 5, 9, 13 and 20 minutes after the start of the infusion (the final observation was 5 minutes after the infusion had ended).

For the gas-breathing protocol, experiments were performed using HT29 tumours only, because of the difficulties encountered with the CaNT tumours in the ATII studies (see **Results**). Animals breathed air at 1 $l.min^{-1}$ through a mask while baseline observations were made. For the treatment group, the gas was then switched to air-5% CO_2, then carbogen, then back to air again for periods of 8 minutes each. The control group breathed air throughout the experiment. Observations were made 5 minutes into each gas-

breathing period (e.g. at 5, 13 and 21 minutes). Observations were made in the control group at the same times.

After the experiment was completed, animals were killed by cervical dislocation. Some tumours were placed in formalin and subsequently stained for αSMA for comparison with subcutaneous tumours.

4.2.5.3 Data analysis for intravital microscopy

The analysis was performed off-line using the video recordings made during the experiments. Measurements were made with the aid of an image overlay hardware system (DAVID, Dimensional Analysis and Video Insertion Device, Brian Reece Scientific ltd, UK). This was calibrated using microscope distance standards (1, 10 and 100 μm) so that the distance between any pairs of selected pixels could be directly read out on the image, in microns. A transparency was placed over the video screen so those vessels suitable for analysis could be marked and tracked for subsequent time points (**Figure 4.4**). Usually 3-4 vessels were chosen per ROI. Suitable vessels were considered to be >10 μm in diameter and contained flowing red cells.

Average diameters were calculated from 5 measurements made per vessel. For each measurement, a line was drawn perpendicular to the red blood cell column and its length measured using the 'DAVID' system, under transmitted light conditions. Diameter measurements were also made for a skin arteriole, where possible.

Red blood cell velocity and flux in all selected vessels were calculated from recorded data on fluorescence ε-illumination. At least 10 fluorescent red blood cells were monitored for velocity measurements over 60 s of recorded images. Velocity was calculated in $\mu m.s^{-1}$ from the number of video frames taken for each red blood cell to travel between two points of measured distance, marked on the vessel image. If, at subsequent time points, no red blood cells were observed within the observation period, a value of 0.85 $\mu m.s^{-1}$ was assumed – the maximum possible velocity of red cells if none appear during the observation period (Tozer et al., 2001). Changes in red blood cell flux were calculated from the number of fluorescent red blood cells crossing a single point marked on the vessel image within the observation period (~1 minute). Blood flow rates through individual vessels were calculated from the red blood cell velocity and diameter

measurements described above (blood flow rate = velocity x $\pi/4$ x (diameter)^2). This assumes that the red blood cells are travelling with bulk plasma flow. A few red cells, which were observed to be travelling slower than the majority, within a particular vessel, were not used for velocity calculations.

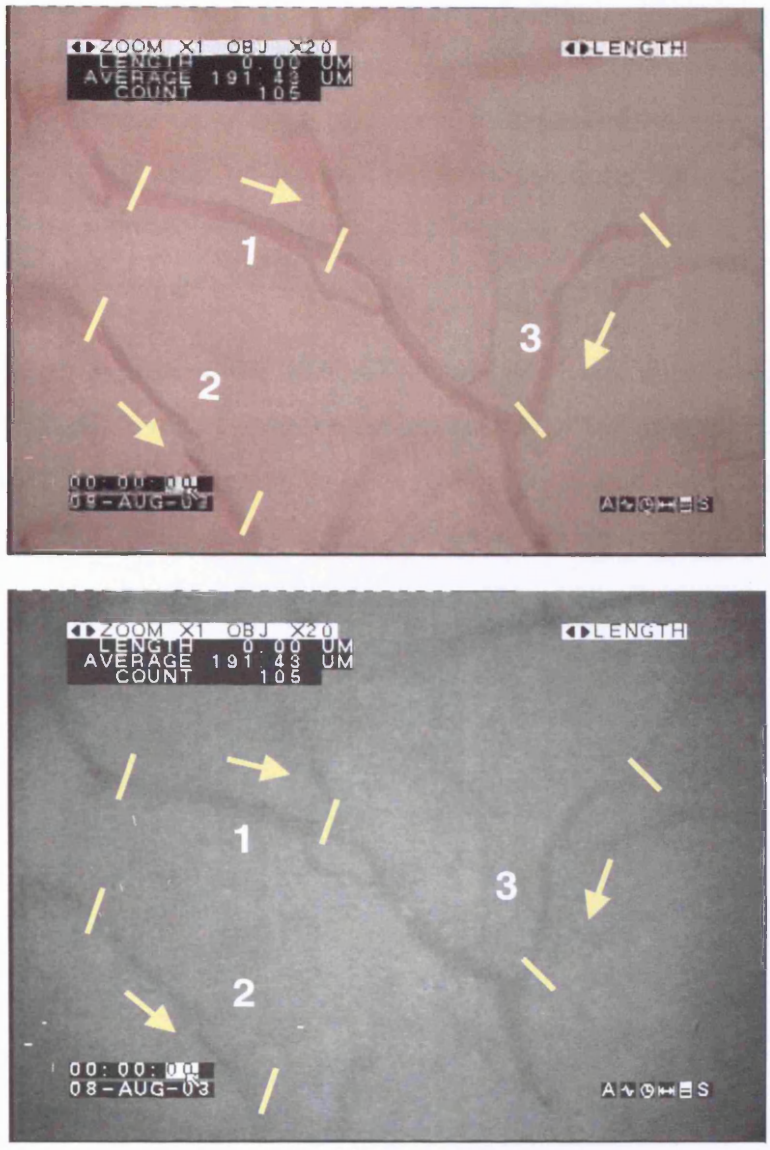

Figure 4.4: video intravital microscopy images viewed with transmitted (upper) and UV light (lower), with DAVID software, to show method for identifying vessels for measurement. The lines demarcate the section of vessel used for velocity measurements, arrows show direction of flow (HT29 tumour shown).

4.2.5.4 Statistics for intravital microscopy

Statistical analysis was carried out using JMP Statistics (version 3.2.6, SAS Institute, Inc, Cary, North Carolina, USA). Intravital microscopy data were fitted to a multivariate model (MANOVA) with repeated measures to determine the effects of the different treatments on vessel diameters and red blood cell velocity, flux and blood flow rate. Analysis was performed using the percentage change of values from baseline rather than absolute values. Responses were fitted to effects using least squares. The effect of variation between individual vessels was accounted for by using a nested design, and any variation between animals was described as random. Differences in response caused by treatment or time were tested for significance using an approximate F test based on comparison with the matrix for the hypothesis sum of squares and cross products with the matrix of the residual. Differences in response were described as significant if the probability corresponding to the F value was <0.05.

It is not possible to represent the MANOVA analysis using simple error bars. For graphical presentation, the mean parameter value was taken for each mouse and then the overall mean value plus the standard error of the mean determined for each time-point.

4.3 Results

4.3.1 Histology: Vascular maturation index

H&E sections showed HT29 tumours to be moderately-to-well differentiated, well-vascularised tumours. In comparison, CaNT tumours were poorly differentiated and less well vascularised but tended to have larger, more sinusoidal vessels than the HT29. T138 tumours showed variable differentiation and the majority had cystic areas and areas of haemorrhagic necrosis. The differences in vascularisation between these tumours are borne out by their functional vascular volumes (measured with Hoechst 33342): 6.3 ±0.4% (9 animals), 4.2 ±0.2% (10 animals) and 8.9 ±1.1% (15 animals) for HT29, CaNT and T138 respectively – Dr SA Hill, personal communication.

Vascular maturation index varied widely between these tumour types: 68.2 ± 7.2%, 1.6 ± 0.6% and 11.5 ± 2.3% for HT29, CaNT and T138 respectively (**Figure 4.5**). **Figure 4.6** shows H&E sections of the three tumours. Histological sections demonstrating αSMA and CD31 antigen staining are shown in **Figure 4.7.**

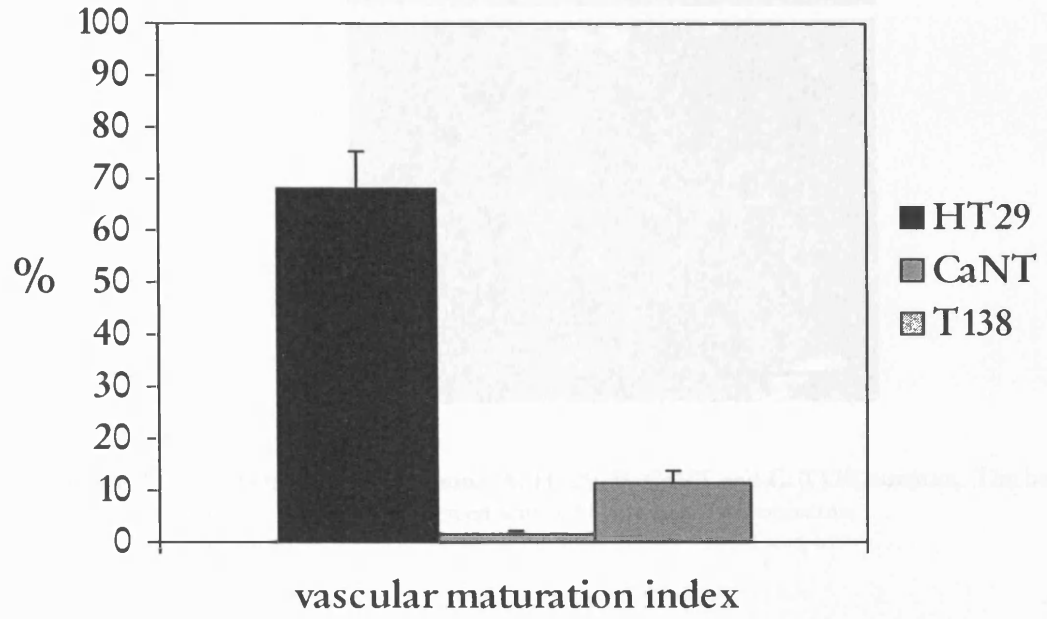

Figure 4.5: Vascular maturation index for HT29, CaNT and T138 tumours

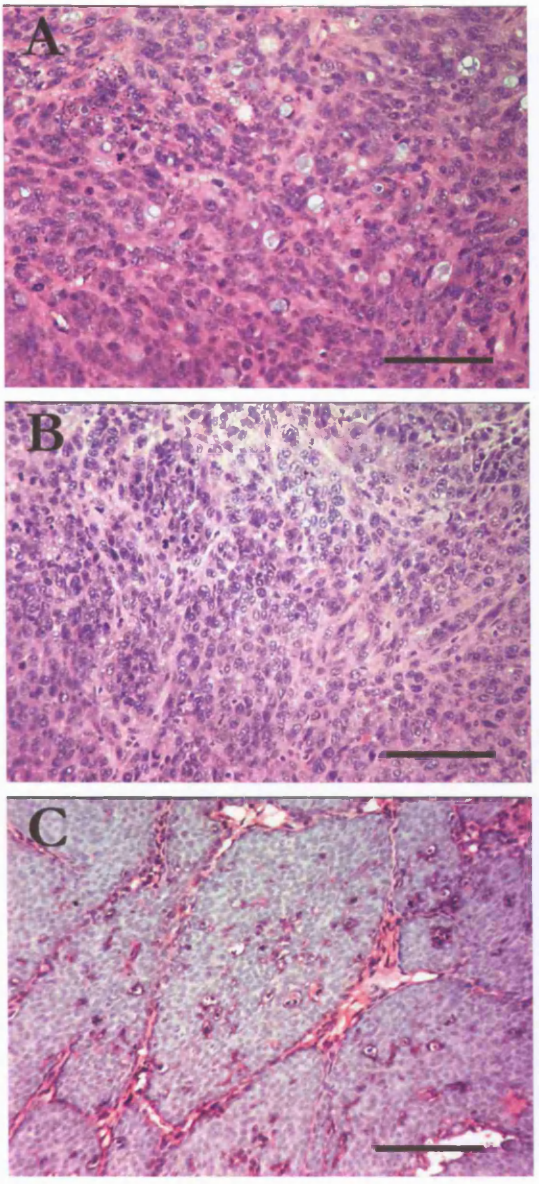

Figure 4.6: H&E histological sections. **A:** HT29, **B**: CaNT and **C:** T138 tumours. The bar represents 100 μm. All sections viewed with x20 magnification objective.

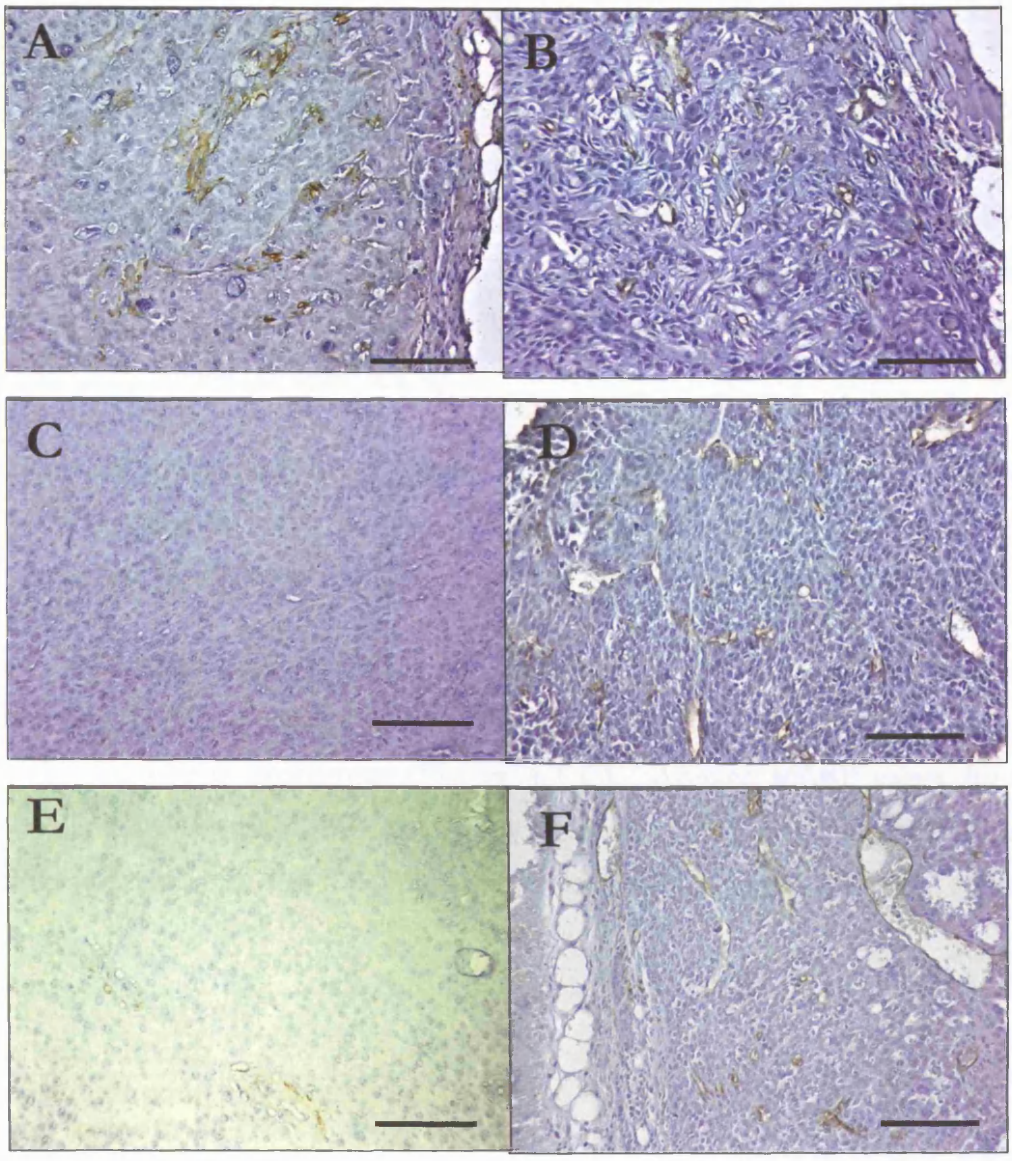

Figure 4.7: Histological sections to show αSMA and CD31 staining. **A:** HT29, αSMA; **B:** HT29, CD31 antigen; **C:** CaNT, αSMA; **D:** CaNT, CD3 antigen, **E:** T138 αSMA; **F:** T138, CD31 antigen. Bar represents 100 μm. All sections viewed with x20 magnification objective.

4.3.2 The effect of treatment on mouse MABP

Figure 4.8 shows the effects on MABP of ATII infusion (A), breathing air-5% CO_2 and carbogen (B) in anaesthetised mice, and the effects of anaesthesia (C). For graphical presentation, the average MABP for each mouse strain is shown at each time point.

There was a significant increase in mouse MABP during ATII infusion for all three mouse strains. Blood pressure rose rapidly following onset, remained stable during ATII infusion then decreased rapidly after termination of the ATII infusion. The average time for blood pressure to rise following the start of the ATII infusion was 2 minutes (range 1-3 minutes). The average time for blood pressure to fall following the end of the ATII infusion was 2.5 minutes (range 1-5 minutes) (**Figure 4.8 A**).

There was no significant change in average MABP when breathing air-5% CO_2 or carbogen compared to breathing air alone for any of the three mouse strains (ANOVA) or when individual treatment blocks were compared to baseline values (control) (**Figure 4.8 B**).

Induction of anaesthesia caused a significant decrease in MABP for all 3 mice strains (-27%, -16% and –35% for T138, SCID and CBA mice respectively) which then remained stable for the rest of the experiment (**Figure 4.7 C**). Average MABP values for un-anaesthetised and anaesthetised mice MABP are shown in **Table 4.1.** CBA MABP (both anaesthetised and unanaesthetised) was significantly lower than that of SCID or T138 mice.

	T138	SCID	CBA
Unanaesthetised, tail cuff	118.2 ±7.3	121.1 ±2.7	96.8 ±3.9
Anaesthetised, tail cuff	87.9 ±3.0	101.4 ±3.3	63.5 ±1.9
Anaesthetised, femoral artery cannulation (prior to ATII)	71.7 ±2.4	95.3 ±9.3	61.6 ±3.7
Anaesthetised, femoral artery cannulation (prior to carbogen)	64.3 ±0.8	90.4 ±1.1	59.8 ±1.0

Table 4.1: Comparison of baseline MABP (in mmHg ± 1 standard error). There was a significant difference between MABP in anaesthetised and unanaesthetised mice (tail cuff experiment) for all three mouse types ($p < 0.05$).

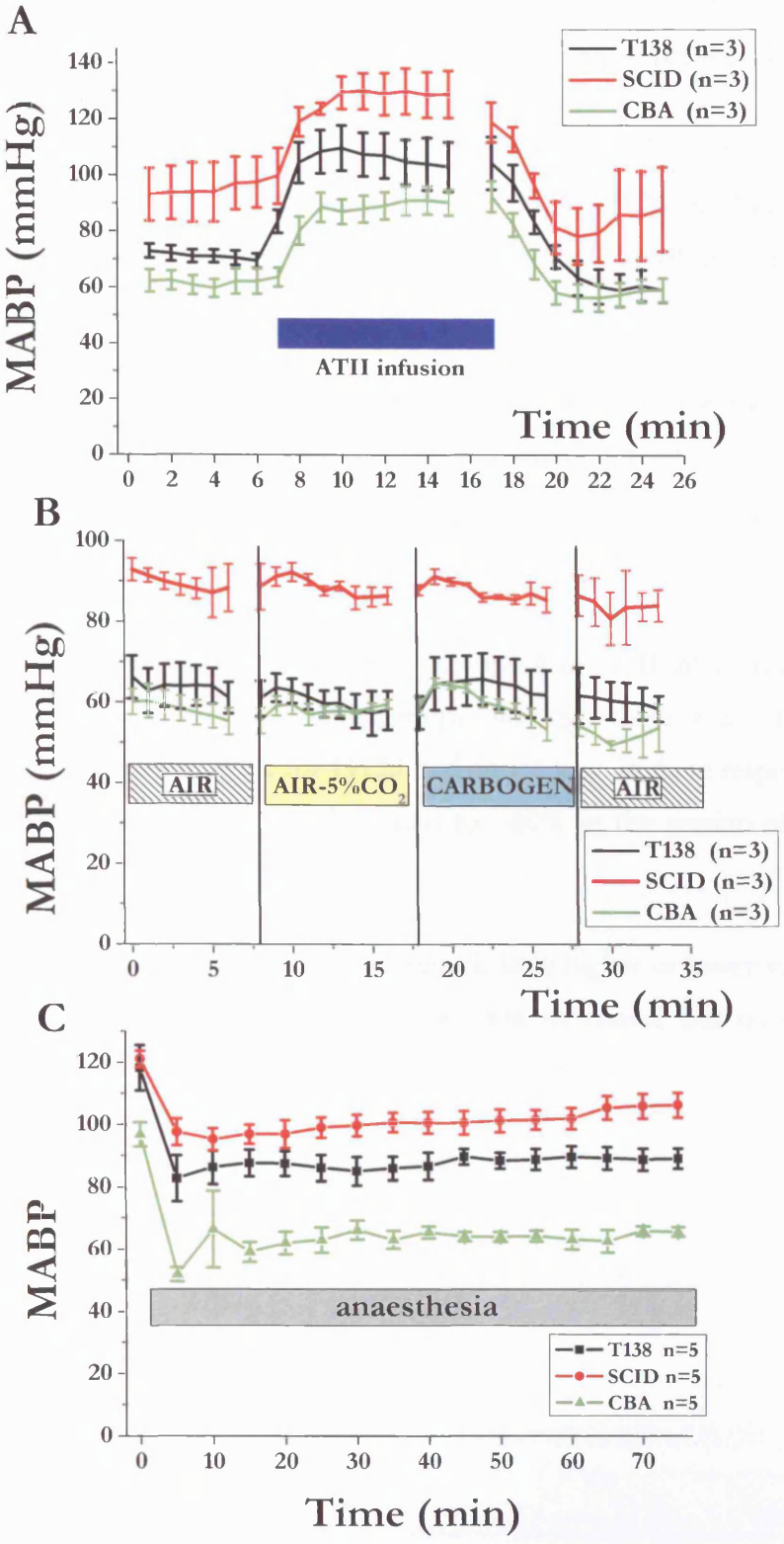

Figure 4.8 A: The effect of ATII infusion on mouse MABP. The graph is truncated during ATII infusion due to variable infusion times. **B:** Effect of breathing air-5% CO_2 or carbogen on mouse MABP. **C:** MABP before (time 0) and during anaesthesia. Graphs show mean ±SEM.

4.3.3 BOLD-MRI results

4.3.3.1 Multi-echo single slice sequence: ATII protocol

A few individual images had to be excluded as there was movement in and out of plane when images were viewed using GIMP software (mean 2 images per mouse, range 0-6).

The average baseline values for T_2* (the mean of the median ROI value for each animal) were 11.1 ±1.6, 13.7 ±2.4, 12.9 ±3.0 and 7.7 ms for T138, HT29 and CaNT tumours and normal kidney (from one of the T138s) respectively, (A_0 is in arbitrary units so baseline values were normalised to 100, see **Methods**).

Baseline tumour R_2* values (obtained by taking the reciprocal of the median baseline T_2* values and then averaging for each tumour group) were 77.3 ±9.9, 90.7 ±11.4 and 75.5 ±10.5 s^{-1} for HT29, CaNT and T138 respectively. These are similar to R_2* values at 4.7 T for other tumours quoted in the literature (Robinson et al., 2003).

There were no significant change in T_2* or A_0 as a result of ATII infusion on ANOVA for any tumour type (n=6 for each tumour group), although there was a trend towards a decrease in A_0 in response to ATII for HT29 and an increase in A_0 in response to ATII for CaNT (**Figure 4.9**). In contrast, A_0 decreased to ~80% in the section of normal kidney imaged (see above).

The percentage of individual pixels that had significantly higher or lower values of T_2* and A_0 during ATII infusion compared to baseline were measured, but no clear pattern of response was seen.

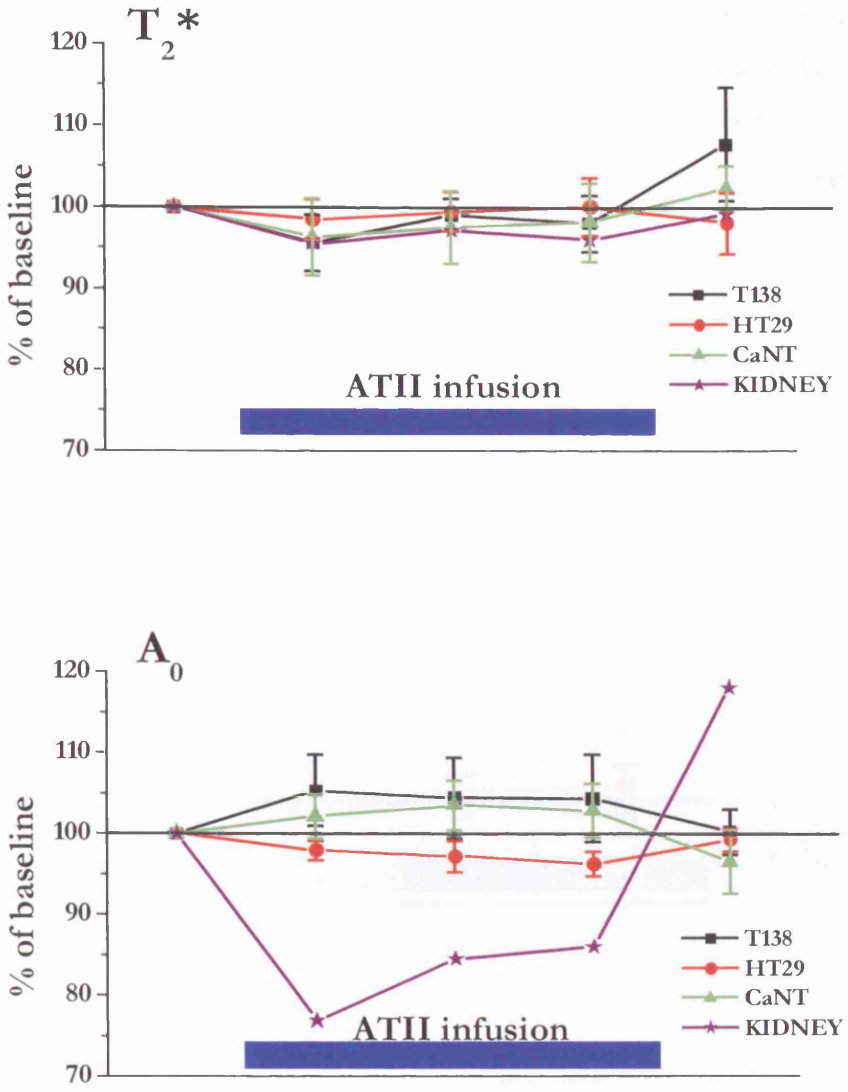

Figure 4.9: Mean percentage chage from baseline for T_2^* and A_0 for the ATII protocol (multi-echo, single slice sequence). Graphs show mean ±SEM.

4.3.3.2 Multi-echo single slice sequence: gas breathing protocol

Three SCID and two T138 mice were excluded from the gas-breathing study as there was movement in and out of plane when the images were viewed using GIMP software. No individual images had to be excluded.

For the gas-breathing protocol, the average baseline values for T_2* (the mean of the median ROI value for each animal) were 27.3 ±8.0 and 19.8 ±6.8 ms for T138 and HT29 respectively. Baseline R_2* values were 48.6 ±11.0 and 66.7 ±12.3 s^{-1} for T138 and HT29 respectively. Again, there was no significant change in T_2* or A_0 with breathing air-5% CO_2 or carbogen compared to baseline for any tumour type (n=5 for each group) (**Figure 4.10**).

The percentage of individual pixels that had significantly higher or lower values of T_2* and A_0 during air-5% $C0_2$ and carbogen compared to baseline were measured – but again no clear pattern of response was seen.

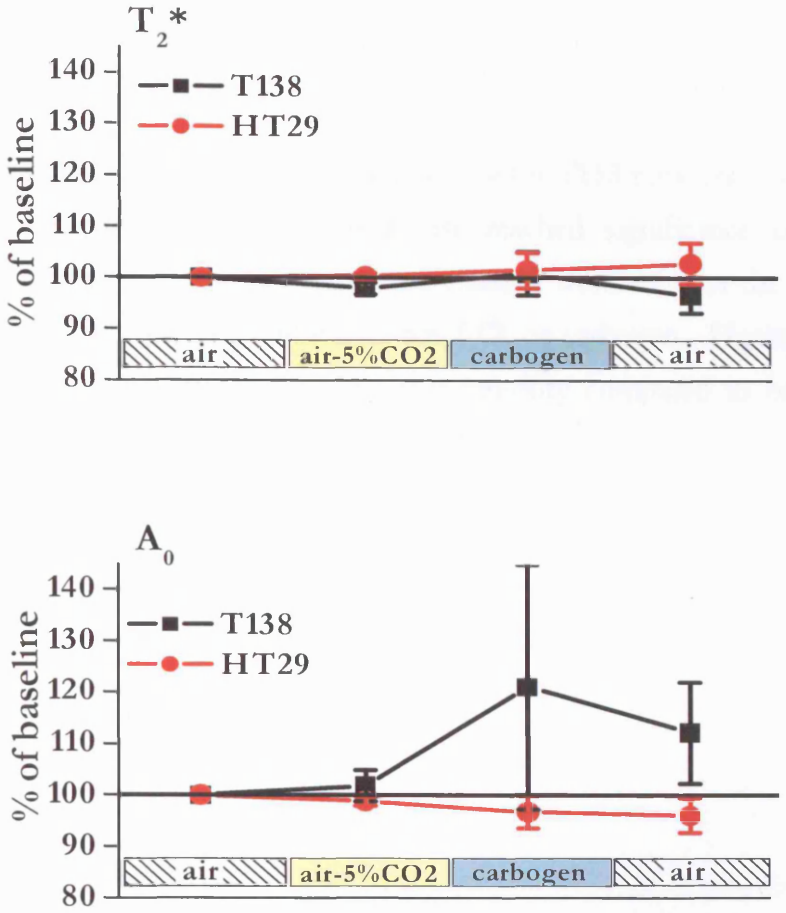

Figure 4.10: Mean percentage change in T_2* and A_0 for gas-breathing protocol compared to baseline (multi-slice, single echo sequence). Graphs show mean ±SEM.

4.3.3.3 Single-echo multi-slice sequence: ATII protocol

No animals or individual images had to be excluded due to movement.

There was no significant change in BOLD signal intensity (TR=600 ms, TE = 20 ms, α = 20°) for HT29 (n=6), CaNT (n=6) or T138 (n=5) tumours in response to ATII. There was no difference between tumour response for the single central slice and when averaged over 5 slices. However, there was a significant decrease in BOLD signal intensity in the kidney for all three mice strains. **Figure 4.11 (A)** shows the mean percentage change in BOLD signal intensity compared to baseline for the three tumour types and for kidney.

Figures 4.12 & 13 show a series of BOLD signal intensity images before, during and after ATII infusion for a HT29 tumour ROI and a kidney ROI respectively.

4.3.3.4 Single-echo multi-slice: gas breathing protocol

No animals or individual images had to be excluded due to movement.

There was an increase in BOLD signal intensity for T138 tumours in response to breathing carbogen compared to baseline that just reached significance on post-test analysis (p=0.046). However, no other significant changes were seen for the different tumours or for kidney in response to breathing air-5% CO_2 or carbogen. **Figure 4.11 (B)** shows the mean percentage change in BOLD signal intensity compared to baseline for the three tumour types (n=6 for each treatment group).

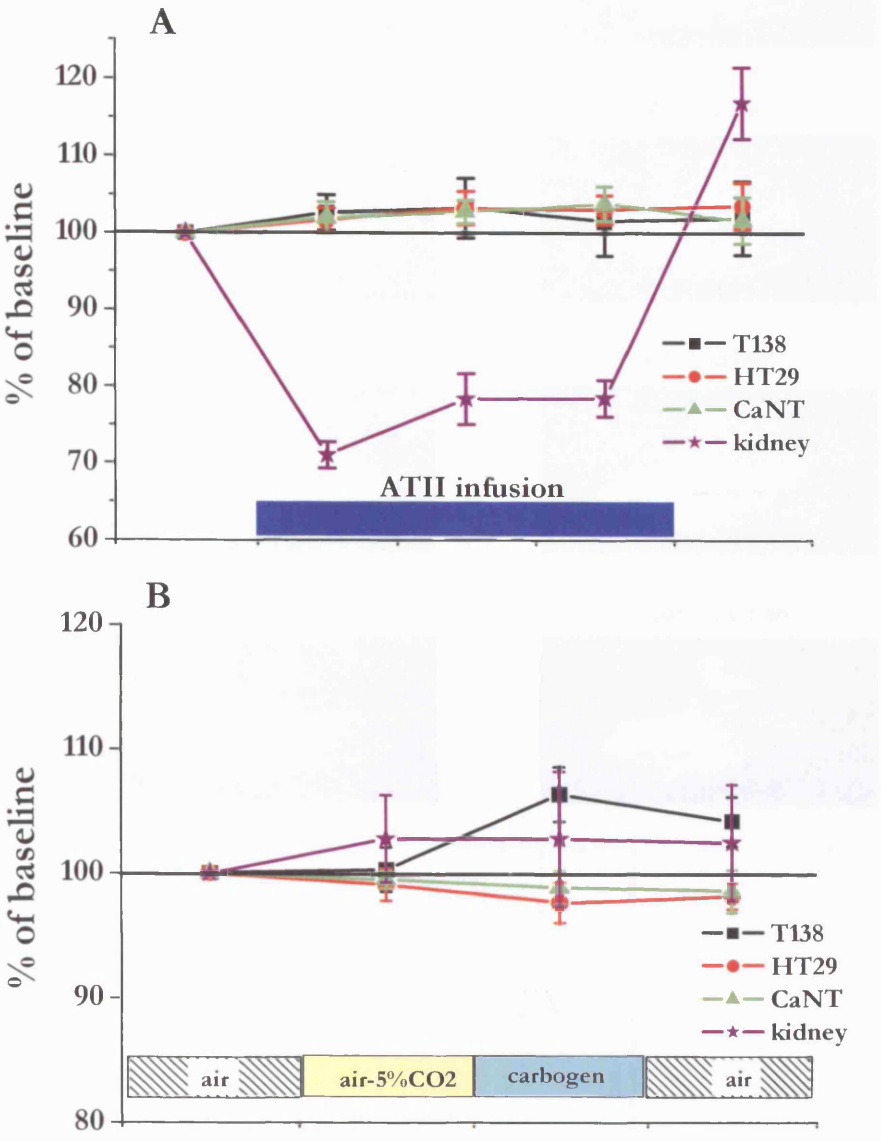

Figure 4.11: Mean percentage change in signal intensity for ATII protocol **(A)** and gas-breathing protocol **(B)** (single echo, multi-slice sequence). Graphs show mean ±SEM.

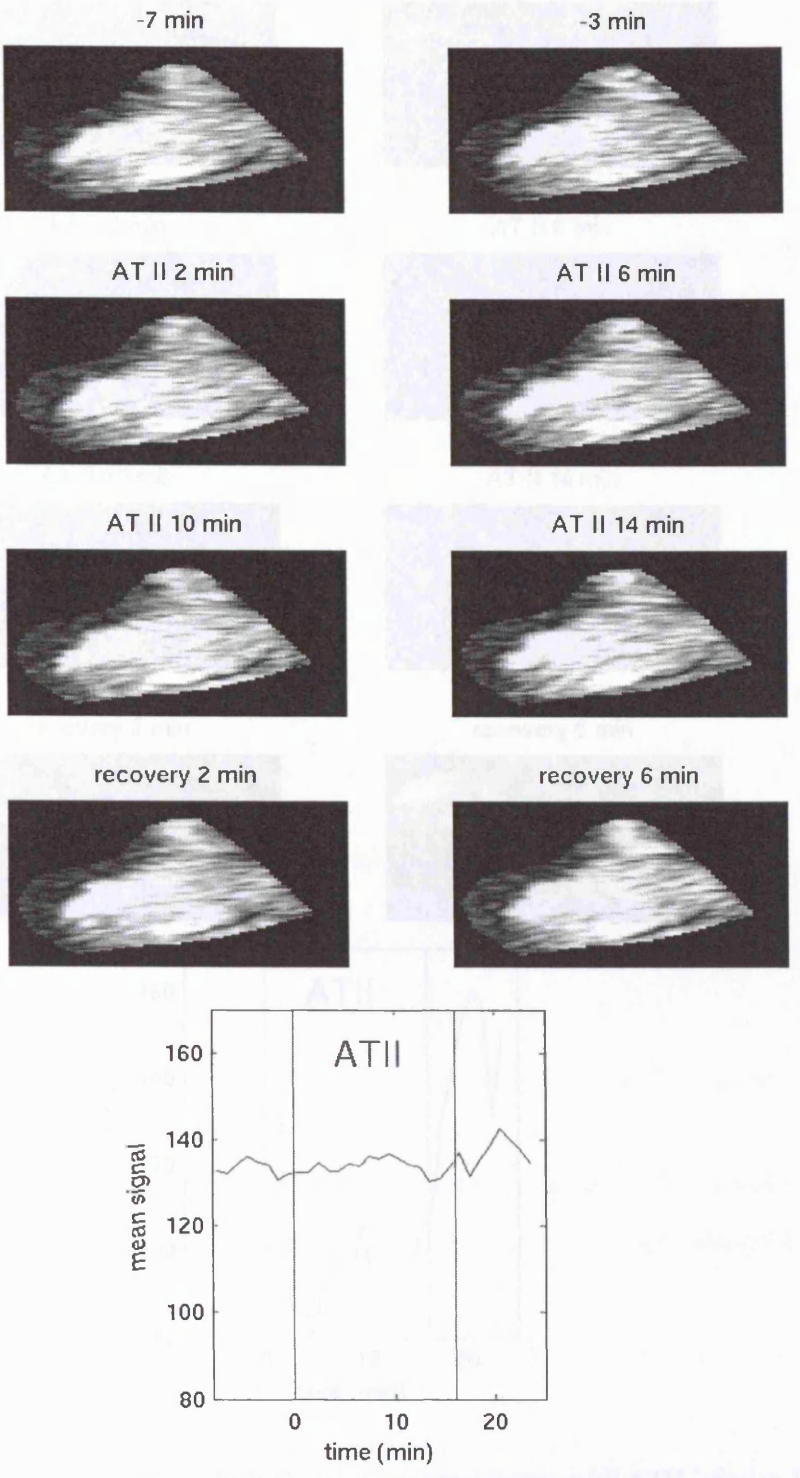

Figure 4.12: Images and graph to show BOLD signal intensity change with ATII infusion for HT29 tumour RO1 (same animal as in **Figure 4.13**).

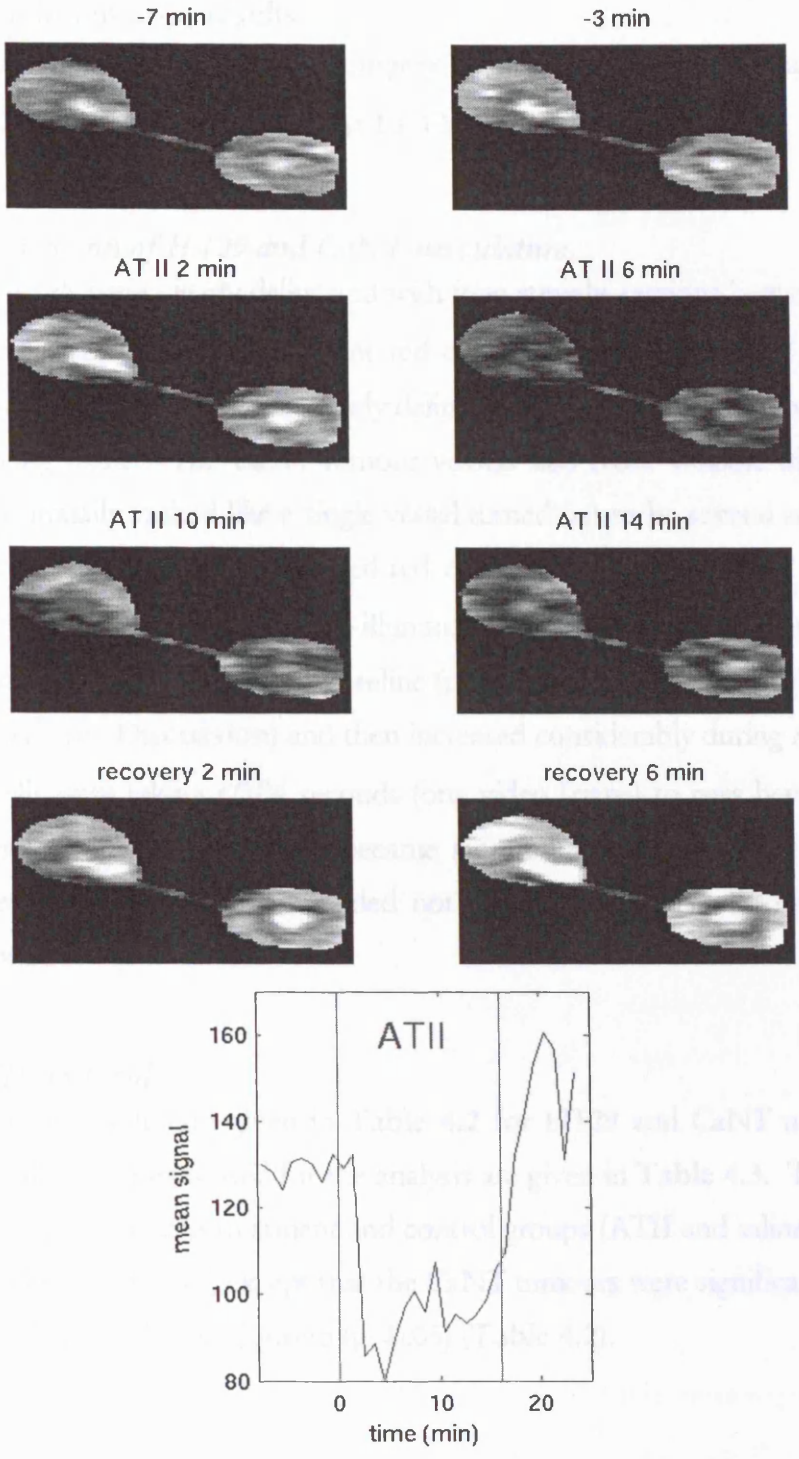

Figure 4.13: Images and graph to show BOLD signal intensity change with ATII infusion for kidney RO1 (same animal as in **Figure 4.13).**

4.3.4 Intravital Microscopy results

The average time from window chamber surgery to intravital microscopy was 13.5 (±0.5) days for HT29 tumours and 11.3 (±0.3) days for CaNT tumours.

4.3.4.1 Comparison of HT29 and CaNT vasculature

HT29 tumour vessels were clearly delineated with long straight sections between branches. On fluorescence ε-illumination, fluorescent red cells could be seen clearly at each time point. CaNT tumour vessels were less clearly delineated and more tortuous, moving in and out of the imaging plane. The CaNT tumour vessels had more variable diameters and, sometimes, what initially looked like a single vessel turned out to be several smaller vessels entangled together. Consequently, labelled-red cells could not be seen as clearly as in HT29 tumour vessels on fluorescence ε-illumination. In some experiments, flux and velocity measurements were very low at baseline (probably due to CBA low blood pressure under anaesthesia – see **Discussion**) and then increased considerably during ATII infusion such that red cells were taking ≤0.04 seconds (one video frame) to pass between the two measurement points. As a result, they became smeared and could not be seen clearly. Because of these difficulties, it was decided not to use the CaNT tumour for the gas breathing protocol.

4.3.4.2 ATII protocol

Baseline parameters results are given in **Table 4.2** for HT29 and CaNT tumours. The number of animals and vessels used for the analysis are given in **Table 4.3**. There were no significant differences between treatment and control groups (ATII and saline) for baseline parameters for HT29 or CaNT, except that the CaNT tumours were significantly larger for the saline group than for the ATII group ($p<0.05$) (**Table 4.2**).

	Tumour surface area (mm^2)	Tumour vessel diameter (μm)	Skin arteriole diameter (μm)	Tumour vessel flux (s^{-1})	Tumour vessel velocity ($\mu m.s^{-1}$)
HT29					
ATII	6.3 (±0.6)	18.1 (±1.1)	80.3 (±8.2)	0.84 (±0.14)	655 (±106)
Saline	7.6 (±0.1.3)	15.7 (±1.2)	84.0 (±20.9)	0.67 (±0.11)	557 (±59)
CaNT					
ATII	6.2 (±0.5)*	23.7 (±1.5)	101.6 (±16.1)	0.70 (±0.12)	541 (±65)
Saline	8.1 (±0.5)*	22.8 (±1.6)	101.7 (±10.4)	1.22 (±0.21)	489 (±59)

Table 4.2: Intravital microscopy: baseline values for ATII protocol (±one standard error of the mean), *significant difference between treatment groups. Mean parameter values are for the vessels chosen for measurement, not the whole tumour.

	Tumour vessel diameter	Skin arteriole diameter	Tumour vessel flux & velocity
HT29			
ATII	8 (32)	6	7 (20)
Saline	7 (24)	4	7 (20)
CaNT			
ATII	12 (29)	8	7 (17)
Saline	12 (35)	8	9 (24)

Table 4.3: Total animal and vessel numbers for ATII protocol. Vessel numbers are given in brackets. Skin arteriole diameter measurements were made on 1 vessel per animal.

Figure 4.14 shows examples of the effect of ATII on vessel diameter for HT29, CaNT and a normal skin arteriole. HT29 tumour vessels vasoconstrict, become paler and some disappear in response to ATII. In contrast, CaNT tumour vessels vasodilate and become hyperaemic in response to ATII. For both SCID and CBA mice, skin arterioles were observed to vasoconstrict and become paler in response to ATII.

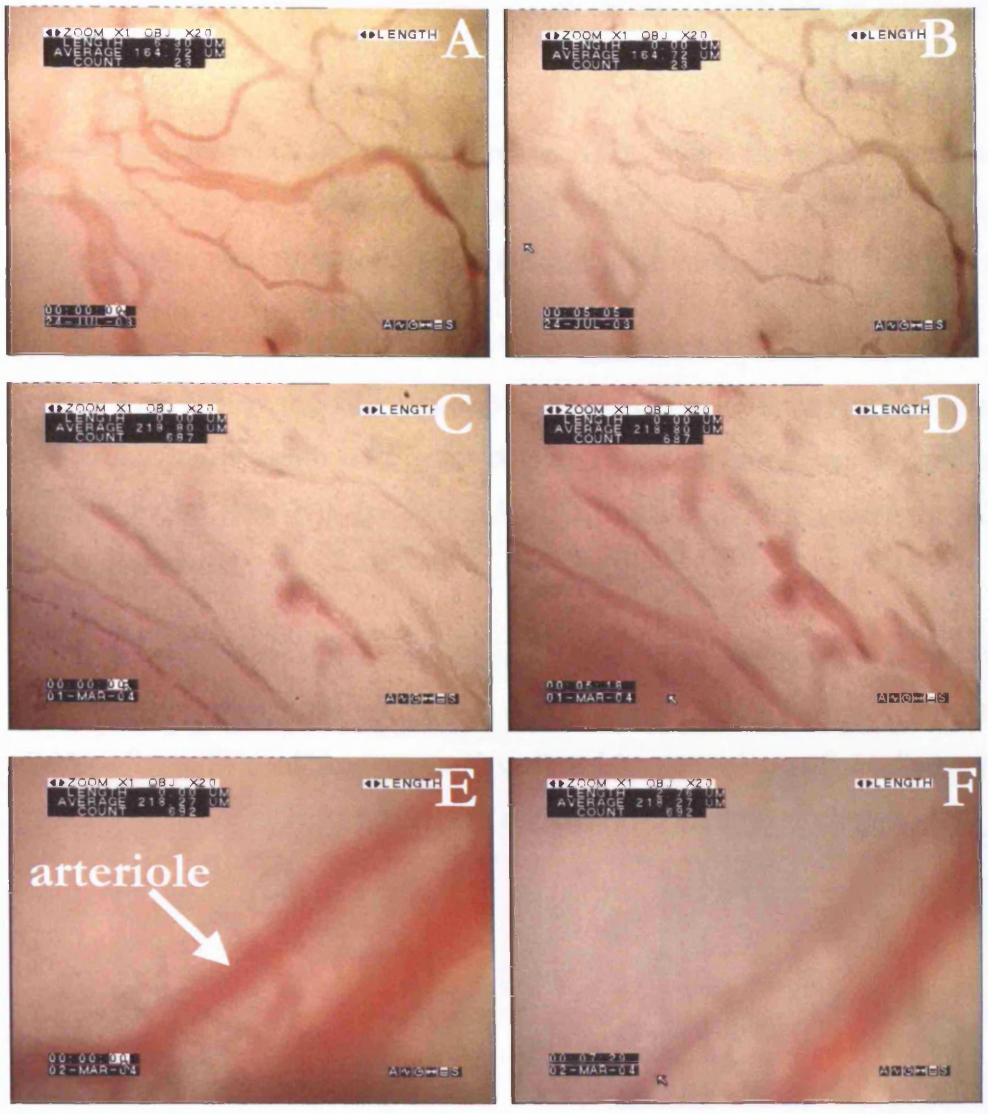

Figure 4.14: Intravital Microscopy images showing the effects of ATII infusion using x20 magnification objective. **A**: HT29 pre-ATII, **B**: HT29 during ATII infusion, **C:** CaNT pre-ATII, **D**: CaNT during ATII infusion, **E:** skin arteriole pre-ATII, **F:** skin arteriole during ATII (from a CaNT tumour preparation).

There was a significant decrease ($p<0.05$, MANOVA) in mean diameter during ATII infusion compared to saline control in both HT29 tumour vessels and normal skin arterioles in the same window chamber preparation (**Figure 4.15**). Therefore, both HT29 tumour vessels and normal skin arterioles were capable of vasoconstriction in response to ATII.

In contrast, CaNT tumour vessels did not respond to ATII. While there was a significant decrease in normal skin arteriole diameter in response to ATII ($p<0.0001$, MANOVA), as above, the CaNT tumour vessels tended to increase in diameter, although this was not significant with the numbers used (**Figure 4.16**).

There was no significant change in HT29 tumour vessel red cell velocity or flux in response to ATII compared to saline controls (**Figure 4.15**). However, there was a significant decrease in tumour blood flow rate ($p<0.01$, MANOVA) that persisted after the ATII infusion had been terminated.

For CaNT tumour vessels, there was a tendency for red cell flux, velocity and blood flow rate to increase in response to ATII compared with saline controls (**Figure 4.16**). This reached significance for individual time points (0 vs 9 and 0 vs 13 minutes for velocity, flux and blood flow rates, all $p<0.05$, MANOVA) but not over the whole analysis period.

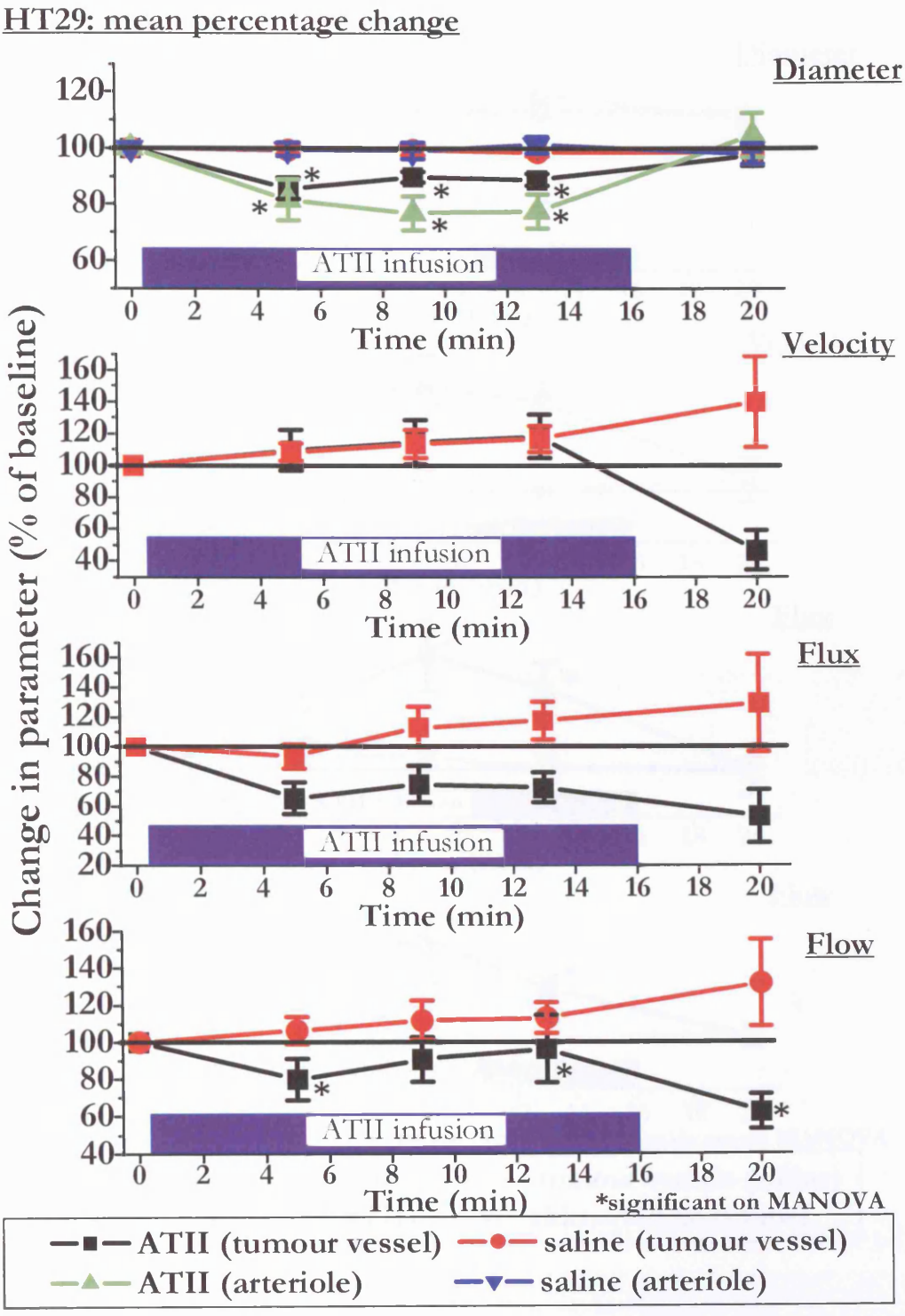

Figure 4.15: Mean percentage change in HT29 parameters for ATII protocol. Graphs show mean ±SEM.

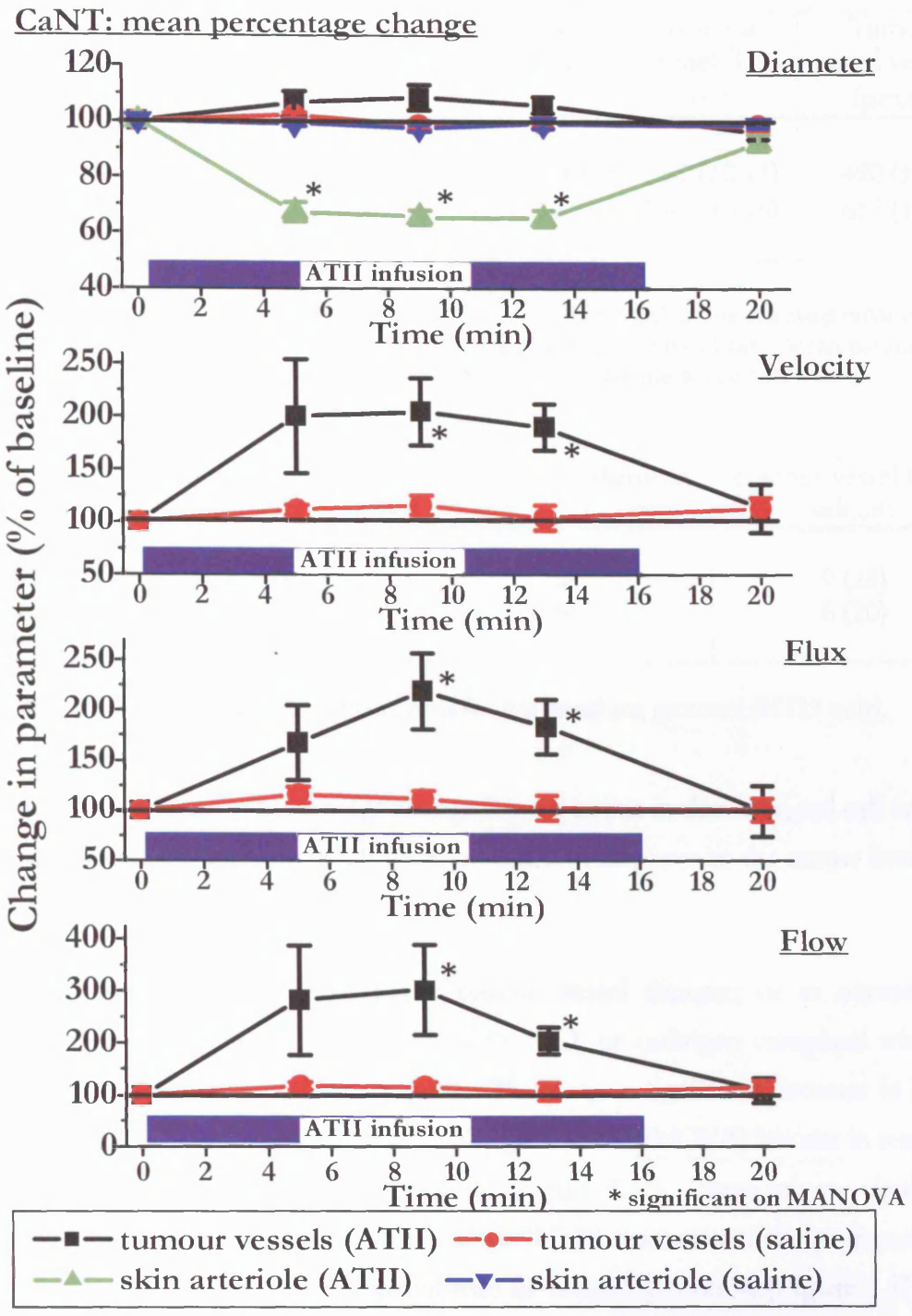

Figure 4.16: Mean percentage change in CaNT parameters for ATII protocol. Graphs show mean ±SEM

4.3.4.3 *Gas breathing protocol (HT29 only)*

There were no significant differences between treatment groups for baseline parameters (**Table 4.4**). The total number of animals and vessels used are given in **Table 4.5.**

	Tumour surface area (mm^2)	Tumour vessel diameter (μm)	Skin arteriole diameter (μm)	Tumour vessel flux (s^{-1})	Tumour vessel velocity ($\mu m.s^{-1}$)
Treatment	5.8 (±0.5)	16.3 (±0.9)	57.2 (±6.6)	0.63 (±0.13)	490 (±67)
Control	5.6 (±0.5)	16.1 (±1.2)	74.5 (±10.3)	0.67 (±0.15)	617 (±65)

Table 4.4 Baseline parameters for gas breathing protocol (HT29 only) (±one standard error of the mean). **Treatment:** air-5% CO_2/carbogen; **Control:** breathing air throughout. Mean parameter values are for the vessels chosen for measurement, not the whole tumour.

	Tumour vessel diameter	Skin arteriole diameter	Tumour vessel flux & velocity
Treatment	9 (32)	5	9 (28)
Control	8 (24)	5	6 (20)

Table 4.5 Mouse and vessel numbers used for gas breathing protocol (HT29 only).

Figure 4.17 shows the mean percentage change from baseline in diameter, red cell velocity and flux, and blood flow rate for HT29 tumour vessels in response to the mouse breathing air-5% CO_2/carbogen or air throughout.

There was no significant change in HT29 tumour vessel diameter or in normal skin arteriole diameter in response to breathing air-5% CO_2 or carbogen compared with air-breathing controls (MANOVA) (**Figure 4.17**). There was a significant decrease in HT29 red cell flux in response to breathing air-5% CO_2 ($p<0.05$, MANOVA) but not in response to carbogen, compared to air-breathing controls (**Figure 4.17**). There was no significant change in red cell velocity or blood flow rate in HT29 tumour vessels in response to breathing air-5% CO_2 or carbogen compared with air-breathing controls (**Figure 4.17**).

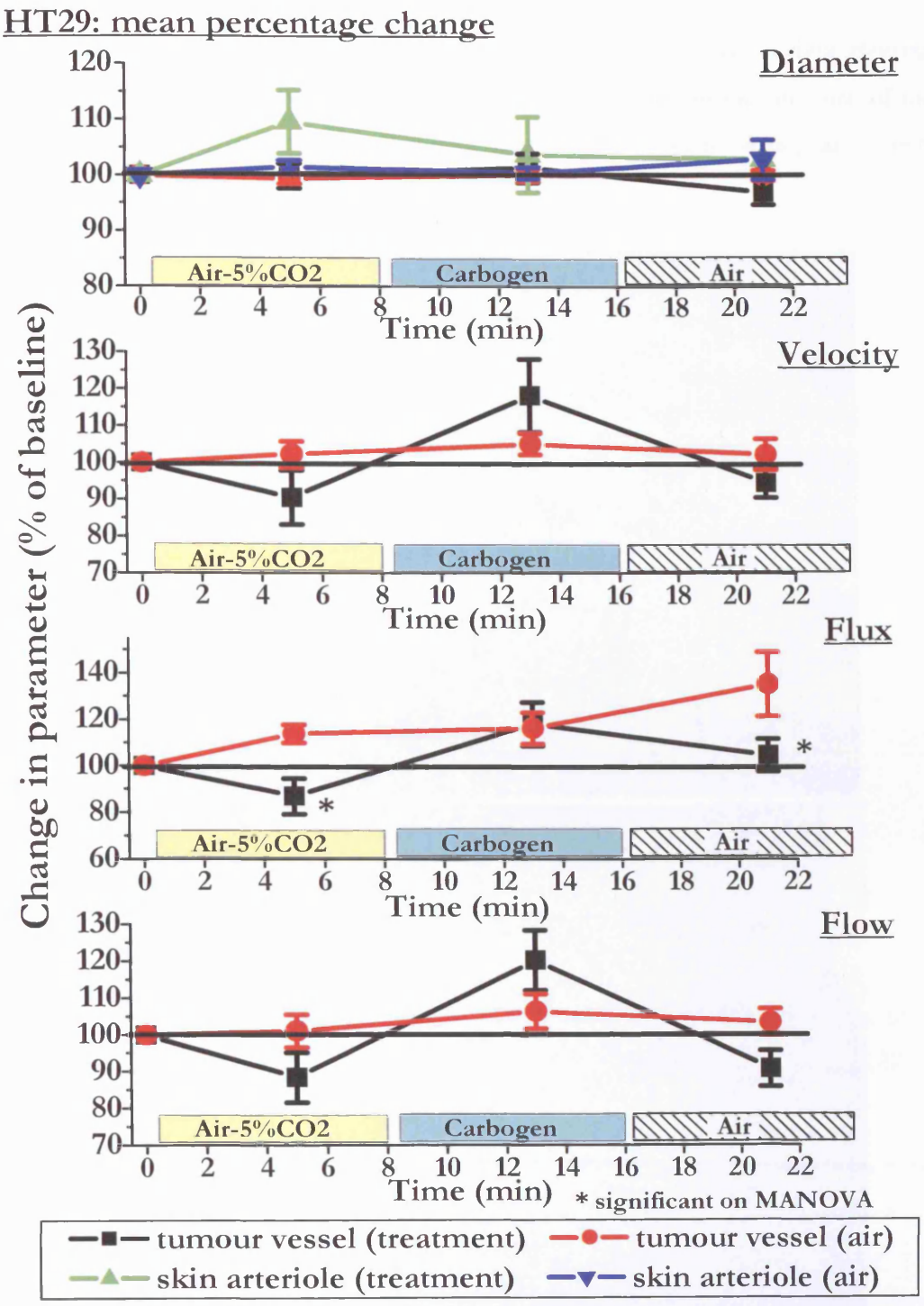

Figure 4.17: Mean percentage change in HT29 parameters on gas breathing protocol. Graphs show mean ±SEM.

4.3.4.4 Intravital Microscopy: Histology

Vessels from HT29 tumours grown in window chambers showed strong staining for αSMA whereas vessels from CaNT tumour did not, confirming the presence of mature vessels in the HT29 window chamber preparation (**Figure 4.18**), as found for subcutaneous tumours (see **Figure 4.7**).

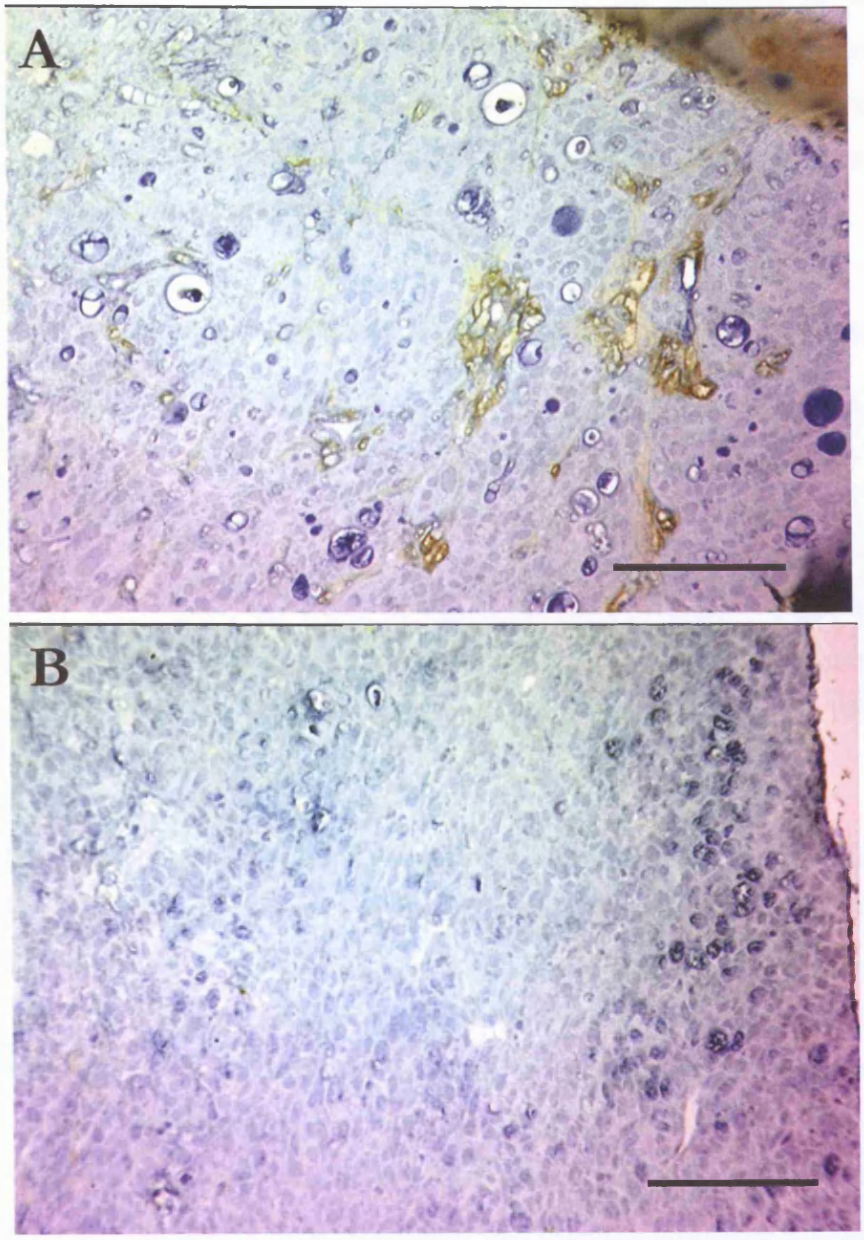

Figure 4.18: αSMA staining of **A:** HT29 and **B:** CaNT tumours taken from window chamber preparations. Taken with x20 magnification objective. Bar shows 100 μm.

4.4 Discussion

4.4.1 T138 tumours

The T138 tumours were included in the protocol as they arise spontaneously and so are more comparable to the clinical situation than xenografted tumours in this respect. They have a variable degree of αSMA staining, but it was unfortunately not possible to compare BOLD responses and vascular maturation index for individual tumours as the amount of haemorrhage and necrosis led to doubts concerning the accuracy of the vascular maturation index measurement. There would have to be confidence in measurements in individual tumours (rather than averaged as a group) for further work to continue using T138 mice. Since data from individual tumours were not considered to be reliable, these mice were not used for intravital microscopy.

4.4.2 Mouse MABP measurements in response to ATII, air-5% CO_2/carbogen and anaesthesia

Mouse MABP increased rapidly in response to ATII and decreased rapidly following the end of the infusion. The time course and magnitude of the change in MABP in response to ATII infusion is similar to that reported previously (Trotter et al., 1991).

Breathing air-5% CO_2 or carbogen had no effect on mouse MABP. Other authors have reported either no response or small increases in blood pressure in anaesthetised rats breathing carbogen (Brizel et al., 1995; Dewhirst et al., 1996; Dunn et al., 1999; Iadecola, 1992; Lanzen et al., 1998).

The values for MABP obtained from un-anaesthetised, restrained T138 and SCID mice are similar to those quoted by other authors for other mouse strains (Cullen & Walker, 1985; Mattson, 1998; Menke & Vaupel, 1988). However, the average MABP in un-anaesthetised CBA mice was ~20% lower. MABP decreased with anaesthesia for all three strains but was pronounced in the CBA mice, such that their average MABP when anaesthetised was only 63.5 mmHg. The inherent low blood pressure of CBA mice and their particular sensitivity to anaesthesia might have affected the ability of BOLD-MRI to detect a CaNT tumour response to the vasoactive agents tested (see below).

4.4.3 Tumour vessel response to angiotensin II as measured by BOLD-MRI and intravital microscopy

A differential response to ATII between HT29 and CaNT tumours could not be detected using BOLD-MRI despite their very different vascular maturation indices. However, BOLD-MRI could detect a response to ATII in kidney as a significant decrease in BOLD signal intensity was seen (and in A_0 and T_2* for the single kidney section imaged) – consistent with a decrease in blood flow. Other studies, using laser Doppler flowmetry or IAP, have also found that ATII infusion reduces kidney blood flow (Badzynska et al., 2002; Huang et al., 1991; Tozer & Shaffi, 1993). (See also **Section 1.3**).

However, the intravital microscopy experiments do show that HT29 and CaNT tumour vessels have a differential response to ATII, as HT29 tumour vessels are capable of vasoconstriction whereas CaNT vessels are not. (The reason for an increase in tumour vessel diameter seen with CaNT is consistent with passive expansion in response to increased perfusion pressure.) Therefore, the two tumour types responded as would be predicted from histological assessment of their vessel maturation status. Also, there must be active ATII receptors and intact downstream signalling machinery on HT29 tumour vessels.

Other explanations for the lack of a differential BOLD-MRI response must therefore be sought. These can be divided into issues concerning the BOLD-MRI protocol, the particular tumour types used and the influence of anaesthesia on mouse blood pressure.

Limitations of the BOLD-MRI technique:

While a positive BOLD response (increase in signal intensity or T_2*) must be associated with an increase in tumour pO_2 (with the size of change modulated by any blood volume change), no response or a negative response cannot be interpreted easily (Howe et al., 2001). An increase in tumour blood flow may not produce a decrease in deoxyHb if the oxygen extraction fraction increases. Conversely, a change in blood volume due to vasodilation or vasoconstriction may mask any changes in haemoglobin oxygenation (Howe et al., 2001).

The aim of the BOLD-MRI study was to develop a technique that could be translated into the clinic. Therefore a body coil (imaging the whole mouse) rather than a surface coil (imaging the tumour only), was used to reflect clinical practice. In addition, a surface coil

would not have been practical for imaging T138 tumours due to their location, nor would it have allowed the acquisition of normal tissue data. However, a surface coil probably would have produced a better signal to noise ratio, better spatial resolution and less movement artefact, as the tumour is fixed into the coil.

The single-echo multi-slice protocol was designed to be selective for changes in blood oxygenation and to minimise in-flow effects, which would have reduced the sensitivity to a change in tumour blood flow. Neeman et al. found that, when their MRI data were analysed so as to be sensitive to in-flow effects, there was a 10-fold increase in the magnitude of response to air-5% CO_2 compared to when the analysis method was not designed to be sensitive to in-flow effects (Neeman et al., 2001). However, the multi-echo single-slice protocol used for the work presented here **was** sensitive to in-flow effects but still did not detect a significant response to ATII in HT29 tumour vessels.

Individual pixel by pixel analysis was done to see if a possible heterogeneous response could be detected. No response was seen, although small changes may have been obscured by movement artefact. The spatial resolution was 0.16 x 0.35 mm and 0.1 x 0.4 mm for the multi-echo and single-echo protocols respectively, so even very slight movement may have affected results.

In conclusion, the BOLD-MRI technique used was not sensitive enough to detect the response of tumour blood vessels to ATII, as detected by intravital microscopy. However, it is possible that small changes in response to ATII infusion could have been detected if the BOLD-MRI protocol had been optimised: e.g. using a surface coil in order to improve spatial resolution and minimise movement. These issues remain to be resolved.

Problems related to the particular tumour types used:

Another possible explanation for lack of BOLD response in the HT29 is tumour vessel size. It has been observed that vessel density and vessel size are important for BOLD-MRI response (Howe et al., 2002; Robinson et al., 2003). Robinson et al. (Robinson et al., 2003) compared the GH3 prolactinoma (strong BOLD response) and the RIF-1 fibrosarcoma (poor BOLD response) and found that the RIF-1 functional vascular density and vessel size were much smaller than for GH3. They estimated vessel size to be 14-21 μm for the GH3 prolactinoma and 5-11 μm for RIF-1. They concluded that there was insufficient deoxyHb in the RIF-1 tumour for a BOLD response to be detected. HT29 tumour vessels

have been reported as having an average diameter of 18 μm (measured using multi-photon fluorescence microscopy) (Tozer et al., 2005), which is similar to the diameters measured in the intravital microscopy experiments (see **Tables 4.2 & 4.4**). Robinson et al.'s (Robinson et al., 2003) diameter estimates were taken from MR measurements, so are not directly comparable with the HT29 measurements, but based on the above, HT29 tumour vessel size should not have been a significant issue.

Influence of anaesthesia on results:

Anaesthesia was required for restraint for these experiments. Hypnorm is known to affect rodent MABP, reducing it by ~25-30%, whereas Hypnovel has no effect (Cullen & Walker, 1985; Menke & Vaupel, 1988). Anaesthesia had a severe effect on CBA mouse blood pressure (**Figure 4.8**). The MABP of CBA mice did increase significantly in response to ATII but the consequent increase in tumour perfusion pressure may have been insufficient to produce a detectable BOLD-MRI response. A recent study has also shown that general anaesthesia in rats had no effect on the vascular response to the vasodilator, sodium nitroprusside, in tumour and a range of normal tissues, despite its effect on MABP (GM Tozer, personal communication). Without repeating the experiments using unanaesthetised animals, it is difficult to judge how anaesthesia has influenced the results.

4.4.4 Tumour vessel response to air-5% CO_2/carbogen as measured by BOLD-MRI and intravital microscopy

A differential response to air-5% CO_2/carbogen between HT29 and CaNT tumours could not be detected using BOLD-MRI despite their very different vascular maturation indices. The intravital microscopy experiments have shown that HT29 tumour vessels, at least, do not vasodilate in response to the mouse breathing air-5% CO_2 or carbogen gas mixtures, despite the presence of αSMA, so it is not surprising that the BOLD-MRI results were negative.

CO_2 does act as a vasodilator in some tumour types: air-5% CO_2 induced a positive BOLD response (increase of ~10-30%) in the GH3 prolactinoma model with a further 40-50% increase in response to carbogen (Robinson et al., 1999) – in keeping with Neeman et al.'s findings, though of a greater magnitude (see **Section 1.3.1.1**).

However, as discussed in **Section 1.3.1.1**, the action of CO_2 on both tumour and normal vasculature is not consistent. In Neeman et al's most recent paper (Gilead et al., 2004), any

change (rather than an increase) in BOLD-MRI signal intensity in response to breathing air-5% CO_2 was taken as being indicative of the presence of mature vessels and quantitative measurements were done on squared values to take into account both significant positive and negative changes. Serial BOLD-MRI measurements were performed on MLS ovarian carcinoma spheroids implanted in nude mice. A MRI vascular maturation index, defined as the fraction of mature vessels (showing response to air-5% CO_2) of the total functioning vessels (showing response to carbogen) normalised to normal control tissue (skin) was obtained which correlated with histological maturation index using αSMA (Gilead et al., 2004). Presumably their argument is that **any** change in BOLD-MRI signal intensity in response to air-5% CO_2 is indicative of vasoreactivity and whether CO_2 is inducing vasodilation or vasoconstriction in individual vessels does not actually matter. However, one could argue that no change might be seen if both vasodilation and vasoconstriction were occurring within the same pixel and that using significant change rather than increase in BOLD signal intensity as the measurement parameter is just a convenient way of getting around that fact that CO_2 may not act consistently as a vasodilator.

4.5 Conclusions

BOLD-MRI failed to discriminate between HT29 and CaNT tumours based on response to ATII. However, the intravital microscopy experiments showed that ATII could distinguish between HT29 and CaNT tumours and a positive BOLD response was seen in kidney. This suggests that the BOLD technique used lacked sufficient sensitivity. How this work could be developed further is discussed in **Chapter 5.**

Neeman et al.'s hypothesis that mature and immature vasculature can be distinguished by differential BOLD-MRI response to breathing air-5% CO_2 and carbogen gas (Neeman et al., 2001)) could not be reproduced - with the particular tumours and protocol used. The explanation for this is that, for HT29 tumour vessels at least, CO_2 does not act as a vasodilator. Based on the intravital microscopy data, CO_2 does not appear to be a suitable agent for the further investigation of tumour vessel maturity.

4.6 References: Chapter 4

Badzynska, B., Grzelec-Mojzesowicz, M., Dobrowolski, L. & Sadowski, J. (2002). Differential effect of angiotensin II on blood circulation in the renal medulla and cortex of anaesthetised rats. *J Physiol*, **538**, 159-66.

Brizel, D.M., Lin, S., Johnson, J.L., Brooks, J., Dewhirst, M.W. & Piantadosi, C.A. (1995). The mechanisms by which hyperbaric oxygen and carbogen improve tumour oxygenation. *Br J Cancer*, **72**, 1120-4.

Cullen, B.M. & Walker, H.C. (1985). The effect of several different anaesthetics on the blood pressure and heart rate of the mouse and on the radiation response of the mouse sarcoma RIF-1. *Int J Radiat Biol Relat Stud Phys Chem Med*, **48**, 761-71.

Dewhirst, M.W., Ong, E.T., Rosner, G.L., Rehmus, S.W., Shan, S., Braun, R.D., Brizel, D.M. & Secomb, T.W. (1996). Arteriolar oxygenation in tumour and subcutaneous arterioles: effects of inspired air oxygen content. *Br J Cancer Suppl*, **27**, S241-6.

Dunn, T., Braun, R., Rhemus, W., Secomb, T., Tozer, G., Chaplin, D. & Dewhirst, M. (1999). The effects of hyperoxic and hypercarbic gases on tumour blood flow. *Br J Cancer*, **80**, 117-126.

Gilead, A., Meir, G. & Neeman, M. (2004). The role of angiogenesis, vascular maturation, regression and stroma infiltration in dormancy and growth of implanted MLS ovarian carcinoma spheroids. *Int J Cancer*, **108**, 524-31.

Hirst, D.G., Hirst, V.K., Shaffi, K.M., Prise, V.E. & Joiner, B. (1991). The influence of vasoactive agents on the perfusion fo tumours growing in three sites in the mouse. *Int J Radiat Biol*, **60**, 211-218.

Howe, F., Robinson, S., Rijken, P., McSheehy, P., van der Sanden, B., Heerschap, A., Stubbs, M., van der Kogel, A. & Griffiths, J. (2002). Determination of tumor vascular morphology and function by susceptibility MRI and immunohistochemistry. In *Proc ISMRM*, Vol. 10. pp. 311: Honolulu, Hawaii.

Howe, F.A., Robinson, S.P., McIntyre, D.J., Stubbs, M. & Griffiths, J.R. (2001). Issues in flow and oxygenation dependent contrast (FLOOD) imaging of tumours. *NMR Biomed*, **14**, 497-506.

Huang, C.L., Davis, G. & Johns, E.J. (1991). A study of the action of angiotensin II on perfusion through the cortex and papilla of the rat kidney. *Exp Physiol*, **76**, 787-98.

Iadecola, C. (1992). Does nitric oxide mediate the increases in cerebral blood flow elicited by hypercapnia? *Proc Natl Acad Sci U S A*, **89**, 3913-6.

Jain, R.K., Munn, L.L. & Fukumura, D. (2002). Dissecting tumour pathophysiology using intravital microscopy. *Nat Rev Cancer*, **2**, 266-76.

Kimura, H., Braun, R.D., Ong, E.T., Hsu, R., Secomb, T.W., Papahadjopoulos, D., Hong, K. & Dewhirst, M.W. (1996). Fluctuations in red cell flux in tumor microvessels can lead to transient hypoxia and reoxygenation in tumor parenchyma. *Cancer Res*, **56**, 5522-8.

Lanzen, J.L., Braun, R.D., Ong, A.L. & Dewhirst, M.W. (1998). Variability in blood flow and pO2 in tumors in response to carbogen breathing. *Int J Radiat Oncol Biol Phys*, **42**, 855-9.

Mattson, D.L. (1998). Long-term measurement of arterial blood pressure in conscious mice. *Am J Physiol*, **274**, R564-70.

Menke, H. & Vaupel, P. (1988). Effect of injectable or inhalational anesthetics and of neuroleptic, neuroleptanalgesic, and sedative agents on tumor blood flow. *Radiat Res*, **114**, 64-76.

Neeman, M., Dafni, H., Bukhari, O., Braun, R. & Dewhirst, M. (2001). In Vivo BOLD Contrast MRI Mapping of Subcutaneous Vascular Function and Maturation: Validation by Intravital Microscopy. *Magn Reson Med*, **45**, 887-898.

Robinson, S.P., Collingridge, D.R., Howe, F.A., Rodrigues, L.M., Chaplin, D.J. & Griffiths, J.R. (1999). Tumour response to hypercapnia and hyperoxia monitored by FLOOD magnetic resonance imaging. *NMR Biomed*, **12**, 98-106.

Robinson, S.P., Rijken, P.F., Howe, F.A., McSheehy, P.M., Van Der Sanden, B.P., Heerschap, A., Stubbs, M., Van Der Kogel, A.J. & Griffiths, J.R. (2003). Tumor vascular architecture and function evaluated by non invasive susceptibility MRI methods and immunohistochemistry. *Magn Reson Imaging*, **17**,445-54

Tozer, G.M., Prise, V.E., Wilson, J., Cemazar, M., Shan, S., Dewhirst, M.W., Barber, P.R., Vojnovic, B. & Chaplin, D.J. (2001). Mechanisms associated with tumor vascular shut-down induced by combretastatin A-4 phosphate: intravital microscopy and measurement of vascular permeability. *Cancer Res*, **61**, 6413-22.

Tozer, G.M. & Shaffi, K.M. (1993). Modification of tumour blood flow using the hypertensive agent, angiotensin II. *Br J Cancer*, **67**, 981-8.

Trotter, M., Chaplin, D. & Olive, P. (1991). Effect of angiotensin II on intermittent tumour blood flow and acute hypoxia in the murine SCCVII carcinoma. *Eur J Cancer*, **27**, 887-893.

Unthank, J.L., Lash, J.M., Nixon, J.C., Sidner, R.A. & Bohlen, H.G. (1993). Evaluation of carbocyanine-labeled erythrocytes for microvascular measurements. *Microvasc Res*, **45**, 193-210.

Chapter 5 Concluding Discussion

The results presented in this thesis demonstrate that

- The platinum and taxane-based chemotherapy regimens tested do not cause acute anti-vascular changes, as detected by DCE-MRI. Therefore, anti-vascular agents such as CA-4-P have a specific action and this gives further confidence to the use of DCE-MRI kinetic endpoints as biomarkers for response to this group of agents. (Tofts et al., 1999; Tofts & Kermode, 1991).

- There is a dose-response relationship for the SW1222 tumour for CA-4-P with a clinically relevant dose (30 $mg.kg^{-1}$) producing a reversible decrease in DCE-MRI kinetic parameters. This dose level significantly increased antibody retention in the tumour, which is promising for the clinical combination of CA-4-P and radioimmunotherapy.

- An arterial input function was obtained for the nude mice used for the SW1222/CA-4-P study. A simultaneous fit of data from the *in-vivo* and blood experiments proved to be the most robust as it incorporated both very early data (*in-vivo* experiment) with quantitative time-points (blood sampling experiment). Calculation of the arterial input function has allowed data to be fitted to the Tofts' model (for calculation of quantitative parameters K^{trans} and v_e).

- BOLD-MRI could not demonstrate a difference between the HT29 and CaNT tumours based on their response to air-5% CO_2/carbogen or to angiotensin II. The intravital microscopy experiments demonstrated that the explanation for the lack of response to air-5% CO_2/carbogen may be because HT29 tumour vessels do not vasodilate in response to 5% CO_2. However, the intravital microscopy experiments showed that HT29 tumour vessels do vasoconstrict in response to angiotensin II and the lack of a BOLD-MRI response in this instance must be due to a lack of sensitivity.

5.1 *Future Work*

5.1.1 Clinical Study: DCE-MRI measurement of acute anti-vascular effects of cytotoxic agents

The experience gained from the clinical study reported here gives us greater confidence in using DCE-MRI as a surrogate marker in clinical trials of vascular disruptive agents. In retrospect, patient selection could have been better as several patients had very cystic tumours, in which only a small percentage of pixels within the tumour ROI took up contrast and so could be analysed. It is important to take time to position the patient carefully to ensure that the same section of tumour is imaged each time. Pelvic tumours are ideal as they do not move with respiration.

In this study, only median parameter values have been quoted. While this is a straightforward method of summarising data, it does not take into account inherent tumour heterogeneity and heterogeneity of response to treatment. Spatial heterogeneity of response was evaluated relatively simply for the CA-4-P/SW1222 study by identifying three regions: tumour rim, an intermediate area and tumour centre (**Chapter 3**). An alternative strategy would be to perform a histogram analysis to determine whether the percentage of pixels with a particular parameter value has increased/decreased in response to treatment (Hayes et al., 2002). How best to evaluate heterogeneity in the clinical setting and how to summarise it statistically needs to be determined.

An individualised arterial input function is the obvious next step in order to improve reproducibility. An artery within the same image slice as tumour could be used as a substitute for tumour-feeding arterioles, but it would have to be at least ~5mm in diameter to avoid partial volume effects as the in-plane resolution for the T_1-weighted sequence was 1.4 x 2.2 mm (pixel size). Computer algorithms can be developed that identify suitable pixels within an artery, e.g. by setting a threshold of the maximum average Gd-DTPA concentration plus two standard deviations (Rijpkema et al., 2001).

An alternative strategy is to normalise to another tissue, such as muscle or spleen, but this is not a simple option. As discussed in **Chapter 2**, muscle parameters were found to have a much worse reproducibility than tumour parameters. Also, normalising to muscle or spleen might confound analysis of tumour response to a vascular disruptive agent, as CA-4-P induces a small but significant acute reduction in blood flow in these tissues (~7

fold and ~2.5 fold at 6 hours following 100 $mg.kg^{-1}$ CA-4-P in spleen and muscle respectively) as well as in tumour (Tozer et al., 1999). Reductions in splenic and muscle blood flow are also seen with lower, 'clinically relevant' doses of CA-4-P (10 and 30 $mg.kg^{-1}$) (Prise et al., 2002).

A reproducibility analysis was obtained for the T_2* parameters, rBV and rBF, for visceral tumours. rBV and rBF may be useful for the evaluation of vascular disruptive agents in visceral tumours but they need to be validated first, by ensuring that changes in rBV and rBF are positively correlated with changes in blood volume and blood flow obtained from 'gold standard' techniques.

For blood flow measurements, radiolabelled iodoantipyrine (IAP) could be used to obtain absolute measurements of blood flow in an animal model (Maxwell et al., 2002; Tozer et al., 1999). Alternatively, the development of the new PET facility at the Gray Cancer Institute means that a comparison between MRI and PET measurements of change in tumour rBF in response to a vascular disruptive agent such as CA-4-P could be made in an animal model. PET has been used in clinical trials to assess changes in tumour blood flow measurements in response to CA-4-P and razoxane, an anti-angiogenic agent, using ^{15}O-labelled water (Anderson et al., 2003a; Anderson et al., 2003b). However, ^{15}O has a half-life of 2 minutes so is more difficult to use if the cyclotron and the PET scanner are separately housed, which is the case at the Mount Vernon site. An alternative would be to use the tracer copper(II) pyruvaldehyde bis(N-4-methylthiosemicarbazone) (Cu-PTSM) labelled with ^{62}Cu, which has a half-life of 9.7 minutes so is short enough to allow repeated measurements after about 40 minutes. Cu-PTSM has been used to measure tumour blood flow in patients using the first-pass extraction technique (Burke et al., 2001). Fluoromethane gas, labelled with ^{18}F, has also been used for blood flow measurements in PET (Celesia et al., 1984; Holden et al., 1981). The advantage of using fluoromethane is that the arterial input function can be inferred from radioactivity in expired air, so arterial puncture is not required (Holden et al., 1981). The advantage of using PET is that the experiments could be translated into the clinic, if so desired.

PET can also be used to measure blood volume using carbon monoxide gas (labelled with either ^{15}O or ^{11}C) (Anderson et al., 2003a; Anderson et al., 2003b; Kurdziel et al., 2003). ^{11}C has a half-life of 20 minutes, so is a more practical choice than ^{15}O. Carbon monoxide binds to haemoglobin to form deoxyhaemoglobin, which remains in the vascular space and

therefore provides a measure of intravascular volume. Alternatively, ^{51}Cr-labelled red blood cells could be used (Tozer & Morris, 1990).

5.1.2 CA-4-P/SW1222 study

The pre-clinical study investigating the acute effects of different dose levels of CA-4-P on the SW1222 tumour has provided data that can be extrapolated to the clinical trial. That is, it has provided an estimate of the magnitude of anti-vascular effect occurring at clinically achievable doses. However, the effect of the combination of a lower, more clinically relevant, dose of CA-4-P (such as 30 mg.kg^{-1}) and ^{131}I-A5B7 on SW1222 tumour growth still needs to be investigated.

How the addition of CA-4-P influences tumour response to ^{131}I-A5B7 could be investigated further. A comparison of the pattern of antibody distribution within tumour with the pattern of anti-vascular effect of CA-4-P (as measured by functional vascular volume, percentage necrosis, or DCE-MRI kinetic parameters) would help determine how much improvement is due to spatial cooperation.

5.1.3 Investigation of tumour vessel maturity

The ultimate aim of the BOLD-MRI experiments was to develop a non-invasive functional index of tumour vessel maturity that could be potentially translated into the clinic and which might help predict which patients are likely to respond to treatment with agents such as CA-4-P.

The BOLD-MRI and intravital microscopy experiments have been helpful in that they have shown that response to ATII is a potential discriminator between tumours with different levels of vessel maturity. However, BOLD-MRI lacks the sensitivity to detect this effect (at least with the particular protocols and tumours used) and so another method of detecting response would be required. As deoxyHb is an endogenous contrast agent, there is no control over the amount present within a tissue and sufficient amounts to be detected may not be present. In addition, from Neeman et al.'s data (Neeman et al., 2001) changes in blood flow are more important than changes in oxygenation. An alternative strategy would be to use an exogenous contrast agent instead to obtain T_2*-susceptibility measurements before and during administration of a vasoactive agent. A blood-pool agent such as Sinerem® (Guerbet, France) would be a suitable candidate. Sinerem is an ultra-small superparamagnetic iron oxide particle (USPIO) that has substantial T_2* relaxation

properties and a prolonged plasma circulation time (36 hours in humans). Sinerem has already been tested in clinical trials (to image lymph nodes, as it is taken up by macrophages) (Anzai, 2004), so is safe for clinical use. Sinerem would be injected intravenously and baseline T_2* measurements made, then a vasoactive agent administered and T_2* measurements repeated. The hypothesis would be that administration of the vasoactive agent would induce vasoconstriction/ vasodilation in vessels capable of response and a consequent change in tumour blood volume and hence in signal intensity and T_2*, as the amount of Sinerem present would be reduced/increased. If a change in blood volume in response to a vasoactive agent could be reliably be detected using Sinerem (or a similar compound) then it could be used to develop a non-invasive index of tumour vessel maturity. Then, of course, it would have to be compared to tumour response to CA-4-P to see whether there was any correlation between the degree of tumour vessel maturity and response to CA-4-P. Drug company approval for the use of Sinerem for this particular indication would be required for translation into clinical trials.

Alternatively, it may be more profitable to investigate whether tumour vessel permeability predicts CA-4-P response better. In this case, DCE-MRI could be used to investigate the relationship between vascular permeability to macromolecules and CA-4-P response. Beauregard et al. have shown that sensitivity to CA-4-P, as measured by DCE-MRI, is proportional to the permeability of the vascular wall to Gd-DTPA bound with albumin, across a range of different rodent tumour types (Beauregard et al., 2001). However, bovine albumin was used, so this compound could not be taken into clinical trials, but permeability to a USPIO might be an alternative option.

The above discussion highlights the need for further work to improve the reproducibility of DCE-MRI and the evaluation of response to vascular disruptive agents using various MR parameters. Whether it will be possible to develop a non-invasive index of tumour vessel maturity and the relevance of this to the assessment of vascular disruptive agents remains to be determined.

5.2 Chapter 5 References

Anderson, H., Yap, J.T., Wells, P., Miller, M.P., Propper, D., Price, P. & Harris, A.L. (2003a). Measurement of renal tumour and normal tissue perfusion using positron emission tomography in a phase II clinical trial of razoxane. *Br J Cancer*, **89**, 262-7.

Anderson, H.L., Yap, J.T., Miller, M.P., Robbins, A., Jones, T. & Price, P.M. (2003b). Assessment of pharmacodynamic vascular response in a phase I trial of combretastatin A4 phosphate. *J Clin Oncol*, **21**, 2823-30.

Anzai, Y. (2004). Superparamagnetic iron oxide nanoparticles: nodal metastases and beyond. *Top Magn Reson Imaging*, **15**, 103-11.

Beauregard, D.A., Hill, S.A., Chaplin, D.J. & Brindle, K.M. (2001). The susceptibility of tumors to the antivascular drug combretastatin A4 phosphate correlates with vascular permeability. *Cancer Res*, **61**, 6811-5.

Burke, D., Davies, M.M., Zweit, J., Flower, M.A., Ott, R.J., Dworkin, M.J., Glover, C., McCready, V.R., Carnochan, P. & Allen-Mersh, T.G. (2001). Continuous angiotensin II infusion increases tumour: normal blood flow ratio in colo-rectal liver metastases. *Br J Cancer*, **85**, 1640-5.

Celesia, G.G., Polcyn, R.E., Holden, J.E., Nickles, R.J., Koeppe, R.A. & Gatley, S.J. (1984). Determination of regional cerebral blood flow in patients with cerebral infarction. Use of fluoromethane labeled with fluorine 18 and positron emission tomography. *Arch Neurol*, **41**, 262-7.

Hayes, C., Padhani, A.R. & Leach, M.O. (2002). Assessing changes in tumour vascular function using dynamic contrast- enhanced magnetic resonance imaging. *NMR Biomed*, **15**, 154-63.

Holden, J.E., Gatley, S.J., Hichwa, R.D., Ip, W.R., Shaughnessy, W.J., Nickles, R.J. & Polcyn, R.E. (1981). Cerebral blood flow using PET measurements of fluoromethane kinetics. *J Nucl Med*, **22**, 1084-88.

Kurdziel, K.A., Figg, W.D., Carrasquillo, J.A., Huebsch, S., Whatley, M., Sellers, D., Libutti, S.K., Pluda, J.M., Dahut, W., Reed, E. & Bacharach, S.L. (2003). Using positron emission tomography 2-deoxy-2-[18F]fluoro-D-glucose, 11CO, and 15O-water for monitoring androgen independent prostate cancer. *Mol Imaging Biol*, **5**, 86-93.

Maxwell, R., Wilson, J., Prise, V., Vojnovic, B., Rustin, G., Lodge, M. & Tozer, G. (2002). Evaluation of the anti-vascular effects of combretastatin in rodent tumours by dynamic contrast enhanced MRI. *NMR Biomed*, **15**, 89-98.

Neeman, M., Dafni, H., Bukhari, O., Braun, R. & Dewhirst, M. (2001). In Vivo BOLD Contrast MRI Mapping of Subcutaneous Vascular Function and Maturation: Validation by Intravital Microscopy. *Magn Reson Med*, **45**, 887-898.

Prise, V.E., Honess, D.J., Stratford, M.R., Wilson, J. & Tozer, G.M. (2002). The vascular response of tumor and normal tissues in the rat to the vascular targeting agent, combretastatin A-4-phosphate, at clinically relevant doses. *Int J Oncol*, **21**, 717-26.

Rijpkema, M., Kaanders, J.H., Joosten, F.B., van der Kogel, A.J. & Heerschap, A. (2001). Method for quantitative mapping of dynamic MRI contrast agent uptake in human tumors. *J Magn Reson Imaging*, **14**, 457-63.

Tofts, P., Brix, G., Buckley, D., Evelhoch, J., Henderson, E., Knopp, M., Larsson, H., Lee, T., Mayr, N., Parker, G., Port, R., Taylor, J. & Weisskoff, R. (1999). Estimating kinetic parameters from dynamic contrast-enhanced T(1)-weighted MRI of a diffusable tracer: standardized quantities and symbols. *J Magn Reson Imaging*, **10**, 223-32.

Tofts, P.S. & Kermode, A.G. (1991). Measurement of the blood-brain barrier permeability and leakage space using dynamic MR imaging. 1. Fundamental concepts. *Magn Reson Med*, **17**, 357-67.

Tozer, G. & Morris, C. (1990). Blood flow and blood volume in a transplanted rat fibrosarcoma: comparison with various normal tissues. *Radiother Oncol*, **17**, 153-65.

Tozer, G.M., Prise, V.E., Wilson, J., Locke, R.J., Vojnovic, B., Stratford, M.R., Dennis, M.F. & Chaplin, D.J. (1999). Combretastatin A-4 phosphate as a tumor vascular-targeting agent: early effects in tumors and normal tissues. *Cancer Res*, **59**, 1626-34.

Appendix

1.1 Conversion of signal intensity into Gd-DTPA concentration

Signal intensity on spoiled gradient echo images (the T_1-weighted sequence used) is given by:

$$S = S_{max} \times \frac{1-\exp(-TR/T_1)}{1-\cos\alpha \times \exp(-TR/T_1)} \times \exp(-TE/T_2^*) \quad (1)$$

where S_{max}. is the maximal signal intensity (for $TR >> T_1$ and $TE << T_2$) and α is the flip angle (Hittmair et al., 1994).

If $TE << T_2^*$, the term $\exp(-TE/T_2^*)$ can be ignored and equation (1) simplified to:

$$S = S_{max} \times [1-\exp(-K \times TR/T_1)] \quad (2)$$

where K is a flip angle correction factor (Hittmair et al., 1994) and is equal to 1.40 for our acquisition conditions (obtained by simulation). The ratio of signal intensity at time t, S_t to baseline (pre-contrast) signal intensity, S_0, is then:

$$S_t/S_0 = \frac{1-\exp[-K \times TR/T_1(t)]}{1-\exp[-K \times TR/T_1(0)]} \quad (3)$$

where $T_1(t)$ is the post-contrast signal intensity at time t, and $T_1(0)$ is the pre-contrast relaxation time respectively.

$T_1(0)$ is calculated from an inversion recovery sequence (see below) and $T_1(t)$ calculated by rearranging equation (3):

$$1/T_1(t) = -\frac{1}{K \times TR} \times \ln\left[1 - \frac{S_t}{S_0}(1-\exp[-K \times TR/T_1(0)]\right] \quad (4)$$

The concentration of Gd-DTPA present at time t, C_t, can then be calculated from equation 5 (Donahue et al., 1994):

$$C_t = \frac{\left(1/T_1(t) - 1/T_1(0)\right)}{r_1} \tag{5}$$

where r_1 is the longitudinal relaxivity of protons *in vivo* due to Gd-DTPA ($mM^{-1}.s^{-1}$).

1.2 Calculation of $T_1(0)$

In an inversion recovery sequence, a 180° pulse is applied which flips the net magnetisation vector down to the –Z axis. When the pulse is removed, longitudinal magnetisation (M_Z) will begin to relax back to alignment with B_0 (along the +Z axis). This is described by equation (6):

$$M_Z = M_0[1 - 2\exp(-t/T_1)] \tag{6}$$

where M_0 is the equilibrium magnetisation.

If a 90° pulse is applied after a time known as 'inversion time', TI (time from the original inverting 180° pulse) then M_Z will be converted into M_{XY} (magnetisation in the transverse (XY) plane) and it will induce a signal. The resultant signal intensity is a measure of M_Z. If a series of 180° and 90° pulses are applied with varying inversion times, then a graph of signal intensity versus inversion time can be plotted and fitted to the equation below:

$$S(TI) = M_Z(TI) = M_0[1 - 2\exp(-TI/T_1)] \tag{7}$$

where S(TI) is the signal intensity at inversion time, TI. As TI $\rightarrow\infty$, full relaxation will have occurred so signal intensity will $\rightarrow M_0$. Values for the two unknown parameters T_1 and M_0 may be obtained from curve-fitting (see **Figure 1.1**).

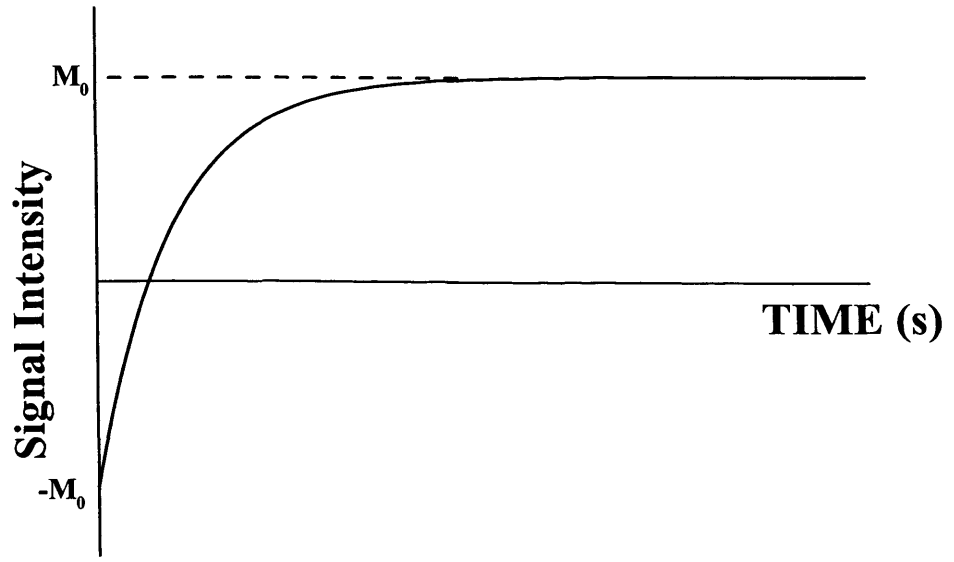

Figure 1.1: Calculation of $T_1(0)$

1.3 References

Donahue, K., Burstein, D., Manning, W. & Gray, M. (1994). Studies of Gd-DTPA relaxivity and proton exchange rates in tissue. *Magn Reson Med*, **32**, 66-76.

Hittmair, K., Gomiscek, G., Langenberger, K., Recht, M., Imhof, H. & Kramer, J. (1994). Method for the quantitative assessment of contrast agent uptake in dynamic contrast-enhanced MRI. *Magn Reson Med* **31**, 567-571.

Publications and presentations arising from this thesis

Submitted for publication:

Effects of platinum/taxane based chemotherapy on perfusion in human pelvic tumours as measured by dynamic MRI
Lankester KJ, Taylor NJ, Stirling JJ, Boxall J, D'Arcy JA, Leach MO, Padhani AR, Rustin GJS. (submitted to *British Journal of Cancer*).

Oral Presentations

Can BOLD-MRI be used as a non-invasive method to investigate tumour vessel maturity using angiotensin II?
British Cancer Research Meeting, Glasgow, 2002.

Magnetic resonance imaging & intravital Microscopy to measure tumour vascular maturity.
British Microcirculation Society 41st Scientific meeting, Sheffield, 2004.

Acute anti-vascular effects of Combretastatin A4-phosphate in the SW1222 tumour as measured by dynamic contrast enhanced (DCE)-MRI,
British Cancer Research Meeting, Manchester, 2004.

Reports

Acute anti-vascular effects of Combretastatin A4 Phosphate (CA4P) on the SW1222 tumour as measured by Dynamic contrast enhanced (DCE)-MRI.
Lankester KJ, Maxwell RJ, Hill SA, Tozer GM. (Cancer Research UK, 2003)

Abstracts

DCE-MRI assessment of acute functional microvascular effects in human tumours treated with cytotoxic chemotherapy.
Lankester KJ, Taylor NJ, Stirling JJ, Boxall J, Rustin GJS, Leach MO, Padhani AR.
Proc Intl Soc Mag Reson Med, 10th Scientific meeting, Honolulu, 2002:2091

Dynamic contrast enhanced MRI assessment of acute microvascular effects with conventional cytotoxic chemotherapy in human tumours.
Lankester KJ, Taylor NJ, Stirling JJ, Boxall J, Rustin GJS, Leach MO, Maxwell RJ, Padhani AR. Proc. British Cancer Research Meeting, Glasgow 2002.
BJC 2002; **86**(suppl 1):S99.

Quantifying heterogeneity of kinetic DCE-MRI parameters to refine the assessment of tumour response to cytotoxic therapy.
Lankester KJ, Taylor NJ, Stirling JJ, Boxall J, Rustin GJS, Leach MO, Padhani AR.
Intl Soc Mag Reson Med Cancer workshop October 2002, Santa Cruz, California.

Application of navigator techniques to breathhold DCE-MRI studies of the liver.
Taylor NJ, **Lankester KJ**, Stirling JJ, Rustin GJS, D'Arcy JA, Leach MO, Padhani AR.
Proc Intl Soc Mag Reson Med 11th Scientific meeting, Toronto, 2003:1306.

Effects of the anti-vascular agent, combretastatin-A4-phosphate, on 1H MRI relaxation times in colon tumour xenografts.
Maxwell RJ, **Lankester KJ**.
Proc Intl Soc Mag Reson Med 11th Scientific meeting, Toronto, 2003:1240.

Conventional cytotoxic chemotherapy agents do not have acute antivascular effects, as measured by dynamic contrast enhanced MRI (DCE-MRI).
Lankester KJ, Taylor NJ, Stirling JJ, Boxall J, Leach MO, Padhani AR, Rustin GJS
ASCO 2003 (A # 588).

Reproducibility of T1 and T2* weighted dynamic contrast-enhanced MRI:
a multiparametric comparison of breast and abdominal tumours
Taylor NJ, **Lankester KJ**, Ah-See MW, Stirling JJ, Rustin GJS, Makris A, D'Arcy JA, Walker-Samuel S, Leach MO, Padhani AR.
Proc Intl Soc Mag Reson Med 12th Scientific meeting, Kyoto, 2004:1975.